

Catalyst and Reaction Development in Conjugated Polymer Synthesis

by

Ariana Olsen Hall

A dissertation submitted in partial fulfillment
of the requirements for the degree of
Doctor of Philosophy
(Chemistry)
in the University of Michigan
2017

Doctoral Committee:

Professor Anne J. McNeil, Chair
Professor Jinsang Kim
Professor Melanie S. Sanford
Professor John P. Wolfe

Ariana O. Hall

aolsenh@umich.edu

ORCID iD: [0000-0002-2720-5992](https://orcid.org/0000-0002-2720-5992)

Acknowledgments

I would like to first thank Anne McNeil for her invaluable mentorship and advice throughout my time in graduate school. I want to thank my labmates Dr. Se Ryeon Lee, Dr. Kelsey King, Dr. Ed Palermo, Dr. Zack Bryan, Dr. Danielle Zurcher, Dr. Mitchell Smith, Pete Goldberg, Kendra Souther, Amanda Leone, Dr. Gesine Veits, Dr. Chen Kong, Matthew Hannigan, Emily Mueller, and Justin Harris. I especially want to thank Se Ryeon for her mentorship when I first joined the group, and for working with me on developing Ni precatalysts. I also owe special thanks to Danielle, Pete and Amanda for proofreading dissertation chapters, especially Danielle, who read and gave insightful feedback for every unpublished chapter. I also want to thank my collaborators: Professor Steven Wheeler, Dr. Jacob Bloom, and Andrea Bootsma, for their work on the computational calculations in Chapter 2, and Professor Stephen Maldonado and Josh DeMuth for letting me to use their equipment and helping me set up and understand electrochemistry. Finally, I want to thank my family and friends. Their support and encouragement was invaluable throughout my PhD.

TABLE OF CONTENTS

ACKNOWLEDGMENTS	ii
LIST OF FIGURES	iv
LIST OF TABLES	ix
LIST OF CHARTS	xi
LIST OF SCHEMES	xii
LIST OF APPENDICES	xiv
ABSTRACT	xv
CHAPTER	
1. Introduction	1
2. Reactive Ligand Influence on Initiation in Phenylene Catalyst-Transfer Polymerization	17
3. Limitations of Using Small Molecules to Identify Catalyst-Transfer Polymerization Reactions	30
4. Single-Electron Reactions for Conjugated Polymer Synthesis	40
5. Conclusions	54
APPENDICES	64

LIST OF FIGURES

FIGURE	
2.1 (A) Time-dependent in situ IR spectra when polymerizing monomer 1 (B) Plot of monomer concentration versus time for the same reaction.	22
2.2. MALDI-TOF-MS data when polymerizing monomer 1 with various (dppe)Ni(RL)X catalysts	25
3.1 Plot of number-average molecular weight and dispersity versus conversion for 5	33
3.2 Plot of the difunctionalized-to-monofunctionalized product ratio versus percent conversion of the limiting reagent for a Kumada and Sonogashira small molecule reaction.	34
4.1 EPR spectra showing radical formation in the reaction of 3 and iPrMgCl.	42
4.2 Cyclic voltammetry curves for 4 , P1 and PDI	46
4.3 Proposed initiator for polymerizing 3	47
S1.1 ³¹ P NMR spectra acquired during the attempted synthesis of S8	75
S1.2 Gas chromatogram (a) for the attempted synthesis of S8 and mass spectrum (b) for peak at 3.4 min	76
S1.3 ¹ H and ³¹ P NMR spectra of 2b	77
S1.4 ¹ H and ³¹ P NMR spectra of S1	78
S1.5 ¹ H and ³¹ P NMR spectra of 2c	79
S1.6 ¹ H and ¹³ C NMR spectra of S2	80
S1.7 ¹ H and ³¹ P NMR spectra of 2d	81
S1.8 ¹ H and ¹³ C NMR spectra of S3	82

S1.9 ^1H and ^{13}C NMR spectra of S4	83
S1.10 ^1H and ^{31}P NMR spectra of 2e	84
S1.11 ^1H and ^{13}C NMR spectra of S6	85
S1.12 ^1H and ^{31}P NMR spectra of S7	86
S1.13 ^1H and ^{31}P NMR spectra of 2f	87
S1.14 Plot of [monomer] versus for the polymerization of monomer 1 catalyzed by 2b	91
S1.15 Plot of [monomer] versus time the polymerization catalyzed by 2c .	92
S1.16 Plots of [monomer] versus time for the polymerization catalyzed by 2d	93
S1.17 Plot of [monomer] versus time for the polymerization catalyzed by 2e	94
S1.18 Plot of [monomer] versus time for the polymerization catalyzed by 2e with PPh_3	95
S1.19 Plot of [monomer] versus time for the polymerization catalyzed by 2f .	96
S1.20 (a) ^{19}F and ^{31}P NMR spectra at the beginning and (b) end of the reaction in Scheme S1.1 .	98
S1.21 Representative ^{19}F NMR spectral array for precatalyst 2e	99
S1.22 Plot of concentration of intermediate (●) and product (○) versus time for the data in Figure S1.21 .	99
S1.23 Plot of M_n and \bar{D} versus conversion for 2b	102
S1.24 Plot of M_n and \bar{D} versus conversion for 2c	103
S1.25 Plot of M_n and \bar{D} versus conversion for 2d	104
S1.26 Plot of M_n and \bar{D} versus conversion for 2e	105
S1.27 a.) Plot of M_n and \bar{D} versus conversion for 2f b.) GPC curves of aliquots removed at 20 and 80% monomer conversion during Run 1.	106
S1.28 a.) Full MALDI-TOF MS spectrum of polyphenylene initiated with precatalyst 2b , b.) MALDI-TOF MS spectrum at 23 repeat units, and c.) MALDI-TOF MS spectrum at 30 repeat units.	108

S1.29 a.) Full MALDI-TOF MS spectrum of polyphenylene initiated with precatalyst 2c , and b.) MALDI-TOF MS spectrum at 23 repeat units.	109
S1.30 a.) Full MALDI-TOF MS spectrum of polyphenylene initiated with precatalyst 2d , and b.) MALDI-TOF MS spectrum at 23 repeat units.	109
S1.31 a.) Full MALDI-TOF MS spectrum of polyphenylene initiated with precatalyst 2f , and b.) MALDI-TOF MS spectrum at 23 repeat units.	111
S1.32 a.) Full MALDI-TOF MS spectrum of polyphenylene initiated with Ni(dppe)tolBr, and b.) MALDI-TOF MS spectrum at 23 repeat units.	111
S1.33 a.) Full MALDI-TOF MS spectrum of polyphenylene initiated with Ni(dppe)Cl ₂ , and b.) MALDI-TOF MS spectrum at 23 repeat units.	112
S2.1 ¹ H and ¹³ C NMR spectra for 1	127
S2.2 ¹ H and ¹³ C NMR spectra for S1	128
S2.3 ¹ H and ¹³ C NMR spectra for 6	129
S2.4 ¹ H and ¹³ C NMR spectra for S2	130
S2.5 ¹ H and ¹³ C NMR spectra for 3	131
S2.6 ¹ H and ¹³ C NMR spectra for 4	132
S2.7 ¹ H and ¹³ C NMR spectra for S4	133
S2.8 ¹ H and ¹³ C NMR spectra for 5	134
S2.9 ¹ H and ¹³ C NMR spectra for S5	135
S2.10 ¹ H and ¹³ C NMR spectra for S6	136
S2.11 ¹ H and ¹³ C NMR spectra for S7	137
S2.12 ¹ H and ¹³ C NMR spectra for S8	138
S2.13 ¹ H and ¹³ C NMR spectra for S9	139
S2.14 ¹ H and ³¹ P NMR spectra for S10	140
S2.15 Plot of M_n and \bar{D} versus conversion utilizing the most favorable small molecule conditions.	149

S2.16 Plot of M_n and \bar{D} versus time utilizing S9 monomer and previously reported chain-growth conditions	150
S2.17 Plot of M_n and \bar{D} versus time utilizing S9 monomer and the most favorable small molecule conditions	152
S2.18 Plot of product ratios versus conversion from Table S2.14 and Table S2.17	157
S2.19 Plot of product ratios versus conversion from Table S2.15 and Table S2.16.	157
S2.20 Calibration curve for 1 , points include error bars	160
S2.21 Calibration curve for 2 , points include error bars	161
S2.22 Calibration curve for 3 , points include error bars	161
S2.23 Calibration curve for 4 , points include error bars	162
S2.24 Calibration curve for S5 , points include error bars	162
S3.1 ^1H and ^{13}C NMR spectra of S1	169
S3.2 ^1H and ^{13}C NMR spectra of 4	170
S3.3 ^1H and ^{13}C NMR spectra of PDI	171
S3.4 EPR spectra of 1 , $i\text{PrMgCl}$, and the reaction of 1 + $i\text{PrMgCl}$	173
S3.5 EPR spectra of 2 , $i\text{PrMgCl}$, and the reaction of 2 + $i\text{PrMgCl}$	173
S3.6 EPR spectra of 3 , $i\text{PrMgCl}$, and the reaction of 3 + $i\text{PrMgCl}$	173
S3.7 (a) ^1H NMR spectrum of unreacted 2 (b). ^1H NMR spectrum of 2 after Zn activation and quenching	175
S3.8 GPC traces for the attempted polymerization of 2	176
S3.9 Undivided cell setup for polymerizing 4	177
S3.10 GPC traces for polymerizing 4 in an undivided cell	178
S3.11 Plot of potential (V) vs time (s) for polymerizing 4 in an undivided cell	178

S3.12 GPC trace of isolated P1	179
S3.13 Divided cell for polymerizing 4	180
S3.14 GPC trace of product isolated from polymerizing 4 in a divided cell	180
S3.15 GPC trace for treating 4 with constant current in the absence of PDI	181
S3.16 GPC trace for treating PDI with constant current in the absence of 4	182
S3.17 GPC trace for combining 4 , PDI , and zinc foil in the absence of current	182
S3.18 GPC trace for polymerizing 4 with constant potential	183
S3.19 Cyclic voltammograms of (a) 4 , (b) P1 , (c) PDI , and (d) M4 , P1 , and PDI overlaid	184

LIST OF TABLES

TABLE

3.1 Selective small molecule analogues and the corresponding CTPs	32
S1.1. Table of k_p values	88
S1.2 Data for the plots in Figure S1.14	91
S1.3 Data for the plots in Figure S1.15	92
S1.4 Data for the plots in Figure S1.16	93
S1.5 Data for the plots in Figure S1.17	94
S1.6 Data for the plots in Figure S1.18	95
S1.7 Data for the plots in Figure S1.18	96
S1.8 Initiation rate constants for 2e	100
S1.9 Data for the plot in Figure S1.23 , Run 1.	102
S1.10 Data for the plot in Figure S1.23 , Run 2.	102
S1.11 Data for the plot in Figure S1.24 , Run 1.	103
S1.12 Data for the plot in Figure S1.24 , Run 2.	103
S1.13 Data for the plot in Figure S1.25 , Run 1.	104
S1.14 Data for the plot in Figure S1.25 , Run 2.	104
S1.15 Data for the plot in Figure S1.26 , Run 1.	105
S1.16 Data for the plot in Figure S1.26 , Run 2.	105
S1.17 Data for the plot in Figure S1.27 , Run 1.	106
S1.18 Data for the plot in Figure S1.27 , Run 2.	107

S1.19 Absolute electronic energies (E) and free energies (G), in hartrees, for reactants and transition states (TS), along with the corresponding change in NPA charges for select species (Δq).	114
S2.1 Data for reactions with 0–2 equiv of SPhos	142
S2.2 Data for reactions with variable Pd precatalysts	143
S2.3 Data for reactions with variable Pd precatalysts.	144
S2.4 Data for reactions with 5-20 equiv PMDTA.	144
S2.5 Data for reactions with 1-20 equiv CuI/PMDTA	144
S2.6 Data for reactions with 0.2-5 equiv of Gen 2 SPhos	144
S2.7 Data for reactions with various bases.	145
S2.8 Data for reactions with 15-100% NEt ₃ volume ratio.	145
S2.9 Data for polymerization screens with NEt ₃ (variable volume)	147
S2.10 Data for reactions with variable Pd precatalysts	147
S2.11 Data for the plot in Figure S2.15	149
S2.12 Data for the plot in Figure S2.16	151
S2.13 Data for the plot in Figure S2.17	152
S2.14 Data for Sonogashira small molecule reaction profile, trial 1	154
S2.15 Data for Sonogashira small molecule reaction profile, trial 2	154
S2.16 Data for Kumada small molecule reaction profile, trial 1	156
S2.17 Data for Kumada small molecule reaction profile, trial 2	156
S3.1 GC areas for attempted polymerization of 2	176
S3.2 Results for polymerizing 4 in an undivided cell with varying equivalents of PDI .	178
S3.3 Cyclic voltammetry results for 4 , P1 , and PDI	184

LIST OF CHARTS

CHART

1.1 First generation precatalysts	4
1.2 High-performing polymers in OPVs	6
2.1 Second-generation reactive ligands	21
2.2 Third-generation reactive ligands	23
4.1 Commercially available monomers screened for radical formation	42
4.2 PDI derivatives to screen as mediators	47
5.1 Efficient thienothiophene polymer for photovoltaics and proposed mediators for indirect electropolymerization	59

LIST OF SCHEMES

SCHEME

1.1 CTP mechanism for 3-hexylthiophene	2
1.2 Initiation of thiophene polymerization with (dppe)Ni(o-tolyl) precatalyst	3
1.3 Small-molecule model to screen for CTP conditions	5
1.4 Chain-walking in thiazole	6
1.5 Proposed indirect electrocatalytic polymerization	8
2.1 First-generation reactive ligands for phenylene polymerization	18
2.2 Structural differences between the model system and the authentic polymerization and their impact on initiation rates	23
3.1 Difunctionalized products can be obtained via two different pathways	31
4.1 Thiazole oligomerization via $S_{RN}1$ reaction	41
4.2 Attempted $S_{RN}1$ polymerization using LiTDBB as a sacrificial donor	43
4.3 Phenyl–pyrrole coupling through indirect electrocatalysis	44
4.4 Electrocatalytic reaction for polymerizing 4 with constant applied current	45
5.1 Fast initiation and narrow dispersity could be achieved with electron-rich catalysts and triphenylphosphine	56
5.2 Summary of results for Chapter 2	56
5.3 Small-molecule screen reported by Noonan and coworkers	57
5.4. Summary of results and future implications for Chapter 3	57

5.5. Results for Chapter 4	58
S1.1. Initiation of precatalyst 2e	97

LIST OF APPENDICES

APPENDIX

- | | |
|--|-----|
| 1. Supporting Information for Chapter 2: Reactive Ligand Influence on Initiation in Phenylene Catalyst-Transfer Polymerization | 64 |
| 2. Supporting Information for Chapter 3: Limitations of Using Small Molecules to Identify Catalyst-Transfer Polycondensation Reactions | 116 |
| 3. Supporting Information for Chapter 4: Single-Electron Reactions for Conjugated Polymer Synthesis | 164 |

Abstract

Conjugated polymers are lightweight, flexible, solution-processible materials which can be used in organic electronic devices, including photovoltaics and light-emitting diodes. Catalyst-transfer polymerization (CTP) is a chain-growth method for synthesizing conjugated polymers with targeted molecular weight and sequence, as well as narrow dispersity. Several factors continue to limit the utility of CTP. Slow precatalyst initiation leads to broad dispersity and limited sequence control. Furthermore, the monomer scope of CTP is limited, especially for electron-deficient monomers. The highest performing polymers in photovoltaic devices are still synthesized by step-growth polymerizations. This thesis describes our efforts to address both limitations of CTP by designing new precatalysts which undergo fast initiation, using model reactions to screen catalysts to expand CTP scope, and finally, to develop new, non-CTP chain-growth syntheses of conjugated polymers through single-electron reactions.

Chapter 1 provides a history of CTP for conjugated polymer synthesis. It describes progress that has been made in precatalyst design to improve dispersity and enhance initiation. We then discuss the use of small-molecule screens to identify catalysts for CTP as a method for expanding the monomer scope. Finally, we briefly introduce the precedent for single-electron reactions, both radical and electrochemical, for conjugated polymer synthesis and explain our proposal to develop chain-growth syntheses by modifying these methods.

Chapter 2 reports our design of a new precatalyst which has faster initiation than propagation. It describes our development of a new method for measuring initiation rates during polymerization, as well as our discovery that adding triphenylphosphine to a polymerization and incorporating a trifluoroethoxy group into a precatalyst both affected initiation rates.

Chapter 3 describes our efforts to identify catalysts and reaction conditions for CTP of phenylene-ethynylene by using a small-molecule reaction to probe for catalyst

association by looking at mono-coupling versus di-coupling. It explains our discovery that small-molecule systems, which we and others have previously used, can have false positives when there are large reactivity differences between substrates, and proposes additional experiments to increase the accuracy of such models for predicting CTP.

Chapter 4 describes our efforts to synthesize conjugated polymers through single-electron reactions rather than CTP. We present the precedent for conjugated polymer synthesis via $S_{RN}1$ reactions, and our attempts to expand the monomer scope to several monomers used in organic photovoltaics. It further explains the history of step-growth electropolymerizations and our efforts to use indirect electrolysis to develop a chain-growth electropolymerization for conjugated polymers. We successfully synthesized one conjugated polymer using a perylene diimide mediator.

Chapter 5 summarizes our progress in catalyst and reaction development for conjugated polymer synthesis and the future directions and impact of each chapter. It describes the impacts that our discoveries in Chapter 2 could have for precatalyst design, rate enhancement, and rate studies. It discusses the impact that our work in Chapter 3 will have on using model systems to identify CTP conditions, including a recent example that citing our work. Finally, it describes the promising results in Chapter 4 and the future directions of indirect electrocatalysis for chain-growth conjugated polymer synthesis. Chain-growth methods are needed to control molecular weight, dispersity, and sequence in conjugated polymer synthesis, to ensure reproducibly high-performing devices.

Chapter 1

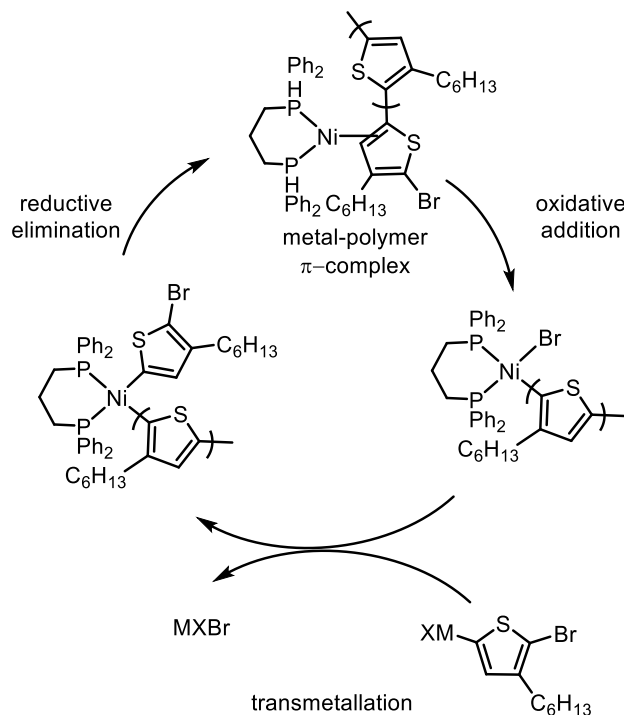
Introduction

Organic π -conjugated polymers are used as lightweight, flexible, solution-processible materials for electronic applications such as organic photovoltaic devices.¹ A bulk heterojunction organic photovoltaic device contains an active layer with a donor, frequently a π -conjugated polymer, and an acceptor. Devices with high efficiency frequently contain complex conjugated polymers with multiple heteroaromatic groups in the repeat unit.² Polymer properties such as molecular weight (M_n)³ and dispersity (\mathcal{D})⁴ impact device performance.⁵ Therefore, fabricating robust electronic devices with high efficiency requires methods to polymerize a broad scope of monomers with targeted M_n and \mathcal{D} . Since the discovery of conductive polymers in 1977,⁶ a variety of synthetic methods have been developed.^{7,8} Early synthetic methods frequently used electrochemical polymerizations, which typically produced insoluble polymer films.⁶

Conjugated polymer synthesis was improved by the discovery of chain-growth catalyst-transfer polymerization (CTP), first discovered independently by Yokozawa⁹ and McCullough¹⁰ in 2004 for polymerizing 3-hexylthiophene with nickel-phosphine catalysts (Scheme 1.1). Since it was discovered, CTP has been expanded to several other monomers, including phenylene,¹¹ fluorene,^{12,13} thiazole,^{14,15} pyrrole,¹⁶ pyridine,¹⁷ and benzotriazole.¹⁸ The catalyst scope has also been expanded to Ni and Pd catalysts ligated by diimines,^{18,19} NHCs,²⁰ phosphines,^{12,21} and Buchwald ligands.^{22,23,24} In addition to Grignard and zinc reagents, boronic acids¹² and esters,^{25,26,27} stannanes,²⁸ organolithium,²⁹ and gold-functionalized³⁰ monomers. Copolymers, including block,^{26,31} gradient,^{24,31r,32,33} alternating,³⁴ and random,^{23,31r} have also been polymerized through CTP. Importantly, we have found that gradient copolymers, which are only accessible through chain-growth polymerizations, can stabilize organic photovoltaic device

performance over heating time (modelling the effects of long-term sun exposure on devices).³⁵

Scheme 1.1. CTP mechanism for polymerizing 3-hexylthiophene. M = Mg, Zn, X = Br, Cl^{9,10}

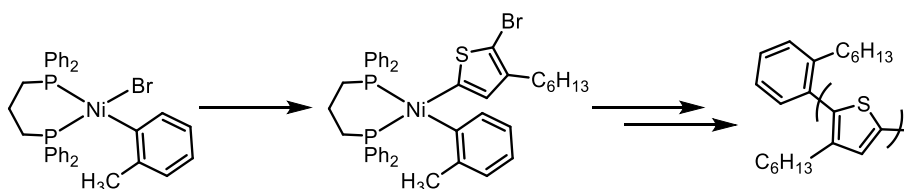


The chain-growth behavior results from a metal-polymer π-complex which forms after reductive elimination (Scheme 1.1) and promotes intramolecular oxidative addition. Catalyst-transfer polymerization produces polymers with narrow dispersities and enables targeted molecular weight by simply varying catalyst-to-monomer ratio. Several studies have provided evidence for the presence of this π-complex: competition studies have shown that catalysts have a high preference for intramolecular oxidative addition, even in the presence of a more reactive “competitive agent”³⁶ and Koeckelburghs observed π-complex formation by ³¹P NMR spectroscopy when attempting to polymerize thienothiophene,³⁷ although the catalyst-thienothiophene π-complex was so stable that polymerization did not occur. Mechanistic studies have provided further insight into CTP and guided catalyst development: kinetic studies show that the rate-determining step in CTP with Ni-phosphines depends on the bite-angle of the ancillary ligand on the precatalyst. Using 1,2-bis(diphenylphosphino)ethane (dppe), the rate-determining step is

reductive elimination, while bis(diphenylphosphino)propane gives rate-determining transmetallation.³⁸ The polymerization rate is enhanced by using electron-deficient dppe derivatives, while electron-rich ligands provide polymers with narrower dispersity.³⁹ However, CTP still has several limitations, including slow precatalyst initiation and limited monomer scope.

Precatalysts that contain reactive ligands which react with monomer to initiate a polymerization are useful for several reasons. The first precatalysts, Ni-phosphine precatalysts with tolyl reactive ligands, were developed as a soluble alternative to Ni-phosphine dihalide precatalysts (Scheme 1.2).⁴⁰ In addition to improving solubility, precatalysts with organic reactive ligands enable targeted sequence when synthesizing copolymers by “blocking” one reactive polymer end with the non-reactive organic group, ensuring unidirectional polymer growth. Furthermore, precatalysts are also used to incorporate various functional groups, including alkynes,⁴¹ silyl ethers,⁴² and esters.⁴³ However, if precatalyst initiation is slower than subsequent propagation reactions, the dispersity will be broader.⁴⁴ Our group found that phenylene polymerizations using Ni-dppe catalysts have initiation that is significantly slower than propagation. To address this limitation we set out to accelerate initiation in phenylene polymerizations.

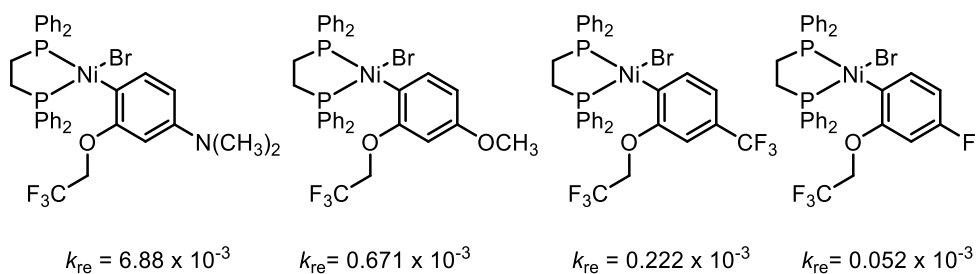
Scheme 1.2. Initiation of thiophene polymerization with (dppe)Ni(o-tolyl) precatalyst⁴⁰



Using Ni precatalysts containing 1,2-diphenylphosphineethane, both initiation and propagation have rate-determining reductive elimination, and therefore changing reaction conditions or ancillary ligands would affect both processes similarly. To selectively enhance initiation over propagation, we designed a series of nickel precatalysts with modified phenyl groups as the reactive ligand.⁴⁵ We anticipated that the reactive ligand should have the strongest effect during initiation, when it is directly forming a bond to a monomer. Theoretical calculations found a correlation between the energy barriers and the change in atomic charge on both organic groups (reactive ligand and monomer) during reductive elimination. To test this, we then developed a model to measure

reductive elimination rates by ^{19}F NMR spectroscopy. We incorporated a trifluoroethoxy tag to the reactive ligand of the precatalyst (Chart 1.1) to directly observe the nickel species during the reaction, enabling calculation of reductive elimination rate constants (k_{re}). With this model, we calculated reductive elimination rates for the precatalysts, and found that the precatalysts containing a para dimethylamino group, had the fastest initiation rate, but was still slower than propagation. Furthermore, its synthesis had an overall yield of just 5% making it impractical for widespread use.

Chart 1.1. First generation precatalysts⁴⁵

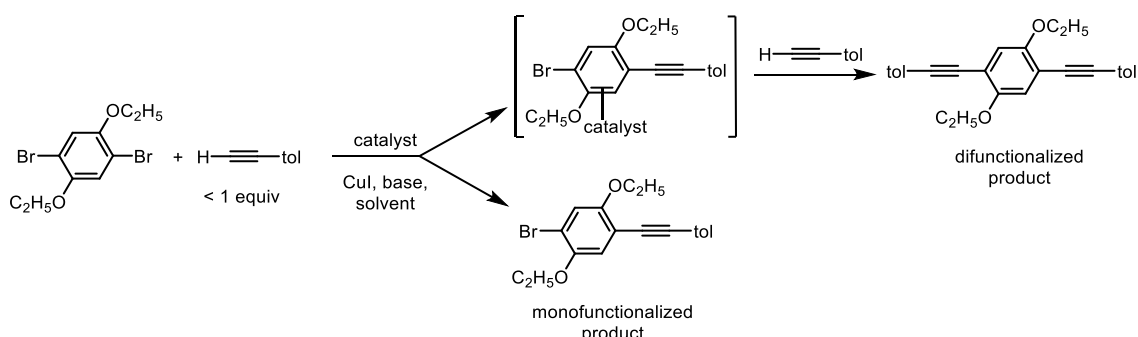


Chapter 2 details our efforts to find a precatalyst with an initiation rate faster than propagation and a less arduous synthesis. We synthesized several precatalysts containing heteroaromatic and biphenyl reactive ligands. To avoid extra synthetic steps needed to install the trifluoroethoxy tag, we derived a method using in situ IR spectroscopy to measure initiation rates during a polymerization. We found that several changes between the polymerization conditions and the single-turnover model system we had previously used had significant effects on the initiation rate. Furthermore, we found that the strongest factor to impact dispersity and living, chain-growth behavior in phenylene polymerization is the ancillary ligand, rather than the reactive ligand. Overall, this chapter provides new insight into the effects of reactive ligands, fluorine tags, and additives on CTP with phenylene.

In addition to slow initiation, monomer scope is an ongoing challenge in CTP. Screening catalysts for living, chain-growth polymerizations of new monomers is challenging because many factors can lead to termination, side reactions and other failures in a polymerization, which make screening and analysis difficult. Small-molecule reactions can predict chain-growth when a difunctionalized product is observed even though monofunctionalized product is stoichiometrically favored (Scheme 1.3). This

selectivity implies that a π -complex forms after reductive elimination, promoting the intramolecular oxidative addition that is essential for chain-growth polymerization. Selective difunctionalization has been used as evidence for catalyst association in thiophene polymerization,¹⁰ and to identify Pd-NHCs as catalysts for CTP with phenylene and thiophene,^{20c,46} and to predict CTP conditions for poly(pyridine)⁴⁷ and several thiophene derivatives.⁴⁸ Chapter 3 details our attempts to use a screening method to identify chain-growth conditions for synthesizing poly(phenylene-ethynylene), a conjugated polymer with applications in LEDs.⁴⁹ While the screening model identified selective dicoupling conditions, they still gave step-growth polymerizations. The observed selectivity arose from monofunctionalized product reacting much faster than the starting material. Ultimately, this chapter elucidates the shortcomings of a common method used to predict chain-growth polymerization conditions, and shows that, in addition to screening for selective dicoupling, one must study the product ratios over time to determine the cause of the selectivity.

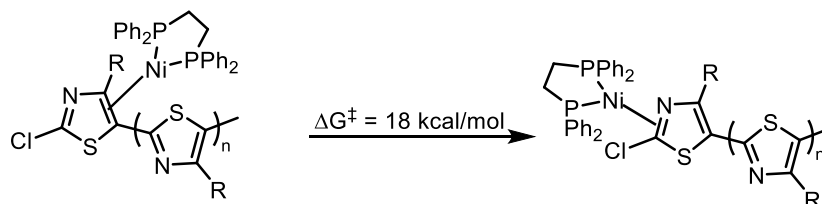
Scheme 1.3. Small-molecule model to screen for CTP conditions



While CTP can produce polymers and copolymers with targeted molecular weight and narrow dispersity, monomer scope remains limited. As described in chapter 3, efforts to identify catalysts for new monomers can be time consuming and difficult. For example, when polymerizing the electron-deficient thiazole, which differs from thiophene by only a single atom, new conditions needed to be found for both activation and polymerization. A mixed-halogen monomer had to be synthesized to ensure controlled activation. Furthermore, while Ni-dppe catalysts perform well for thiophene polymerizations, when polymerizing thiazole, computations reveal a high energy barrier for the catalyst to “walk” from the C–C bond of a monomer unit to the C–N bond prior to oxidative addition (Scheme

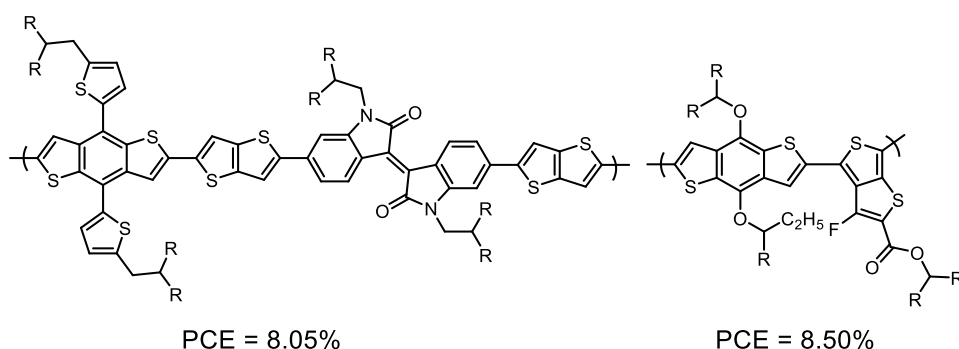
1.4). The high barrier enables a chain-transfer-to-monomer side reaction to occur, and so a more rigid phosphine ligand was needed to suppress this process.

Scheme 1.4. Chain-walking in thiazole



The high chain-walking barrier observed when polymerizing thiazole are especially concerning because polymers with higher power conversion efficiency (PCE) in OPVs typically contain large monomers with multiple rings of different electronic properties (Chart 1.2).^{2b,50} A successful CTP mechanism requires the catalyst to efficiently “walk” across all the rings without getting trapped on a bond or dissociating; in other words, the energy barriers for each step must be low enough that the catalyst is not displaced from the polymer, which could lead to step-growth polymerization. The high barrier to chain-walking in a single thiazole ring raises concerns for CTP with large, complex monomers where many chain-walking steps between electronically different bonds must occur. To address this limitation, we explored alternative mechanisms that could provide chain-growth polymerization.

Chart 1.2. High-performing polymers in OPVs^{3b,50}



Single-electron mechanisms may provide an alternative method for polymerizing electron-deficient monomers. Radical polymerizations are effective for polymerizing alkene-functionalized monomers, and can be controlled through various techniques by

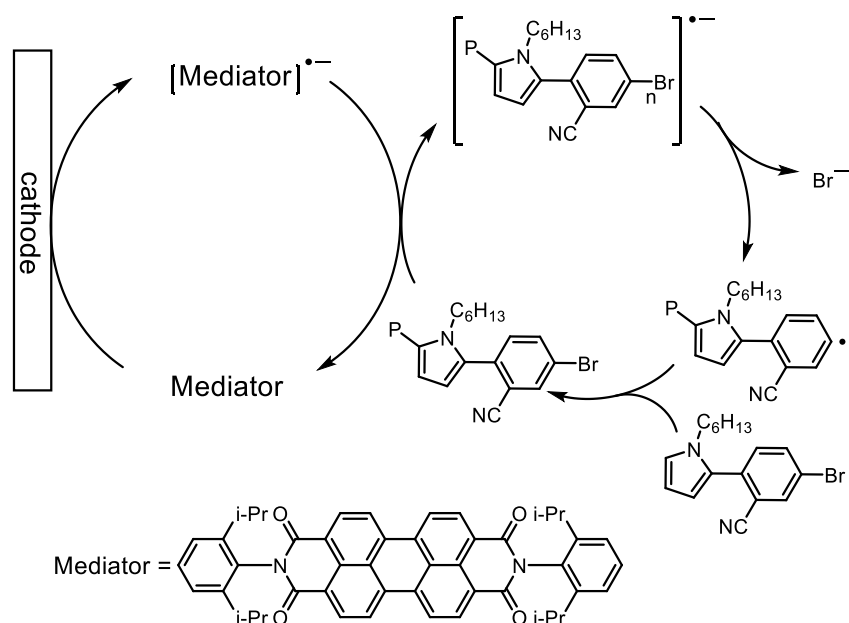
manipulating the concentration of active radicals.⁵¹ While analogous radical mechanisms are rarely used for conjugated polymer synthesis, Studer and coworkers have used radical-anion mechanisms to polymerize poly(metaphenylene),⁵² poly(paraphenylene), poly(naphthalene),⁵³ and poly(paraphenylene sulfide).⁵⁴ Kiriya discovered a radical activation method for perylene diimide-thiophene monomers, though polymerization still requires a nickel catalysts.⁵⁵ The McNeil group recently discovered that an electron-deficient thiazole Grignard monomer undergoes spontaneous oligomerization through a radical-anion $S_{RN}1$ mechanism. Chapter 4 describes our efforts to expand this reaction to other monomers.

In addition to chemically-induced radical polymerization, electrochemical polymerizations are a widely used method. Initial efforts to synthesize conjugated polymer films frequently employed oxidative electropolymerization techniques, which were used to synthesize poly(thiophene),⁵⁶ poly(thienothiophene),^{57,58} poly(pyrrole),⁵⁹ poly(aniline),⁶⁰ and poly(carbazole),⁶ among others. Reductive electropolymerization has also been used with nickel catalysts to synthesize poly(thiophene)⁶¹ and other conjugated polymers. In direct electropolymerizations, the reaction must occur at the surface of the oxidizing or reducing electrode, making chain-growth difficult, as all polymer chains would have to remain on or near the surface throughout the entire polymerization, or diffuse more rapidly than monomer.

To address the limitations of previous reductive electropolymerizations we propose that indirect electrocatalysis could provide a chain-growth polymerization. This method uses a mediator, which is reduced or oxidized at the electrode, and then reduces or oxidizes a substrate, returning to a neutral state. Using a mediator enables the reaction to proceed at a lower potential than is needed to directly reduce the reactant, and to occur in the bulk solution as well as at the electrode. Wan and coworkers recently published indirect electrocatalyzed cross-couplings of aryl halides and pyrroles.⁶² In this case, an organic perylene diimide (PDI) compound was used as the mediator. The PDI is reduced at a working electrode, and it in turn reduces the phenyl halide to a radical anion, which undergoes halide cleavage to produce a radical species that forms a new bond to pyrrole. This synthetic method is intriguing for controlled polymerizations, because the extended π -system of a polymer could lead to a less negative reduction potential compared to

monomer (proposed polymerization in Scheme 1.5). Therefore, after an initiation step, a polymerization could be conducted at a constant potential targeting selective reduction of polymer rather than monomer, such that initiated polymer chains would continuously grow, leading to a chain-growth process.⁶³ Chapter 4 describes efforts to develop single-electron methods for synthesizing conjugated polymers, exploring both $S_{RN}1$ reactions and electrocatalysis.

Scheme 1.5. Proposed indirect electrocatalytic polymerization



Overall, this thesis details our efforts to address the limitations of slow initiation in CTP and monomer scope in chain-growth methods for conjugated polymer synthesis. It describes our efforts to selectively enhance initiation rates through precatalyst design, as well as the insight this work gave into model systems and rate effects in phenylene polymerization. We further discuss our efforts to expand the monomer scope of CTP to phenylene-ethynylene, and the limitations learned about small-molecule systems as catalyst screening tools. Finally, it discusses our efforts to move beyond CTP to single-electron mechanisms to polymerize electron-deficient monomers. The discoveries we made about reactive ligand and additive rate effects will improve precatalyst development in CTP. The limitations we identified of small-molecule screens leads to more accurate models to discover new catalysts. Lastly, we have discovered a promising new method

for synthesizing electron-deficient conjugated polymers which could lead to chain-growth polymerizations.

References

(1) Recent reviews: (a) Dou, L.; You, J.; Hong, Z.; Xu, Z.; Li, G.; Street, R.A.; Yang, Y. 25th Anniversary Article: A Decade of Organic/Polymeric Photovoltaic Research *Adv. Mater.* **2013**, *25*, 6642–6671. (b) Zhang, S.; Ye, L.; Jianhui Hou, J. Breaking the 10% Efficiency Barrier in Organic Photovoltaics: Morphology and Device Optimization of Well-Known PBDTTT Polymers *Adv. Energy Mater.* **2016**, *6*, 1502529. (c) Ostroverkhova, O. Organic Optoelectronic Materials: Mechanisms and Applications *Chem. Rev.* **2016**, *116*, 13279–13412.

(2) (a) Cai, M.; Xichang Bao, X.; Wang, X.; Zhang, H.; Qiu, M.; Yang, R.; Yang, C.; Wan, X. From Isoindigo to Dibenzonaphthyridinedione: A Building Block for Wide-Bandgap Conjugated Polymers with High Power Conversion Efficiency *Chem. Mater.* **2016**, *28*, 6196–6206. (b) Liuyuan, L.; Zhiming, C.; Qin, H.; Lei, Y.; Rui, Z.; Feng, L.; Thomas P., R.; Fei, H.; Yong, C. High-Performance Polymer Solar Cells Based on a Wide-Bandgap Polymer Containing Pyrrolo[3,4-f]benzotriazole-5,7-dione with a Power Conversion Efficiency of 8.63% *Adv. Sci.* **2016**, *3*, 1600032. (c) Lin, Y.; Zhao, F.; He, Q.; Huo, L.; Wu, Y.; Parker, T.C.; Ma, W.; Sun, Y.; Wang, C.; Zhu, D.; Heeger, A. J.; Marder, S. R.; Zhan, X. High-Performance Electron Acceptor with Thienyl Side Chains for Organic Photovoltaics *J. Am. Chem. Soc.* **2016**, *138*, 4955–4961.

(3) (a) Li, W.; Yang, L.; Tumbleston, J. R.; Yan, L.; Ade, H.; You, W. “Controlling Molecular Weight of a High Efficiency Donor-Acceptor Conjugated Polymer and Understanding Its Significant Impact on Photovoltaic Properties” *Adv. Mater.* **2014**, *26*, 4456–4462. (b) Liu, C.; Wang, K.; Hu, X.; Yang, Y.; Hsu, C. H.; Zhang, W.; Xiao, S.; Gong, X.; Cao, Y. “Molecular Weight Effect on the Efficiency of Polymer Solar Cells” *ACS Appl. Mater. Interfaces* **2013**, *5*, 12163–12167. (c) Chu, T.-Y.; Lu, J.; Beaupré, S.; Zhang, Y.; Pouliot, J.-R.; Zhou, J.; Najari, A.; Leclerc, M.; Tao, Y. “Effects of the Molecular Weight and the Side-Chain Length on the Photovoltaic Performance of Dithienosilole/Thienopyrrolodione Copolymers” *Adv. Funct. Mater.* **2012**, *22*, 2345–2351. (d) Schilinsky, P.; Asawapirom, U.; Scherf, U.; Biele, M.; Brabec, C. “Influence of the Molecular Weight of Poly(3-hexylthiophene) on the Performance of Bulk Heterojunction Solar Cells” *Chem. Mater.* **2005**, *17*, 2175–2180.

(4) (a) Lu, L.; Zheng, T.; Xu, T.; Zhao, D.; Yu, L. Mechanistic Studies of Effect of Dispersity on the Photovoltaic Performance of PTB7 Polymer Solar Cells *Chem. Mater.* **2015**, *27*, 537–543. (b) Meager, I.; Ashraf, R.S.; Nielsen, C.B.; Donaghey, J.E.; Huang, Z.; Bronstein, H.; Durrant, J. R.; McCulloch, I. Power conversion efficiency enhancement in diketopyrrolopyrrole based solar cells through polymer fractionation *J. Mater. Chem. C.* **2014**, *2*, 8593–8598.

- (5) (a) Guo, X.; Baumgarten, M. Müllen, K. Designing π -Conjugated Polymers for Organic Electronics *Progress in Polymer Science* **2013**, *38*, 1832–1908. (b) Katsouras, A.; Gasparini, N.; Koulogiannis, C.; Spanos, M.; Ameri, T.; Brabec, C.J.; Chochos, C.L.; Avgeropoulos, A. Systematic Analysis of Polymer Molecular Weight Influence on the Organic Photovoltaic Performance *Macromol. Rapid Commun.* **2015**, *36*, 1778–1797.
- (6) Shirakawa, H.; Louis, E.J.; MacDiarmid, A.G.; Chiang, C.K.; Heeger, A.J. Synthesis of Electrically Conducting Organic Polymers: Halogen Derivatives of Polyacetylene, $(\text{CH})_x$ *J.C.S. Chem. Comm.* **1977** 578–580.
- (7) Malhotra, B.D.; Kumar, N.; Chandra, S. Recent Studies of Heterocyclic and Aromatic Conducting Polymers *Prog. Polym. Sci.* **1986**, *12*, 179–218.
- (8) Babudri, F.; Farinola, G.M.; Naso, F. Synthesis of Conjugated Oligomers and Polymers: the Organometallic Way *J. Mater. Chem.*, **2004**, *14*, 11–34.
- (9) Yokoyama, A.; Miyakoshi, R.; Yokozawa, T. Chain-Growth Polymerization for Poly(3-hexylthiophene) with a Defined Molecular Weight and a Low Polydispersity *Macromolecules*, **2004**, *37*, 1169–1171.
- (10) Sheina, E.E.; Liu, J.; Iovu, M.C.; Laird, D.W.; McCullough, R.D Chain Growth Mechanism for Regioregular Nickel-Initiated Cross-Coupling Polymerizations *Macromolecules* **2004**, *37*, 3526–3528.
- (11) Miyakoshi, R.; Shimono, K.; Yokoyama, A.; Yokozawa, T. Catalyst-Transfer Polycondensation for the Synthesis of Poly(p-phenylene) with Controlled Molecular Weight and Low Polydispersity *J. Am. Chem. Soc.* **2006**, *128*, 16012–16013.
- (12) Yokoyama, A.; Suzuki, H.; Kubota, Y.; Ohuchi, K.; Higashimura, H.; Yokozawa, T. Chain-Growth Polymerization for the Synthesis of Polyfluorene via Suzuki–Miyaura Coupling Reaction from an Externally Added Initiator Unit *J. Am. Chem. Soc.* **2007**, *129*, 7236–7237.
- (13) Sui, A.; Shi, X.; Wu, S.; Tian, H.; Geng, Y.; Wang, F. Controlled Synthesis of Polyfluorenes via Kumada Catalyst Transfer Polycondensation with Ni(acac)₂/dppp as the Catalyst *Macromolecules* **2012**, *45*, 5436–5443.
- (14) Pammer, F.; Jager, J.; Rudolf, B.; Sun, Y. Soluble Head-to-Tail Regioregular Polythiazoles: Preparation, Properties and Evidence for Chain-Growth Behaviour in the Synthesis via Kumada-Coupling Polycondensation *Macromolecules* **2014**, *47*, 5904–5912.
- (14) Smith, M.L.; Leone, A.K.; Zimmerman, P.M.; McNeil, A.J. Impact of Preferential π -Binding in Catalyst-Transfer Polycondensation of Thiazole Derivatives *ACS Macro Lett.* **2016**, *5*, 1411–1415.

- (16) Yokoyama, A.; Kato, A.; Miyakoshi, R.; Yokozawa, T. Precision Synthesis of Poly(N-hexylpyrrole) and Its Diblock Copolymer with Poly(p-phenylene) via Catalyst-Transfer Polycondensation *Macromolecules* **2008**, *41*, 7271–7273.
- (17) Nanashima, Y.; Yokoyama, A.; Yokozawa, T. Synthesis of novel blue-light-emitting polypyridine *J. Polym. Sci. A Polym. Chem.* **2012**, *50*, 1054–1061.
- (18) Bridges, C.R.; Yan, H.; Pollit, A.A.; Seferos, D.S. Controlled Synthesis of Fully π -Conjugated Donor–Acceptor Block Copolymers Using a Ni(II) Diimine Catalyst *ACS Macro Lett.* **2014**, *3*, 671–674.
- (19) Magurudeniya, H. D.; Sista, P.; Westbrook, J. K.; Ourso, T. E.; Nguyen, K.; Maher, M. C.; Alemseghed, M. G.; Biewer, M. C.; Stefan, M. C. Nickel(II) α -Diimine Catalyst for Grignard Metathesis (GRIM) Polymerization *Macromol. Rapid Commun.* **2011**, *32*, 1748–1752.
- (20) For Ni-NHCs: (a) Tamba, S.; Shono, K.; Sugie, A.; Mori, A. C–H Functionalization Polycondensation of Chlorothiophenes in the Presence of Nickel Catalyst with Stoichiometric or Catalytically Generated Magnesium Amide *J. Am. Chem. Soc.* **2011**, *133*, 9700–9700. (b) Qiu, Y.; Worch, J.C.; Fortney, A.; Gayathri, C.; Gil, R.R.; Noonan, K.J.T Nickel-Catalyzed Suzuki Polycondensation for Controlled Synthesis of Ester-Functionalized Conjugated Polymers *Macromolecules* **2016**, *49*, 4757–4762. (c) For Pd-NHCs: Bryan, Z.J.; Smith, M.L.; McNeil, A.J Chain-Growth Polymerization of Aryl Grignards Initiated by a Stabilized NHC-Pd Precatalyst *Macromol Rapid Commun.* **2012**, *33*, 842–847.
- (21) Zhang, H.H.; Xing, C.H.; Hu, Q.S. Controlled Pd(0)/t-Bu₃P-Catalyzed Suzuki Cross-Coupling Polymerization of AB-Type Monomers with PhPd(t-Bu₃P)I or Pd₂(dba)₃/t-Bu₃P/ArI as the Initiator *J. Am. Chem. Soc.* **2012**, *134*, 13156–13159.
- (22) Verswyvel, M.; Steverlynck, J.; Mohamed, S.H.; Trabelsi, M.; Champagne, B.; Koeckelberghs, G. All-Conjugated ABC-block-copolymer Formation with a Varying Sequence via an Unassociated Catalyst *Macromolecules* **2014**, *47*, 4668–4675.
- (23) Willot, P.; Steverlynck, J.; Moerman, D.; Leclere, P.; Lazzaroni, R.; Koeckelberghs, G. Poly(3-alkylthiophene) with Tuneable Regioregularity: Synthesis and Self-Assembling Properties *Polym. Chem.* **2013**, *4*, 2662–2671.
- (24) Hardeman, T.; Koeckelberghs, G. The Synthesis of Poly(thiophene-co-fluorene) Gradient Copolymers *Macromolecules* **2015**, *48*, 6987–6993.
- (25) Sui, A.; Shi, X.; Tian, H.; Geng, Y.; Wang, F. Suzuki–Miyaura Catalyst-Transfer Polycondensation with Pd(IPr)(OAc)₂ as the Catalyst for the Controlled Synthesis of Polyfluorenes and Polythiophenes *Polym. Chem.* **2014**, *5*, 7072–7080.

- (26) Yokozawa, T.; Kohno, H.; Yoshihiro, O.; Yokoyama, A. Catalyst-Transfer Suzuki–Miyaura Coupling Polymerization for Precision Synthesis of Poly(p-phenylene) *Macromolecules* **2010**, *43*, 7095–7100.
- (27) Elmalem, E.; Kiriya, A.; Huck, W.T.S. Chain-Growth Suzuki Polymerization of n-Type Fluorene Copolymers *Macromolecules* **2011**, *44*, 9057–9061.
- (28) Qiu, Y.; Mohin, J.; Tsai, C.H.; Tristram-Nagle, S.; Gil, R.R.; Kowalewski, T.; Noonan, K.J.T. Stille Catalyst-Transfer Polycondensation Using Pd-PEPPSI-IPr for High-Molecular-Weight Regioregular Poly(3-hexylthiophene) *Macromol. Rapid Commun.* **2015**, *36*, 840–844.
- (29) Fuji, K.; Tamba, S.; Shono, K.; Sugie, A.; Mori, A. Murahashi Coupling Polymerization: Nickel(II)–N-Heterocyclic Carbene Complex-Catalyzed Polycondensation of Organolithium Species of (Hetero)arenes *J. Am. Chem. Soc.* **2013**, *135*, 12208–12211.
- (30) Suraru, S.L.; Lee, J.A.; Luscombe, C.K. Preparation of an Arylated Alkylthiophene Monomer via C–H Activation for Use in Pd-PEPPSI-iPr Catalyzed-Controlled Chain Growth Polymerization *ACS Macro Lett.* **2016**, *5*, 533–536.
- (31) (a) Iovu, M.C.; Sheina, E.E.; Gil, R.R.; McCullough, R.D. Experimental Evidence for the Quasi-“Living” Nature of the Grignard Metathesis Method for the Synthesis of Regioregular Poly(3-alkylthiophenes) *Macromolecules* **2005**, *38*, 8649–8656. (b) Wu, P.T.; Ren, G.; Li, C.; Mezzenga, R.; Jenekhe, S.A. Crystalline Diblock Conjugated Copolymers: Synthesis, Self-Assembly, and Microphase Separation of Poly(3-butylthiophene)-b-poly(3-octylthiophene) *Macromolecules* **2009**, *42*, 2317–2320. (c) Zhang, Y.; Tajima, K.; Hirota, K.; Hashimoto, K. Synthesis of All-Conjugated Diblock Copolymers by Quasi-Living Polymerization and Observation of Their Microphase Separation *J. Am. Chem. Soc.* **2008**, *130*, 7812–7813. (d) Van den Bergh, K.; Huybrechts, J.; Verbiest, T.; Koeckelberghs, G. Transfer of Supramolecular Chirality in Block Copoly(thiophene)s *Chem. Eur. J.* **2008**, *14*, 9122–9125. (e) Chan, S.H.; Lai, C.S.; Chen, H.L.; Ting, C.; Chen, C.P. Highly Efficient P3HT: C60 Solar Cell Free of Annealing Process *Macromolecules* **2011**, *44*, 8886–8891. (f) Ouhib, F.; Khoukh, A.; Ledeuil, J.B.; Martinez, H.; Desbrieres, J.; Lartigau, C.D. Diblock and Random Donor/Acceptor “Double Cable” Polythiophene Copolymers via the GRIM Method *Macromolecules* **2008**, *41*, 9736–9743. (g) Ouhib, F.; Hiorns, R.C.; de Bettignies, R.; Bailly, S.; Desbrieres, J.; Lartigau, C.D. Photovoltaic Cells Based on Polythiophenes Carrying Lateral Phenyl Groups *Thin Solid Film* **2008**, *516*, 7199–7204. (h) Clément, S.; Meyer, F.; De Winter, J.; Coulembier, O.; Vande Velde, C. M. L.; Zeller, M.; Gerbaux, P.; Balandier, J.Y.; Sergeev, S.; Lazzaroni, R.; Geerts, Y.; Dubois, P. Synthesis and Supramolecular Organization of Regioregular Polythiophene Block Oligomers *J. Org. Chem.* **2010**, *75*, 1561–1568. (i) Verswyvel, M.; Goossens, K.; Koeckelberghs, G. Amphiphilic chiral block-poly(thiophene)s: tuning the blocks *Polym. Chem.* **2013**, *4*, 5310–5320. (j) Wu, P.-T.; Ren, G.; Kim, F. S.; Li, C.; Mezzenga, R.; Jenekhe, S. A. Poly(3-hexylthiophene)-b-Poly(3-cyclohexylthiophene): Synthesis, Microphase Separation, Thin Film Transistors, and

Photovoltaic Applications *J. Polym. Sci. A Polym. Chem.* **2010**, *48*, 614–626. (j) Ho, C.C.; Liu, Y.C.; Lin, S.H.; Su, W.F. Synthesis, Morphology, and Optical and Electrochemical Properties of Poly(3-hexylthiophene)-b-poly(3-thiophene hexylacetate) *Macromolecules* **2012**, *45*, 813–820. (k) Benanti, T.L.; Kalaydjian, A.; Venkataraman, D. Protocols for Efficient Postpolymerization Functionalization of Regioregular Polythiophenes *Macromolecules* **2008**, *41*, 8312–8315. (l) Ohshimizu, K.; Ueda, M. Well-Controlled Synthesis of Block Copolythiophenes *Macromolecules* **2008**, *41*, 5289–5294. (m) Higashihara, T.; Ohshimizu, K.; Ryo, Y.; Sakurai, T.; Takahashi, A.; Nojima, S.; Ree, M.; Ueda, M. Synthesis and Characterization of Block Copolythiophene with Hexyl and Triethylene Glycol Side Chains *Polymer* **2011**, *52*, 3687–3695. (n) Kozyccz, L.M.; Gao, D.; Hollinger, J.; Seferos, D.S. Donor–Donor Block Copolymers for Ternary Organic Solar Cells *Macromolecules*, **2012**, *45*, 5823–5832. (o) Miyakoshi, R.; Yokoyama, A.; Yokozawa, T. Importance of the Order of Successive Catalyst-transfer Condensation Polymerization in the Synthesis of Block Copolymers of Polythiophene and Poly(p-phenylene) *Chemistry Letters* **2008**, *37*, 1022–1023. (p) Wu, S.; Bu, L.; Huang, L.; Yu, X.; Han, Y.; Geng, Y.; Wang, F. Synthesis and characterization of phenylene-thiophene all-conjugated diblock copolymers *Polymer* **2009**, *50*, 6245–6251. (q) Javier, A.E.; Varshney, S.R.; McCullough, R.D. Chain-Growth Synthesis of Polyfluorenes with Low Polydispersities, Block Copolymers of Fluorene, and End-Capped Polyfluorenes: Toward New Optoelectronic Materials *Macromolecules* **2010**, *43*, 3233–3237. (r) Palermo, E.F.; McNeil, A.J. Impact of Copolymer Sequence on Solid-State Properties for Random, Gradient and Block Copolymers containing Thiophene and Selenophene *Macromolecules*, **2012**, *45*, 5948–5955. (s) Hollinger, J.; DiCarmine, P.M.; Karl, D.; Seferos, D.S. Heterocycle-Induced Phase Separation in Conjugated Polymers *Macromolecules* **2012**, *45*, 3772–3778.

(32) Locke, J. R.; McNeil, A. J. Syntheses of Gradient π -Conjugated Copolymers of Thiophene *Macromolecules* **2010**, *43*, 8709–8710.

(33) Palermo, E.F.; van der Laan, H.L.; McNeil, A.J. Impact of π -Conjugated Gradient Sequence Copolymers on Polymer Blend Morphology *Polym. Chem.* **2013**, *4*, 4606–4611.

(34) (a) Ono, R.J.; Kang, S.; Bielawski, C.W. Controlled Chain-Growth Kumada Catalyst Transfer Polycondensation of a Conjugated Alternating Copolymer *Macromolecules* **2012**, *45*, 2321–2326. (b) Todd, A.D.; Bielawski, C.W. Controlled Synthesis of an Alternating Donor–Acceptor Conjugated Polymer via Kumada Catalyst-Transfer Polycondensation *ACS Macro Lett.* **2015**, *4*, 1254–1258. (c) Bronstein, H.; Hurhangee, M.; Collado-Fregoso, E.; Beatrup, D.; Soon, Y. W.; Huang, Z.; Hadipour, A.; Tuladhar, P.S.; Rossbauer, S.; Sohn, E.H.; Shoaee, S.; Dimitrov, S.D.; Frost, J.M.; Ashraf, R.S.; Kirchartz, T.; Watkins, S.E.; Song, K.; Anthopoulos, T.; Nelson, J.; Rand, B. P.; Durrant, J.R.; McCulloch, I. Isostructural, Deeper Highest Occupied Molecular Orbital Analogues of Poly(3-hexylthiophene) for High-Open Circuit Voltage Organic Solar Cells *Chem. Mater.* **2013**, *25*, 4239–4249. (d) Tsai, C.H.; Fortney, A.; Qiu, Y.; Gil, R.R.; Yaron, D.; Kowalewski, T.; Noonan, K. J. T. Conjugated Polymers with Repeated Sequences of Group 16 Heterocycles Synthesized through Catalyst-Transfer Polycondensation *J. Am.*

Chem. Soc. 2016, 138, 6798–6804. (e) Qiu, Y.; Fortney, A.; Tsai, C.H.; Baker, M.A.; Gil, R.R.; Kowalewski, T.; Noonan, K. J. T. Synthesis of Polyfuran and Thiophene-Furan Alternating Copolymers Using Catalyst-Transfer Polycondensation *ACS Macro Lett.* 2016, 138, 332–336.

(35) Palermo, E. F.; Darling, S. B.; McNeil, A. J. π -Conjugated Gradient Copolymers Suppress Phase Separation and Improve Stability in Bulk Heterojunction Solar Cells *J. Mater. Chem. C* **2014**, 2, 3401–3406.

(36) Bryan, Z. J.; McNeil, A. J. Evidence for a Preferential Intramolecular Oxidative Addition in Ni-catalyzed Cross-Coupling Reactions and Their Impact on Chain-Growth Polymerizations *Chem. Sci.* **2013**, 4, 1620–1624.

(37) Willot, P.; Koeckelberghs, G. Evidence for Catalyst Association in the Catalyst Transfer Polymerization of Thieno[3,2-b]thiophene *Macromolecules* **2014**, 47, 8548–8555.

(38) Lanni, E. L.; McNeil, A. J. Evidence for Ligand-Dependent Mechanistic Changes in Nickel-Catalyzed Chain-Growth Polymerizations *Macromolecules* **2010**, 43, 8039–8044.

(39) Lee, S. R.; Bryan, Z. J.; Wagner, A. M.; McNeil, A. J. Effect of ligand electronic properties on precatalyst initiation and propagation in Ni-catalyzed cross-coupling polymerizations *Chem. Sci.* **2012**, 3, 1562–1566.

(40) Bronstein, H.A.; Luscombe, C.K. Externally Initiated Regioregular P3HT with Controlled Molecular Weight and Narrow Polydispersity *J. Am. Chem. Soc.* **2009**, 131, 12894–12895.

(41) Van den Bergh, K.; Willot, P.; Cornelis, D.; Verbiest, T.; Koeckelberghs, G. Influence of the Presence and Length of an Alkyl Spacer on the Supramolecular Chirality of Block Copoly(thiophene)s *Macromolecules* **2011**, 44, 728–735.

(42) Smeets, A.; Van den Bergh, K.; De Winter, J.; Gerbaux, P.; Verbiest, T.; Koeckelberghs, G. Incorporation of Different End Groups in Conjugated Polymers Using Functional Nickel Initiators *Macromolecules* **2009**, 42, 7638–7641.

(43) Smeets, A.; Willot, P.; De Winter, J.; Gerbaux, P.; Verbiest, T.; Koeckelberghs, G. End Group-Functionalization and Synthesis of Block-Copolythiophenes by Modified Nickel Initiators *Macromolecules* **2011**, 44, 6017–6025.

(44) Sanchez, I.C. Irreversible Anionic Polymerization Kinetics Revisited *Ind. Eng. Chem. Res.* **2010**, 49, 11890–11895

(45) Lee, S. R.; Bloom, J. W. G.; Wheeler, S. E.; McNeil, A.J. Accelerating Ni(II) Precatalyst Initiation Using Reactive Ligands and its Impact on Chain-Growth Polymerizations *Dalton Trans.* **2013**, 42, 4218–4222.

- (46) Larrosa, I.; Somoza, C.; Banquy, A.; Goldup, S.M. Two Flavors of PEPPSI-IPr: Activation and Diffusion Control in a Single NHC-Ligated Pd Catalyst? *Org. Lett.* **2011**, *13*, 146–149.
- (47) Nanashima, Y.; Yokoyama, A.; Yokozawa, T. Synthesis of Well-Defined Poly(2-alkoxypyridine-3,5-diyl) via Ni-Catalyst-Transfer Condensation Polymerization *Macromolecules* **2012**, *45*, 2609–2613.
- (48) Qiu, Y.; Worch, J.C.; Fortney, A.; Gayathri, C.; Gil, R.R.; Noonan, K.J.T. Nickel-Catalyzed Suzuki Polycondensation for Controlled Synthesis of Ester-Functionalized Conjugated Polymers *Macromolecules* **2016**, *49*, 4757–4762.
- (49) Grimsdale, A.C.; Chan, K.L.; Martin, R.E.; Jokisz, P.G.; Holmes, A.B. Synthesis of Light-Emitting Conjugated Polymers for Applications in Electroluminescent Devices *Chem. Rev.* **2009**, *109*, 897–1091.
- (50) Zhu, L.; Wang, M.; Li, B.; Jiang, C.; Li, Q. High Efficiency Organic Photovoltaic Devices Based on Isoindigo Conjugated Polymers with a Thieno[3,2-b]thiophene π -Bridge *J. Mater. Chem. A* **2016**, *4*, 16064–16072.
- (51) Cowie, J.M.G.; Arrighi, V. *Polymers: Chemistry and Physics of Modern Materials*; CRC Press, Taylor & Francis Group: Boca Raton, FL, 2008.
- (52) Murarka, S.; Mobus, J.; Erker, G.; Muck-Lichtenfeld, C.; Studer, A. TEMPO-Mediated Homocoupling of Aryl Grignard Reagents: Mechanistic Studies *Org. Biomol. Chem.* **2015**, *13*, 2762–2767.
- (53) Murarka, S.; Studer, A. Radical/Anionic $S_{RN}1$ -Type Polymerization for Preparation of Oligoarenes *Angew. Chem. Int. Ed.* **2012**, *51*, 12362–12366.
- (54) Heine, N. B.; Studer, A. Poly(paraphenylene sulfide) and Poly(metaphenylene sulfide) via Light-Initiated $S_{RN}1$ -Type Polymerization of Halogenated Thiophenols *Macromol. Rapid Commun.* **2016**, *37*, 1494–1498.
- (55) Senkovskyy, V.; Tkachov, R.; Komber, H.; Sommer, M.; Heuken, M.; Voit, B.; Huck, W. T. S.; Kataev, V.; Petr, A.; Kiriya, A. Chain-Growth Polymerization of Unusual Anion-Radical Monomers Based on Naphthalene Diimide: A New Route to Well-Defined n-Type Conjugated Copolymers *J. Am. Chem. Soc.* **2011**, *133*, 19966–19970.
- (56) Tourillon, G.; Garnier, F. New Electrochemically Generated Organic Conducting Polymers *J. Electroanal Chem.* **1982**, *135*, 173–178.
- (57) Lazzaroni, R.; De Pryck, A.; Debaisieux, C.; Riga, J.; Verbist, J. Electronic Structure of Conducting Polymers from Heteroaromatic Bicyclic Compounds *Synth. Met.* **1987**, *21*, 189–195.

- (58) Danieli, R.; Taliani, C.; Zamboni, R. Optical, Electrical and Electrochemical Characterization of Electrosynthesized Polythieno(3,2-b)thiophene *Synth. Met.* **1986**, *13*, 325–328.
- (59) Diaz, A.F.; Kanazawa, K.K.; Gardini, G.P. Electrochemical Polymerization of Pyrrole *J. Chem. Soc., Chem. Commun.* **1979**, *14*, 635–636.
- (60) Ohsaka, T.; Ohnuki, Y.; Oyama, N. IR Absorption Spectroscopic Identification of Electroactive and Electroinactive Polyaniline Films Prepared by the Electrochemical Polymerization of Aniline *J. Electroanal Chem.* **1984**, *161*, 399–405.
- (61) Xu, Z.; Horowitz, G.; Garnier, F. Cathodic Electropolymerization of Polythiophene on Platinum and Various Semiconducting Electrodes. *J. Electroanal Chem.* **1988**, *246*, 467–472.
- (62) Sun, G.; Ren, S.; Zhu, X.; Huang, M.; Wan, Y. Direct Arylation of Pyrroles via Indirect Electroreductive C–H Functionalization Using Perylene Bisimide as an Electron-Transfer Mediator *Org. Lett.* **2016**, *18*, 544–547.
- (63) Yokoyama, A.; Yokozawa, T. Converting Step-Growth to Chain-Growth Condensation Polymerization *Macromolecules* **2007**, *40*, 4093–4101.

Chapter 2

Reactive Ligand Influence on Initiation in Phenylene Catalyst-Transfer Polymerization¹

INTRODUCTION

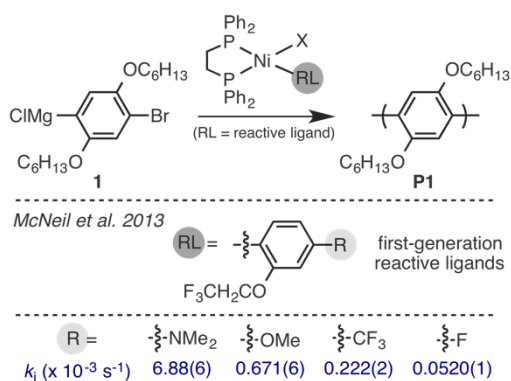
Catalyst-transfer polymerization (CTP) is a chain-growth method for synthesizing π -conjugated polymers with control over both the polymer length and sequence.^{1,2} Though limited in scope, these methods have substantially impacted the field by enabling unprecedented access to materials such as gradient sequence copolymers³ and a cyclic polymer.⁴ Nevertheless, many challenges remain, including broadening the scope to include electron-deficient monomers, narrowing the polymer dispersities, and reducing the air- and moisture-sensitivities of the reagents. Broad dispersities in a chain-growth polymerization reflect underlying problems, including chain-transfer and chain-termination pathways, as well as slow initiation.

Conventional CTP catalyst design has largely focused on the ancillary ligand and metal identity.^{2a} In contrast, the mechanistic impact of reactive ligands has remained largely unexplored.⁵ Most studies focus on altering the reactive ligand for other purposes, such as growing polymers off surfaces⁶ and synthesizing block⁷ or cyclic polymers.⁴ We recently demonstrated that reactive ligands substantially impact the precatalyst initiation rate in phenylene CTP (Scheme 2.1).⁵ For example, the initiation rate was 132-fold faster with a *para*-dimethylaminobenzene as the reactive ligand compared to the otherwise analogous *para*-fluorobenzene. To rationalize these results, the initiation rates were evaluated computationally, wherein a correlation between the activation barrier for reductive elimination was found with the change in charge on the reactive ligands (as

¹ Reproduced with permission from Hall, A. O., Lee, S. R., Bootsma, A. N., Bloom, J. W. G., Wheeler, S. E. and McNeil, A. J. Reactive Ligand Influence on Initiation in Phenylene Catalyst-Transfer Polymerization. *J. Polym. Sci. Part A: Polym. Chem.* **2017**, 1530–1535.

computed by Natural Population Analysis) en route to the rate-limiting transition state. Although the theoretical model identified potential reactive ligands with higher reactivity, their functional groups were incompatible with the Grignard-based polymerization (e.g., NO₂). As a consequence, we describe herein a second and third generation of reactive ligands and their initiation rates. At the same time, we report an improved method for measuring initiation rates using in situ infrared (IR) spectroscopy.

Scheme 2.1. First-generation reactive ligands for phenylene polymerization.^{5,1}



Herein, we describe how this combined theoretical/experimental approach led to a new, fast-initiating precatalyst for CTP of monomer **1**. We anticipated that this precatalyst would lead to polymer samples with narrower dispersities (\mathcal{D}) because most polymer chains would initiate before any significant propagation occurred. Instead, the dispersities were on par with commonly utilized precatalysts (e.g., (dppe)NiCl₂ where dppe is 1,2-bis(diphenylphosphino)ethane).⁸ End-groups analysis revealed similar ratios of living/non-living chains, which suggests that other factors (e.g., chain-transfer) are currently more significant contributors to the dispersity. Last, we found that small differences between the original model system and the authentic polymerization conditions led to significantly different initiation rates. Combined, these studies provide useful insight into the effect of reactive ligands on initiation, many of which should be generalizable to CTP of other monomers.

EXPERIMENTAL

Synthesis of Precatalyst **2f**

In the glovebox, Ni(cod)₂ (138 mg, 0.502 mmol, 1.0 equiv), and triphenyl phosphine (Ph₃P) (262 mg, 1.00 mmol, 2.0 equiv) were dissolved in THF (3 mL) in a 20 mL vial with stirring. In a separate 4 mL vial, 1-chloro-2-methoxy-4-phenyl-benzene (142 mg, 0.650 mmol, 1.3 equiv) was dissolved in THF (2 mL). This solution was then added to the vial containing the Ni/Ph₃P and stirred at rt for 4 h, during which time a yellow precipitate formed. The solvent was removed under vacuum until approx. 0.5 mL remained. Hexanes (approx. 15 mL) were then added, and the yellow precipitate was collected by vacuum filtration, giving 157 mg (79% yield). In a 20 mL vial, the isolated yellow powder (157 mg, 0.196 mmol, 1.0 equiv) and 1,2-bis(diphenylphosphino)ethane (94 mg, 0.24 mmol, 1.2 equiv) were dissolved in THF (2.5 mL) and stirred at rt for 1 h. (Note: A yellow precipitate was observed after 5 min.) After 1 h, hexanes (approx. 15 mL) were added, and the solution was placed in a -30 °C freezer overnight. The product was collected by vacuum filtration, giving 100 mg of **2f** as a yellow powder (59% yield). ¹H NMR (500 MHz, CD₂Cl₂) δ 8.41 (br, 2H) 8.27 (at, *J* = 9.0 Hz, 2H), 7.71 (at, *J* = 8.5 Hz, 2H), 7.61–7.40 (m, 11H), 7.34 (at, *J* = 7.5 Hz, 2H), 7.27–7.22 (m, 2H), 7.17 (at, *J* = 7.0 Hz, 2H), 7.07 (at, *J* = 6.6, 2 H) 6.85 (at, *J* = 9.1 Hz, 2H), 6.77 (dt, *J* = 6.1 Hz, 1.5 Hz, 1H), 6.15 (at, *J* = 2.1 Hz, 1 H), 3.37 (s, 3H), 2.39–2.21 (m, 3H), 1.63–1.62 (m, 1H). ³¹P NMR (202 MHz, CD₂Cl₂) δ 59.85 (d, *J* = 27.5 Hz), 38.37 (d, *J* = 27.5 Hz).

Representative Procedure for Generating Monomer **1**

In a glovebox, a 20 mL vial was charged with 1,4-dibromo-2,6-bis(hexyloxy)benzene (1.09 g, 2.50 mmol, 1 equiv) and THF (2.5 mL). Then, isopropylmagnesium chloride (1.7 M in THF, 1.32 mL, 2.25 mmol, 0.9 equiv)⁹ was added and the solution stirred at rt for 19 h. The concentration of **1** was determined by titration with salicylaldehyde phenylhydrazone.¹⁰

General Procedure for Polymerizations Monitored via In Situ IR Spectroscopy

The IR probe was inserted through an O-ring-sealed 14/20 ground-glass adapter (custom-made) into an oven-dried 50 mL 2-neck flask equipped with a stir bar. The other neck was fitted with a three-way flow-control adapter with a septum for injections/aliquot sampling and an N₂ line. The oven-dried flask was cooled under vacuum, then filled with N₂. The flask was re-evacuated and filled for two additional cycles. The flask was charged with THF (6.7 mL) and cooled to 0 °C for 15 min. After recording a background spectrum,

monomer **1** (2.3 mL, 0.44 M in THF, 1.0 equiv) was added by syringe and equilibrated at 0 °C for at least 5 min. Then the precatalyst solution (1.0 mL, 0.015 M, 0.015 equiv) was injected and spectra were recorded every 15 s. To account for mixing and temperature equilibration, spectra recorded in the first 60 s were not analyzed.

Aliquots (approx. 0.5 mL) were taken via syringe and immediately quenched with aq. HCl (approx. 1 mL, 12 M). The resulting solution was then extracted with CH₂Cl₂ (2 x 1.5 mL) (with mild heating if polymer had precipitated), dried over MgSO₄, filtered, and then concentrated. At approximately 80% conversion, the polymerization was poured into aq. HCl (20 mL, 12 M), extracted with CH₂Cl₂ (3 x 25 mL), washed with H₂O (1 x 25 mL), brine (1 x 25 mL), dried over MgSO₄, filtered, and concentrated. The samples (both aliquots and the final reaction mixture) were each dissolved in THF (with heating), and passed through a 0.2 μm poly(tetrafluoroethylene) filter for analysis by gel permeation chromatography (GPC). The monomer conversion versus time data was calculated from the IR spectra using a calibration curve.

General Procedure for Polymerizations Analyzed by MALDI-TOF-MS

In a glovebox, a precatalyst stock solution was made by combining **2f** (11.2 mg, 0.0165 mmol) with THF (3.3 mL) in a 4 mL vial. (Note: For Ni(dppe)Cl₂, a pre-initiation protocol was followed wherein monomer **1** (0.23 mL, 5 equiv) was added to the precatalyst and stirred until homogeneous). The precatalyst solution (3.0 mL, 0.015 mmol, 1 equiv) and THF (3.8 mL) were combined in a 50 mL Schlenk tube, sealed with a Teflon stopper, and then removed from the glovebox and put under N₂ pressure. The solution was cooled to 0 °C for 20 min. Then monomer solution (3.2 mL, 1.0 mmol, 66 equiv) was added. After 30 min, an aliquot was removed by syringe, then quenched with aq. HCl (approx. 1.0 mL, 12 M), extracted with CH₂Cl₂ (2 x 1 mL), dried over MgSO₄, filtered, concentrated, and then analyzed by MALDI-TOF MS analysis (SI). After 4 h, the polymerization was poured in aq. HCl (20 mL, 12 M), extracted with CH₂Cl₂ (3 x 25 mL), washed with water (1 x 25 mL), brine (1 x 25 mL), dried over MgSO₄, filtered, and concentrated. Both the aliquot and the bulk polymerization were analyzed by GPC.

Computational Methods

Computations were performed with the BP86 DFT functional¹¹ paired with the 6-311+G(d) basis set¹² was used for all non-metal atoms and the SDB-cc-pVTZ basis set with the

small core, fully relativistic effective core potential¹³ was used for Ni. All computations were performed using Gaussian09.

RESULTS AND DISCUSSION

Influence of Reactive Ligand Structure on Activation Barriers and Rates

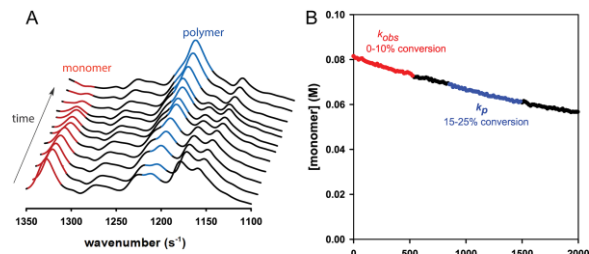
We focused on reactive ligands with a carbon-metal bond (Chart 2.1) because C–C reductive eliminations (i.e., the rate-limiting step) are reported to be faster than the analogous C–Y (where Y = N, O, S) reductive eliminations.¹⁴ In addition, we focused on sp²–sp² reductive eliminations because they are known to be faster than both sp²–sp and sp²–sp³ reductive eliminations.¹⁵ Our theoretical model predicted that alkenyl reactive ligands (e.g., **2a**) would exhibit the lowest barrier (and thus fastest rates) for reductive elimination (Supporting Information, SI). Unfortunately, alkenyl-substituted precatalysts decomposed during synthesis, presumably via disproportionation (SI).¹⁶ A biphenyl-based reactive ligand (**2b**) was prepared based on the rationale that its structural similarity to the polymer would lead to an initiation rate that is similar to propagation. In addition, heteroaryl groups were investigated, including thiophene (**2c**) and benzothiophene (**2d**).

Chart 2.1. Second-generation reactive ligands.¹

$\Delta G_{\text{calc}}^{\ddagger}$ (kcal/mol)	6.5	11.4	11.4	11.9
k_i ($\times 10^{-3} \text{ s}^{-1}$)	n/a	3.1	1.9(6)	1.40(2)

In situ IR spectroscopy was used to measure initiation rates under authentic polymerization conditions using monomer **1** (Figure 2.1A). When precatalyst initiation is slower than propagation, the initiation rate constant (k_i) can be extracted from the overall rate constant (k_{obs}) at low monomer conversions (i.e., 0–10%, equation 1 and SI).¹⁷ This analysis requires accurately measuring the propagation rate constant (k_p), which can be obtained by monitoring monomer consumption rates at later conversions (e.g., 15–25% conversion) or in a separate experiment (Figure 1B and SI). Precatalysts **2b–d** exhibited initiation rate constants (k_i) on par with our previous best precatalyst (c.f., Scheme 2.1).⁵ On the basis of these studies, it appeared that the potentially more reactive precatalysts (e.g., **2a**) are too unstable to isolate while the more stable precatalysts (**2b–d**) cannot initiate faster than propagation ($k_p = 10(2) \times 10^{-3} \text{ s}^{-1}$).

Figure 2.1. (A) Time-dependent in situ IR spectra when polymerizing monomer **1** (0.08 M) with precatalyst **2f** (0.015 M) in THF at 0 °C. (B) Plot of monomer concentration versus time for the same reaction.



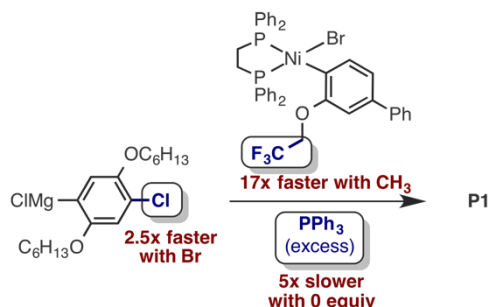
$$k_{\text{obs}} = k_i (e^{-k_i t}) + k_p (1 - e^{-k_i t}) \quad (1)$$

Comparing Initiation Rates Under Authentic Conditions versus the Model System

With the ability to measure initiation rates under the authentic polymerization conditions using in situ IR spectroscopy, the question arose as to whether the original model system (which used ^{19}F NMR spectroscopy) measured the true initiation rates. Second-generation precatalyst **2b** was used as the test case, and it was modified and evaluated in the same manner as the first-generation reactive ligands.⁵ As highlighted in Scheme 2.2, there were three substantial changes made to the authentic system. First, the bromine atom on the monomer was replaced with a chlorine atom, effectively preventing a second catalyst turnover. Isolating just this modification, a 2.5x slower initiation rate was observed.¹⁸ This modest rate difference reflects the minor impact of switching a Cl to a Br on the monomer's charge density during the reductive elimination. Next, the influence of Ph_3P was examined, which was added in the model system to scavenge $\text{Ni}(0)$ generated from the first turnover. These studies revealed a surprising 5x initiation rate enhancement with added Ph_3P .¹⁹ One possible explanation is that a five-coordinate square pyramidal species is generated via Ph_3P coordination prior to or during reductive elimination.²⁰ Five-coordinate metal complexes are known to undergo faster reductive eliminations than their four-coordinate counterparts.¹⁴ Related intermediates have been invoked to explain the accelerating effect of added arenes²¹ and alkenes²² on $\text{Ni}(\text{II})$ - and $\text{Pd}(\text{II})$ -based reductive eliminations. Overall, this Ph_3P -based rate acceleration has broader implications for CTP: For example, it may already be accelerating initiation

with precatalysts that are generated in situ from Ph_3P -based precursors (e.g., $(\text{PPh}_3)_2\text{NiX}_2$ followed by ancillary ligand exchange).²³ Alternatively, adding exogenous Ph_3P may be a simple method to accelerate initiation.¹⁹

Scheme 2.2. Structural differences between the model system (in blue) and the authentic polymerization and their impact on initiation rates (in red).



The final difference was the *ortho*-trifluoroethoxy ($\text{CF}_3\text{CH}_2\text{O}$) substituent, which was added to provide an NMR spectroscopic handle. The relatively short CH_2O linker between the CF_3 tag and the reactive arene was a compromise between minimizing the electronic perturbation of the fluorine on reductive elimination while maximizing the likelihood of observing unique ^{19}F signals for each intermediate in the NMR spectrum. The initiation rates with precatalyst **2e** were >17x slower than precatalyst **2f**, suggesting that the fluorine-based inductive effect on reductive elimination is significant (Chart 2.2). Indeed, our computational model found a lower activation barrier when the CF_3 was removed. Such a large inductive effect is reasonable considering the significant difference in $\text{p}K_a$ values for $\text{CF}_3\text{CH}_2\text{OH}$ (12.5) versus CH_3OH (15.5).²⁴

Chart 2.2. Third-generation reactive ligands.

$\Delta G_{\text{calc}}^\ddagger$ (kcal/mol)	10.4	11.4	12.5
k_i ($\times 10^{-3} \text{ s}^{-1}$)	>10.9(6)	3.1	0.64(03)

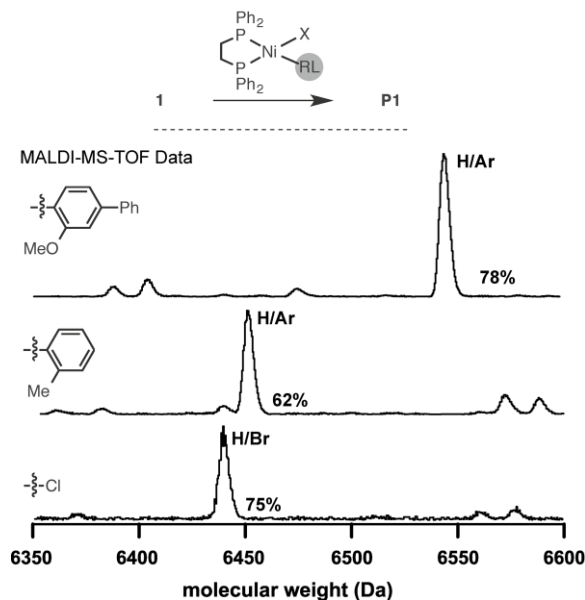
Combined, these studies provide a cautionary tale about model systems: that is, they can become “talking lions”,²⁵ which report only on the model system and do not reflect the authentic system.²⁶ In many cases, including the one described herein, it is only when new methods become available that one can probe the differences between model and authentic systems.

Slow Initiation is Just One Contributor to Broad Dispersities

When comparing the model system versus authentic conditions, we serendipitously discovered that precatalyst **2f** has the fastest initiation rate measured to date. Our computational model supported this experimental result, wherein the precatalyst **2f** exhibited a 1 kcal/mol lower activation barrier than precatalyst **2b**. This result is consistent with our earlier observations⁵ that resonance-based substituents lead to smaller changes in charge on the reactive ligands during reductive elimination, leading to lower activation barriers and faster rates.

Once this fast initiating precatalyst was identified, we anticipated that the resulting polymer samples would exhibit the narrowest dispersities reported for polymer **P1**. Instead, the dispersities for soluble precatalyst **2f** ($\bar{M}_w/\bar{M}_n = 1.45$) were on par with another soluble precatalyst that is widely used ($(dppe)Ni(o\text{-tolyl})Br$, $\bar{M}_w/\bar{M}_n = 1.54$) and commercially available insoluble precatalyst $(dppe)NiCl_2$ ($\bar{M}_w/\bar{M}_n = 1.41$). Importantly, these polymerization results were obtained using the same monomer batch on the same day and were reproducible. The resulting polymers were analyzed by matrix-assisted laser-desorption ionization time-of-flight mass spectrometry (MALDI-TOF-MS) to identify the polymer end-groups (Figure 2.2).²⁷ Regardless of which precatalyst was used,²⁸ the majority of polymer chains exhibited end-groups consistent with a living, chain-growth polymerization. The other polymer chains had undergone unproductive pathways such as early termination or chain-transfer. Combined, these results suggest that the ancillary ligand – dppe – needs to be replaced to achieve lower dispersities. Previous studies suggest that a more electron-rich analogue, such as 1,2-bis(diethylphosphino)ethane (depe), would be better due to its stronger metal-polymer associative complex and/or increased reactivity in the subsequent oxidative addition. In practice, however, these air-unstable Ni precatalysts are more difficult to prepare because their synthesis requires transmetalation with $(depe)NiCl_2$ (rather than ligand exchange from $(PPh_3)_2NiArBr$), leading to challenging purifications to remove both unreacted starting material and multiple by-products.

Figure 2.2. MALDI-TOF-MS data when polymerizing monomer **1** (0.10 M) with various (dppe)Ni(RL)X catalysts (1.5 mM; RL is shown) in THF at 0 °C. The major peak corresponds to polymer **P1** with 23 repeat units.



CONCLUSIONS

Using a combined theoretical and experimental approach, as well as a new method for measuring initiation, a precatalyst with an initiation rate comparable to propagation was discovered. This faster initiating precatalyst contains a reactive ligand (*o*-methoxybiphenyl) that closely resembles the polymer structure. These results suggest that more broadly, one may be able to engineer a faster initiating precatalyst by simply focusing on a reactive ligand that is structurally similar to the polymer. Unexpectedly, the polymer dispersities remained quite broad, suggesting that chain-transfer events (e.g., catalyst dissociation) may be prevalent in these polymerizations. This conclusion is supported by the observed 20% of polymer chains that were nonliving. These unproductive events obscured the impact of slow initiation on the dispersities. Nevertheless, we anticipate that these fast-initiating precatalysts will lead to narrower polymer dispersities in phenylene polymerization when alternative ancillary ligands that provide living conditions are used.

References

- (1) (a) Sheina, E.E.; Liu, J.; Iovu, M.C.; Laird, D.W.; McCullough, R.D. Chain Growth Mechanism for Regioregular Nickel-Initiated Cross-Coupling Polymerizations *Macromolecules* **2004**, *37*, 3526–3528. (b) Yokoyama, A.; Miyakoshi, R.; Yokozawa, T. Chain-Growth Polymerization for Poly(3-hexylthiophene) with a Defined Molecular Weight and a Low Polydispersity *Macromolecules* **2004**, *37*, 1169–1171. (c) Miyakoshi, R.; Yokoyama, A.; Yokozawa, T. Synthesis of Poly(3-hexylthiophene) with a Narrower Polydispersity *Macromol. Rapid Commun.* **2004**, *25*, 1663–1666.
- (2) For recent reviews, see: (a) Leone, A.K.; McNeil, A.J. Matchmaking in Catalyst-Transfer Polycondensation: Optimizing Catalysts based on Mechanistic Insight *Acc. Chem. Res.* DOI: 10.1021/acs.accounts.6b00488. (b) Yokozawa, T.; Ohta, Y. Transformation of Step-Growth Polymerization into Living Chain-Growth Polymerization *Chem. Rev.* **2016**, *116*, 1950–1968. (c) Grisorio, R.; Suranna, G.P. Intramolecular Catalyst Transfer Polymerisation of Conjugated Monomers: from Lessons Learned to Future Challenges *Polym. Chem.* **2015**, *6*, 7781–7795. (d) Bryan, Z.J.; McNeil, A.J. Conjugated Polymer Synthesis via Catalyst-Transfer Polycondensation (CTP): Mechanism, Scope, and Applications *Macromolecules* **2013**, *46*, 8395–8405.
- (3) For recent examples of gradient copolymers, see: (a) Hardeman, T.; Koeckelberghs, G. The Synthesis of Poly(thiophene-co-fluorene) Gradient Copolymers *Macromolecules* **2015**, *48*, 6987–6993. (b) Amonoo, J.A.; Li, A.; Purdum, G.E.; Sykes, M.E.; Huang, B.; Palermo, E.F.; McNeil, A.J.; Shtein, M.; Loo, Y.-L.; Green, P.F. An All-Conjugated Gradient Copolymer Approach for Morphological Control of Polymer Solar Cells *J. Mater. Chem. A* **2015**, *3*, 20174–20184. (c) Palermo, E. F.; Darling, S.B.; McNeil, A. J. π -Conjugated Gradient Copolymers Suppress Phase Separation and Improve Stability in Bulk Heterojunction Solar Cells *J. Mater. Chem. C* **2014**, *2*, 3401–3406. (d) Palermo, E.F.; van der Laan, H.L.; McNeil, A.J. Impact of π -Conjugated Gradient Sequence Copolymers on Polymer Blend Morphology *Polym. Chem.* **2013**, *4*, 4606–4611.
- (4) G. R. McKeown, G.R.; Fang, Y.; Obhi, N.K.; Manion, J.G.; Perepichka, D.F.; Seferos, D.S. Synthesis of Macrocyclic Poly(3-hexylthiophene) and Poly(3-heptylselenophene) by Alkyne Homocoupling *ACS Macro Lett.* **2016**, *5*, 1075–1079.
- (5) Lee, S. R.; Bloom, J. W. G.; Wheeler, S. E.; McNeil, A. J. Accelerating Ni(II) Precatalyst Initiation Using Reactive Ligands and its Impact on Chain-Growth Polymerizations *Dalton Trans.* **2013**, *42*, 4218–4222.
- (6) For a recent example, see: Huddleston, N.E.; Roy, A.; Bilbrey, J.A.; Zhao, Y.; Locklin, J. Functionalization of Reactive End Groups in Surface-Initiated Kumada Catalyst-Transfer Polycondensation *Macromol. Symp.* **2015**, *351*, 27–36.

- (7) For recent examples, see: (a) Smeets, A.; Willot, P.; De Winter, J.; Gerbaux, P.; Verbiest, T.; Koeckelberghs, G. End Group-Functionalization and Synthesis of Block-Copolythiophenes by Modified Nickel Initiators *Macromolecules* **2011**, *44*, 6017–6025. (b) E. Kaul, V. Senkovskyy, R. Tkachov, V. Bocharova, H. Komber, M. Stamm, A. Kiriya, Synthesis of a Bifunctional Initiator for Controlled Kumada Catalyst-Transfer Polycondensation/Nitroxide-Mediated Polymerization and Preparation of Poly(3-hexylthiophene)–Polystyrene Block Copolymer Therefrom *Macromolecules* **2010**, *43*, 77–81.
- (8) (a) Miyakoshi, R.; Shimono, K.; Yokoyama, A.; Yokozawa, T. Catalyst-Transfer Polycondensation for the Synthesis of Poly(p-phenylene) with Controlled Molecular Weight and Low Polydispersity *J. Am. Chem. Soc.* **2006**, *128*, 16012–16013. (b) Lanni, E. L.; McNeil, A. J. Mechanistic Studies on Ni(dppe)Cl₂-Catalyzed Chain-Growth Polymerizations: Evidence for Rate-Determining Reductive Elimination *J. Am. Chem. Soc.* **2009**, *131*, 16573–16579.
- (9) Excess iPrMgCl can terminate polymer chains via reacting with the catalyst during CTP. As a consequence, less than 1 equiv iPrMgCl is typically used.
- (10) Love, B.E.; Jones, E.G. The Use of Salicylaldehyde Phenylhydrazone as an Indicator for the Titration of Organometallic Reagents *J. Org. Chem.* **1990**, *45*, 1924–1930.
- (11) (a) Becke, A.D. Density-Functional Exchange-Energy Approximation with Correct Asymptotic Behavior *Phys. Rev. A* **1988**, *38*, 3098–3100. (b) Perdew, J.P. Density-Functional Approximation for the Correlation Energy of the Inhomogeneous Electron Gas *Phys. Rev. B* **1986**, *33*, 8822–8824.
- (12) (a) Raghavachari, K.; Binkley, J.S.; Seeger, R.; Pople, J.A. Self-Consistent Molecular Orbital Methods. XX. A Basis Set for Correlated Wave Functions *J. Chem. Phys.* **1980**, *72*, 650–654. (b) McLean, A.D.; Chandler, G.S. Contracted Gaussian Basis Sets for Molecular Calculations. I. Second Row Atoms, Z=11–18 *J. Chem. Phys.* **1980**, *72*, 5639–5648. (c) Clark, T.; Chandrasekhar, J.; Spitznagel, G.W.; Schleyer, P.v.R. Efficient Diffuse Function-Augmented Basis Sets for Anion Calculations. III. The 3-21+G Basis Set for First-Row Elements, Li–F *J. Comp. Chem.* **1983**, *4*, 294–301.
- (13) (a) Dolg, M.; Wedig, U.; Stoll, H.; Preuss, H.; Energy-Adjusted ab initio Pseudopotentials for the First Row Transition Elements *J. Chem. Phys.* **1987**, *86*, 866–872. (b) Martin, J.M.L.; Sundermann, A. Correlation Consistent Valence Basis Sets for Use with the Stuttgart–Dresden–Bonn Relativistic Effective Core Potentials: The atoms Ga–Kr and In–Xe *J. Chem. Phys.* **2001**, *114*, 3408–3420.
- (14) J. F. Hartwig, Reductive Elimination. In *Organotransition Metal Chemistry: From Bonding to Catalysis*. University Science Books, Sausalito, CA, 2010, p 321–345.

- (15) Ananikov, V.P.; Musaev, D.G.; Morokuma, K. Theoretical Insight into the C–C Coupling Reactions of the Vinyl, Phenyl, Ethynyl, and Methyl Complexes of Palladium and Platinum *Organometallics* **2005**, *24*, 715–723.
- (16) When the alkene was 2-butene, the crude reaction mixture contained the homodimerization product, consistent with disproportionation (Appendix 1).
- (17) Note that the initiation rate constant (k_i) cannot be obtained using equation 1 when it exceeds the propagation rate constant (k_p).
- (18) Note that the length of the alkyl chains has also changed, from methyl in the model system to hexyl in the polymerization.
- (19) In contrast, the propagation rate constant (k_p) was approx. 25% slower with Ph_3P present.
- (20) (a) Levine, A.M.; Stockland, R.A., Jr; Clark, R.; Guzei, I. Direct Observation of P(O)–C Bond Formation from $(\text{N}\curvearrowright\text{N})\text{PdMe}(\text{P}(\text{O})(\text{OPh})_2)$ Complexes. Rate Enhancement of Reductive Elimination by Addition of Triarylphosphines *Organometallics* **2002**, *21*, 3278–3284. (b) Bertani, R.; Berton, A.; Carturan, G.; Camprostrini, R. Reaction of $\text{Pd}(\eta^3\text{-C}_3\text{H}_5)_2$ with Cyano-Olefins; Reductive Coupling of Allyl Groups in the Presence of Triphenylphosphine *J. Organomet. Chem.* **1988**, *349*, 263–268. (c) McKinney, R.J.; Roe, D.C. The Mechanism of Nickel-Catalyzed Ethylene Hydrocyanation. Reductive Elimination by an Associative Process *J. Am. Chem. Soc.* **1986**, *108*, 5167–5173. (d) Tatsumi, K.; Nakamura, A.; Komiya, S.; Yamamoto, A.; Yamamoto, T. An Associative Mechanism for Reductive Elimination of $d^8 \text{NiR}_2(\text{PR}_3)_2$ *J. Am. Chem. Soc.* **1984**, *106*, 8181–8188. (e) Komiya, S.; Abe, Y.; Yamamoto, A.; Yamamoto, T. Phosphine-Induced Reductive Elimination from Cis-Arylmethylnickel(II) Complexes Having a 1,2-Bis(dimethylphosphino)ethane Ligand *Organometallics* **1983**, *2*, 1466–1468.
- (21) (a) Yamamoto, T.; Abla, M.; Murakami, Y. Promotion of Reductive Elimination Reaction of Diorgano(2,2'-bipyridyl)nickel(II) Complexes by Electron-Accepting Aromatic Compounds, Lewis Acids, and Brønsted Acids. *Bull. Chem. Soc. Jpn.* **2002**, *75*, 1997–2009. (b) Giovannini, R.; Studemann, T.; Devasagayaraj, A.; Dussin, G.; Knochel, P. *J. Org. Chem.* New Efficient Nickel-Catalyzed Cross-Coupling Reaction between Two Csp^3 Centers **1999**, *64*, 3544–3553. (c) Yamamoto, T.; Abla, M. Reductive elimination of Et–Et from $\text{NiEt}_2(\text{bpy})$ promoted by electron-accepting aromatic compounds *J. Organomet. Chem.* **1997**, *535*, 209–211.
- (22) (a) Huang, C.-Y.; Doyle, A.G. Electron-Deficient Olefin Ligands Enable Generation of Quaternary Carbons by Ni-Catalyzed Cross-Coupling *J. Am. Chem. Soc.* **2015**, *137*, 5638–5641. (b) Huang, C.-Y.; Doyle, A.G. Nickel-Catalyzed Negishi Alkylations of Styrenyl Aziridines *J. Am. Chem. Soc.* **2012**, *134*, 9541–9544. (c) Estévez, L.; Tuxworth, L.W.; Sotiropoulos, J.-M.; Dyer, P.W.; Miqueu, K. Combined DFT and

Experimental Studies of C–C and C–X Elimination Reactions Promoted by a Chelating Phosphine–Alkene Ligand: the Key Role of Penta-Coordinate Pd^{II} *Dalton Trans.* **2014**, *43*, 11165–11179. (b) Johnson, J.B.; Rovis, T.; More than Bystanders: The Effect of Olefins on Transition-Metal-Catalyzed Cross-Coupling Reactions *Angew. Chem. Int. Ed.* **2008**, *47*, 840–871. (c) Kurosawa, H.; Ohnishi, H.; Emoto, M.; Chatani, N.; Kawasaki, Y.; Murai, S.; Ikeda, I. Preparation and Reductive Elimination of (η^3 -allyl)(aryl)nickel(II) Complexes: Unusually Facile η^3 -allyl-aryl Coupling on Nickel Having an 18-electron Configuration *Organometallics* **1990**, *9*, 3038–3042. (d) Kurosawa, H.; Ohnishi, H.; Emoto, M.; Kawasaki, Y.; Murai, S. Unusually Lower Barrier to Reductive Elimination in an 18-Electron η^3 -allyl(organo)nickel(II) Complex Than Those for the 16-Electron η^3 -allyl Counterpart and its 16-Electron η^1 -allyl Isomer *J. Am. Chem. Soc.* **1988**, *110*, 6272–6273. (e) Yamamoto, T.; Yamamoto, A.; Ikeda, S. Organo (Dipyridyl) Nickel Complexes. I. Stability and Activation of the Alkyl-Nickel Bonds of Dialkyl (Dipyridyl) Nickel by Coordination with Various Substituted Olefins *J. Am. Chem. Soc.* **1971**, *93*, 3350–3359.

(23) Bronstein, H.A.; Luscombe, C.K. Externally Initiated Regioregular P3HT with Controlled Molecular Weight and Narrow Polydispersity *J. Am. Chem. Soc.* **2009**, *131*, 12894–12895. (b) Boyd, S.D.; Jen, K.-Y.; Luscombe, C.K. Steric Stabilization Effects in Nickel-Catalyzed Regioregular Poly(3-hexylthiophene) Synthesis *Macromolecules* **2009**, *42*, 9387–9389.

(24) Evans' pKa Table. http://evans.rc.fas.harvard.edu/pdf/evans_pKa_table.pdf (accessed December 6, 2016)

(25) The phrase refers to a quote by philosopher Ludwig Wittgenstein, who posited that “if a lion could talk, we would not understand him.” For reference, see: L. Wittgenstein, *Philosophical Investigations*, translated by G.E.M. Anscombe, P.M.S. Hacker and J. Schulte, 4th ed. Blackwell Publishing Ltd, United Kingdom, 2009, p. 327.

(26) A common interpretation is that although we *would* be able to understand a talking lion, s/he would not be able to tell us about normal (non-talking) lions. S. Budiansky, *If a Lion Could Talk: Animal Intelligence and the Evolution of Consciousness*. Free Press, 1998.

(27) The percentages refer to the relative area ratios for each DP.

(28) Similar ratios of end-groups were observed with precatalysts **2b–d** (Appendix 1).

Chapter 3

Limitations of Using Small Molecules to Identify Catalyst-Transfer Polymerization Reactions¹

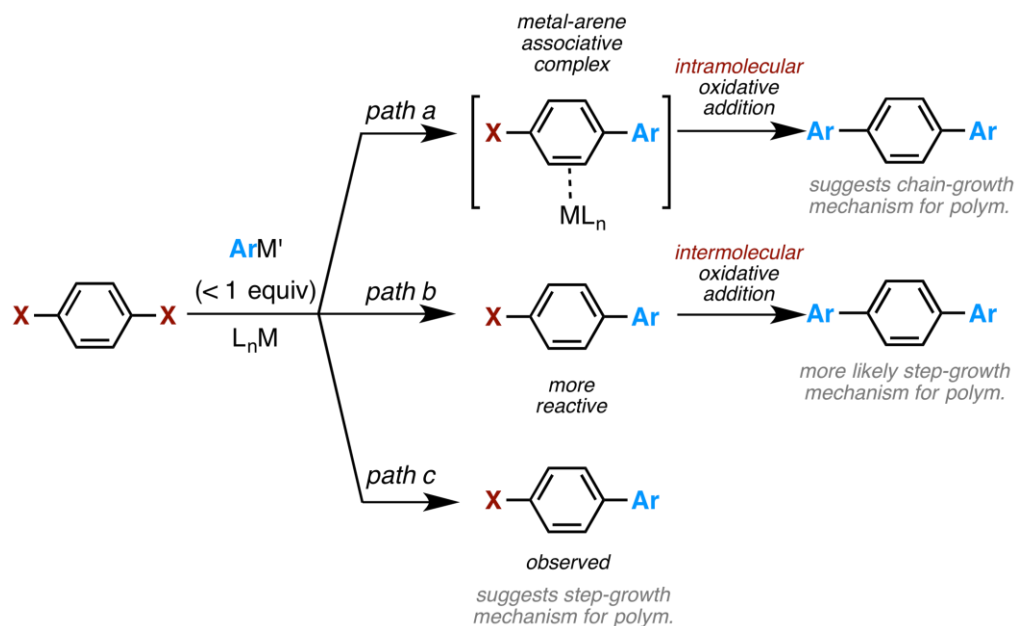
Conjugated polymers continue to garner considerable interest due to their light-harvesting, light-emitting and semi-conducting properties.¹ Step-growth methods dominated the synthetic landscape for many decades until a chain-growth method, now referred to as catalyst-transfer polymerization (CTP), was reported in 2004.² The CTP method has been used to access controlled sequence copolymers (e.g., block,³ gradient⁴), end-functionalized polymers,⁵ and surface-functionalized polymers.⁶ Despite a decade of research on CTP, the scope remains limited to a handful of monomers, most of which are electron-rich (hetero)arenes, and the reasons for this limitation are not entirely clear.⁷

To identify new CTP reactions, we and others have used small molecule difunctionalizations as an analogue for the polymerization.⁸ The experiments are performed with substoichiometric amounts of coupling partner so if the difunctionalized product is predominant, then an associative intermediate with a subsequent intramolecular oxidative addition is suggested (Scheme 3.1, path a). This pathway is analogous to the chain-growth mechanism in CTP. Another way to obtain selective difunctionalization is if the monofunctionalized product is more reactive than the starting material, outcompeting it in an intermolecular oxidative addition (Scheme 3.1, path b). In this case, the analogous polymerization is likely to follow a step-growth mechanism.⁹ If, on the other hand, the monofunctionalized product is favored, then a step-growth mechanism for the polymerization is expected (Scheme 3.1, path c).

¹ Reproduced with permission from Bryan, Z. J.; Hall, A. O.; Zhao, C. T.; Chen, J.; McNeil, A. J. Limitations of Using Small Molecules to Identify Catalyst-Transfer Polycondensation reactions *ACS Macro Lett.* **2016**, *5*, 69–72

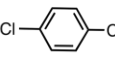
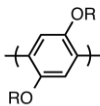
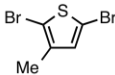
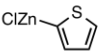
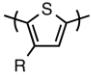
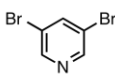
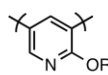
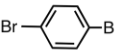
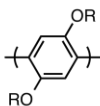
² A.O.H. synthesized and conducted polymerization of the stannyl-functionalized monomer to compare catalysts between this work and previously published results.

Scheme 3.1. Difunctionalized products can be obtained via two different pathways.



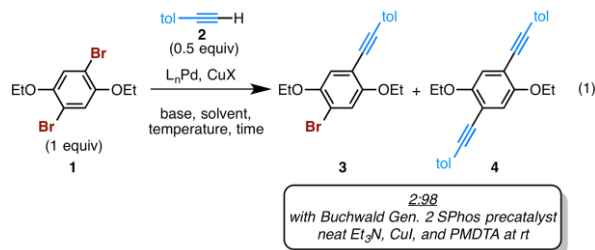
An early example of a relevant small molecule difunctionalization was performed by Kumada in 1976 (Table 3.1, entry 1).¹⁰ Using dichlorobenzene and substoichiometric butyl magnesium chloride, Kumada and co-workers observed >96% of the difunctionalized arene. These reaction conditions bear a striking resemblance to the chain-growth synthesis of poly(2,5-bis(hexyloxy)phenylene) reported by Yokozawa and coworkers in 2006, suggesting that the small molecule reaction proceeded through an associative intermediate (Scheme 3.1, path a).¹¹ McCullough and coworkers used a related small molecule analogue to support the claim of an associative intermediate in CTP with thiophene monomers (Table 3.1, entry 2).^{2c} Using the polymerization catalyst and substoichiometric thienyl zinc, they observed >97% difunctionalization of the 2,5-dibromo-3-methyl-thiophene. In 2012, Yokozawa and coworkers used a small molecule analogue to support the claim of CTP in poly(2-alkoxypyridine-3,5-diyl) synthesis (Table 3.1, entry 3).^{8b-c} In 2012, we reported a new CTP method^{8a} based on a reported selective multi-functionalization of arenes using Pd catalysts (Table 3.1, entry 4).¹² Motivated by these examples, we examined small molecule analogues for a variety of challenging monomers, aimed at broadening the scope of CTP. Herein we describe one of these small molecule studies and the lessons learned from its implementation.

Table 3.1. Selective small molecule analogues^{2c,8b-c,10,12} and the corresponding CTPs.^{2c,8,11}

entry	substrate	limiting reagent	catalyst	di:mono	CTP
1		nBuMgCl	Ni(bpy)Cl ₂	96:4	
2		ClZn 	Ni(dppp)Cl ₂	97:3	
3		PhMgCl	Ni(dppp)Cl ₂	100:0	
4		nBuZnBr	PEPPSI-IPr	>99:1	

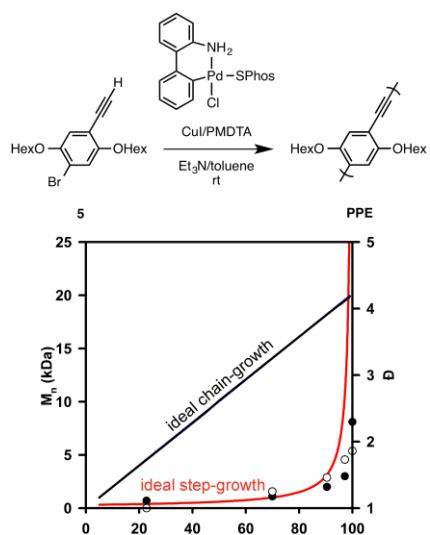
Polyphenylene ethynylenes (PPEs) were selected because at the time we started this work there were no known chain-growth methods for their synthesis. PPEs are highly fluorescent polymers with a variety of applications, including light emitting diodes¹³ and sensors.¹⁴ While the Sonogashira polymerization could proceed through an associative complex, the impact of the additional metal (i.e., copper) and π -bonds (i.e., alkynes) on this key intermediate was unknown. While this work was in progress, Bielawski and coworkers reported a chain-growth synthesis of PPEs using PhPdP(tBu)₃Br; however, stoichiometric tin was used, ultimately limiting its applications.¹⁵

Our small molecule analogue used 1,4-diethoxy-2,5-dibromobenzene (**1**) and 4-tolylacetylene (**2**) as the starting materials because their steric and electronic properties mirror those of known PPE monomers.¹⁶ In our standard conditions, a 4:1 ratio of Br:alkyne was used (eq 1). Conversion of starting materials and products was determined by gas chromatography, enabling rapid iteration and efficient screening (SI). Hundreds of small molecule reactions were performed to examine the impact of the precatalyst/ligand, co-catalyst/ligand, base, solvent, and temperature (SI). Ultimately, we found that selective difunctionalization could be achieved with Buchwald-type Pd precatalysts and amine-ligated copper in toluene/Et₃N at room temperature. With further optimization, the highest product ratio obtained in these small molecule studies was 98:2 (**4:3**; eq 1), which is similar to the analogues that correlate with CTPs (Table 3.1).^{2c,8b-c,10,12}



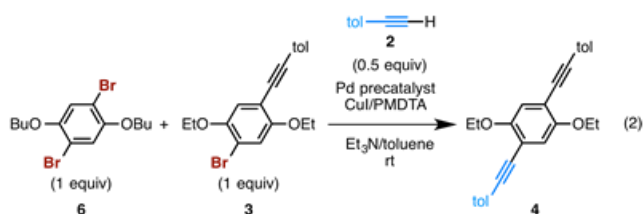
To determine whether this selective Sonogashira difunctionalization translates to a chain-growth PPE synthesis, monomer **5** was synthesized in four steps with a moderate yield (SI).¹⁷ Polymerizing monomer **5** using the most selective small molecule conditions surprisingly led to a step-growth polymerization, as evident by the gradual increase in the number-average molecular weight (M_n) and molecular weight distribution (\mathcal{D}) with conversion (Figure 1). This result led us to reconsider the common assumption that difunctionalization results from an associative intermediate (Scheme 3.1, path a). Instead, the observed difunctionalization could simply result from a large difference in the intermolecular oxidative addition rates between starting material **1** and monofunctional product **3** (Scheme 3.1, path b).

Figure 3.1. Plot of number-average molecular weight (M_n , ●) and dispersity (\mathcal{D} , ○) versus conversion ($[5] = 0.085$ M, $[\text{precatalyst}] = 1.3$ mM, $[\text{CuI}]$ and $[\text{PMDTA}] = 6.3$ mM, Et_3N (2.5 mL), toluene (7.5 mL), rt, 30 h).



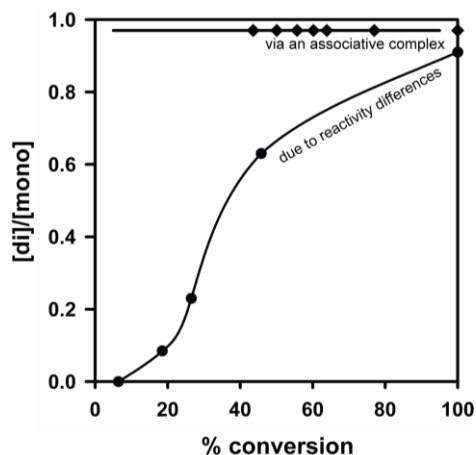
To test this hypothesis, we performed a competition experiment where equimolar concentrations of dibromoarene **6** and monobromoarene **3** competed for a limiting

amount of alkyne **2** (eq 2). To readily distinguish the two possible difunctionalized products, butyloxy groups were used in arene **6**. Notably, the only product observed in this reaction is difunctional **4** via reaction of monobromoarene **3**. Based on the 5 mol% of Pd present, we can estimate that **3** is at least 20x more reactive than **6**. These results suggest that the high selectivity for difunctionalized product was solely due to reactivity differences. Because monomer **5** and the polymer (“PPE”) are more structurally similar than our model system (eq 2), we would expect smaller differences in their relative reactivities during polymerization.



To minimize such “false positives” in future studies, we designed a simple experiment to distinguish whether the small molecule difunctionalizations result from an associative complex or reactivity differences. Monitoring the product ratio as a function of the conversion will either give (a) a constant, high di-to-monofunctionalization ratio (via associative complex), or (b) a ratio that favors monofunctionalization at low conversions and difunctionalization at high conversions (via reactivity differences) (Figure 2, Appendix 2).¹⁸

Figure 3.2. Plot of the difunctionalized-to-monofunctionalized product ratio versus percent conversion of the limiting reagent for a Kumada (◆) and Sonogashira (●) small molecule reaction. See Appendix 3 for experimental details.



The lack of chain-growth behavior herein was surprising, particularly in light of Bielawski and co-workers observed chain-growth polymerization using $\text{PhPd}(\text{PtBu}_3)\text{Br}$ and a tributyltin-activated monomer.¹⁵ We initially suspected that the difference in alkyne functional group (i.e., an “H” compared to a “ Bu_3Sn ”) was important, and that the strongly π -coordinating, relatively unhindered alkyne in **5** might competitively displace the polymer from the associative complex, leading to step-growth behavior. To test this hypothesis, we synthesized the tributyltin monomer and polymerized it using both our optimized conditions as well as those reported by Bielawski and co-workers (Appendix 2).¹⁵ Consistent with the earlier report, chain-growth behavior was observed with $\text{PhPd}(\text{PtBu}_3)\text{Br}$ whereas step-growth behavior was observed under our difunctionalization conditions.¹⁵ Combined, these results suggest that the difference in the ancillary ligands (i.e., PtBu_3 versus SPhos), is the key factor, rather than the alkyne functional group. That is, the more strongly σ -donating trialkyl phosphine likely promotes formation and reactivity of the associative intermediate in the chain-growth pathway.¹⁹ In summary, although small molecule reactions have been useful in identifying new chain-growth polymerization conditions, the results can vary. Selective difunctionalization, in the presence of a limiting reagent, can stem from one of two pathways: (a) an associative intermediate, or (b) from reactivity differences. Only in the former case are the small molecule results likely to correspond to a chain-growth polymerization. Following the mono/difunctionalization ratios at low and high conversions can elucidate which of these pathways is dominant, unless the reactivity differences are exceedingly large. Despite these limitations, small molecule analogues remain a useful tool to target new monomers for CTP.

References

(1) For reviews, see: (a) Yeh, N.; Yeh, P. Organic solar cells: Their developments and potentials *Renew. Sust. Energ. Rev.* **2013**, *21*, 421–431. (b) Cataldo, S.; Pignataro, B. Polymeric Thin Films for Organic Electronics: Properties and Adaptive Structures *Materials* **2013**, *6*, 1159–1190. (c) Li, G.; Zhu, R.; Yang, Y. Polymer Solar Cells *Nature Photonics* **2012**, *6*, 153–161. (d) Boudreault, P.-L. T.; Najari, A.; Leclerc, M. Processable Low-Bandgap Polymers for Photovoltaic Applications *Chem. Mater.* **2011**, *23*, 456–469.

(e) Facchetti, A. π -Conjugated Polymers for Organic Electronics and Photovoltaic Cell Applications *Chem. Mater.* **2011**, *23*, 733–758.

(2) (a) Yokoyama, A.; Miyakoshi, R.; Yokozawa, T. Chain-Growth Polymerization for Poly(3-hexylthiophene) with a Defined Molecular Weight and a Low Polydispersity *Macromolecules*, **2004**, *37*, 1169–1171. (b) Miyakoshi, R.; Yokoyama, A.; Yokozawa, T. Synthesis of Poly(3-hexylthiophene) with a Narrower Polydispersity *Macromol. Rapid Commun.* **2004**, *25*, 1663–1666. (c) Sheina, E. E.; Liu, J. S.; Iovu, M. C.; Laird, D. W.; McCullough, R. D. Chain Growth Mechanism for Regioregular Nickel-Initiated Cross-Coupling Polymerizations *Macromolecules*, **2004**, *37*, 3526–3528.

(3) For recent examples, see: (a) Sui, A.; Shi, X.; Tian, H.; Geng, Y.; Wang, F. Suzuki–Miyaura Catalyst-Transfer Polycondensation with Pd(IPr)(OAc)₂ as the Catalyst for the Controlled Synthesis of Polyfluorenes and Polythiophenes *Polym. Chem.* **2014**, *5*, 7072–7080. (b) Erdmann, T.; Back, J.; Tkachov, R.; Ruff, A.; Voit, B.; Ludwigs, S.; Kiriya, A. Dithienosilole-Based All-Conjugated Block Copolymers Synthesized by a Combination of Quasi-Living Kumada and Negishi Catalyst-Transfer Polycondensations *Polym. Chem.* **2014**, *5*, 5383–5390. (c) Sui, A.; Shi, X.; Wu, S.; Tian, H.; Geng, Y.; Wang, F. Controlled Synthesis of Polyfluorenes via Kumada Catalyst Transfer Polycondensation with Ni(acac)₂/dppp as the Catalyst *Macromolecules* **2012**, *45*, 5436–5443. (d) Verswyvel, M.; Koeckelberghs, G. Chirality in Conjugated Polymers: When Two Components Meet *Polym. Chem.* **2012**, *3*, 3203–3216.

(4) For recent examples, see: (a) Hardeman, T.; Koeckelberghs, G. The Synthesis of Poly(thiophene-co-fluorene) Gradient Copolymers *Macromolecules* **2015**, *48*, 6987–6993 (b) Palermo, E. F.; Darling, S. B.; McNeil, A. J. π -Conjugated Gradient Copolymers Suppress Phase Separation and Improve Stability in Bulk Heterojunction Solar Cells *J. Mater. Chem. C* **2014**, *2*, 3401–3406. (c) Palermo, E.F.; van der Laan, H.L.; McNeil, A.J. Impact of π -Conjugated Gradient Sequence Copolymers on Polymer Blend Morphology *Polym. Chem.* **2013**, *4*, 4606–4611. (e) Palermo, E. F.; McNeil, A. J. Palermo, E.F.; McNeil, A.J. Impact of Copolymer Sequence on Solid-State Properties for Random, Gradient and Block Copolymers containing Thiophene and Selenophene *Macromolecules* **2012**, *45*, 5948–5955. (e) Locke, J. R.; McNeil, A. J. Syntheses of Gradient π -Conjugated Copolymers of Thiophene *Macromolecules* **2010**, *43*, 8709–8710.

(5) For recent examples, see: (a) Handa, N. V.; Serrano, A. V.; Robb, M. J.; Hawker, C. J. Exploring the Synthesis and Impact of End-Functional Poly(3-hexylthiophene) *J. Polym. Sci., Part A: Polym. Chem.* **2015**, *53*, 831–841. (b) Okamoto, K.; Luscombe, C. K. Simple Procedure for Mono- and Bis-End-Functionalization of Regioregular Poly(3-hexylthiophene)s Using Chalcogens *Chem. Commun.* **2014**, *50*, 5310–5312. (c) Yuan, M. J.; Okamoto, K.; Bronstein, H. A.; Luscombe, C. K. Constructing Regioregular Star Poly(3-hexylthiophene) via Externally Initiated Kumada Catalyst-Transfer Polycondensation *ACS Macro Lett.* **2012**, *1*, 392–395. (d) Elmalem, E.; Biedermann, F.;

Johnson, K.; Friend, R. H.; Huck, W. T. S. Synthesis and Photophysics of Fully π -Conjugated Heterobis-Functionalized Polymeric Molecular Wires via Suzuki Chain-Growth Polymerization *J. Am. Chem. Soc.* **2012**, *134*, 17769–17777.

(6) For recent examples, see: (a) Huddleston, N. E.; Sontag, S. K.; Bilbrey, J. A.; Sheppard, G. R.; Locklin, J. Palladium-Mediated Surface-Initiated Kumada Catalyst Polycondensation: A Facile Route Towards Oriented Conjugated Polymers *Macromol. Rapid Commun.* **2012**, *33*, 2115–2120. (b) Sontag, S. K.; Sheppard, G. R.; Usselman, N. M.; Marshall, N.; Locklin, J. Surface-Confined Nickel Mediated Cross-Coupling Reactions: Characterization of Initiator Environment in Kumada Catalyst-Transfer Polycondensation *Langmuir* **2011**, *27*, 12033–12041.

(7) For recent reviews, see: (a) Bryan, Z. J.; McNeil, A. J. Conjugated Polymer Synthesis via Catalyst-Transfer Polycondensation (CTP): Mechanism, Scope, and Applications *Macromolecules* **2013**, *46*, 8395–8405. (b) Yokozawa, T.; Ohta, Y. Scope of Controlled Synthesis via Chain-Growth Condensation Polymerization: from Aromatic Polyamides to π -Conjugated Polymers *Chem. Commun.* **2013**, *49*, 8281–8310. (c) Yokozawa, T.; Nanashima, Y.; Ohta, Y. Precision Synthesis of n-Type π -Conjugated Polymers in Catalyst-Transfer Condensation Polymerization *ACS Macro. Lett.* **2012**, *1*, 862–866.

(8) (a) Bryan, Z. J.; Smith, M. L.; McNeil, A. J. Chain-Growth Polymerization of Aryl Grignards Initiated by a Stabilized NHC-Pd Precatalyst *Macromol. Rapid Commun.* **2012**, *33*, 842–847. (b) Nanashima, Y.; Shibata, R.; Miyakoshi, R.; Yokoyama, A.; Yokozawa, T. Investigation of Catalyst-Transfer Condensation Polymerization for the Synthesis of n-Type π -Conjugated Polymer, Poly(2-dioxaalkylpyridine-3,6-diyl) *J. Polym. Sci. Pol. Chem.* **2012**, *50*, 3628–3640. (c) Nanashima, Y.; Yokoyama, A.; Yokozawa, T. Synthesis of Well-Defined Poly(2-alkoxypyridine-3,5-diyl) via Ni-Catalyst-Transfer Condensation Polymerization *Macromolecules* **2012**, *45*, 2609–2613. (d) See also 2c.

(9) If the reactivity differences are substantial, this pathway can result in a chain-growth polymerization. For a review, see: Yokozawa, T.; Yokoyama, A. Chain-growth Polycondensation: The Living Polymerization Process in Polycondensation *Prog. Polym. Sci.* **2007**, *32*, 147–172. For an example with conjugated polymers, see: Verswyvel, M; Verstappen, P.; De Cremer, L.; Verbiest, T.; Koeckelberghs, G. Development of a Universal Chain-Growth Polymerization Protocol of Conjugated Polymers: Toward a Variety of All-Conjugated Block-Copolymers *Polym. Chem.* **2011**, *49*, 5339–5349. Although linear M_n versus conversion plots were obtained, there was almost no dependence of M_n on the monomer/initiator ratio, suggesting competing chain-transfer or termination reactions.

(10) Tamao, K.; Sumitani, K.; Kiso, Y.; Zembayashi, M.; Fujioka, A.; Kodama, S.; Nakajima, I.; Minato, A.; Kumada, M. *Bull. Chem. Soc. Jpn.* Nickel-Phosphine Complex-Catalyzed Grignard Coupling. I. Cross-Coupling of Alkyl, Aryl, and Alkenyl Grignard

Reagents with Aryl and Alkenyl Halides: General Scope and Limitations **1976**, *49*, 1958–1969.

(11) Miyakoshi, R.; Shimono, K.; Yokoyama, A.; Yokozawa, T. Catalyst-Transfer Polycondensation for the Synthesis of Poly(p-phenylene) with Controlled Molecular Weight and Low Polydispersity *J. Am. Chem. Soc.* **2006**, *128*, 16012–16013.

(12) Larrosa, I.; Somoza, C.; Banquy, A.; Goldup, S. M. Two Flavors of PEPPSI-IPr: Activation and Diffusion Control in a Single NHC-Ligated Pd Catalyst? *Org. Lett.* **2011**, *13*, 146–149.

(13) (a) Grimsdale, A. C.; Leok Chan, K.; Martin, R. E.; Jokisz, P. G.; Holmes, A. B. Synthesis of Light-Emitting Conjugated Polymers for Applications in Electroluminescent Devices *Chem. Rev.* **2009**, *109*, 897–1091. (b) Pschirer, N. G.; Miteva, T.; Evans, U.; Roberts, R. S.; Marshall, A. R.; Neher, D.; Myrick, M. L.; Bunz, U. H. F. Blue Solid-State Photoluminescence and Electroluminescence from Novel Poly(para-phenyleneethynylene) Copolymers *Chem. Mater.* **2001**, *13*, 2691–2696.

(14) (a) Thomas, S. W.; Joly, G. D.; Swager, T. M. Chemical Sensors Based on Amplifying Fluorescent Conjugated Polymers *Chem. Rev.* **2007**, *107*, 1339–1386. (b) Yang, J.-S.; Swager, T. M. Fluorescent Porous Polymer Films as TNT Chemosensors: Electronic and Structural Effects *J. Am. Chem. Soc.* **1998**, *120*, 11864–11873.

(15) Although a tin-free polymerization was also reported, no evidence supporting a chain-growth mechanism was provided. For reference, see: Kang, S.; Ono, R. J.; Bielawski, C. W. Controlled Catalyst Transfer Polycondensation and Surface-Initiated Polymerization of a p-Phenyleneethynylene-Based Monomer *J. Am. Chem. Soc.* **2013**, *135*, 4984–4987.

(16) (a) Allara, D. L.; Arnold, J. J.; Bumm, L. A.; Burgin, T. P.; Cygan, M. T.; Dunbar, T. D.; Jones, L., II; Tour, J. M.; Weiss, P. S. Are Single Molecular Wires Conducting? *Science* **1996**, *271*, 1705–1707. (b) See also refs 13 and 14.

(17) (a) Lanni, E. L.; McNeil, A. J. Mechanistic Studies on Ni(dppe)Cl₂-Catalyzed Chain-Growth Polymerizations: Evidence for Rate-Determining Reductive Elimination *J. Am. Chem. Soc.* **2009**, *131*, 16573–16579. (b) Caddick, S.; Delisser, V. M.; Doyle, V. E.; Khan, S. Studies Toward the Synthesis of Natural and Unnatural Dienediyne 1. Approaches to a Functionalised Bicyclic Ring System *Tetrahedron*, **1999**, *55*, 2737–2754.

(18) Note that extremely large reactivity differences could result in a constant product ratio (favoring difunctionalization) even though it does not proceed through an associative intermediate. In these cases, the polymerization data is needed to distinguish between the two possible mechanisms.

(19) Bryan, Z. J.; McNeil, A. J. Evidence for a Preferential Intramolecular Oxidative Addition in Ni-Catalyzed Cross-Coupling Reactions and their Impact on Chain-Growth Polymerizations *Chem. Sci.* **2013**, *4*, 1620–1624.

Chapter 4

Single-Electron Reactions for Conjugated Polymer Synthesis

Introduction

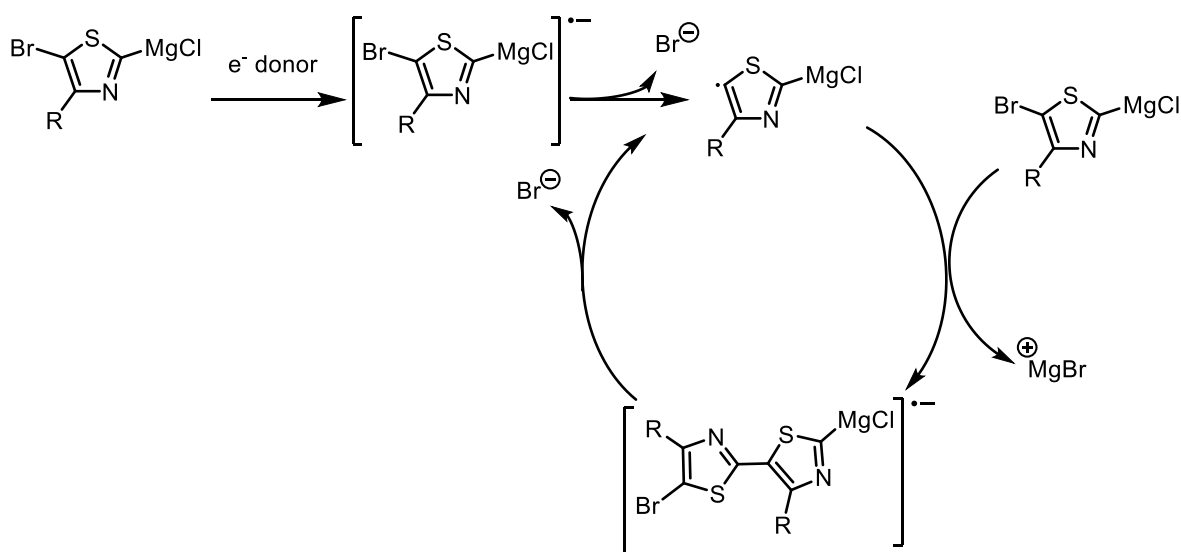
Since catalyst transfer polymerization (CTP) was first discovered for poly(thiophene), the scope has been expanded to many electron-rich monomers, but efforts to polymerize electron-deficient monomers have yielded fewer results, often with low molecular weight (M_n) or broad dispersity (\mathcal{D}).¹ The highest-performing polymers in organic photovoltaics are still synthesized by step-growth polymerizations, most commonly Stille couplings, which yield polymers with broad \mathcal{D} .² Using CTP, minor changes in monomer structure can impact the polymerization results (e.g., the addition of a nitrogen atom in thiazole led to a high-energy chain walking step, enabling side reactions to occur³), making it necessary to screen catalysts for each new monomer. Looking beyond metal-catalyzed polymerizations, single-electron reactions may be key to expanding monomer scope beyond what is accessible through CTP. Living chain-growth radical polymerizations have been developed for many monomers,⁴ especially for alkenyl-functionalized monomers,⁵ but few examples have been reported for conjugated polymers.^{6,7,8} Poly(thiophene) and other conjugated polymers have been synthesized through oxidative electropolymerization, but targeted molecular weight, which can affect conductivity and device performance,⁹ are hard to achieve with this method that more commonly produces insoluble polymer films.¹⁰ This chapter details efforts to develop chain-growth polymerizations for electron-deficient monomers through two single-electron-based approaches: expanding radical polymerization methods to conjugated polymers, and modifying electrochemical polymerization methods to target chain-growth.

Radical $S_{RN}1$ Polymerizations

There is some precedent for radical anion polymerizations of conjugated polymers. Studer has reported radical-anion reactions for polymerizing aryl Grignard reagents to obtain poly(metaphenylene),⁶ poly(paraphenylene),⁷ poly(naphthalene),⁷ and

poly(paraphenylene sulfide),⁸ using TEMPO to initiate polymerizations. We were further inspired to try radical polymerizations of electron-deficient monomers by a recent discovery in our group that a thiazole monomer spontaneously oligomerizes without any transition metal catalyst after activation by magnesium-halogen exchange (Scheme 4.1).³ EPR spectroscopy revealed radical formation in the activated monomer solution, consistent with oligomers formation through a radical-anion $S_{RN}1$ mechanism. Similar radical-anion mechanisms have been reported in small molecule aryl–aryl couplings.¹¹ In this mechanism, thiazole Grignard accepts an electron from a donor (magnesium or a Grignard reagent) to generate a radical anion. The radical anion undergoes halide cleavage to form a neutral radical species which attacks a second monomer, forming a bis(thiazole) radical anion. Subsequent halide cleavage regenerates a neutral radical. Using an external EPR standard, it was found that only 0.07% of the thiazole monomer contained a radical. The observation of high monomer conversion along with low M_n and low radical concentration suggests frequent activation and quenching of radicals. We also found that electronics have a significant impact on the reaction: the oligomerization was approximately 1000 times slower when a different regioisomer of the monomer was used, while no oligomers formed when bromide was replaced with chloride, likely due to a higher energy barrier for chloride cleavage. Based on these results, we attempted to further develop $S_{RN}1$ reactions for synthesizing electron-deficient conjugated polymers.

Scheme 4.1. Thiazole oligomerization via $S_{RN}1$ reaction



Because poly(thiazole) derivatives have limited solubility and are not commonly used in photovoltaics,^{6,12} we decided to explore other monomers for $S_{RN}1$ polymerizations. We began by screening three commercially available electron-deficient monomers which have been used in organic electronics: a bis(thienyl)diketopyrrolopyrrole (**1**),¹³ a dioctylbenzothiadiazole (**2**),¹⁴ and a naphthalene-diimide (**3**),¹⁵ which has been previously observed to form radical anions when exposed to zinc¹⁶ (Chart 4.1). We treated each monomer with isopropylmagnesium chloride and analyzed the reactions by EPR spectroscopy) to see if spontaneous radical formation was possible. We observed a new radical signal in each reaction (Figure 4.1, Appendix 3). The quenched reactions were analyzed by gel permeation chromatography (GPC) but no polymer formed, even after 24 hours.

Chart 4.1. Commercially available monomers screened for radical formation

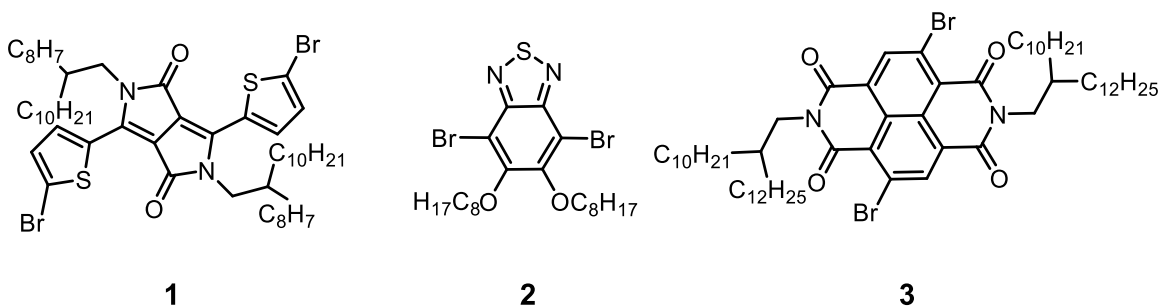
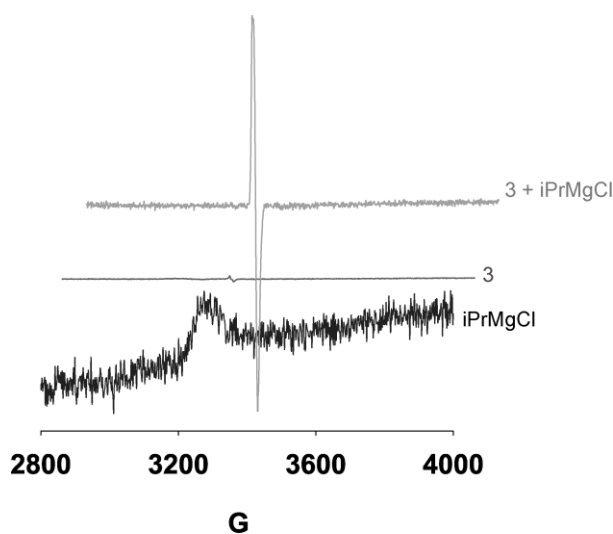
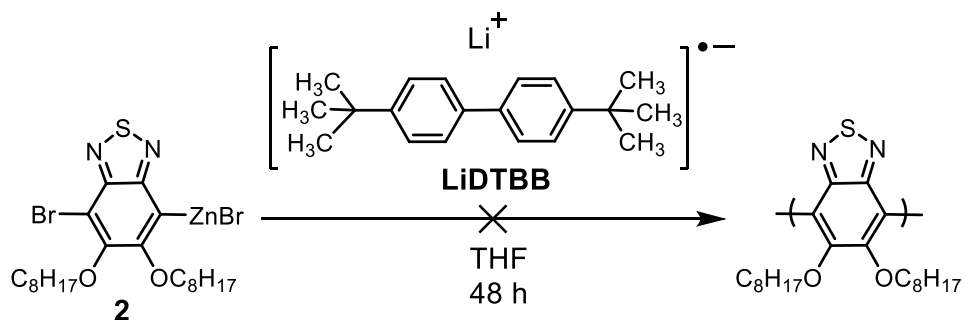


Figure 4.1. EPR spectra for the reaction of **3** and *i*PrMgCl.



We next used a sacrificial electron donor as a potential initiator. We used direct zinc insertion to activate **2**, then exposed it to lithium 4,4'-di-*tert*-butylbiphenylide (LiDTBB) (0.05 equiv), a radical anion which is reported to initiate S_{RN}1 reactions¹⁷ (Scheme 4.2, Appendix 3). We observed no polymer formation after 48 hours. The steric crowding of the two octyloxy side chains may have prevented bond formation. These efforts demonstrate the spontaneous S_{RN}1 reaction observed with thiazole is not readily expanded to other monomers, even with sacrificial electron-donors.

Scheme 4.2. Attempted S_m1 polymerization using LiDTBB as a sacrificial donor



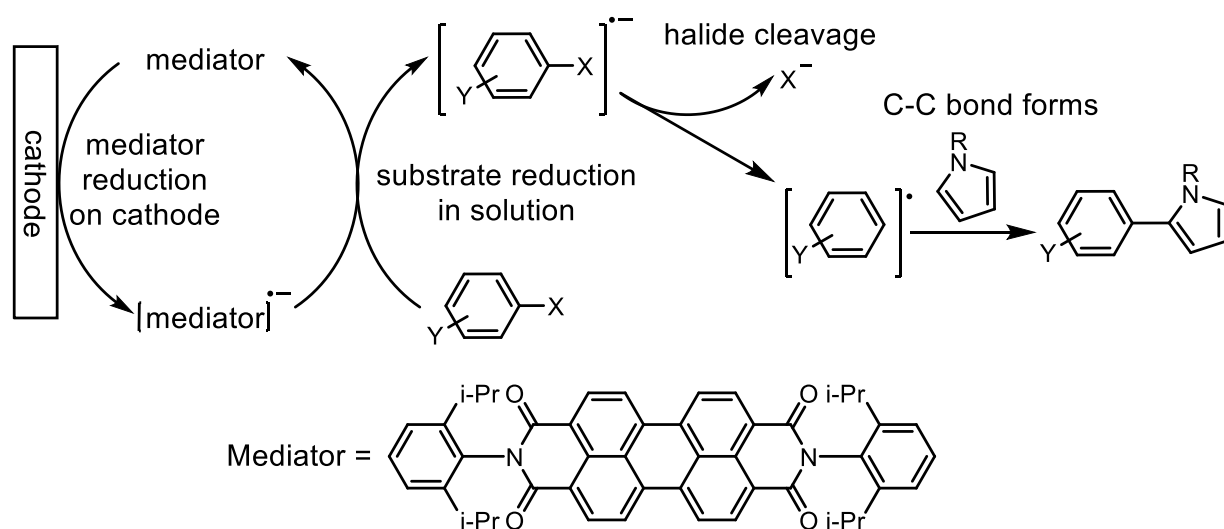
Electrocatalytic polymerization

Because we were unable to induce polymerization through S_{RN}1 reactions, we turned to electropolymerizations, which also proceed through single-electron mechanisms. Oxidative electropolymerizations have been developed for several conjugated polymers.¹⁸ Reductive electropolymerization with nickel catalysts has been used to synthesize poly(thiophene),¹⁹ poly(phenylene),²⁰ poly(furan),²¹ poly(fluorene),²² poly(fluorenone),²³ poly(naphthalene),²⁴ and poly(pyridine).²⁵ The proposed mechanism involves oxidative addition of Ni(0) into the aryl–halide bond, followed by cathodic reduction to reform Ni(0) and aryl–aryl bonds.¹⁹ While these examples show that reductive electropolymerization is possible for conjugated polymers, the reaction still occurs only at the electrode surface and therefore for chain-growth to occur, all polymers must remain on or near the surface during polymerization.

We propose an alternative route using indirect electrocatalysis instead to develop chain-growth polymerizations based on recently reported small-molecule coupling.²⁶ Using an electrocatalytic mediator enables reduction to occur in solution rather than solely on the electrode surface. In this process, the mediator is reduced at the cathode. The

reduced mediator can then diffuse in solution and reduce a substrate, which then undergoes further reactions. Indirect electrocatalysis enables the reaction to occur in solution rather than solely at the electrode surface. Furthermore, by using a mediator with a lower reduction potential, the reaction can be conducted at a lower potential than would be required to directly reduce the substrate, which can improve selectivity and avoid side-reactions and product decomposition that might occur at high potentials. Wan and coworkers used a perylene-diimide (**PDI**) mediator for electrocatalytic small-molecule aryl–aryl couplings (Scheme 4.3).²⁶

Scheme 4.3. Phenyl–pyrrole coupling through indirect electrocatalysis²⁶

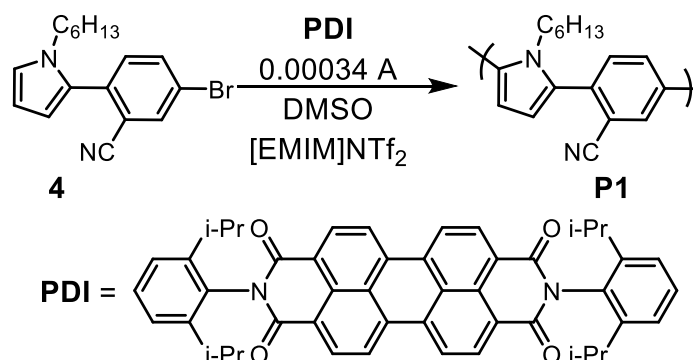


We envision that differences in reduction potential between monomer and polymer could be used to give chain-growth polymerization. Differences in reactivity between polymer and monomer have been reported to lead to chain-growth polymerization with Pd-catalyzed poly(aniline) polymerization.²⁷ The increased conjugation length in a polymer compared to a monomer could lower the energy barrier for accepting an electron, thus favoring polymer reduction over monomer reduction to give a chain-growth polymerization.

To expand electrocatalysis to conjugated polymers, we began with a phenyl-pyrrole monomer (**4** in Scheme 4.4). Excitingly, we synthesized a polymer using the reported **PDI** mediator, solvent, supporting electrolyte, and constant current reactions conditions,²⁶ albeit with $\bar{D} = 2.9$ and $M_n = 6$ kDa (for isolated polymer, see Appendix 3). As a control, we applied the same reaction conditions to a solution containing only

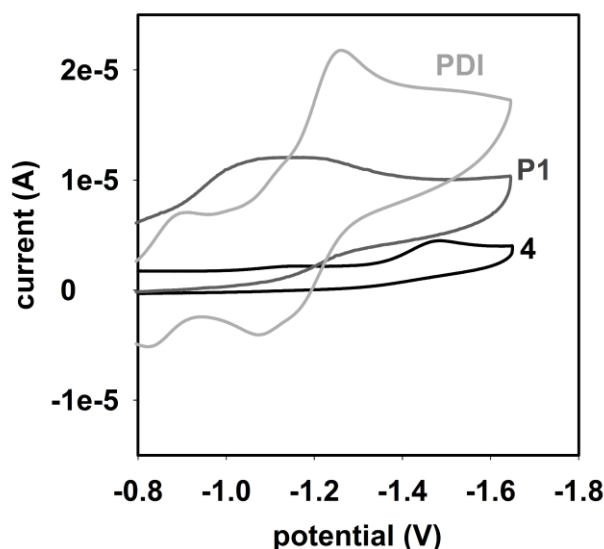
monomer, and separately to a solution containing only **PDI**, and observed no polymer. We then combined **PDI** and **4** with zinc foil (the material for the sacrificial electrode) with no applied current, and again observed no polymer. The control experiments suggest that **P1** forms through an indirect electrocatalytic mechanism.

Scheme 4.4. Electrocatalytic reaction for polymerizing **4** with constant applied current



Following the successful polymerization, we isolated the polymer (**P1**) and compared **4**, **P1**, and **PDI** using cyclic voltammetry (Figure 4.2). We observed that **PDI** and **P1** are reduced at potentials of -0.9 V and -1.1 V, respectively, while monomer requires a potential of -1.5 V. These differences in potential inspired us to target chain growth by applying a constant potential, rather than constant current, to selectively reduce **PDI** and **P1**. To initiate the polymerization, we first applied a high potential of -2.9 V (the potential of the solution that was measured during the constant current experiment, Appendix 3), then reduced the potential to -1.1 V. This method did not produce any observable polymer, suggesting that initiation may be difficult to induce or propagation requires a higher potential. We observed no polymer when we repeated the constant current method using a divided cell, where the zinc counter electrode was separated from the reaction mixture by a frit (Appendix 3), suggesting a possible non-innocent role of zinc in the polymerization. Doubling the reaction time for the constant current reaction gave highly insoluble material, which may suggest we synthesized a polymer with an M_n above the solubility limit for GPC analysis.

Figure 4.2. Cyclic voltammetry curves for **4**, **P1** and **PDI** (relative to Ag/Ag⁺ reference electrode).

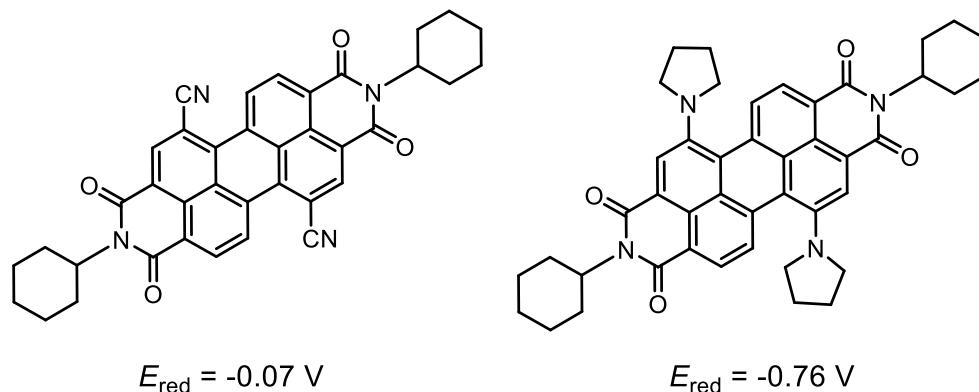


Conclusions and Future Directions

Polymer forming only when electrolysis is combined with mediator and monomer is a promising first step for chain-growth polymerization of conjugated polymers with electrocatalysis. The relationship between reaction time or the amount of charge passed and M_n would provide greater insight into the mechanism, but the insolubility of **P1** limits characterization of larger polymers. Therefore, future efforts should focus on polymerizing other, more soluble, electron-deficient monomers. Our observation that **1** and **3** can rapidly form radicals with Grignard activation shows that both monomers can accept electrons, and so could be explored further under reductive electrocatalytic conditions. Other monomers will likely require different mediators for optimal catalysis. Modified perylene diimide structures are expected to be optimal mediators. Straightforward syntheses have been developed to alter perylene diimide core structures by adding electron-donating or electron-withdrawing groups, which can significantly change the reduction potential.²⁸ While several other organic mediators have been reported for indirect reductive dehalogenation of various compounds, including quinoxilane for vinyl halides,²⁹ and pyrene, anthracene, and fluoranthene for bromoesters,³⁰ all have reported reduction potentials higher than -1.5 V.^{30,31} To reduce these mediators, the reaction would require potentials negative enough to reduce electron-deficient monomers, making them

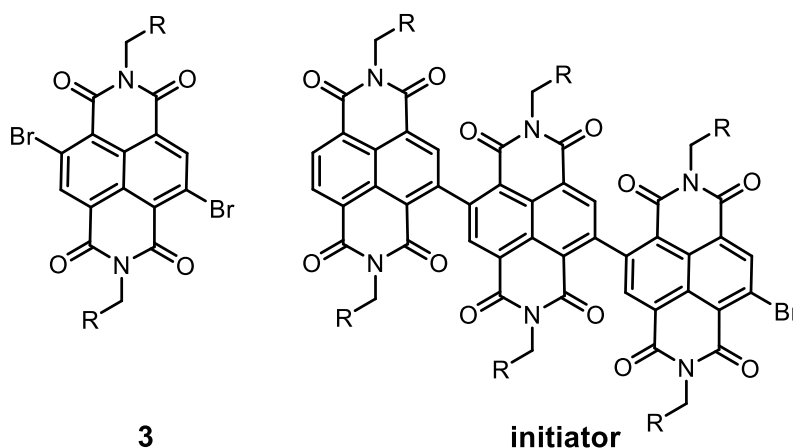
less selective for reducing polymer over monomer. Transition metal mediators such as nickel³² and cobalt³³ have also been reported, but could undergo step-growth polymerization via oxidative addition into monomer followed by cathodic reduction. Cyclic voltammetry can help select an appropriate mediator based on reduction potentials of monomer and polymer.

Chart 4.2. PDI derivatives to screen as mediators (E_{red} relative to SCE) ^{28b,c}



The failure of the constant potential experiment suggests that initiation may be a challenge for these polymerizations. An external initiator could be used instead of relying on high potentials to induce spontaneous initiation. A dimer or trimer of the desired monomer would be expected to have a lower reduction potential, and therefore could initiate the reaction at a lower potential. Combining an external initiator (Figure 4.3) with gradual monomer addition could further ensure that polymerization is initiated in a targeted manner.

Figure 4.3. Proposed initiator for polymerizing **3**



After selecting a monomer, mediator, and initiator, spectroelectrochemistry could be used to analyze mediator, initiator, and monomer reduction, separately and combined, under both constant current and constant potential reaction conditions, to better understand the potential and reaction time required to initiate the reaction. Reduction of perylene diimides has been observed using in situ UV-vis spectroscopy.²⁶ In situ EPR spectroscopy has also been used to observe electrochemical processes such as thiophene oxidation and dimerization at room temperature.³⁴ To summarize, we have shown that we can synthesize one conjugated polymer through an electrocatalytic process. Future work will focus on expanding the scope by synthesizing soluble polymers through optimizing the mediator and initiator, guided by a mechanistic understanding of the reaction.

References

- (1) (a) Todd, A.D.; Bielawski, C.W. Controlled Synthesis of an Alternating Donor–Acceptor Conjugated Polymer via Kumada Catalyst-Transfer Polycondensation *ACS Macro Lett.* **2015**, *4*, 1254–1258. (b) Bridges, C.R.; McCormick, T.M.; Gibson, G.L.; Hollinger, J.; Seferos, D.S. Designing and Refining Ni(II)diimine Catalysts Toward the Controlled Synthesis of Electron-Deficient Conjugated Polymers *J. Am. Chem. Soc.* **2013**, *135*, 13212–13219. (c) Duck, B.C.; Dastoor, P.C.; Rasmussen, M.C. Poly(2,3-dihexylthieno[3,4-b]pyrazine) via GRIM Polymerization: Simple Preparation of a Solution Processable, Low-Band-Gap Conjugated Polymer *Macromolecules* **2008**, *41*, 4576–4578.
- (2) For recent examples with power conversion efficiency over 5%, see: (a) Cai, M.; Xichang Bao, X.; Wang, X.; Zhang, H.; Qiu, M.; Yang, R.; Yang, C.; Wan, X. From Isoindigo to Dibenzonaphthyridinedione: A Building Block for Wide-Bandgap Conjugated Polymers with High Power Conversion Efficiency *Chem. Mater.* **2016**, *28*, 6196–6206. (b) Zhu, L.; Wang, M.; Li, B.; Jiang, C.; Li, Q. High Efficiency Organic Photovoltaic Devices Based on Isoindigo Conjugated Polymers with a Thieno[3,2-b]thiophene p-Bridge *J. Mater. Chem. A* **2016**, *4*, 16064–16072. (c) Fan, Q.; Su, W.; Guo, X.; Guo, B.; Li, W.; Zhang, Y.; Wang, K.; Zhang, M.; Li, Y. A New Polythiophene Derivative for High Efficiency Polymer Solar Cells with PCE over 9% *Adv. Energy Mater.* **2016**, *6*, 1600430 (d) Casey, A.; Green, J.P.; Tuladhar, P.S.; Kirkus, M.; Han, Y.; Anthopoulos, T.D.; Heeney, M. *J. Mater. Chem. A* Cyano Substituted Benzotriazole Based Polymers for Use in Organic Solar Cells **2017**, *5*, 6465–6470. (e) Hwang, J.; Park, J.; Kim, Y.J.; Ha, Y.H.; Park, C.E.; Chung, D.S.; Kwon, S.-K.; Kim, Y.-H. Indolo[3,2-b]indole-Containing Donor–Acceptor Copolymers for High-Efficiency Organic Solar Cells *Chem. Mater.* **2017**, *29*, 2135–2140. (Note: Suzuki, not Stille, conditions were used, but the

polymerization was step-growth) (f) Zhang, Z.; Lu, Z.; Zhang, J.; Liu, Y.; Feng, S.; Wu, L.; Hou, R.; Xu, X.; Bo, Z. High Efficiency Polymer Solar Cells Based on Alkylthio Substituted Benzothiadiazole-Quaterthiophene Alternating Conjugated Polymers *Organic Electronics* **2017**, *40*, 36–41. (g) Hea, D.; Qiu, L.; Yuana, J.; Zhang, Z-H.; Lib, Y.; Zou, Y. Synthesis and Photovoltaic Properties of Alkylthio Phenyl Substituted Benzodifuran (BDF)-Based Conjugated Polymers *Synth. Met.* **2017**, *226*, 31–38. (h) Liuyuan, L.; Zhiming, C.; Qin, H.; Lei, Y.; Rui, Z.; Feng, L.; Thomas P., R.; Fei, H.; Yong, C. High-Performance Polymer Solar Cells Based on a Wide-Bandgap Polymer Containing Pyrrolo[3,4-f]benzotriazole-5,7-dione with a Power Conversion Efficiency of 8.63% *Adv. Sci.* **2016**, *3*, 1600032. (i) Bang, S.-M.; Kang, S.; Lee, Y.-S.; Lim, B.; Heo, H.; Lee, J.; Lee, Y.; Na, S.-I. A Novel Random Terpolymer for High-Efficiency Bulk-Heterojunction Polymer Solar Cells *RSC Adv.* **2017**, *7*, 1975–1980. (j) Tao, Q.; Liu, T.; Duan, L.; Cai, Y.; Xiong, W.; Wang, P.; Tan, H.; Lei, G.; Pei, Y.; Zhu, W.; Yang, R.; Sun, Y. Wide Bandgap Copolymers with Vertical Benzodithiophene Dicarboxylate for High Performance Polymer Solar Cells with an Efficiency up to 7.49% *J. Mater. Chem. A* **2016**, *4*, 18792–18803. (k) Wei, H.; Chao, Y.-H.; Kang, C.; Li, C.; Lu, H.; Gong, X.; Dong, H.; Hu, W.; Hsu, C.-S.; Bo, Z. High-Efficiency Large-Bandgap Material for Polymer Solar Cells *Macromol. Rapid Commun.* **2015**, *36*, 84–89. (l) Constantinou, I.; Lai, T.-H.; Zhao, D.; Klump, E. D.; Deininger, J. J.; Lo, C. K.; Reynolds, J. R.; So, F. High Efficiency Air-Processed Dithienogermole-Based Polymer Solar Cells *ACS Appl. Mater. Interfaces*, **2015**, *7*, 4826–4832. (m) Lin, Y.; Zhao, F.; He, Q.; Huo, L.; Wu, Y.; Parker, T.C.; Ma, W.; Sun, Y.; Wang, C.; Zhu, D.; Heeger, A. J.; Marder, S. R.; Zhan, X. High-Performance Electron Acceptor with Thienyl Side Chains for Organic Photovoltaics *J. Am. Chem. Soc.* **2016**, *138*, 4955–4961. (n) Huo, L.; Liu, T.; Fan, B.; Zhao, Z.; Sun, X.; Wei, D.; Yu, M.; Liu, Y.; Sun, Y. *Adv. Mater.* Organic Solar Cells Based on a 2D Benzo[1,2-b:4,5-b']-difuran-Conjugated Polymer with High-Power Conversion Efficiency **2015**, *27*, 6969–6975.

(3) Smith, M.L.; Leone, A.K.; Zimmerman, P.M.; McNeil, A.J. Impact of Preferential π -Binding in Catalyst-Transfer Polycondensation of Thiazole Derivatives *ACS Macro Lett.* **2016**, *5*, 1411–1415.

(4) Editors: Matyjaszewski, K.; Sumerlin, B.S.; Tsarevsky, N.V.; Chiefari, J.; *Controlled Radical Polymerization: Mechanisms*; American Chemical Society: Washington, DC., 2014.

(5) Cowie, J.M.G.; Arrighi, V. *Controlled Radical Polymerization: Mechanisms*; American Chemical Society: Washington, D.C. 2015.

(6) Murarka, S.; Mobus, J.; Erker, G.; Muck-Lichtenfeld, C.; Studer, A. TEMPO-Mediated Homocoupling of Aryl Grignard Reagents: Mechanistic Studies *Org. Biomol. Chem.* **2015**, *13*, 2762–2767.

(7) Murarka, S.; Studer, A. Radical/Anionic $S_{RN}1$ -Type Polymerization for Preparation of Oligoarenes *Angew. Chem. Int. Ed.* **2012**, *51*, 12362–12366.

(8) Heine, N. B.; Studer, A. Poly(paraphenylene sulfide) and Poly(metaphenylene sulfide) via Light-Initiated $S_{RN}1$ -Type Polymerization of Halogenated Thiophenols *Macromol. Rapid Commun.* **2016**, *37*, 1494–1498.

(9) (a) Li, W.; Yang, L.; Tumbleston, J. R.; Yan, L.; Ade, H.; You, W. Controlling Molecular Weight of a High Efficiency Donor-Acceptor Conjugated Polymer and Understanding Its Significant Impact on Photovoltaic Properties *Adv. Mater.* **2014**, *26*, 4456–4462. (b) Liu, C.; Wang, K.; Hu, X.; Yang, Y.; Hsu, C. H.; Zhang, W.; Xiao, S.; Gong, X.; Cao, Y. Molecular Weight Effect on the Efficiency of Polymer Solar Cells *ACS Appl. Mater. Interfaces* **2013**, *5*, 12163–12167. (c) Chu, T.-Y.; Lu, J.; Beaupré, S.; Zhang, Y.; Pouliot, J.-R.; Zhou, J.; Najari, A.; Leclerc, M.; Tao, Y. Effects of the Molecular Weight and the Side-Chain Length on the Photovoltaic Performance of Dithienosilole/Thienopyrrolodione Copolymers *Adv. Funct. Mater.* **2012**, *22*, 2345–2351. (d) Schilinsky, P.; Asawapirom, U.; Scherf, U.; Biele, M.; Brabec, C. Influence of the Molecular Weight of Poly(3-hexylthiophene) on the Performance of Bulk Heterojunction Solar Cells *Chem. Mater.* **2005**, *17*, 2175–2180.

(10) Malhotra, B.D.; Kumar, N.; Chandra, S. Recent studies of Heterocyclic and Aromatic Conducting Polymers *Prog. Polym. Sci.*, **1986**, *12*, 179–218.

(11) Shiraka, E.; Hayashi, T. Transition-metal-free Coupling Reactions of Aryl Halides *Chem. Lett.* **2012**, *41*, 130–134.

(12) (a) Pammer, F.; Passlack, U. Head-to-Tail Regioregular Polythiazole Prepared via Kumada-Coupling Polycondensation *ACS Macro Lett.* **2014**, *3*, 170-174. (b) Pammer, F.; Jager, J.; Rudolf, B.; Sun, Y. Soluble Head-to-Tail Regioregular Polythiazoles: Preparation, Properties and Evidence for Chain-Growth Behaviour in the Synthesis via Kumada-Coupling Polycondensation *Macromolecules* **2014**, *47*, 5904–5912.

(13) (a) Zoombelt, A.P.; Mathijssen, S.G.J.; Turbiez, M.G.R.; Wienk, M.M.; Janssen, R. A. J. Small Band Gap Polymers Based on Diketopyrrolopyrrole *J. Mater. Chem.* **2010**, *20*, 2240–2246. (b) Qu, S.; Tian, H. Diketopyrrolopyrrole (DPP)-Based Materials for Organic Photovoltaics *Chem. Commun.*, **2012**, *48*, 3039–3051 (c) Yi, Z.; Wang, S.; Liu, Y.; Design of High-Mobility Diketopyrrolopyrrole-Based π -Conjugated Copolymers for Organic Thin-Film Transistors *Adv. Mater.*, **2015**, *27*, 3589–3606.

(14) (a) Yi, H.; Al-Faifi, S.; Iraqi, A.; Watters, D. C.; Kingsley, J.; Lidzey, D. G. Carbazole and Thienyl Benzo[1,2,5]thiadiazole Based Polymers with Improved Open Circuit Voltages and Processability for Application in Solar Cells *J. Mater. Chem.* **2011**, *21*, 13649–13656 (b) Lee, W.; Cha, H.; Kim, Y. J.; Jeong, J.-E.; Hwang, S.; Park, C. E.; Woo, H. Y. Amorphous Thieno[3,2-b]thiophene and Benzothiadiazole Based Copolymers for Organic Photovoltaics *ACS Applied Materials & Interfaces* **2014**, *6*, 20510–20518 (c) Lee, W.; Choi, H.; Hwang, S.; Kim, J. Y.; Woo, H. Y. Efficient Conventional- and Inverted-Type Photovoltaic Cells Using a Planar Alternating Polythiophene Copolymer *Chem. Eur. J.* **2012**, *18*, 2551–2558.

- (15) Sommer, M. Conjugated Polymers Based on Naphthalene Diimide for Organic Electronics *J. Mater. Chem. C* **2014**, *2*, 3088–3098.
- (16) Senkovskyy, V.; Tkachov, R.; Komber, H.; Sommer, M.; Heuken, M.; Voit, B.; Huck, W. T. S.; Kataev, V.; Petr, A.; Kiriya, A. Chain-Growth Polymerization of Unusual Anion-Radical Monomers Based on Naphthalene Diimide: A New Route to Well-Defined n-Type Conjugated Copolymers *J. Am. Chem. Soc.* **2011**, *133*, 19966–19970.
- (17) Shirakawa, E.; Hayashi, Y.; Itoh, K.-I.; Watabe, R.; Uchiyama, N.; Konagaya, W.; Masui, S.; Hayashi, T. Cross-Coupling of Aryl Grignard Reagents with Aryl Iodides and Bromides through S_{RN}1 Pathway *Angew. Chem. Int. Ed.* **2012**, *51*, 218–221.
- (18) (a) Tourillon, G.; Garnier, F. New Electrochemically Generated Organic Conducting Polymers *J. Electroanal. Chem.* **1982**, *135*, 173–178. (b) Lazzaroni, R.; De Pryck, A.; Debaisieux, C.; Riga, J.; Verbist, J. Electronic Structure of Conducting Polymers from Heteroaromatic Bicyclic Compounds *Synth. Met.* **1987**, *21*, 189–195. (c) Danieli, R.; Taliani, C.; Zamboni, R. Optical, Electrical and Electrochemical Characterization of Electrosynthesized Polythieno(3,2-b)thiophene *Synth. Met.* **1986**, *13*, 325–328. (d) Diaz, A.F.; Kanazawa, K.K.; Gardini, G.P. Electrochemical Polymerization of Pyrrole *J. Chem. Soc., Chem. Commun.* **1979**, *14*, 635–636. (e) Ohsaka, T.; Ohnuki, Y.; Oyama, N. IR Absorption Spectroscopic Identification of Electroactive and Electroinactive Polyaniline Films Prepared by the Electrochemical Polymerization of Aniline *J. Electroanal. Chem.* **1984**, *161*, 399–405.
- (19) Xu, Z.; Horowitz, G.; Garnier, F. Cathodic Electropolymerization of Polythiophene on Platinum and Various Semiconducting Electrodes. *J. Electroanal. Chem. Interfacial Electrochem.* **1988**, *246*, 467–472.
- (20) Fauvarque, J-F.; Petit, M-A.; Pfluger, F.; Jutand, A.; Chevrot, C.; Troupel, M. Preparation of Poly(1,4-phenylene) by Nickel(0) Complex Catalyzed Electropolymerization *Macromol. Chem. Rapid Commun.* **1983**, *4*, 455–457.
- (21) Zotti, G.; Schiavon, G.; Comisso, N. Electrochemical Synthesis and Characterization of Polyconjugated Polyfuran *Synth. Met.* **1990**, *36*, 337–351.
- (22) Schiavon, G.; Zotti, G. Anodic and Cathodic Deposition of Electroactive Polyfluorene Films: A Comparison Between the Two Methods *J. Electroanal. Chem.* **1985**, *186*, 191–199.
- (23) Zecchin, S.; Schiavon, G.; Tomat, R.; Zotti, G. Redox Polymer Films from Cathodic Coupling of 4,4'-Dibromobenzophenone and 2,7-Dibromofluorenone *J. Electroanal. Chem.* **1986**, *215*, 377–383.

- (24) Tomat, R.; Zecchin, S.; Shiavon, G.; Zotti, G. 2,6-Polynaphthylene Films from Cathodic Coupling of an Organonickel(II) Complex of 2,6-Dibromonaphthalene *J Electroanal. Chem.* **1988**, *252*, 215–219.
- (25) Alcock, N.W.; Bartlett, P.N.; Eastwick-Field, V.M.; Pike, G.A.; Pringle, P.G. Reinvestigation of the Nickel Phosphine Catalysed Electrochemical Synthesis of Poly(2,5-pyridine). X-Ray Crystal Structures of $[\text{Ni}_2\text{Br}_2(\mu\text{-5-BrC}_5\text{H}_3\text{N-C}^2\text{,N})_2(\text{PPh}_3)_2]$ and $[\text{PtBr}(5\text{-BrC}_5\text{H}_3\text{N-C}^2)(\text{PPh}_3)_2]$ *J. Mater. Chem.* **1991**, *1*, 569–576.
- (26) Sun, G.; Ren, S.; Zhu, X.; Huang, M.; Wan, Y. Direct Arylation of Pyrroles via Indirect Electroreductive C–H Functionalization Using Perylene Bisimide as an Electron-Transfer Mediator *Org. Lett.* **2016**, *18*, 544–547.
- (27) Yokoyama, A.; Yokozawa, T. Converting Step-Growth to Chain-Growth Condensation Polymerization *Macromolecules* **2007**, *40*, 4093–4101.
- (28) (a) Huang, C.; Barlow, S.; Marder, S.R. Perylene-3,4,9,10-tetracarboxylic Acid Diimides: Synthesis, Physical Properties, and Use in Organic Electronics *J. Org. Chem.* **2011**, *76*, 2386–2407. (b) Zhao, Y.; Wasielewski, M. R. 3,4:9,10-Perylenebis(dicarboximide) Chromophores that Function as Both Electron Donors and Acceptors *Tetrahedron Lett.* **1999**, *40*, 7047–7050. (c) Jones, B. A.; Facchetti, A.; Wasielewski, M. R.; Marks, T. J. Tuning Orbital Energetics in Arylene Diimide Semiconductors. Materials Design for Ambient Stability of n-Type Charge Transport *J. Am. Chem. Soc.* **2007**, *129*, 15259–15278.
- (29) Gatti, N.; Jugelt, W.; Lund, H. Indirect Electrochemical Reduction of Vinyl Halides and Related Compounds *Acta Chimica Scandinavica A* **1987**, *41*, 646–652.
- (30) Inesi, A. J. Indirect Reduction of Bromoesters: The Catalytic Efficiency Related to the Structure and Reactivity of the Intermediates *Electroanal. Chem. Interfacial Electrochem.* **1984**, *165*, 293–297.
- (31) Crawford, P.W.; Scamehorn, R.G.; Hollstein, U.; Ryan, M.D.; Kovacic, P. Cyclic Voltammetry of Phenazines and Quinoxalines Including Mono- and Di-N-oxides. Relation to Structure and Antimicrobial Activity *Chem. Biol. Interact.* **1986**, *60*, 67–82
- (32) Ozaki, S.; Matsushita, H.; Ohmori, H. Indirect Electroreductive Radical Cyclization of Halogeno Ethers Using Nickel(II) Complexes as Electron-Transfer Catalysts *J. Chem. Soc., Chem. Commun.* **1992**, 1120–1122.
- (33) Páramo-Garcío, U.; Ávila-Rodríguez, M.; García-Jiménez, M. G.; Gutiérrez-Granados, S.; Ibáñez-Cornejo, J. G. Electrochemical Reduction of Hexachlorobenzene with Co(II)Salen as Catalyst *Electroanalysis* **2006**, *18*, 904–910.

(34) Rapta, P.; Dmitrieva, E.; Popov, A.A.; Dunsch, L. In Situ Spectroelectrochemistry of Organic Compounds. In *Organic Electrochemistry, Fifth Edition*; Hammermich, O.; Speiser B., Ed.; CRC: Boca Raton, FL, 2015; pp 169–190.

Chapter 5

Conclusions

While catalyst-transfer polymerization has enhanced the field of conjugated polymer synthesis by enabling targeted molecular weight (M_n), dispersity (\mathcal{D}), and sequence, it still has several limitations. This thesis first describes our efforts to overcome slow precatalyst initiation. While precatalysts, which contain reactive ligands that react during the first monomer turnover, can promote sequence control and introduce functional end-groups,¹ they can also have slow initiation which can lead to polymers with broad \mathcal{D} and undesired sequences. A greater challenge is the monomer scope: 13 years after the discovery of CTP,² there are still limited examples of electron-deficient conjugated polymers with narrow \mathcal{D} and high M_n .³ In this work, we designed fast-initiating precatalysts, and in the process gained insight into the effect of fluorine tags and additives on initiation rates. Our efforts to expand CTP monomer scope to phenylene-ethynylene also provided information about the flaws of a commonly used dicoupling model system. Finally, we developed an indirect electrocatalytic polymerization as a step towards a new chain-growth polymerization of conjugated polymers.

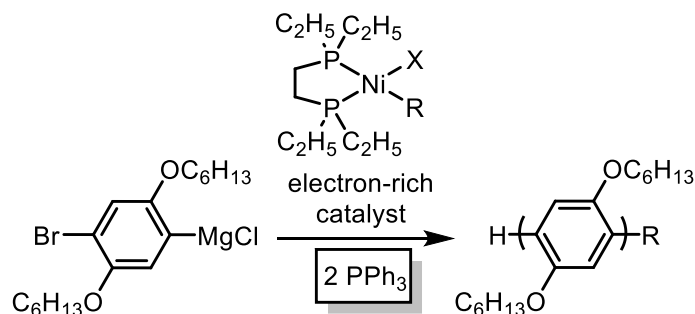
Chapter 2 describes our efforts to design a fast-initiating precatalyst for phenylene polymerization. While carrying out this goal, we developed an improved method to measure initiation rates during a reaction by in situ IR spectroscopy. This method could be applied to other reactions which utilize precatalysts where the reactants and product have distinct IR signals. Nickel and palladium precatalysts have been used in a variety of cross-couplings, including Suzuki,^{4,5} Negishi,⁶ Sonogashira,⁶ Kumada,⁶ and Heck,⁶ as well as other reactions including aminations⁷ and carbonyl-ene reactions.⁸ Nova and coworkers recently reported a comparison of activation rates for Pd-NHC precatalysts with different allyl reactive ligands that are commonly used in Suzuki reactions.⁹ They developed a complex model using ¹H NMR spectroscopy to measure precatalyst activation with base, which used a divinyl siloxane species as a Pd(0) trap as well as a

crown ether to solubilize the base. While NMR spectroscopy provided detailed structural information about the metal species present in a reaction, we have found that using additives can alter the rates. In contrast, for studies comparing precatalysts, our IR methodology would enable measurement of catalyst activation rates during a Suzuki reaction, streamlining the rate studies and enabling measurement of rates under authentic conditions.

In chapter 2, we also found that the fluorine tag installed for spectroscopic rate measurements also decreased initiation rate, suggesting that caution is needed when extrapolating rates from fluorinated systems to non-fluorinated systems. Our group has previously reported initiation rates in CTP using fluorine tags.¹⁰ Espinet and coworkers have also used fluorinated arenes to conduct detailed rate studies and propose mechanisms in Stille coupling.¹¹ They measured transmetalation rates by ¹⁹F NMR spectroscopy using 3,5-dichloro-2,4,6-trifluoro-1-iodobenzene and vinyl stannanes and concluded that transmetalation occurred via an associated mechanism with a 5-coordinate transition state, rather than a previously proposed dissociative mechanism wherein a ligand dissociated from Pd prior to transmetalation. The strongly electron-withdrawing nature of the fluorinated arene, however, could inhibit ligand dissociation that may occur if an electron-rich arene were used. Going forward, we now have a method to measure initiation rates for new catalysts without relying on electron-withdrawing fluorine groups as spectroscopic tags.

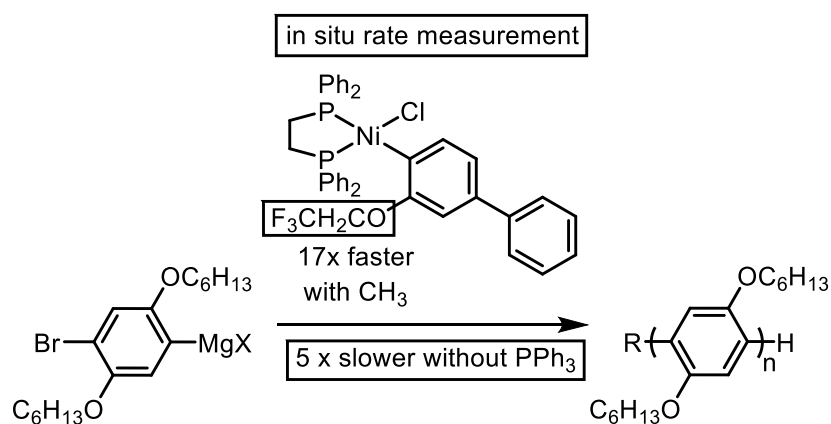
We also discovered that triphenylphosphine (PPh₃) enhanced initiation rate. Several examples of CTP use precatalysts that are generated in situ from Ni-PPh₃ complexes¹² or Pd-NHC¹³ and Ni-NHC¹⁴ precatalysts that are stabilized by labile pyridine or phosphine ligands. Our work suggests these labile ligands may have significant rate effects which should be examined further. Computational studies have found that the labile 3-chloropyridine ligand affects both initiation and propagation rates in CTP for thiophene with Pd-NHC catalysts.¹⁵ Additive rate effects could be explored to enhance rates with slow catalysts. Our group has found that while electron-rich ancillary ligands suppress side reactions in CTP, giving polymers with narrow Đ, they also decrease polymerization rate (Scheme 5.1).^{7,16} Combining labile ligands with electron-rich catalysts might accelerate rates while maintaining narrow Đ.

Scheme 5.1. Fast initiation and narrow dispersity could be achieved with electron-rich catalysts and triphenylphosphine



Finally, Chapter 2 provides a template for future catalyst design. We found that fast initiation occurs when the reactive ligand resembles the polymer; in this case, biphenyl reactive ligands showed faster initiation than monoaryl ligands. This suggests a simple strategy for improving initiation rates in other polymerizations: designing a precatalyst with a dimer-like reactive ligand.

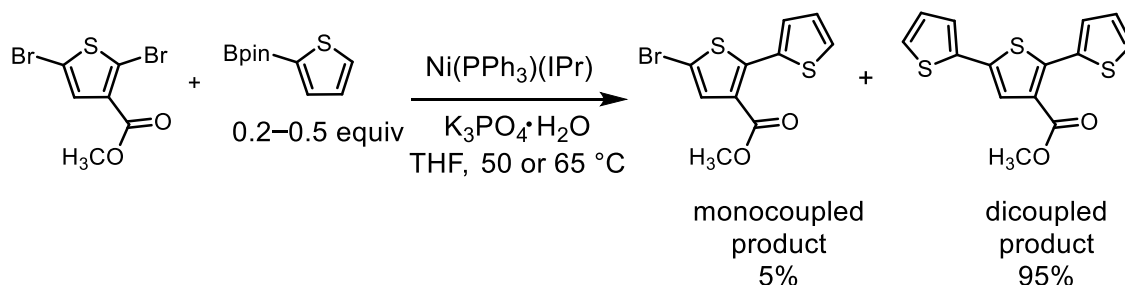
Scheme 5.2. Summary of results for Chapter 2



Chapter 3 describes the limitations of small-molecule catalyst screens, models which are used for identifying CTP conditions.^{2b,17,18} We observed that false positives can arise from reactivity differences between substrates in a model system, and propose a second experiment to probe more deeply for evidence of a π -complex. Noonan and coworkers recently used a similar model to identify catalysts for polymerizing an ester-substituted thiophene by comparing ratios of monocoupled and dicoupled products (Scheme 5.3).¹⁸ Inspired by our results, after observing selective dicoupling with Ni-NHCs, they altered the reaction conditions which could affect the rate (temperature and

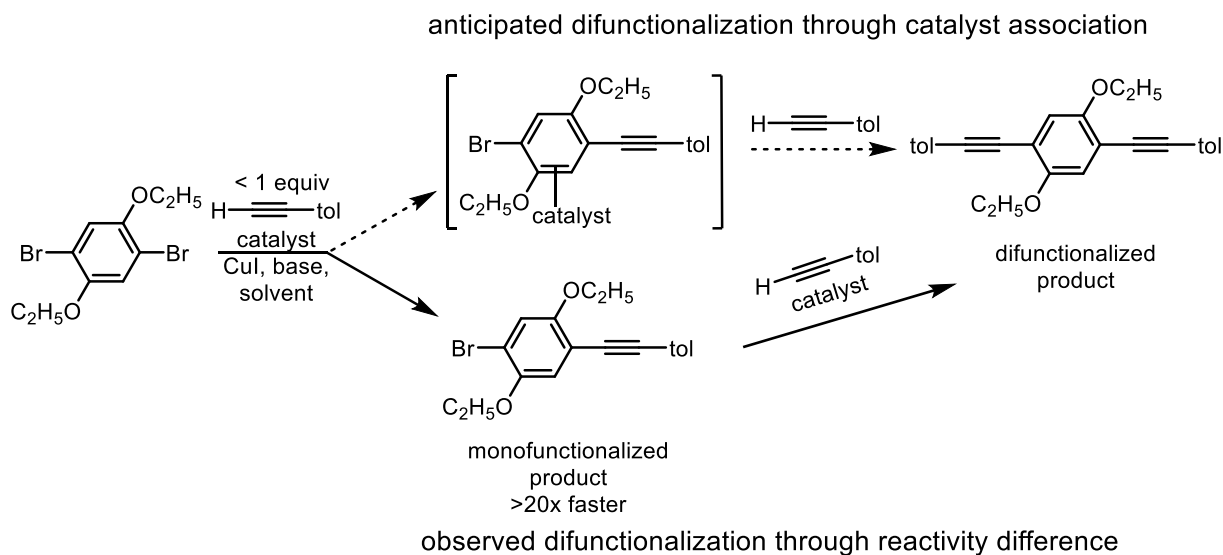
ratio of coupling partners). They observed similar di:mono ratios at all conditions, suggesting that rate differences were unlikely to be the cause of the selective dicoupling. This example highlights our work has led others to reexamine and improve model systems for identifying CTP conditions.

Scheme 5.3. Small-molecule screen reported by Noonan and coworkers.¹⁸



As we and others continue to use small-molecule cross coupling to identify catalysts for CTP, these more informative screens will be better guides for identifying chain-growth conditions (Scheme 5.4).

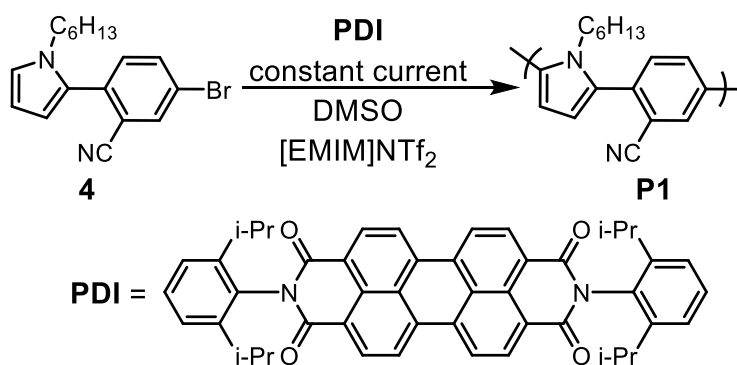
Scheme 5.4. Summary of results and future implications for Chapter 3



Chapter 4 describes our efforts to expand the scope of chain-growth polymerizations of electron-deficient π -conjugated polymers using single-electron reactions. Inspired by previous results,¹⁹ we first attempted to expand the scope of $\text{S}_{\text{RN}}1$ polymerizations. While we successfully induced radical formation with several monomers, we did not obtain polymers. We next targeted indirect electrocatalysis as a new route to

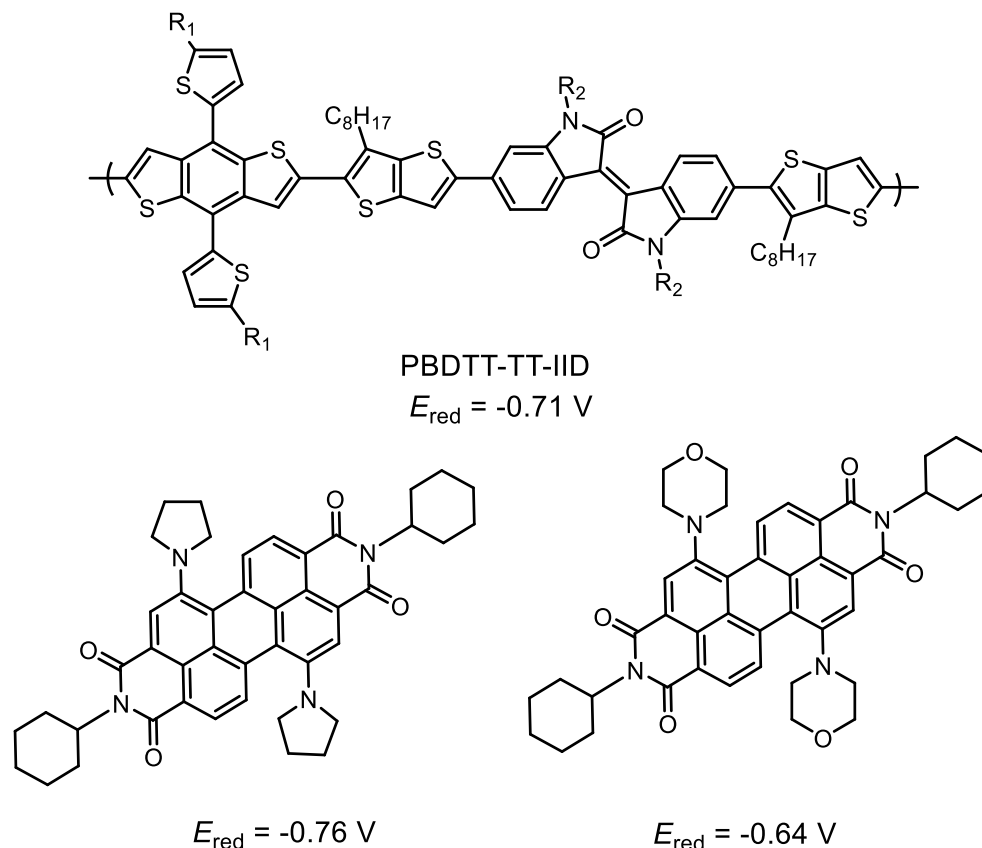
chain-growth polymerizations of conjugated polymers and successfully polymerized one phenyl-pyrrole monomer. Importantly, control reactions show that mediator is required for the polymerization to occur, providing evidence for indirect electrocatalysis. We were unable to definitively characterize larger polymers due to low solubility, so future efforts will target more soluble polymers. Although the polymer had a broad \bar{M}_n and low M_n , optimizing mediators and using external initiators could lead to chain-growth with other monomers. Modifying the reaction setup by using a rotating-disk electrode could also improve control by controlling steady-state current through controlled solution flow-rate.²⁰

Scheme 5.5. Results for Chapter 4: indirect electrocatalytic polymerization



The future of this project should focus on developing electrocatalysis for synthesizing high-performing polymers for organic photovoltaics, which are still made through step-growth methods. A logical next step is to target polymers difficult to polymerize with CTP. For example, Koeckelberghs and coworkers report trapping of Ni(0) by thienothiophene,²¹ a structure present in several high-performing polymers.²² Li and coworkers report organic photovoltaic devices with a benzodithiophene-thienothiophene-isoindigo (PBDTT-TT-IID) polymer have a high PCE of 8.05% (Chart 5.1). The polymer had a reduction potential of -0.71 V (versus a saturated calomel electrode, SCE),^{22f} which is similar to the reduction potentials of two substituted perylene diimides²³ (versus SCE) (Chart 5.1). The similar reduction potentials mean that these PDI derivatives may be effective mediators for this polymerization.

Chart 5.1. Efficient thienothiophene polymer for photovoltaics^{22f} and proposed mediators for indirect electropolymerization²³



Organic π -conjugated polymers are useful materials for electronic applications such as organic photovoltaic devices.²⁴ This work has aimed to solve two problem in conjugated polymer synthesis: slow precatalyst initiation and limited monomer scope. In chapter 2, we designed a precatalyst with a reactive ligand resembling the polymer to achieve initiation that was faster than propagation. We also developed an in situ method for measuring precatalyst initiation rates, and discovered rate effects of triphenylphosphine and fluorinated groups. These results inform future precatalyst design to accelerate initiation with other monomers. The initiation rate enhancement we observed with triphenylphosphine could also be used to enhance rates for slow catalysts. Finally, the in situ rate measurement method could be expanded to other reactions utilizing precatalysts. Our efforts to identify CTP conditions for phenylene-ethynylene led us to discover a flaw in the design of commonly used model system, which has led others to modify their own model systems. Finally, in chapter 4 we explored non-CTP routes to

develop new chain-growth polymerizations for electron-deficient monomers. While we could not induce $S_{RN}1$ polymerizations, we successfully synthesized a conjugated polymer through indirect electrocatalysis, a promising first step for using indirect electrocatalysis to synthesize conjugated polymers. Future efforts should focus on optimizing the method to achieve chain-growth and expanding the scope to synthesize high-performing conjugated polymers.

References

- (1) Van den Bergh, K.; Willot, P.; Cornelis, D.; Verbiest, T.; Koeckelberghs, G. Influence of the Presence and Length of an Alkyl Spacer on the Supramolecular Chirality of Block Copoly(thiophene)s *Macromolecules* **2011**, *44*, 728–735. (b) Smeets, A.; Van den Bergh, K.; De Winter, J.; Gerbaux, P.; Verbiest, T.; Koeckelberghs, G. Incorporation of Different End Groups in Conjugated Polymers Using Functional Nickel Initiators *Macromolecules* **2009**, *42*, 7638–7641. (c) Smeets, A.; Willot, P.; De Winter, J.; Gerbaux, P.; Verbiest, T.; Koeckelberghs, G. End Group-Functionalization and Synthesis of Block-Copolythiophenes by Modified Nickel Initiators *Macromolecules* **2011**, *44*, 6017–6025.
- (2) (a) Yokoyama, A.; Miyakoshi, R.; Yokozawa, T. Chain-Growth Polymerization for Poly(3-hexylthiophene) with a Defined Molecular Weight and a Low Polydispersity *Macromolecules*, **2004**, *37*, 1169–1171. (b) Sheina, E.E.; Liu, J.; Iovu, M.C.; Laird, D.W.; McCullough, R.D Chain Growth Mechanism for Regioregular Nickel-Initiated Cross-Coupling Polymerizations *Macromolecules* **2004**, *37*, 3526–3528.
- (3) Recent examples of CTP with electron-poor monomers: (a) Todd, A.D, Bielawski, C.W. Controlled Synthesis of an Alternating Donor–Acceptor Conjugated Polymer via Kumada Catalyst-Transfer Polycondensation *ACS Macro Lett.* **2015**, *4*, 1254–1258. (b) Bridges, C.R., McCormick, T.M., Gibson, G.L., Hollinger, J., Seferos, D.S. Designing and Refining Ni(II)diimine Catalysts Toward the Controlled Synthesis of Electron-Deficient Conjugated Polymers *J. Am. Chem. Soc.* **2013**, *135*, 13212–13219. (c) Duck, B.C.; Dastoor, P.C.; Rasmussen, M.C. Poly(2,3-dihexylthieno[3,4-b]pyrazine) via GRIM Polymerization: Simple Preparation of a Solution Processable, Low-Band-Gap Conjugated Polymer *Macromolecules* **2008**, *41*, 4576–4578.
- (4) (a) Chen, Q.; Fan, X.-H.; Zhang, L.-P.; Yang, L.-M. Nickel-catalyzed Cross-coupling of Carboxylic Anhydrides with Arylboronic Acids *RSC Adv.* **2014**, *4*, 53885–53890 (b) Shields, J.D.; Gray, E.E.; Doyle, A.G. A Modular, Air-Stable Nickel Precatalyst *Org. Lett.* **2015**, *17*, 2166–2169. (c) Malineni, J.; Jezorek, R.L.; Zhang, N.; Percec, V. Ni(II)Cl(1-Naphthyl)(PCy₃)₂, An Air-Stable σ -Ni(II) Precatalyst for Quantitative Cross-Coupling of Aryl C–O Electrophiles with Aryl Neopentylglycolboronates *Synthesis* **2016**, *48*, 2808–2815. (d) Mohadjer Beromi, M.; Nova, A.; Balcells, D.; Brasacchio, A.M.; Brudvig, G.W.; Guard, L.M.; Hazari, N.; Vinyard, D. Mechanistic Study of an Improved Ni

Precatalyst for Suzuki–Miyaura Reactions of Aryl Sulfamates: Understanding the Role of Ni(I) Species *J. Am. Chem. Soc.*, **2017**, *139*, 922–936.

(5) Bastug, G.; Nolan, S.P. [Pd(IPr*^{OMe})(cin)Cl] (cin = Cinnamyl): A Versatile Catalyst for C–N and C–C Bond Formation *Organometallics* **2014**, *33*, 1253–1258.

(6) Magano, J.; Monfette, S. Development of an Air-Stable, Broadly Applicable Nickel Source for Nickel-Catalyzed Cross-Coupling *ACS Catal.* **2015**, *5*, 3120–3123.

(7) (a) Lavoie, C.M.; MacQueen, P.M.; Rotta-Loria, N.L.; Sawatzky, R.S.; Borzenko, A.; Chisholm, A.J.; Hargreaves, B.K.V.; McDonald, R.; Ferguson, M. J.; Stradiotto Challenging Nickel-catalysed Amine Arylations enabled by Tailored Ancillary Ligand Design *Nature Communications* **2016**, *7*, 11073 (b) Park, N.H.; Teverovskiy, G.; Buchwald, S.L. Development of an Air-Stable Nickel Precatalyst for the Amination of Aryl Chlorides, Sulfamates, Mesylates, and Triflates *Org. Lett.* **2014**, *16*, 220–223. (c) Clark, J. S. K.; Lavoie, C. M.; MacQueen, P. M.; Ferguson, M. J.; Stradiotto, M. A Comparative Reactivity Survey of Some Prominent Bisphosphine Nickel(II) Pre-Catalysts in C–N Cross-Coupling *Organometallics* **2016**, *35*, 3248–3254.

(8) Standley, E.A.; Smith, S.J.; Muller, P.; Jamison, T.F. A Broadly Applicable Strategy for Entry into Homogeneous Nickel(0) Catalysts from Air-Stable Nickel(II) Complexes *Organometallics* **2014**, *33*, 2012–2018.

(9) Melvin, R.P.; Balcells, D.; Hazari, N.; Nova, A. Understanding Precatalyst Activation in Cross-Coupling Reactions: Alcohol Facilitated Reduction from Pd(II) to Pd(0) in Precatalysts of the Type (η^3 -allyl)Pd(L)(Cl) and (η^3 -indenyl)Pd(L)(Cl) *ACS Catal.*, **2015**, *5*, 5596–5606

(10) Lee, S. R.; Bryan, Z. J.; Wagner, A. M.; McNeil, A. J. Effect of Ligand Electronic Properties on Precatalyst Initiation and Propagation in Ni-catalyzed Cross-coupling Polymerizations *Chem. Sci.* **2012**, *3*, 1562–1566.

(11) (a) Casado, R.L.; Espinet, P. Mechanism of the Stille Reaction. 1. The Transmetalation Step. Coupling of R¹I and R²SnBu₃ Catalyzed by *trans*-[PdR¹IL₂] (R¹ = C₆Cl₂F₃; R² = Vinyl, 4-Methoxyphenyl; L = AsPh₃) *J. Am. Chem. Soc.* **1998**, *120*, 8978–8985. (b) Casado, R.L.; Espinet, P.; Gallego, A.M. Mechanism of the Stille Reaction. 2. Couplings of Aryl Triflates with Vinyltributyltin. Observation of Intermediates. A More Comprehensive Scheme *J. Am. Chem. Soc.* **2000**, *122*, 11771–11782.

(12) (a) Bronstein, H.A.; Luscombe, C.K. Externally Initiated Regioregular P3HT with Controlled Molecular Weight and Narrow Polydispersity *J. Am. Chem. Soc.* **2009**, *131*, 12894–12895; (b) S. D. Boyd, A. K.-Y. Jen, C. K. Luscombe, Steric Stabilization Effects in Nickel-Catalyzed Regioregular Poly(3-hexylthiophene) Synthesis *Macromolecules* **2009**, *42*, 9387–9389.

- (13) Bryan, Z.J.; Smith, M.L.; McNeil, A.J Chain-growth Polymerization of Aryl Grignards Initiated by a Stabilized NHC-Pd Precatalyst *Macromol Rapid Commun.* **2012**, *33*, 842–847.
- (14) (a) Tamba, S.; Shono, K.; Sugie, A.; Mori, A. C–H Functionalization Polycondensation of Chlorothiophenes in the Presence of Nickel Catalyst with Stoichiometric or Catalytically Generated Magnesium Amide *J. Am. Chem. Soc.* **2011**, *133*, 9700–9703.
- (15) Y. Zhao, A. J. Nett, A. J. McNeil, P. M. Zimmerman Computational Mechanism for Initiation and Growth of Poly(3-hexylthiophene) Using Palladium *N*-Heterocyclic Carbene Precatalysts *Macromolecules* **2016**, *49*, 7632–7641.
- (16) Bryan, Z. J.; McNeil, A. J. Evidence for a Preferential Intramolecular Oxidative Addition in Ni-catalyzed Cross-coupling Reactions and their Impact on Chain-growth Polymerizations. *Chem. Sci.* **2013**, *4*, 1620–1624.
- (17) (a) Nanashima, Y.; Yokoyama, A.; Yokozawa, T. Synthesis of Well-Defined Poly(2-alkoxypyridine-3,5-diyl) via Ni-Catalyst-Transfer Condensation Polymerization *Macromolecules* **2012**, *45*, 2609–2613. (b) Qiu, Y.; Mohin, J.; Tsai, C.-H.; Tristram-Nagle, S.; Gil, R. R.; Kowalewski, T.; Noonan, K. J. T. Stille Catalyst-Transfer Polycondensation Using Pd-PEPPSI-IPr for High-Molecular-Weight Regioregular Poly(3-hexylthiophene) *Macromol. Rapid Commun.* **2015**, *36*, 840–844.
- (18) Qiu, Y.; Worch, J.C.; Fortney, A.; Gayathri, C.; Gil, R.R.; Noonan, K.J.T Nickel-Catalyzed Suzuki Polycondensation for Controlled Synthesis of Ester-Functionalized Conjugated Polymers *Macromolecules* **2016**, *49*, 4757–4762.
- (19) Smith, M.L.; Leone, A.K.; Zimmerman, P.M.; McNeil, A.J. Impact of Preferential π -Binding in Catalyst-Transfer Polycondensation of Thiazole Derivatives *ACS Macro Lett.* **2016**, *5*, 1411–1415.
- (20) Amatore, C. Basic Concepts. In *Organic Electrochemistry, Fifth Edition*; Hammermich, O.; Speiser B., Ed.; CRC: Boca Raton, FL, 2015; pp 169–190.
- (21) Willot, P.; Koeckelberghs, G. Evidence for Catalyst Association in the Catalyst Transfer Polymerization of Thieno[3,2-b]thiophene *Macromolecules* **2014**, *47*, 8548–8555.
- (22) (a) Son, H.J.; Wang, W.; Xu, T.; Liang, Y.; Wu, Y.; Li, G.; Yu, L. Synthesis of Fluorinated Polythienothiophene-co-benzodithiophenes and Effect of Fluorination on the Photovoltaic Properties *J. Am. Chem. Soc.* **2011**, *133*, 1885–1894. (b) Meager, I.; Ashraf, R. S.; Mollinger, S.; Schroeder, B. C.; Bronstein, H.; Beatrup, D.; Vezie, M. S.; Kirchartz, T.; Salleo, A.; Nelson, J.; McCulloch, I. Photocurrent Enhancement from Diketopyrrolopyrrole Polymer Solar Cells through Alkyl-Chain Branching Point Manipulation *J. Am. Chem. Soc.* **2013**, *135*, 11537–11540 (c) Liu, P.; Zhang, K.; Liu, F.; Jin, Y.; Liu, S.; Russell, T. P.; Yip, H.-L.; Huang, F.; Cao, Y. Effect of Fluorine Content in

Thienothiophene-Benzodithiophene Copolymers on the Morphology and Performance of Polymer Solar Cells *Chem. Mater.* **2014**, *26*, 3009–3017 (d) Kim, J.-H.; Park, J.B.; I. H. Jung, I.H.; Yoon, S.C.; Kwak, J.; Hwang, D.-H. New alkylthio-thieno[3,2-*b*]thiophene-Substituted Benzodithiophene-based Highly Efficient Photovoltaic Polymer *J. Mater. Chem. C* **2015**, *3*, 4250–4253. (e) Kim, J.-H.; Park, J.B.; I. H. Jung, I.H.; Grimsdale, A.C.; Yoon, S.C.; Yang, H.; Hwang, D.-H. Well-controlled Thieno[3,4-*c*]pyrrole-4,6-(5*H*)-dione Based Conjugated Polymers for High Performance Organic Photovoltaic Cells with the Power Conversion Efficiency Exceeding 9% *Energy Environ. Sci.* **2015**, *8*, 2352–2356. (f) Zhu, L.; Wang, M.; Li, B.; Jiang, C.; Li, Q. High Efficiency Organic Photovoltaic Devices Based on Isoindigo Conjugated Polymers with a Thieno[3,2-*b*]thiophene π -Bridge *J. Mater. Chem. A* **2016**, *4*, 16064–16072.

(23) Zhao, Y.; Wasielewski, M. R. 3,4:9,10-Perylenebis(dicarboximide) Chromophores that Function as Both Electron Donors and Acceptors *Tetrahedron Lett.* **1999**, *40*, 7047–7050.

(24) (a) Dou, L.; You, J.; Hong, Z.; Xu, Z.; Li, G.; Street, R.A.; Yang, Y. 25th Anniversary Article: A Decade of Organic/Polymeric Photovoltaic Research *Adv. Mater.* **2013**, *25*, 6642–6671. (b) Zhang, S.; Ye, L.; Jianhui Hou, J. Breaking the 10% Efficiency Barrier in Organic Photovoltaics: Morphology and Device Optimization of Well-Known PBDDTT Polymers *Adv. Energy Mater.* **2016**, *6*, 1502529. (c) Ostroverkhova, O. Organic Optoelectronic Materials: Mechanisms and Applications *Chem. Rev.* **2016**, *116*, 13279–13412.

Appendix 1

Supporting Information for Chapter 2

Reactive Ligand Influence on Initiation in Phenylene Catalyst-Transfer Polymerization

I. Materials

iPrMgCl (2M in THF) was purchased in 100 mL quantities from Aldrich. Bis(cyclooctadiene)nickel (Ni(cod)₂) and 1,2-bis(diphenylphosphino)ethane (dppe) were purchased from Strem. All other reagent grade materials and solvents were purchased from Aldrich, Acros, EMD, or Fisher and used without further purification unless otherwise noted. THF was dried and deoxygenated using an Innovative Technology (IT) solvent purification system composed of activated alumina, copper catalyst, and molecular sieves. *N*-Bromosuccinimide (NBS) was recrystallized from hot water and dried over P₂O₅. Flash chromatography was performed on SiliCycle silica gel (40–63 μm) and thin layer chromatography was performed on Merck TLC plates pre-coated with silica gel 60 F254. Compounds **S2**,¹ and **2b–2f**² were prepared from modified literature procedures.

II. General Experimental

NMR Spectroscopy: Unless otherwise noted, ¹H, ¹³C, ¹⁹F and ³¹P NMR spectra for all compounds were acquired at rt in CD₂Cl₂ or CDCl₃ on a Varian vnmrs 700 operating at 700, 176, 660, and 283 MHz and Varian vnmrs 500 operating at 500, 126, 470, and 202 MHz, respectively. For ¹H and ¹³C spectra in deuterated solvents, the chemical shift data are reported in units of δ (ppm) relative to tetramethylsilane (TMS) and referenced with residual solvent. ¹⁹F NMR spectra were reported relative to CFCl₃ and ³¹P NMR spectra were relative to H₃PO₄. For ¹H, ¹⁹F and ³¹P NMR spectra in non-deuterated THF, the chemical shift data are reported in units of δ (ppm) and referenced with the THF peak at 3.58 ppm in the ¹H NMR spectrum which is then applied to all nuclei. Multiplicities are

reported as follows: singlet (s), doublet (d), doublet of doublets (dd), triplet (t), quartet (q), multiplet (m), broad resonance (br), and apparent triplet (at).

Mass Spectrometry: HRMS data were obtained on a Micromass AutoSpec Ultima Magnetic Sector mass spectrometer.

IR Spectroscopy: Samples were recorded using a Mettler Toledo ReactIR iC10 fitted with a Mercury Cadmium Telluride (MCT) detector, and AgX probe (9.5 mm x 1.5 mm) with a SiComp tip. The spectra were processed using icIR 4.0 software and raw absorbances were exported into Microsoft Excel or Sigma Plot 10 or 13 for analysis.

MALDI-TOF MS: MALDI-TOF mass spectra were recorded using a Bruker AutoFlex Speed in linear or reflectron mode at masses between 5000 and 15000. The matrix *trans*-2-[3-(4-*tert*-butylphenyl)-2-methyl-2-propenylidene]malononitrile (DCTB), was prepared at a concentration of 0.1M in CHCl₃. The matrix sinapic acid was prepared as a saturated solution in a mixture of 30/70 (v/v) MeCN/0.1% TFA in H₂O. The instrument was calibrated with a mixture of peptides in the sinapic acid matrix or with a sample of polyphenylene with H/Br endgroups. The polymer sample was dissolved in THF or CH₂Cl₂ to obtain a approx. 1 mg/mL solution. A 2.5 μL aliquot of polymer solution was mixed with 2.5 μL of the DCTB or sinapic acid matrix solution. This mixture (1 μL) was placed on the target plate and then air-dried. The data was analyzed using flexAnalysis and the percentages refer to the relative area ratios for each DP.

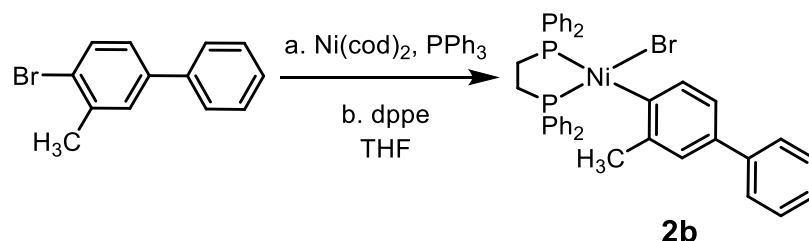
Gel-Permeation Chromatography: Polymer molecular weights were determined by comparison with polystyrene standards (Varian, EasiCal PS-2 MW 580-377,400) on a Waters 1515 HPLC instrument equipped with Waters Styragel® (7.8 x 300 mm) THF HR 0.5, THF HR 1, and THF HR 4 type columns in sequence and analyzed with Waters 2487 dual absorbance detector (254 nm) or on a Malvern Viscotek GPCMax VE2001 equipped with two Viscotek LT-5000L 8 mm (ID) x 300 mm (L) columns and analyzed with Viscotek TDA 305 (with R.I., UV-PDA Detector Model 2600 (190–500 nm), RALS/LALS, and viscometer). Samples were dissolved in THF (with mild heating) and passed through

a 0.2 μm PTFE filter prior to analysis.

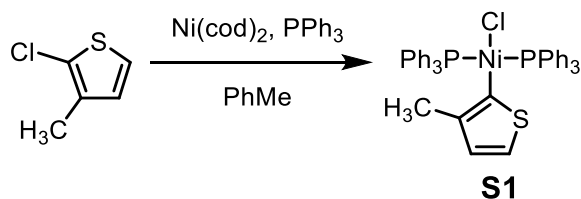
Titrations of the Grignard Reagents: An accurately weighed sample of salicylaldehyde phenylhydrazone³ (typically between 290–310 mg) was dissolved in 5.00 mL of THF. A 0.50 mL aliquot of this solution was stirred at rt while ArMgCl was added dropwise using a 500 μL syringe. The initial solution is yellow and turns bright orange at the end-point.

Statistical Analysis: Reported quantitative data represents the average of 2–3 experiments and the error bars represent standard deviation.

III. Synthetic Procedures

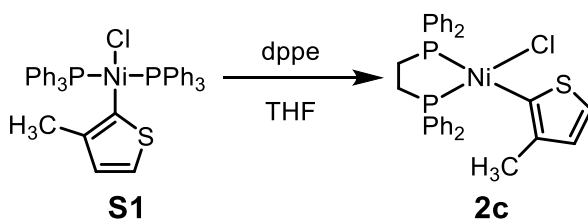


[1,2-bis(diphenylphosphino)ethane](2-methylbiphenyl)nickel(II) bromide (2d). In a glovebox, a 20 mL vial was equipped with a stir bar. Sequentially, Ni(cod)₂ (83.5 mg, 0.310 mmol, 1.00 equiv), PPh₃ (161 mg, 0.615 mmol, 2.00 equiv) and THF (2 mL) were added. The solution was stirred for 5 min and 4-bromo-3-methylbiphenyl (86 mg, 0.35 mmol, 1.1 equiv) and THF (2 mL) were added. The solution was stirred at rt for 2 h. To the deep red solution, dppe (134 mg, 0.335 mmol, 1.10 equiv) and THF (2 mL) were added. The solution was stirred for another 2 h. The orange solution was concentrated in vacuo until approx. 1 mL of solution was left. Addition of hexanes (18 mL) led to a yellow orange precipitate. The solid was filtered and washed with hexanes (20 mL). The resulting solid was recrystallized from approx. 1/3 (v/v) THF/hexanes (approx. 20 mL), to give 106 mg of **2d** as an orange solid (50% yield). Elemental Analysis: Calcd for C₃₉H₃₅BrNiP₂, C, 66.51; H, 5.01; found C, 66.57; H, 5.16.

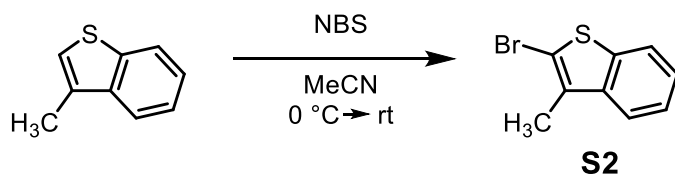


[Bis(triphenylphosphine)](3-methylthiophene)nickel(II) chloride (S1). A 20 mL vial was equipped with a stir bar in the glovebox. Sequentially, Ni(cod)₂ (139 mg, 0.506 mmol, 1.00 equiv), PPh₃ (262 mg, 1.00 mmol, 1.98 equiv), toluene (4 mL), and 2-chloro-3-methylthiophene (82 μL, 0.75 mmol, 1.5 equiv) were added. The solution was stirred at rt

for 30 min and turned from dark red homogeneous solution to orange heterogeneous mixture. The reaction was removed from the glovebox. Addition of hexanes (30 mL) led to an orange precipitate. The solid was filtered and washed with hexanes (20 mL) and cold MeOH (5 mL). The resulting solid was recrystallized from 1/3 (v/v) THF/hexanes (approx. 20 mL), to give 299 mg of **S1** as an orange solid (84% yield). Elemental analysis: Calcd for C₄₁H₃₅ClNiP₂S, C, 68.79; H, 4.93; Found C, 68.49; H, 4.88.

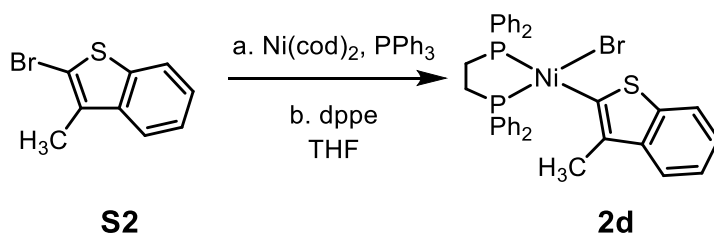


[1,2-bis(diphenylphosphino)ethane](3-methylthiophene)nickel(II) chloride (2c). In a glovebox, a 20 mL vial was equipped with a stir bar. Sequentially, **S1** (144 mg, 0.200 mmol, 1.00 equiv), dppe (89 mg, 0.22 mmol, 1.1 equiv), and THF (4 mL) were added. The solution was stirred at rt for 1 h. The heterogeneous orange solution was concentrated in vacuo until approx. 1 mL of solution remained. Addition of hexanes (18 mL) led to an orange precipitate. The solid was collected by vacuum filtration and washed with hexanes (20 mL). The resulting solid was recrystallized from 1/3 (v/v) THF/hexanes (approx. 20 mL), to give 78 mg of **2c** as an orange solid (66% yield). The product is air-sensitive and prone to decomposition.

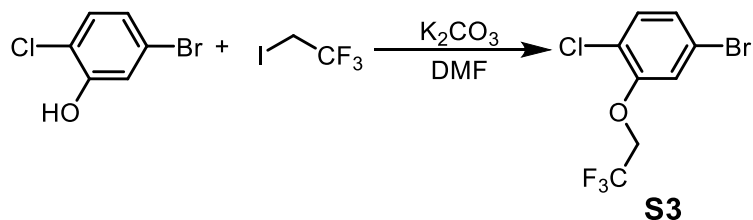


2-bromo-3-methylbenzo[b]thiophene (S2). A 10 mL round-bottom flask was equipped with a stir bar and cooled to 0 °C with an ice-water bath. Sequentially, 3-

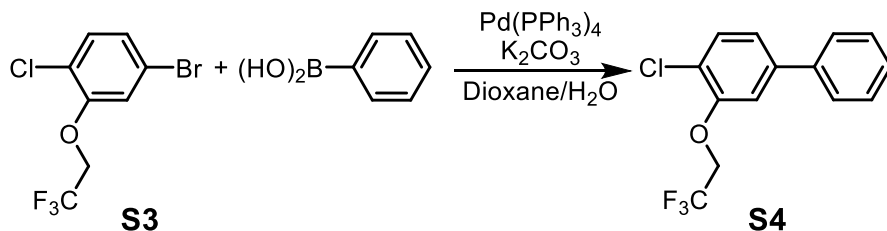
methylbenzothiophene (402 μ L, 3.00 mmol, 1.00 equiv), MeCN (3.5 mL), and NBS (561 mg, 3.15 mmol, 1.05 equiv) were added. The ice-water bath was removed after 5 min and the solution was stirred at rt for 30 min. The reaction was quenched with water (15 mL) and extracted with CH_2Cl_2 (3 x 10 mL). The combined organic layers were dried over MgSO_4 , filtered, and concentrated in vacuo. The resulting oil was purified via silica gel chromatography, using 100% hexanes as the eluent, to give 618 mg of **S2** as a clear liquid (91% yield). HRMS (EI): $[\text{M}^+]$ Calcd for $\text{C}_9\text{H}_7\text{BrS}$, 225.9452; found, 225.9450.



[1,2-bis(diphenylphosphino)ethane](3-methylbenzo[b]thiophene)nickel(II) bromide (2d). A 20 mL vial was equipped with a stir bar in the glovebox. Sequentially, $\text{Ni}(\text{cod})_2$ (82 mg, 0.30 mmol, 1.0 equiv), PPh_3 (158 mg, 0.602 mmol, 2.00 equiv) and THF (3 mL) were added. The solution was stirred for 5 min and **S2** (1.04 mL, 0.460 mmol, 1.5 equiv) and THF (1 mL) were added. The solution was stirred at rt for 1.5 h. To the deep red solution, dppe (2.0 mL, 0.17M in THF, 0.33 mmol, 1.1 equiv) were added. The solution was stirred for another 2 h. The orange solution was concentrated in vacuo until approx. 1 mL of solution was left. Addition of hexanes (18 mL) led to a yellow precipitate. The solid was filtered and washed with hexanes (5 mL). The resulting solid was recrystallized from approx. 1/3 (v/v) THF/hexanes (approx. 20 mL), to give 133 mg of **2d** as a dark orange solid (65% yield). Elemental Analysis: Calcd for $\text{C}_{35}\text{H}_{31}\text{BrNiP}_2\text{S}$, C, 61.44; H, 4.57; Found C, 61.33; H, 4.68.

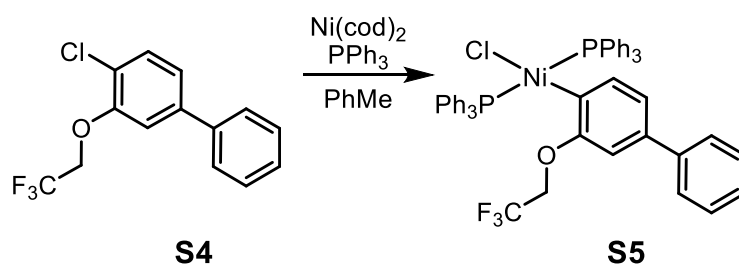


4-bromo-1-chloro-2-(2,2,2-trifluoroethoxy)benzene (S3). A 250 mL bomb flask was equipped with a stir bar. Sequentially, 5-bromo-2-chlorophenol (3.41 g, 16.4 mmol, 1.00 equiv), K_2CO_3 (6.80 g, 49.2 mmol, 3.00 equiv), DMF (35 mL), and 2-iodo-1,1,1-trifluoroethane (6.5 mL, 65 mmol, 4.0 equiv) were added. The mixture was stirred for 6 d at 65 °C. The mixture was poured into water (70 mL) and extracted with CH_2Cl_2 (3 x 50 mL). The organic layers were combined, washed with brine (25 mL), dried over $MgSO_4$, and concentrated in vacuo. The resulting oil was purified by silica gel chromatography using 5:95 (v/v) CH_2Cl_2 /hexanes as the eluent to give 2.26 g of **S3** as a colorless oil (48% yield). HRMS (EI): $[M^+]$ Calcd for $C_8H_5BrClF_3O$, 287.9164; found, 287.9170.

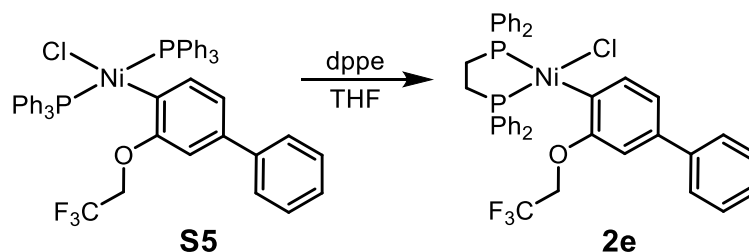


4-chloro-3-(2,2,2-trifluoroethoxy)-1,1'-biphenyl (S4). In a glovebox under a N_2 atmosphere, a 25 mL Schlenk flask was equipped with a stir bar and charged with $Pd(PPh_3)_4$ (139 mg, 0.120 mmol, 0.030 equiv). The flask was sealed with a septum, removed from the glovebox and charged with phenyl boronic acid (740 mg, 6.00 mmol, 1.50 equiv) and K_2CO_3 (1.66 g, 12.0 mmol, 3.00 equiv). A solution of 1,4-dioxane and water (9:1) was sparged with N_2 for 30 min, and 8 mL was added to the Schlenk flask. Then, **S3** (1.18 g, 4.07 mmol, 1.00 equiv) was dissolved in the dioxane/water solution (5.0 mL) and added to the reaction mixture. The reaction mixture was heated to 90 °C overnight. The reaction was quenched with satd. aq. $NaHCO_3$ (30 mL) and extracted with EtOAc (3 x 30 mL). The organic layers were combined and washed with brine (25 mL),

dried over MgSO_4 , and concentrated in vacuo. The product was purified by silica gel chromatography using 5/95 (v/v) EtOAc/hexanes to give 866 mg of **S4** as a colorless oil, which slowly crystallized into a white solid (76% yield). HRMS (EI): $[\text{M}^+]$ Calcd for $\text{C}_{14}\text{H}_{10}\text{ClF}_3\text{O}$, 286.0372; found, 286.0383.

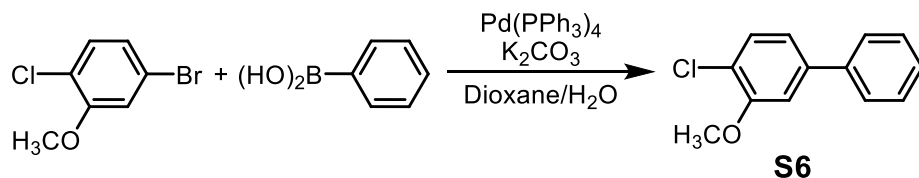


[Bis(triphenylphosphine)](3-(2,2,2-trifluoroethoxy)-1,1'-biphenyl)nickel(II) chloride (S5). In a glovebox, $\text{Ni}(\text{cod})_2$ (68.8 mg, 0.250 mmol, 1.00 equiv) and triphenylphosphine (131 mg, 0.490 mmol, 2.00 equiv) and **S4** (94.6 mg, 0.330 mmol, 1.30 equiv) were dissolved in toluene (2.5 mL) in a 20 mL vial. The reaction mixture was stirred at rt for 2.5 h, then concentrated until approx. 0.5 mL toluene remained. Hexanes (approx. 15 mL) was added, and the yellow precipitate was isolated by vacuum filtration, giving 149 mg of a yellow powder (68% crude yield) which was carried on without further purification.

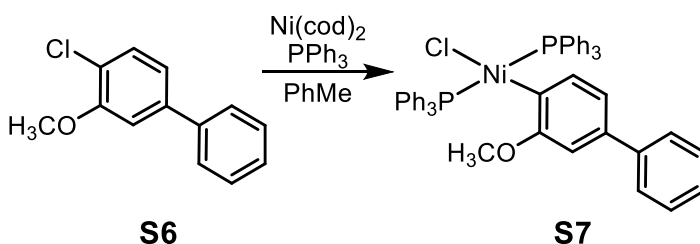


[1,2-bis(diphenylphosphino)ethane](3-(2,2,2-trifluoroethoxy)-1,1'-biphenyl)nickel(II) chloride (2e). In a glovebox, **S5** (149 mg, 0.170 mmol, 1.00 equiv) and dppe (76.5 mg, 0.187 mmol, 1.10 equiv) were dissolved in THF (2.5 mL) in a 20 mL vial. The solution was stirred at rt for 1 h, then concentrated until approx. 0.5 mL THF remained. Hexanes (approx. 15 mL) was added, and the yellow precipitate was isolated by vacuum filtration. The product was recrystallized from approx. 1/3 (v/v) THF/hexanes (approx. 20

mL), giving 100 mg of a yellow powder (79% yield.) Elemental Analysis: Calcd for $C_{40}H_{34}ClF_3NiOP_2$, C, 64.59; H, 4.61; Found C, 64.37; H, 4.65.

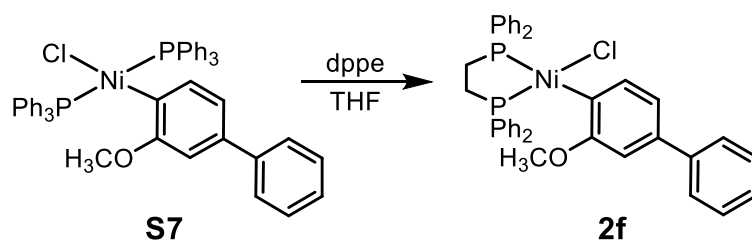


4-chloro-3-methoxy-1,1'-biphenyl (S6). A 25 mL Schlenk flask was equipped with a stir bar in the glovebox and charged with $Pd(PPh_3)_4$ (104 mg, 0.0900 mmol, 0.0600 equiv). The Schlenk flask was then removed from the glovebox and charged with phenylboronic acid (274 mg, 2.30 mmol, 1.50 equiv) and K_2CO_3 (622 mg, 4.50 mmol, 3.00 equiv). A solution of 1,4-dioxane and water (9:1) was sparged with N_2 for 30 min, and 7 mL were added to the Schlenk flask. Then, 4-bromo-1-chloro-2-methoxybenzene (332 mg, 1.50 mmol, 1.00 equiv) was dissolved in the dioxane/water solution (5 mL) and added to the reaction mixture. The reaction mixture was heated to 90 °C for 6 h. The reaction was quenched with saturated NH_4Cl (35 mL), extracted with EtOAc (3 x 35 mL), washed with brine (35 mL), dried over $MgSO_4$, and concentrated in vacuo. The product was purified by silica gel chromatography using 10/90 (v/v) toluene/hexanes to give 232 mg of a colorless oil (71% yield). HRMS (EI): $[M^+]$ Calcd for $C_{13}H_{11}ClO$, 218.0498; found, 286.0500.



[Bis(triphenylphosphine)](3-methoxy-1,1'-biphenyl)nickel(II) chloride (S7). In the glovebox, $Ni(cod)_2$ (138 mg, 0.502 mmol, 1.0 equiv), and triphenyl phosphine (Ph_3P) (262 mg, 1.00 mmol, 2.0 equiv) were dissolved in THF (3 mL) in a 20 mL vial with stirring. In a

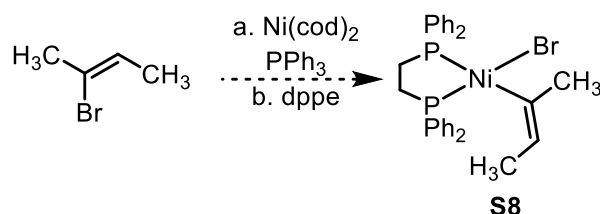
separate 4 mL vial, 1-chloro-2-methoxy-4-phenyl-benzene (142 mg, 0.650 mmol, 1.3 equiv) was dissolved in THF (2 mL). This solution was then added to the vial containing the Ni/Ph₃P and stirred at rt for 4 h, during which time a yellow precipitate formed. The solvent was removed under vacuum until approx. 0.5 mL remained. Hexanes (approx. 15 mL) were then added, and the yellow precipitate was collected by vacuum filtration, giving 157 mg of **S7** as a yellow powder (79% crude yield). The product was used immediately without further purification.



[1,2-bis(diphenylphosphino)ethane](3-methoxy-1,1'-biphenyl)nickel(II) chloride (2f). In a glovebox, in a 20 mL vial, **S7** (157 mg, 0.196 mmol, 1.0 equiv) and dppe (94 mg, 0.24 mmol, 1.2 equiv) were dissolved in THF (2.5 mL) in a 20 mL vial. The reaction mixture was stirred at rt for 1 h. (Note: a yellow precipitate was observed after 5 min.) After 1 h, hexanes (approx. 15 mL) was added, and the solution was cooled in a freezer at -30 °C overnight. The product was collected by vacuum filtration, giving 100 mg of **2f** as a yellow powder (59% yield). Elemental Analysis: Calcd for C₃₉H₃₅ClNiOP₂, C, 69.31; H, 5.22; Found C, 67.96; H, 5.22.

IV. Attempted Synthesis of [1,2-bis(diphenylphosphino)ethane](2-butenyl)nickel(II) Chloride

Precatalyst synthetic procedure:



[1,2-bis(diphenylphosphino)ethane](2-butenyl)nickel(II) chloride (S8). In a glovebox, Ni(cod)₂ (37.1 mg, 0.125 mmol) and PPh₃ (76.2 mg, 0.250 mmol) were dissolved in THF (1.0 mL). In a separate vial, Z-2-bromo-2-butene (24 μL, 0.24 mmol) was dissolved in THF (0.2 mL), and the vial was sealed with a septum. The Ni solution (0.80 mL, containing 0.10 mmol Ni(cod)₂ and 0.20 mmol PPh₃) was transferred to a J. Young NMR tube which was sealed with a septum and removed from the glovebox along with the vial containing Z-2-bromo-2-butene. The alkene solution (0.10 mL, 0.12 mmol, 1.2 equiv relative to Ni(cod)₂) was added to the NMR tube, and a ³¹P NMR spectrum was immediately acquired, showing Ni(PPh₃)₂(cod) and a singlet at 20 ppm. A second ³¹P NMR spectrum was acquired 5 min later, showing formation of several other peaks, as well as Ni(PPh₃)₂(cod). After 1 hr, another ³¹P NMR spectrum was acquired, showing complete consumption of Ni(PPh₃)₂(cod). Then, a solution of dppe in THF (0.20 mL, 0.57M, 1.1 equiv) was added and a final ³¹P NMR spectrum was acquired, showing primarily Ni(dppe)₂. The product was analyzed by GCMS, showing a peak with m/z = 110, the mass of 3,4-dimethylhexa-2,4-diene (the expected organic product from a ligand disproportionation reaction followed by reductive elimination).

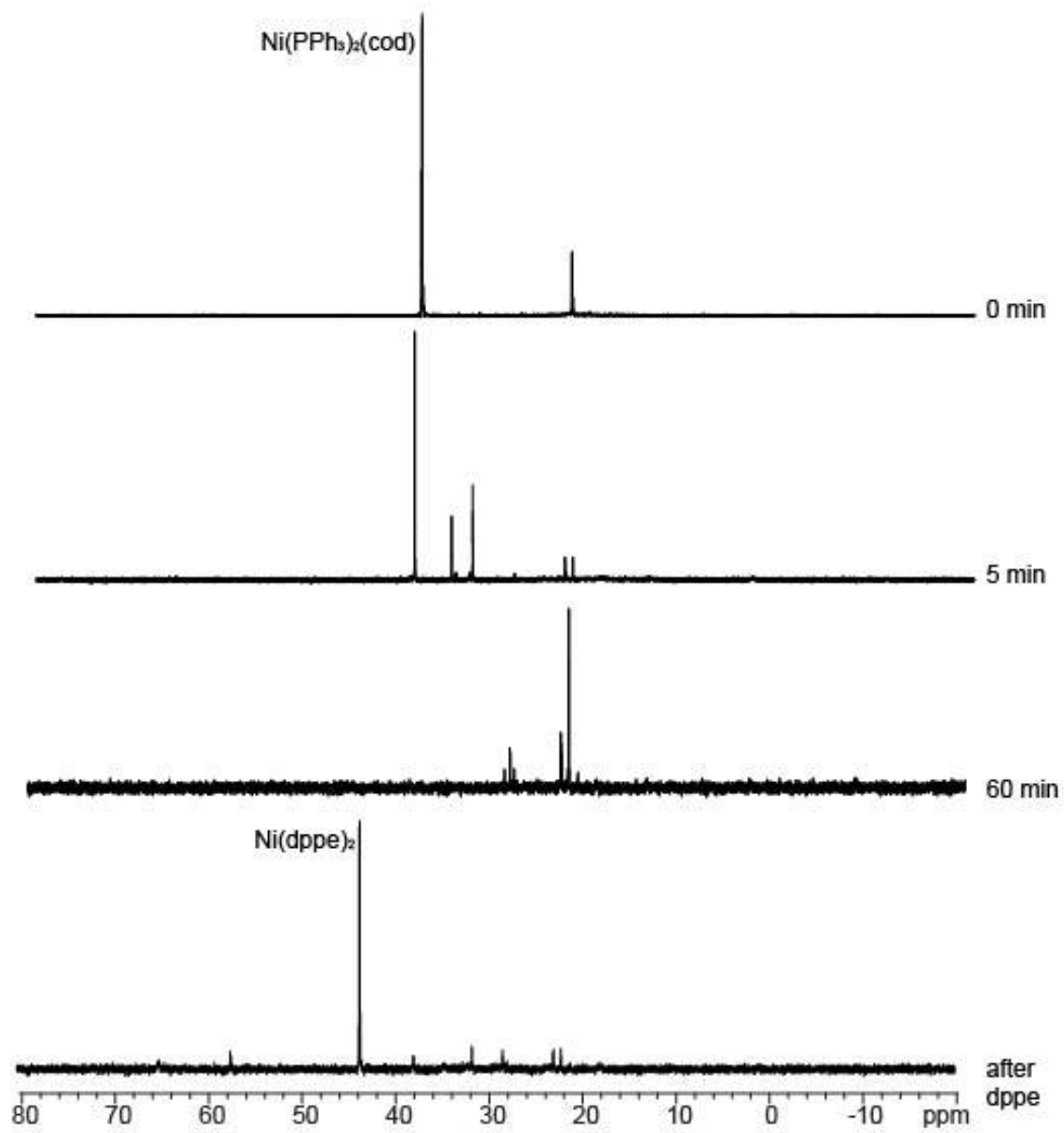
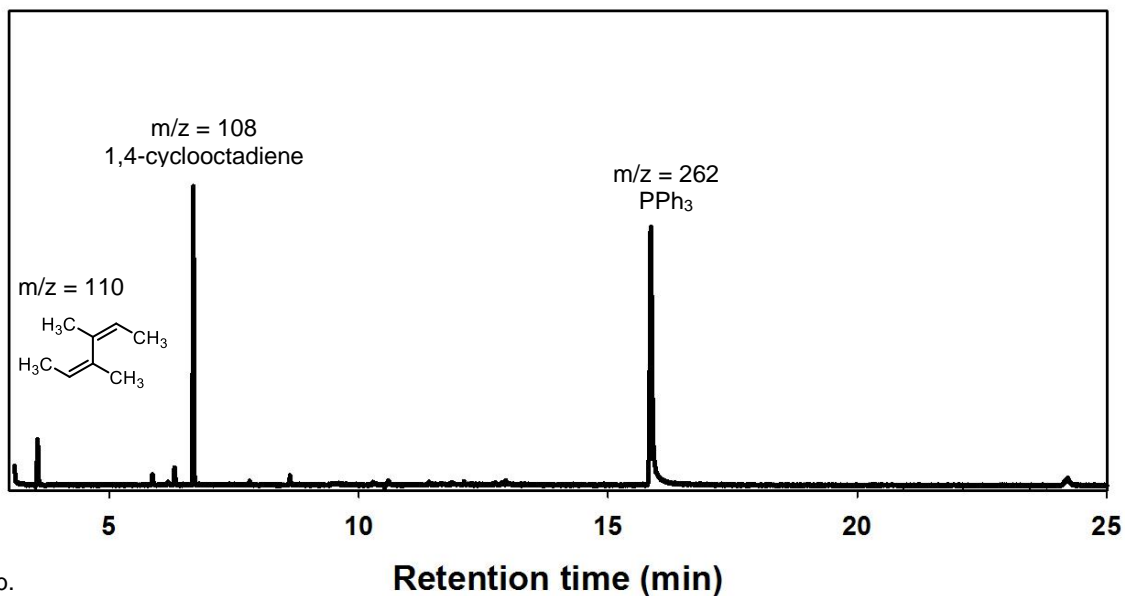


Figure S1.1. ^{31}P NMR spectra acquired during the attempted synthesis of **S8**

a.



b.

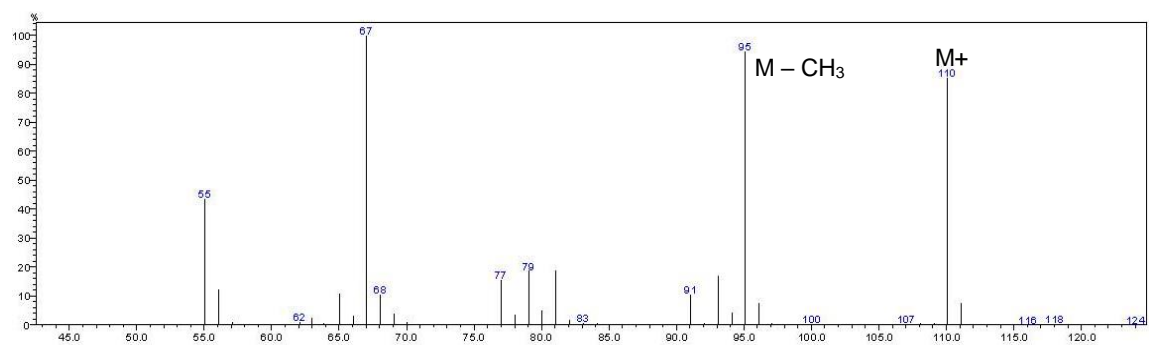


Figure S1.2. Gas chromatogram (a) for the attempted synthesis of **S8** and mass spectrum (b) for peak at 3.4 min

IV. NMR Spectra

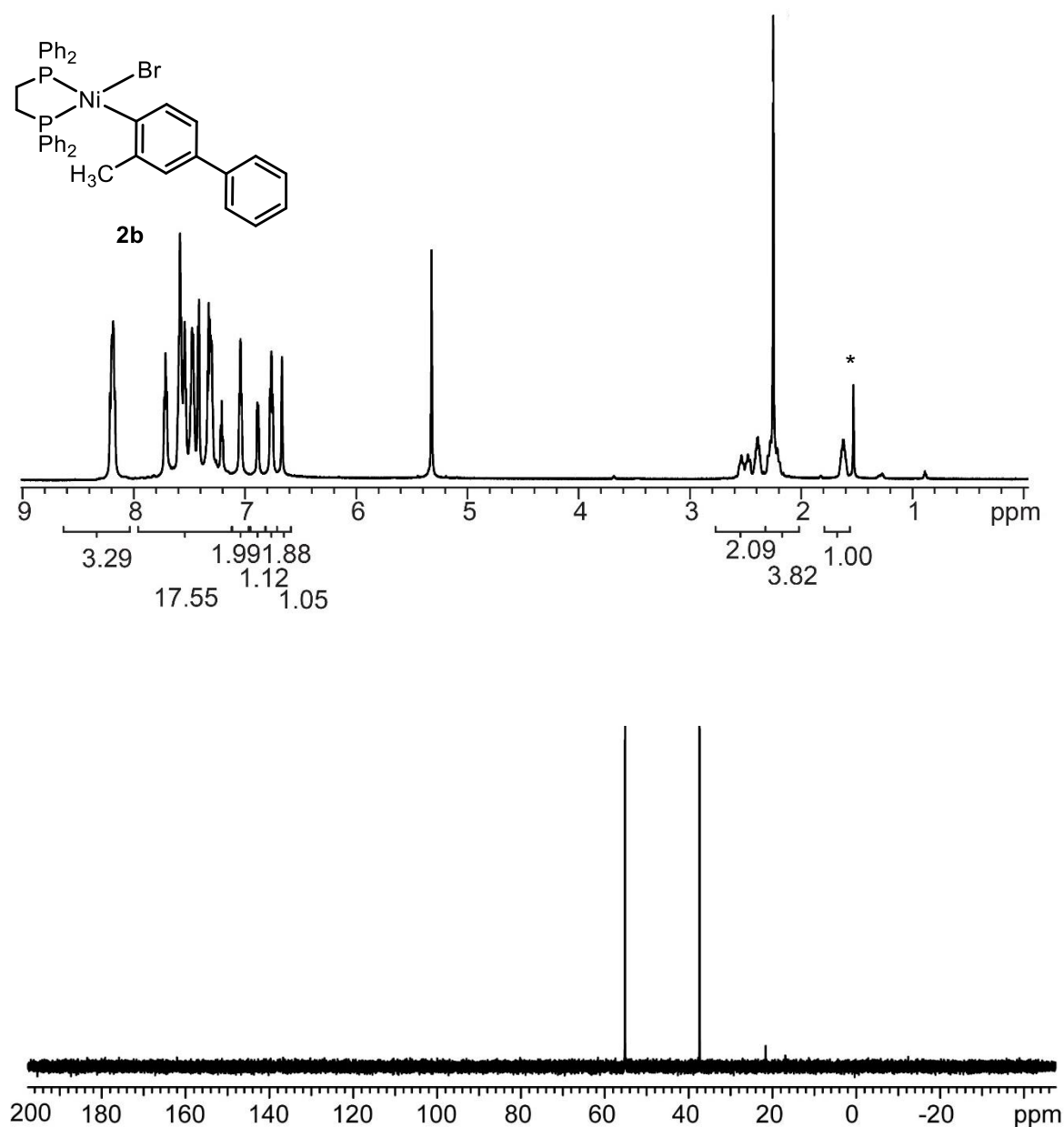


Figure S1.3. ¹H and ³¹P NMR spectra of **2b** ¹H NMR (700 MHz, CD₂Cl₂) δ 8.21–8.17 (m, 4H), 7.71–7.21 (m, 18 H), 7.04 (at, *J* = 6.3 Hz, 2H), 6.88 (d, *J* = 7.7 Hz, 1H), 6.76 (at, *J* = 9.8 Hz, 2H), 6.68 (s, 1H), 2.51 (dt, *J* = 40.6, 13.3 Hz, 1H), 2.41–2.37 (m, 1H), 2.28–2.22 (m, 1H), 2.25 (s, 3H), 1.63–1.62 (m, 1H). *denotes residual H₂O
³¹P NMR (283 MHz, CD₂Cl₂) δ 55.16 (d, *J* = 19.0 Hz), 37.4 (d, *J* = 20.1 Hz).

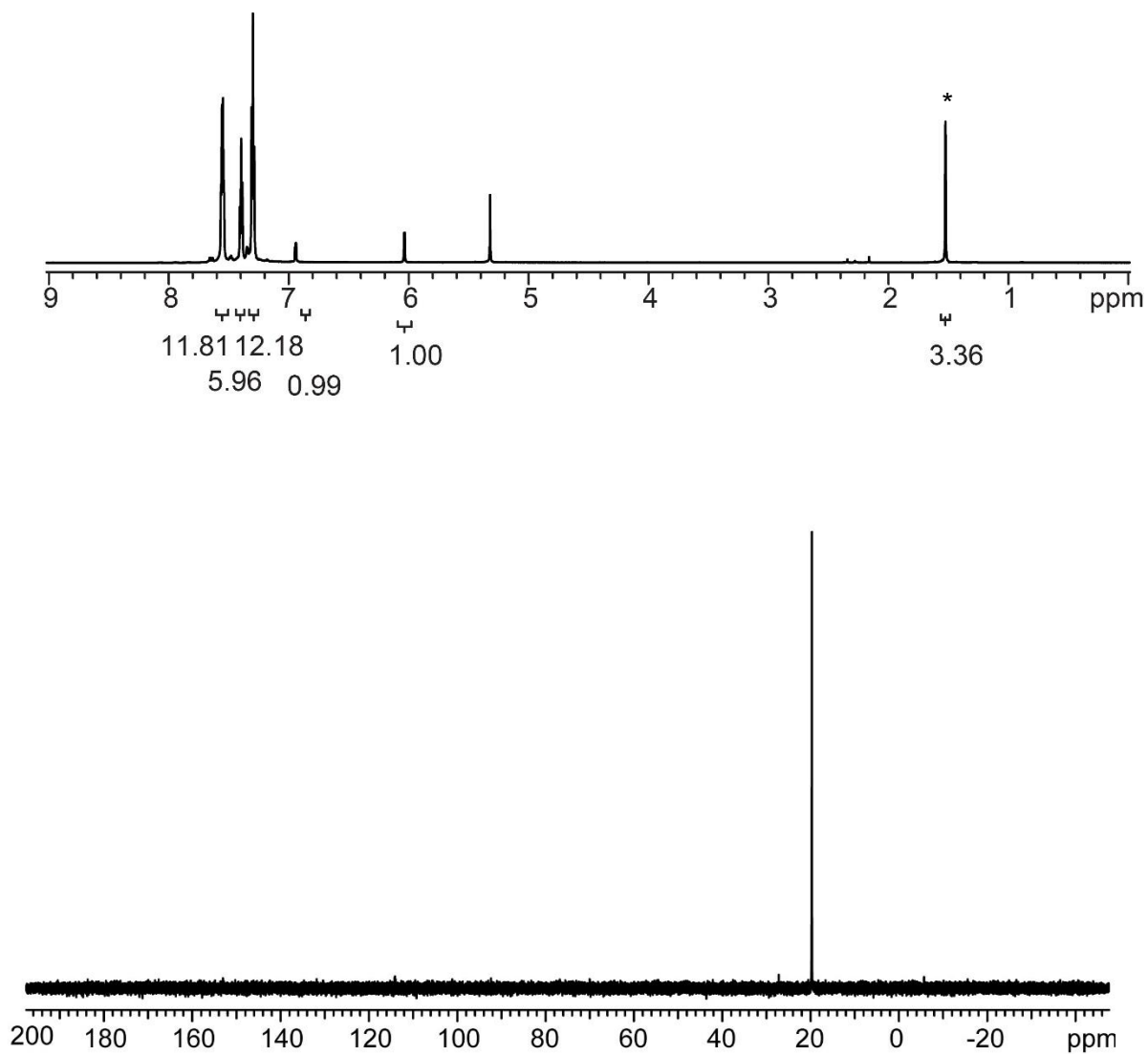
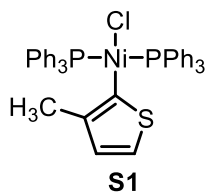


Figure S1.4. ^1H and ^{31}P NMR spectra of **S1**. ^1H NMR (700 MHz, CD_2Cl_2) δ 7.55 (dd, J = 6.6 Hz, 5.5 Hz, 12H), 7.40 (t, J = 7.4 Hz, 6H), 7.30 (at, J = 7.4 Hz, 12H), 6.94 (d, J = 4.2 Hz, 1H), 6.04 (d, J = 4.2 Hz, 1H), 1.52 (s, 3H). *denotes residual H_2O
 ^{31}P NMR (283 MHz, CD_2Cl_2) δ 19.69.

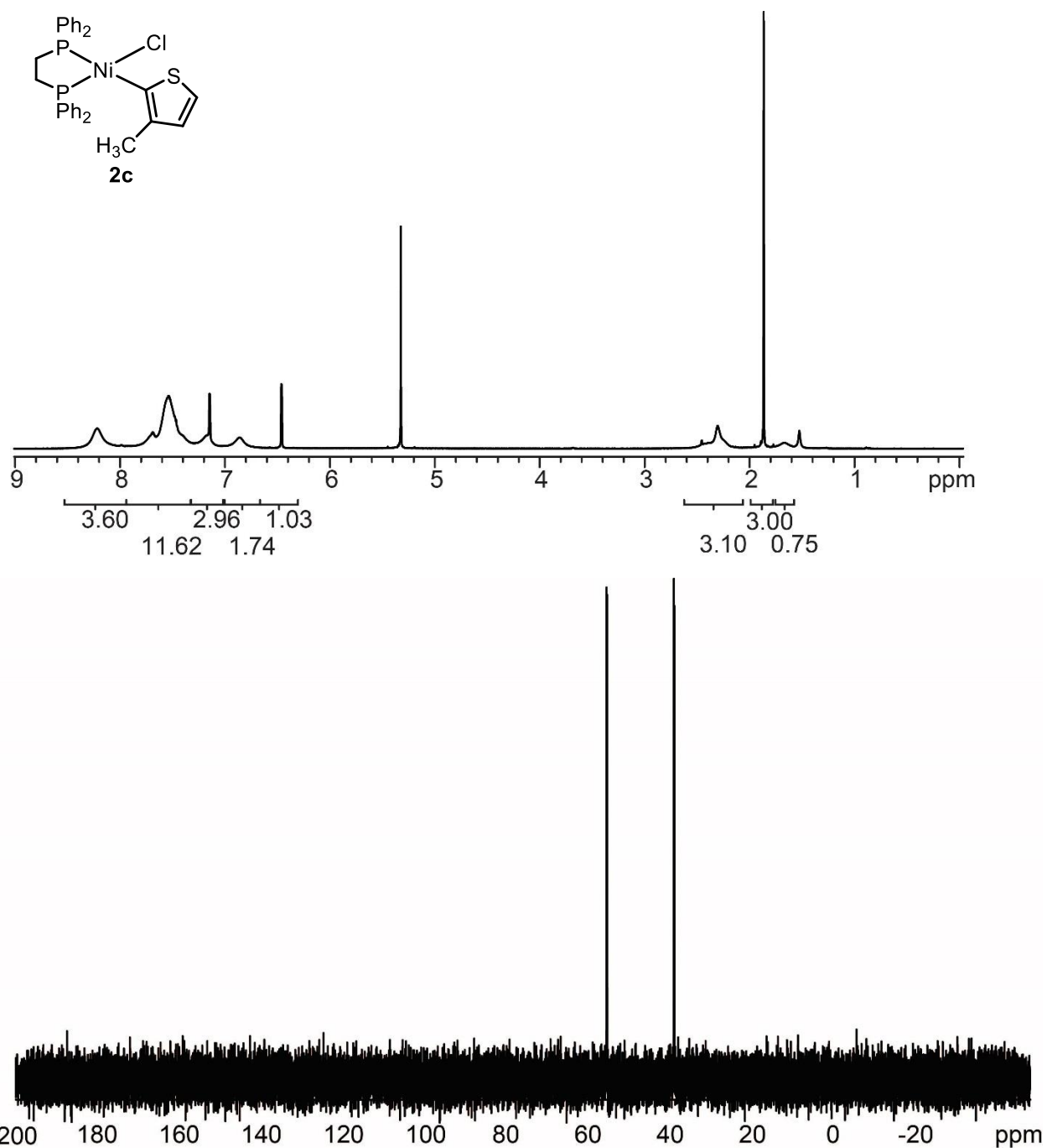


Figure S1.5. ^1H and ^{31}P NMR spectra of **2c**. ^1H NMR (500 MHz, C_6D_6) δ 8.05 (bs, 4H), 7.69–7.47 (m, 12 H), 7.15–7.14 (m, 3H), 7.20–6.96 (m, 3H), 6.89 (bs, 2H), 6.46 (s, 1H), 3.60–3.56 (m, 1H), 2.33 (s, 3H), 1.73 (bs, 2H), 1.44–1.41 (m, 1H). ^{31}P NMR (202 MHz, C_6D_6) δ 54.59 (d, $J = 33.5$ Hz), 38.20 (d, $J = 33.5$ Hz). This compound is unstable and prone to decomposition.

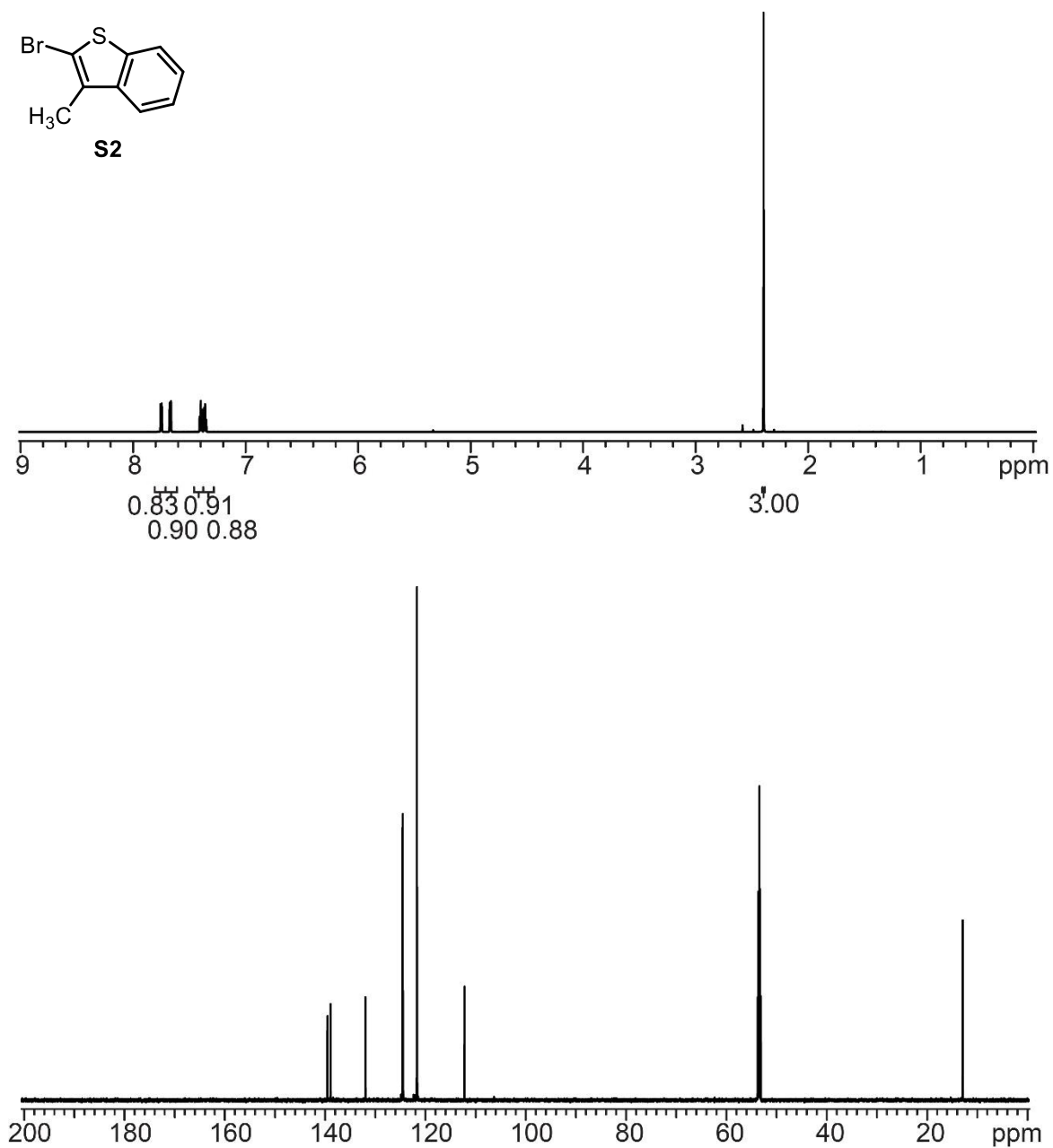
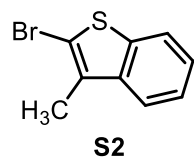


Figure S1.6. ^1H and ^{13}C NMR spectra of **S2**. ^1H NMR (700 MHz, CD_2Cl_2) δ 7.75 (dd, $J = 7.5$ Hz, 0.85 Hz, 1H), 7.66 (dd, $J = 7.5$ Hz, 0.51 Hz, 1H), 7.39 (at, $J = 7.7$ Hz, 1H), 7.36 (at, $J = 7.7$ Hz, 1H), 2.40 (s, 3H). ^{13}C NMR (176 MHz, CD_2Cl_2) δ 139.53, 138.89, 131.97, 124.57, 124.49, 121.68 (2 C), 112.20, 12.86.

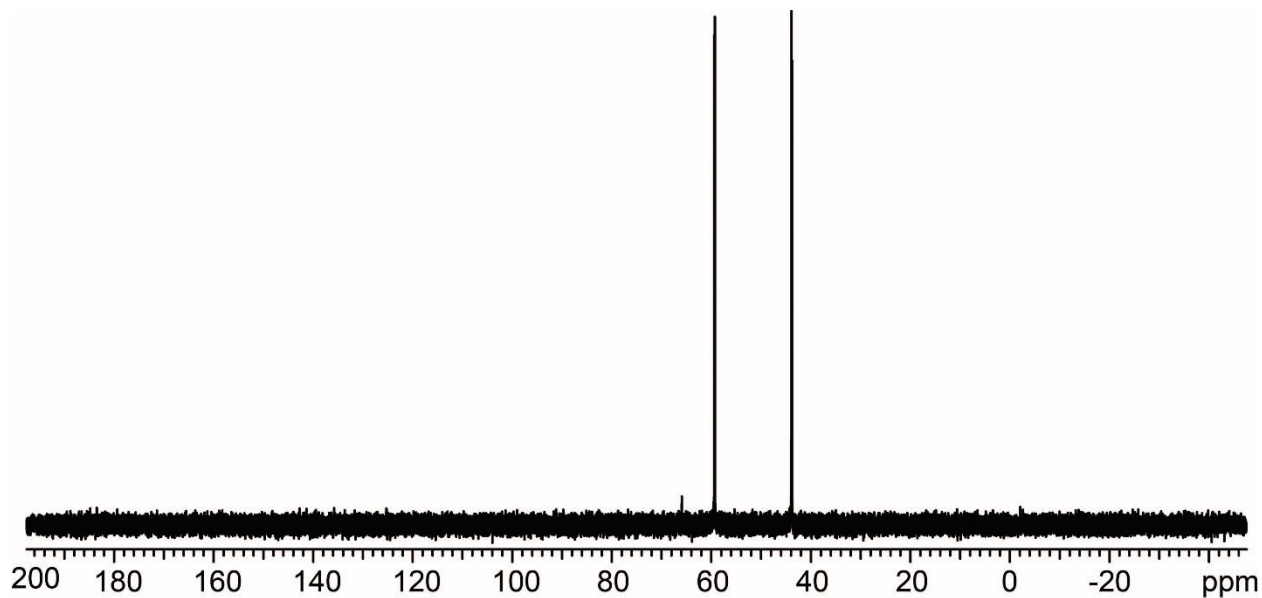
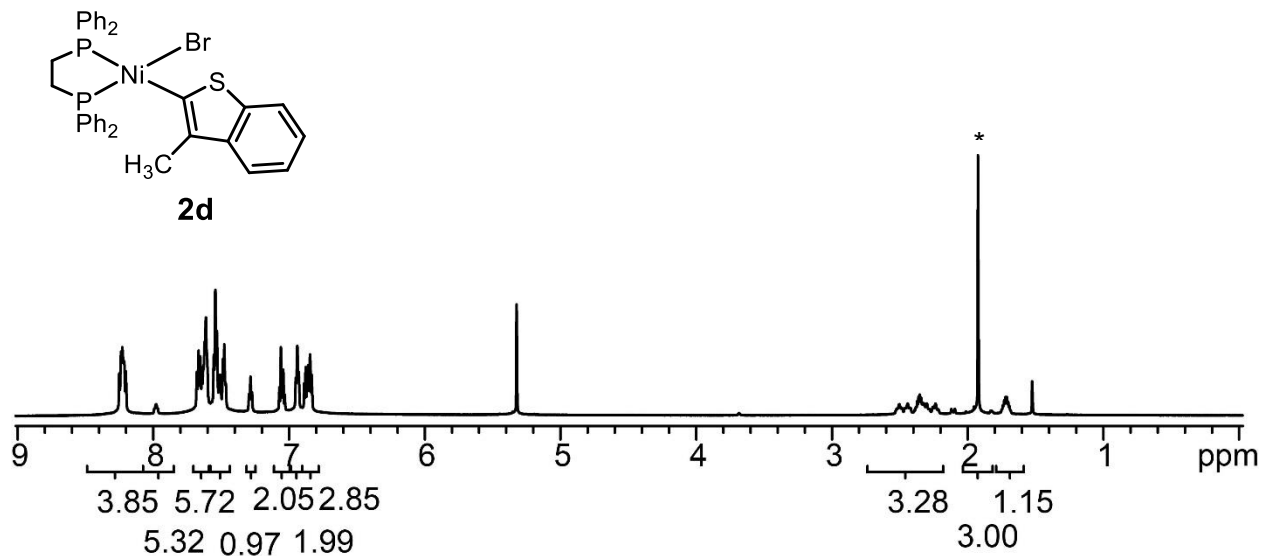
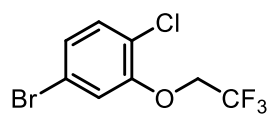


Figure S1.7. ^1H and ^{31}P NMR spectra of **2d**. ^1H NMR (700 MHz, CD_2Cl_2) δ 8.25–8.20 (m, 4H), 7.68–7.61 (m, 5H), 7.55–7.46 (m, 6H), 7.28 (at, $J = 7.3$ Hz, 1H), 7.07–7.03 (m, 2H), 6.94 (at, $J = 7.7$ Hz, 2H), 6.89–6.83 (m, 3H), 2.47 (td, $J = 42.7, 11.2$ Hz, 1H), 2.38–2.22 (m, 2H), 1.92 (s, 3H), 1.74–1.69 (m, 1H). *denotes residual H_2O
 ^{31}P NMR (283 MHz, CD_2Cl_2) δ 59.32 (d, $J = 35.9$ Hz), 43.82 (d, $J = 35.9$ Hz).



S3

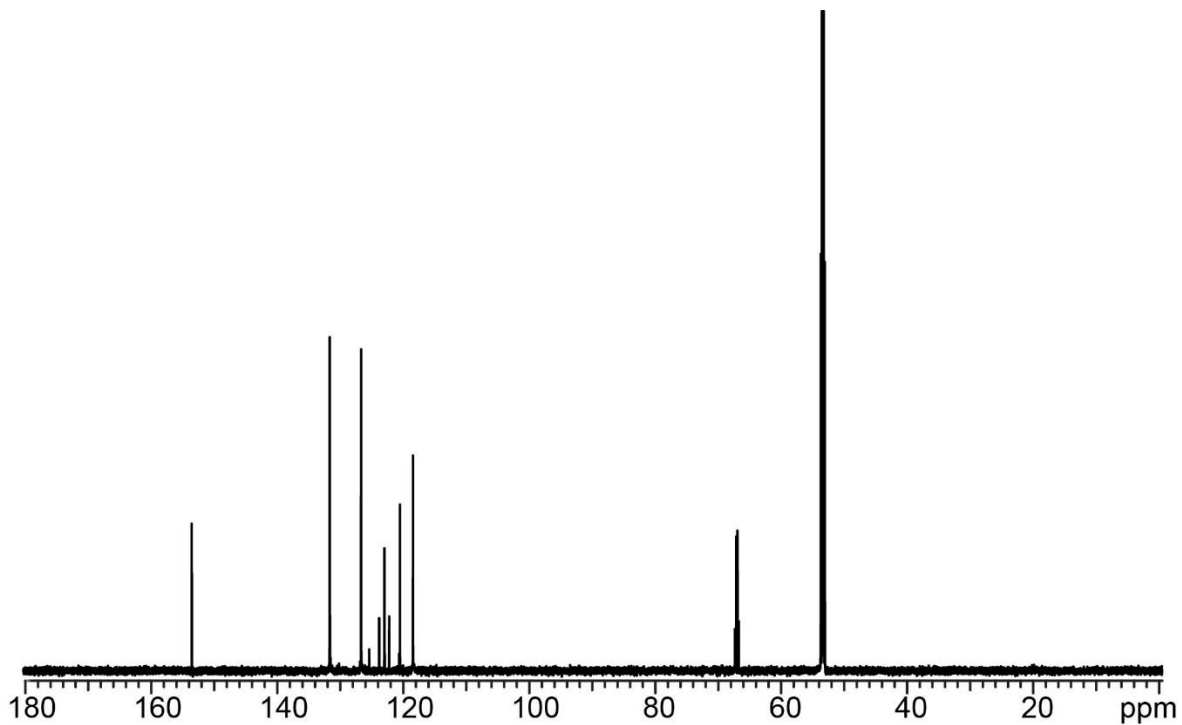
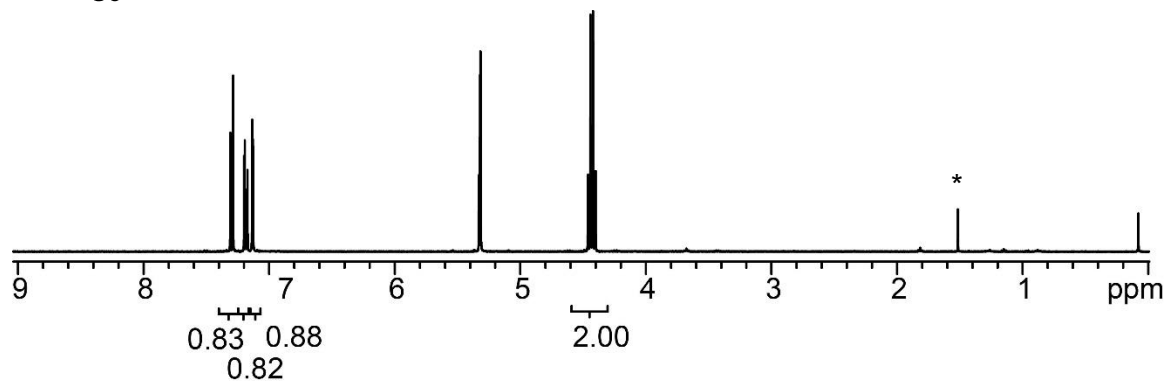
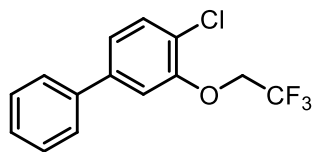


Figure S1.8. ^1H and ^{13}C NMR spectra of **S3**. ^1H NMR (400 MHz, CD_2Cl_2) δ 7.30 (d, $J = 8.4$ Hz, 1H), 7.19 (dd, $J = 8.4$ Hz, 2.1 Hz, 1 H), 7.13 (d, $J = 2.1$ Hz, 1 H), 4.43 (q, $J_{\text{H-F}} = 8.0$ Hz) *denotes residual H_2O
 ^{13}C NMR (176 MHz, CD_2Cl_2) δ 153.56, 131.66, 126.87, 123.02 (q, $J_{\text{C-F}} = 278.6$ Hz), 122.97, 120.51, 118.45, 67.04 (q, $J_{\text{C-F}} = 72.3$ Hz)



S4

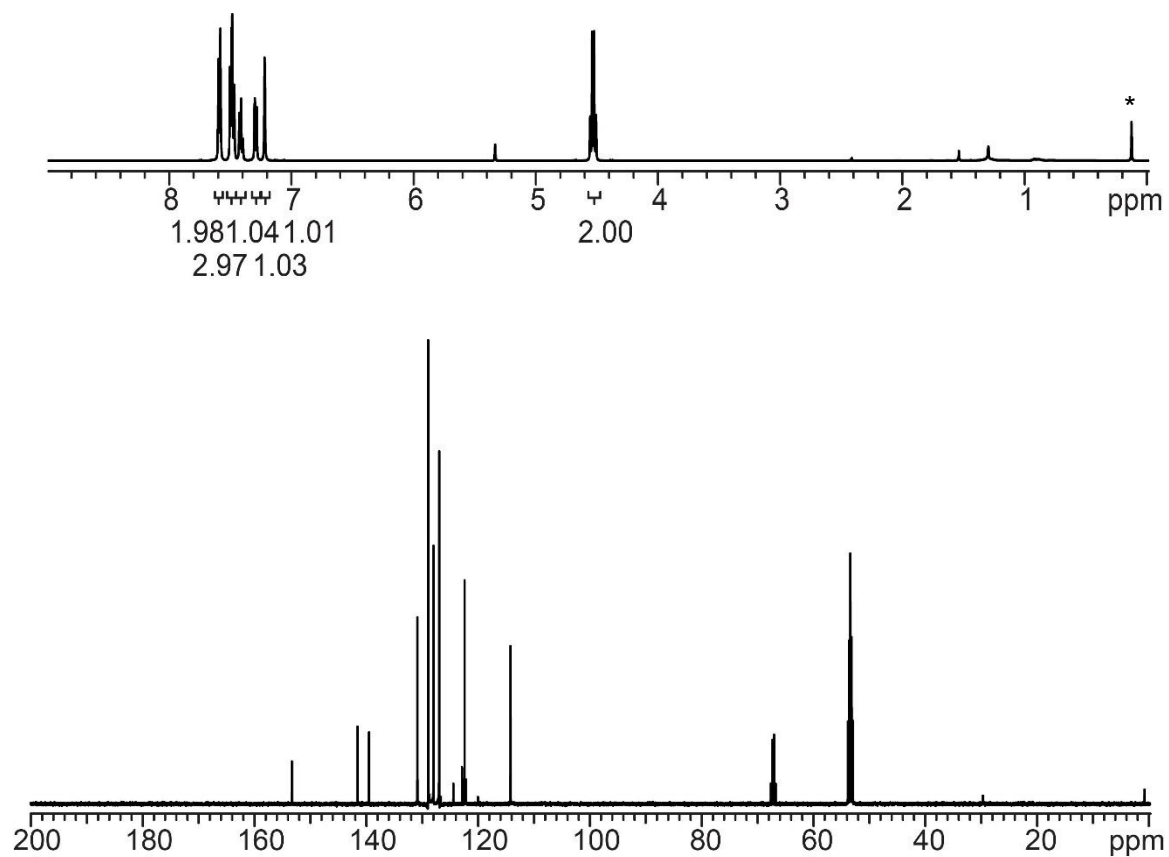


Figure S1.9. ^1H and ^{13}C NMR spectra of **S4**. ^1H NMR (700 MHz, CD_2Cl_2) δ 7.59 (d, J = 7.8 Hz, 2H), 7.50–7.47 (m, 3H), 7.41 (t, J = 7.3 Hz, 1H), 7.28 (dd, J = 8.2 Hz, 1.7 Hz, 1H) 7.20 (d, J = 1.5 Hz, 1H), 4.53 (q, $J_{\text{H-F}}$ = 8.2 Hz, 2H), *denotes residual grease. ^{13}C NMR (176 MHz, CD_2Cl_2) δ 153.31, 141.56, 139.49, 130.84, 128.92, 127.98, 123.31 (q, $J_{\text{C-F}}$ = 278.2 Hz), 122.89, 122.42, 114.19, 67.18 (q, $J_{\text{C-F}}$ = 36.2 Hz).

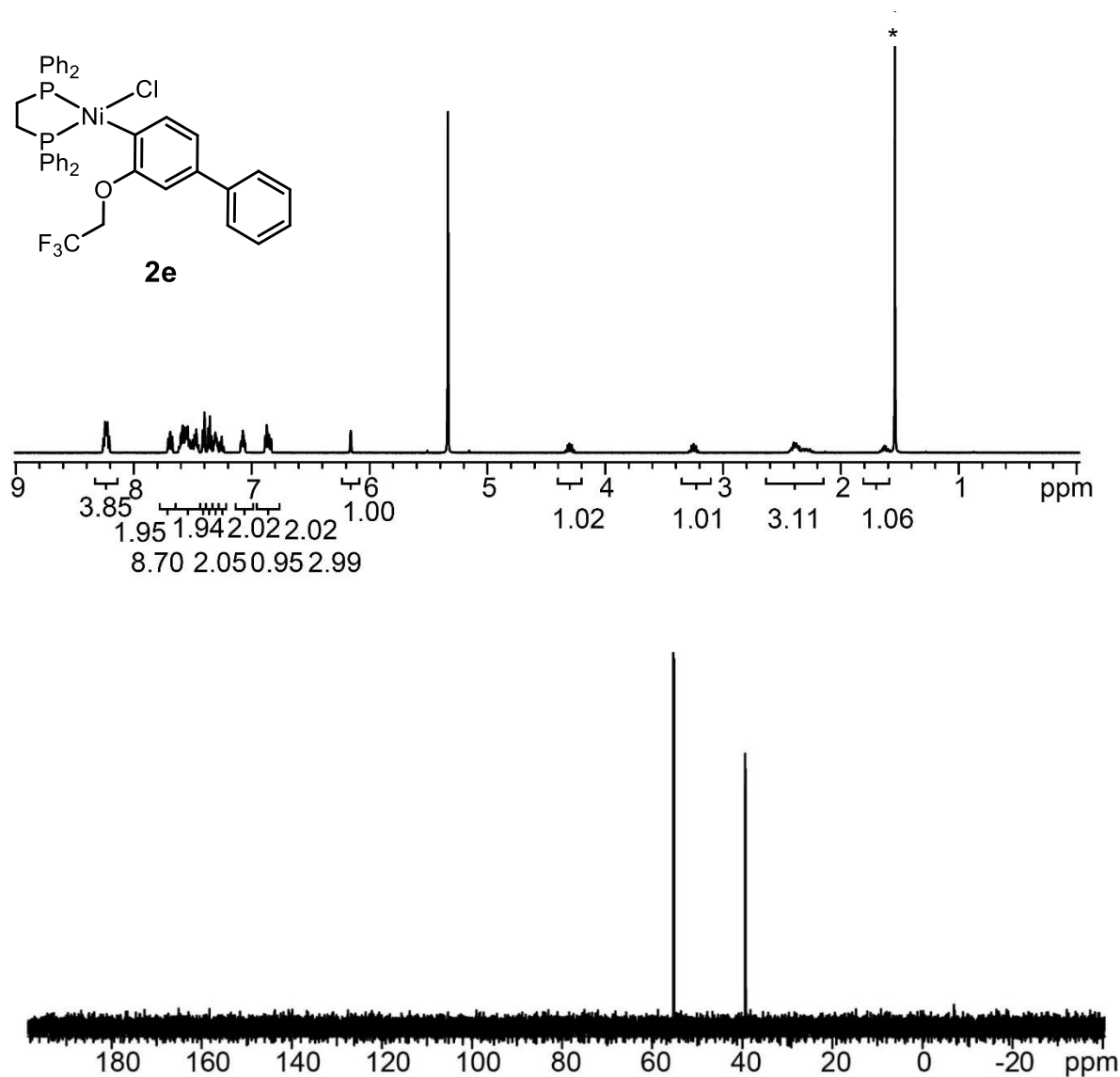


Figure S1.10. ^1H and ^{31}P NMR spectra of **2e**. ^1H NMR (500 MHz, CD_2Cl_2) δ 8.23 (m, 4H) 7.69 (dd, $J = 9.8, 1.7$ Hz, 2H), 7.60–7.47 (m, 9H), 7.41 (d, $J = 7.5$ Hz, 2H), 7.35 (at, $J = 7.5$ Hz, 2H), 7.32–7.29 (m, 2H), 7.27–7.24 (m, 2H), 7.09–7.06 (m, 2H), 6.88–6.83 (m, 3H), 6.16 (s, 1 H), 4–34–4.26 (m, 1H), 3.28–3.21 (m, 1H) 2.43–2.24 (m, 3H), 1.66–1.59 (m, 1H). *denotes residual H_2O
 ^{31}P NMR (202 MHz, CD_2Cl_2) δ 55.20 (d, $J = 30.3$ Hz), 39.31 (d, $J = 28.9$ Hz).

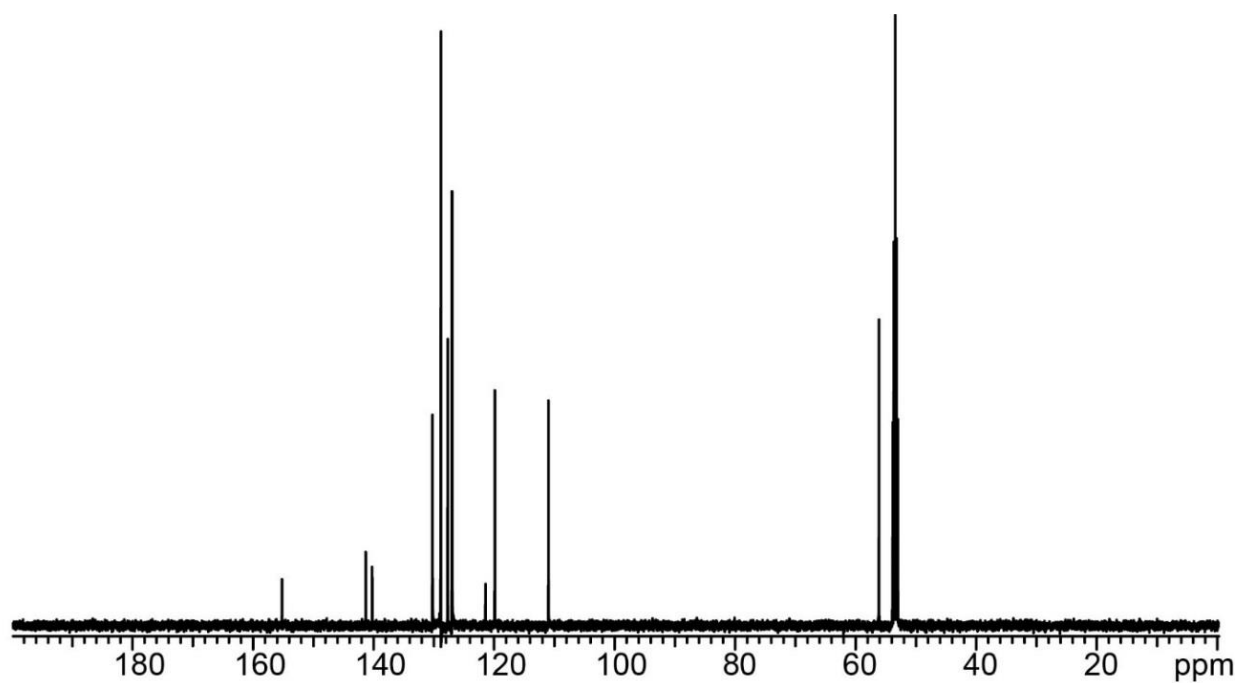
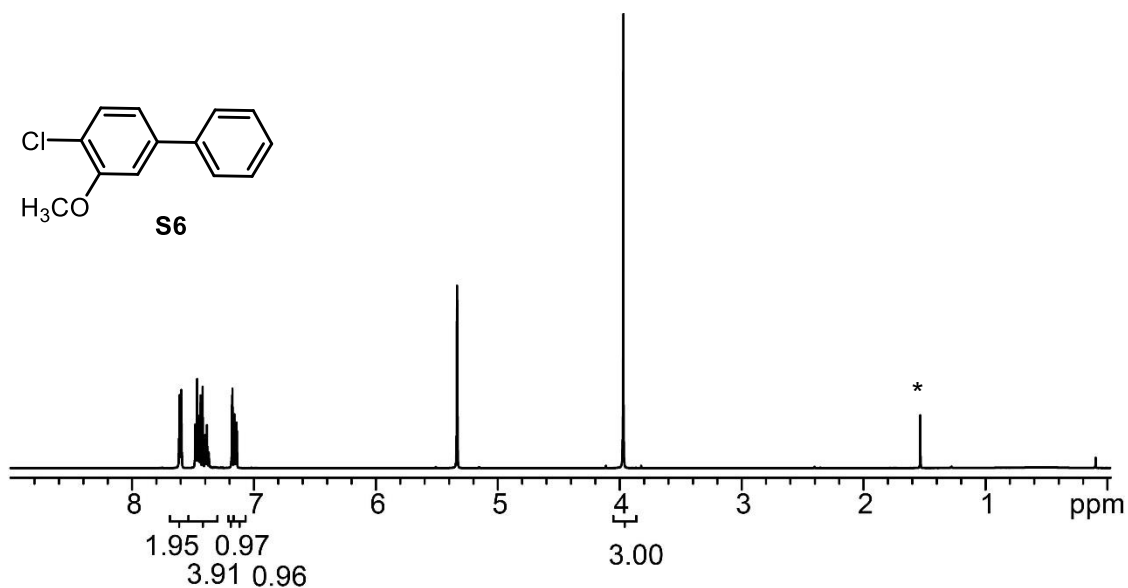


Figure S1.11. ^1H and ^{13}C NMR spectra of **S6**. ^1H NMR (500 MHz, CD_2Cl_2) δ 7.61–7.59 (m, 2H), 7.48–7.37 (m, 4H), 7.18 (d, $J = 2.0$ Hz, 2H), 7.15 (dd, $J = 8.1$ Hz, 2.0 Hz, 1H), 3.97 (s, 3H), *denotes residual H_2O . *denotes residual H_2O . ^{13}C NMR (176 MHz, CD_2Cl_2) 155.18, 141.28, 140.23, 130.23, 126.82, 128.79, 127.70, 126.97, 121.41, 119.86, 110.98, 56.11.

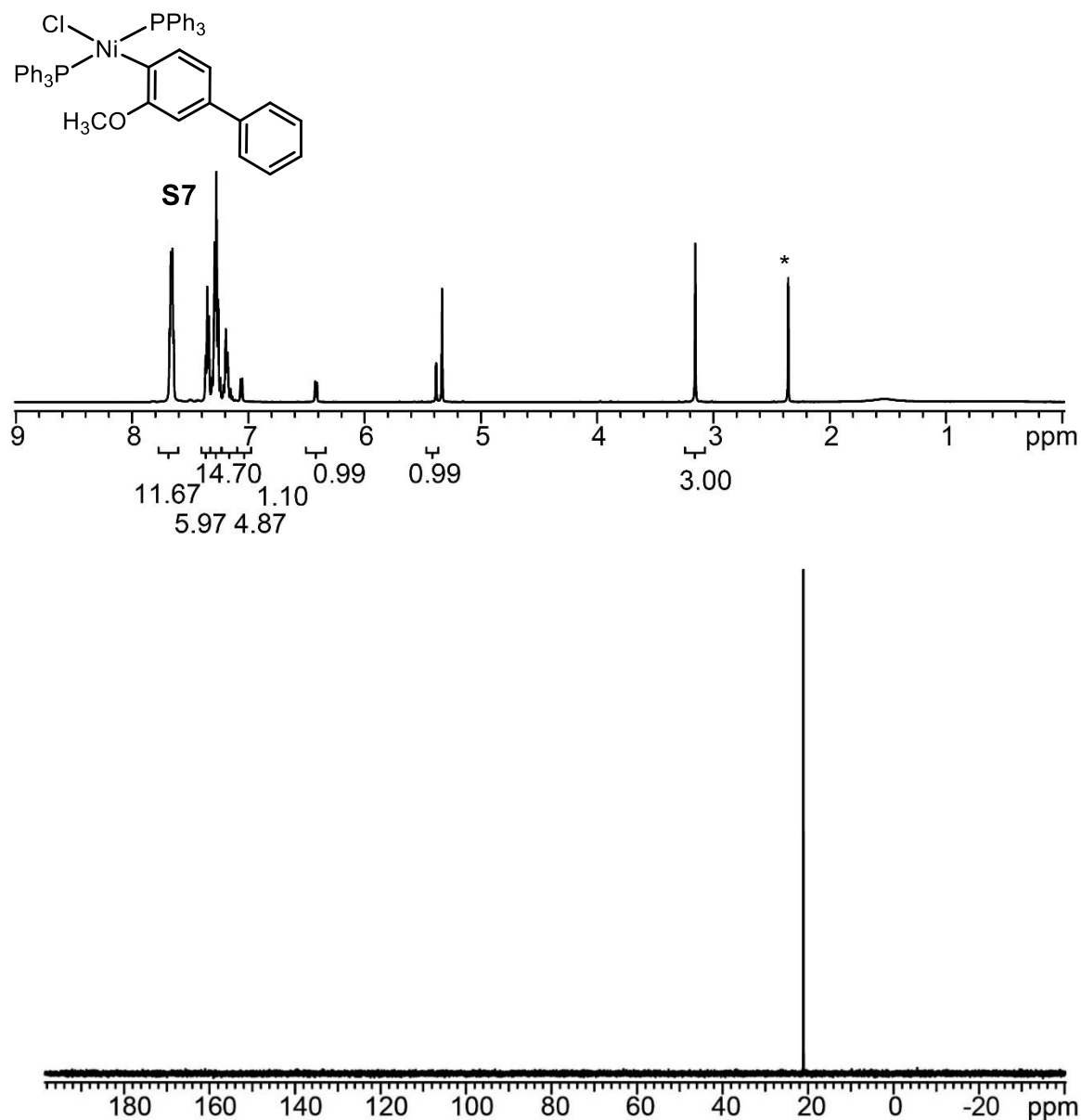


Figure S1.12. ^1H and ^{31}P NMR spectra of **S7**. ^1H NMR (500 MHz, CD_2Cl_2) δ 7.66 (dd, $J = 12.0, 5.1$, 12H) 7.35 (at, $J = 7.2$, 6 H) 7.31–7.24 (m, 15 H), 7.21–7.15 (m, 5H), 7.06 (d, $J = 7.5$ Hz, 1H), 6.41 (d, $J = 7.5$ Hz, 1H), 5.38 (s, 1H), 3.12 (s, 3H) * denotes residual toluene

^{31}P NMR (202 MHz, CD_2Cl_2) δ 21.08.

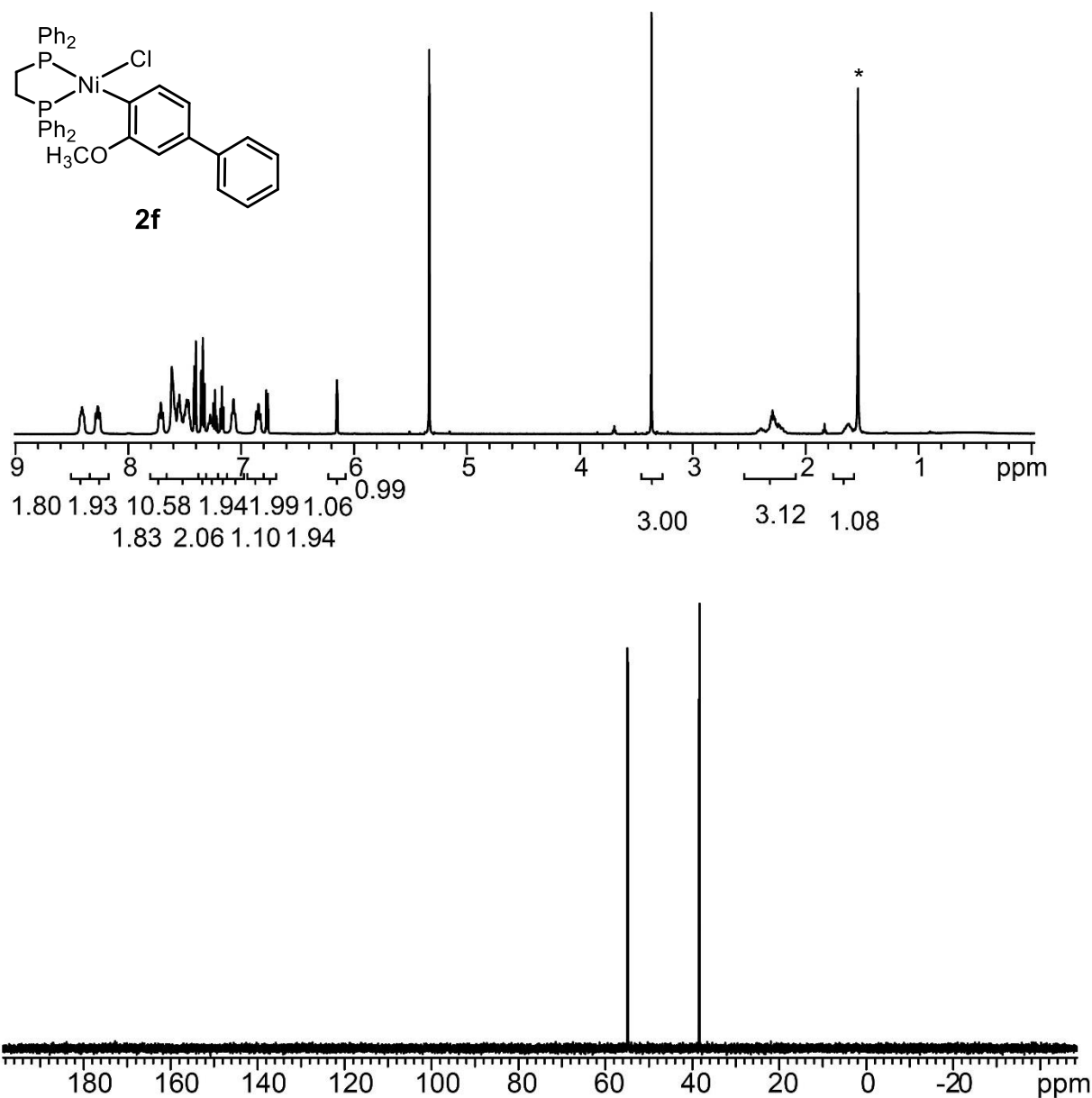


Figure S1.13. ^1H and ^{31}P NMR spectra of **2f**. ^1H NMR (500 MHz, CD_2Cl_2) δ 8.41 (br, 2H) 8.27 (at, $J = 9.0$ Hz, 2H), 7.71 (at, $J = 8.5$ Hz, 2H), 7.61–7.40 (m, 11H), 7.34 (at, $J = 7.5$ Hz, 2H), 7.27–7.22 (m, 2H), 7.17 (at, $J = 7.0$ Hz, 2H), 7.07 (at, $J = 6.6$, 2 H) 6.85 (at, $J = 9.1$ Hz, 2H), 6.77 (dt, $J = 6.1$ Hz, 1.5 Hz, 1H), 6.15 (at, $J = 2.1$ Hz, 1 H), 3.37 (s, 3H), 2.39–2.21 (m, 3H), 1.63–1.62 (m, 1H). *denotes residual H_2O
 ^{31}P NMR (202 MHz, CD_2Cl_2) δ 59.85 (d, $J = 27.5$ Hz), 38.37 (d, $J = 27.5$ Hz).

VI. Initiation Rate Studies

Representative Procedure for Performing React IR Propagation Rate Studies:

The IR probe was inserted through an O-ring sealed 14/20 ground glass adapter (custom-made) into an oven-dried 50 mL 2-neck flask equipped with a stir bar. The other neck was fitted with a three-way flow control adapter with a septum for injections/aliquot sampling and an N₂ line. The oven-dried flask was cooled under vacuum. The flask was then filled with N₂ and evacuated again for a total of three cycles. The flask was charged with a solution of precatalyst **2f** (3.0 mL, 0.005M in THF, 1.00 equiv) and cooled to 0 °C over 20 min. After recording a background spectrum, monomer (0.42 mL, 0.35M in THF, 10 equiv) was added by syringe and the reaction was stirred at 0 °C until monomer consumption stalled for 10 min. Then, THF (3.8 mL) and a second portion of monomer solution (2.8 mL, 0.35M in THF, 65 equiv) were injected and spectra were recorded every 15 s over the entire reaction. To account for mixing and temperature equilibration, spectra recorded in the first 60 s of the reaction were not analyzed. The propagation rate constant (k_p) was calculated by plotting [monomer] versus time over the first 10% conversion of monomer (the second addition). When PPh₃ was included, 2 equiv relative to precatalyst was added in the precatalyst stock solution.

Table S1.1. Table of k_p values

k_p without PPh ₃ (s ⁻¹ x 10 ⁻³)	k_p with PPh ₃ (s ⁻¹ x 10 ⁻³)
10.9	6.7
8.9	8.4
12.0	9.0
11.4	6.7
7.28	6.66
Average = 10 ± 2	Average = 7.5 ± 1

Representative Procedure for Performing React IR Initiation Rate Studies:

The IR probe was inserted through an O-ring sealed 14/20 ground glass adapter (custom-made) into an oven-dried 50 mL 2-neck flask equipped with a stir bar. The other neck was fitted with a three-way flow control adapter with a septum for injections/aliquot sampling and an N₂ line. The oven-dried flask was cooled under vacuum. The flask was then filled with N₂ and evacuated again for a total of three cycles. The flask was charged with THF (6.7 mL) and cooled to 0 °C for 15 min. After recording a background spectrum, monomer (2.3 mL, 0.44M in THF, 1.0 equiv) was added by syringe and allowed to equilibrate at 0 °C for at least 5 min before proceeding. The catalyst solution (1.0 mL, 0.015M, 0.015 equiv) was then injected and spectra were recorded every 15 s over the entire reaction. To account for mixing and temperature equilibration, spectra recorded in the first 60 s of the reaction were not analyzed.

Representative Procedure for k_{obs} Calculation:

The absorbance was converted to concentration using the appropriate calibration curves. The initial rate was obtained from 10% conversion and converted to the observed rate constant (k_{obs}) using equation S1:

$$initial\ rate = -\frac{d[monomer]}{dt} = k_{obs} [Ni]_{total} \quad (S1)$$

Derivation and Representative Procedure for k_i Calculation:

The observed rate constant (k_{obs}) is a weighted average of rate constant of initiation (k_i)

$$k_{obs} = k_i \frac{[Ni]_i}{[Ni]_{total}} + k_p \frac{[Ni]_p}{[Ni]_{total}}$$

and propagation (k_p) during the beginning of polymerization.

The concentration of nickel precatalyst undergoing initiation ($[Ni]_i$) is determined by an

$$[Ni]_i = [Ni]_{i(0)} e^{-k_i t}$$

exponential decay dependent on k_i , time, and the initial concentration of nickel ($[Ni]_{i(0)}$):

Assuming that all precatalyst undergoes initiation, $[\text{Ni}]_{i(0)} = [\text{Ni}]_{\text{total}}$, so we rearranged the exponential decay as follows:

We assume all nickel species in solution are undergoing initiation or propagation;

$$\frac{[\text{Ni}]_i}{[\text{Ni}]_{\text{total}}} = e^{-k_i t}$$

therefore,

$$[\text{Ni}]_{\text{total}} = [\text{Ni}]_i + [\text{Ni}]_p$$

By dividing each side by $[\text{Ni}]_{\text{total}}$, we reach

$$\frac{[\text{Ni}]_{\text{total}}}{[\text{Ni}]_{\text{total}}} = \frac{[\text{Ni}]_i}{[\text{Ni}]_{\text{total}}} + \frac{[\text{Ni}]_p}{[\text{Ni}]_{\text{total}}}$$

and by rearranging and plugging in the exponential decay equation, we derive:

$$\frac{[\text{Ni}]_p}{[\text{Ni}]_{\text{total}}} = 1 - \frac{[\text{Ni}]_i}{[\text{Ni}]_{\text{total}}} = 1 - e^{-k_i t}$$

By substituting the new definitions for k_i and k_p into the equation defining k_{obs} , we arrive at equation 2:

$$k_{\text{obs}} = k_i(e^{-k_i t}) + k_p(1 - e^{-k_i t}) \quad (1)$$

The solve function of Mathematica was utilized to calculate k_i for each catalyst, using reaction time for 10% monomer conversion, and k_{obs} obtained from the initiation study. The propagation rate constant (k_p) was measured experimentally as described in the previous section.

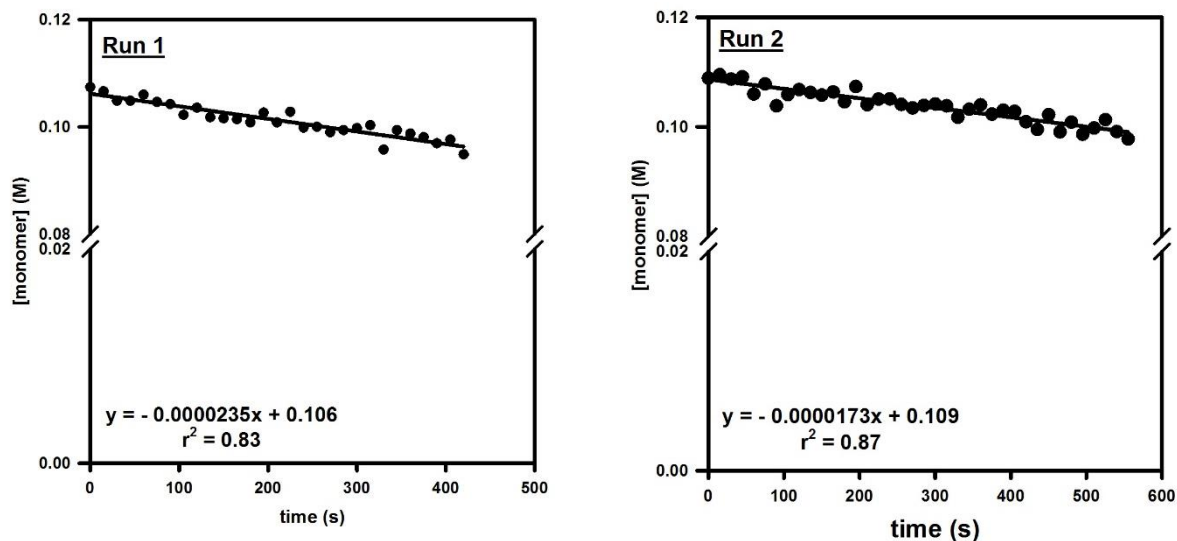


Figure S1.14. Plot of [monomer] versus for the polymerization of **monomer 1** catalyzed by **2b**. (temp = 0 °C, [**2b**] = 0.0015 M, [**monomer**] = 0.11M (Run 1), 0.11M (Run 2)). The initiation rate constant k_i was not calculated for run 1 because equation 1 fails when $k_{obs} > k_p$.

Table S1.2. Table of data for the plots in **Figure S1.14**.

Run	Initial rate ($10^{-6} \times \text{M s}^{-1}$)	k_{obs} ($10^{-3} \times \text{s}^{-1}$)	Time at 10% conversion (s)	Calculated k_i ($10^{-3} \times \text{s}^{-1}$)
1	23.5	15.7	420	n/a
2	17.3	11.5	555	3.1
average	20 ± 4	13 ± 3		

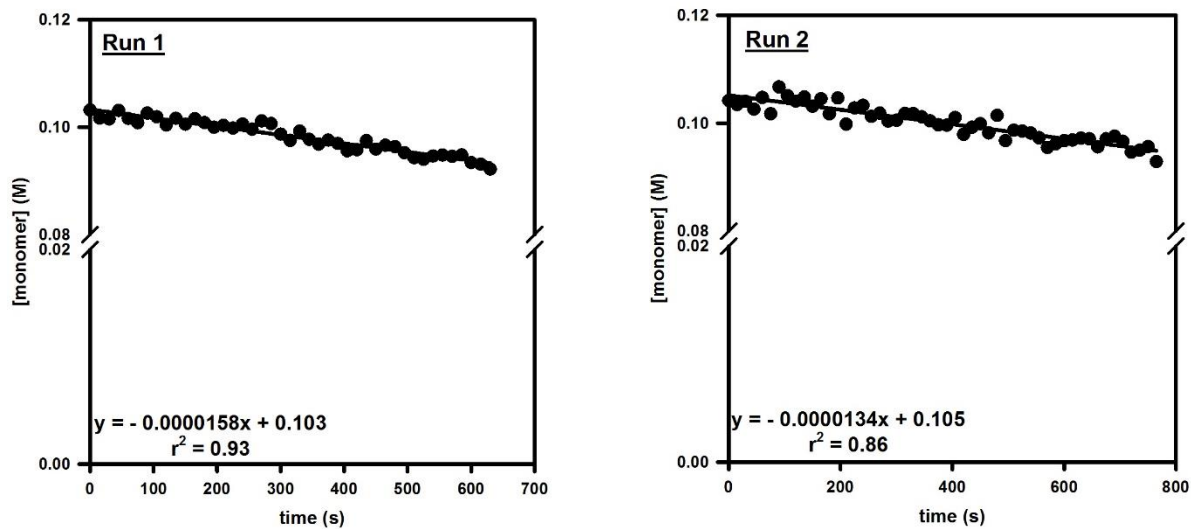


Figure S1.15. Plot of [monomer] versus time the polymerization catalyzed by **2c**. (temp = 0 °C, [2c] = 0.0015M, [monomer] = 0.10M (Run 1), 0.11M (Run 2)).

Table S1.3. Table of data for the plots in **Figure S1.15**.

Run	Initial rate ($10^{-6} \times \text{M s}^{-1}$)	k_{obs} ($10^{-3} \times \text{s}^{-1}$)	Time at 10% conversion (s)	Calculated k_i ($10^{-3} \times \text{s}^{-1}$)
1	15.8	10.5	630	2.35
2	13.4	8.93	735	1.39
average	14 ± 2	9 ± 1		1.9 ± 0.6

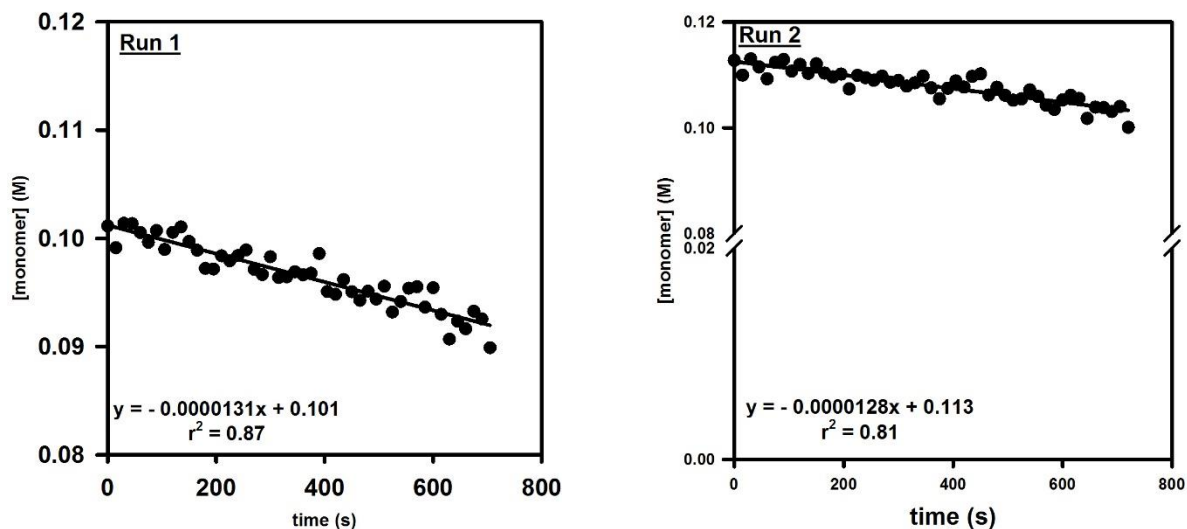


Figure S1.16. Plots of [monomer] versus time for the polymerization catalyzed by **2d**. (temp = 0 °C, [**2d**] = 0.0015M, [monomer] = 0.10M (Run 1), 0.10M (Run 2)). *Due to low solubility of precatalyst **2d**, a more dilute catalyst solution (2.0 mL, 0.0075M, 0.015 equiv) was used.

Table S1.4. Table of data for the plots in **Figure S1.16**.

Run	Initial rate ($10^{-6} \times \text{M s}^{-1}$)	k_{obs} ($10^{-3} \times \text{s}^{-1}$)	Time at 10% conversion (s)	Calculated k_i ($10^{-3} \times \text{s}^{-1}$)
1	13.1	8.56	705	1.38
2	12.8	8.74	720	1.41
average	13.0 ± 0.2	8.7 ± 0.1		1.40 ± 0.02

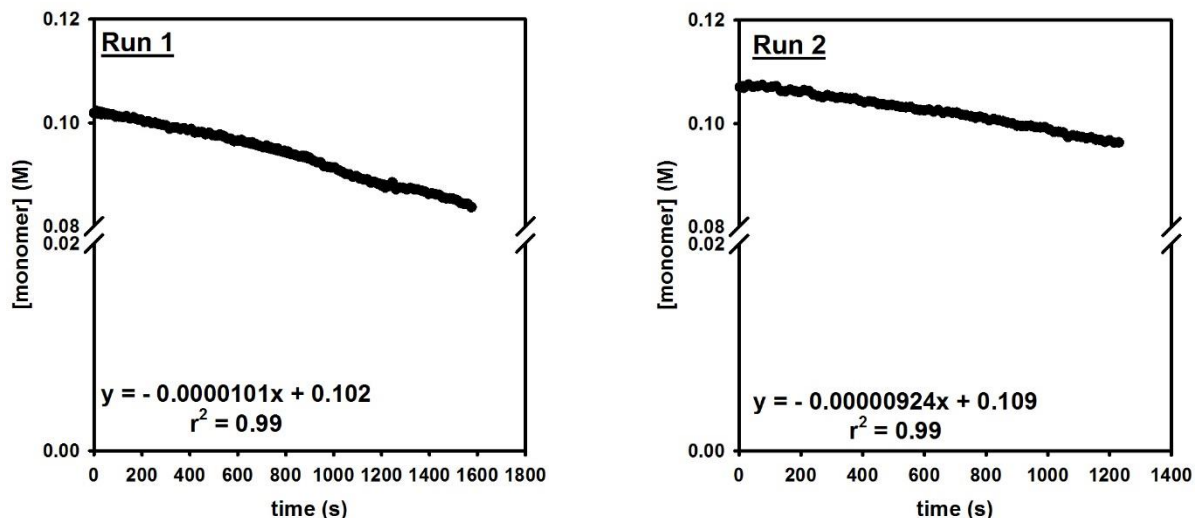


Figure S1.17. Plot of [monomer] versus time for the polymerization catalyzed by **2e**. (temp = 0 °C, [2e] = 0.0015M, [monomer] = 0.10M (Run 1), 0.11M (Run 2)).

Table S1.5. Table of data for the plot in **Figure S1.17**.

Run	Initial rate ($10^{-6} \times \text{M s}^{-1}$)	k_{obs} ($10^{-3} \times \text{s}^{-1}$)	Time at 10% conversion (s)	Calculated k_i ($10^{-3} \times \text{s}^{-1}$)
1	10.08	7.95	990	0.656
2	9.24	6.16	1260	0.616
average	9.7 ± 0.6	7 ± 1		0.64 ± 0.03

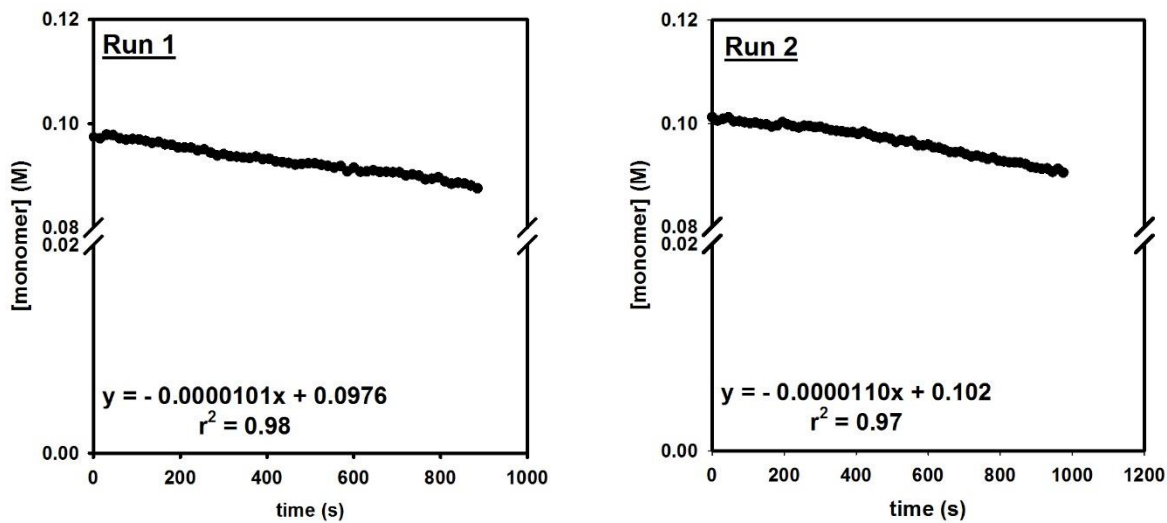


Figure S1.18. Plot of [monomer] versus time for the polymerization catalyzed by **2e** with PPh₃. (temp = 0 °C, [**2e**] = 0.0015M, [PPh₃] = 0.0030 [monomer] = 0.096M (Run 1), 0.11M (Run 2)).

Table S1.6. Table of data for the plot in **Figure S1.18**.

Run	Initial rate (10 ⁻⁶ x M s ⁻¹)	<i>k</i> _{obs} (10 ⁻³ x s ⁻¹)	Time at 10% conversion (s)	Calculated <i>k</i> _i (10 ⁻³ x s ⁻¹)
1	10.1	7.18	885	1.28
2	11.0	7.35	975	1.00
average	10.6 ± 0.7	7.3 ± 0.1		1.1 ± 0.1

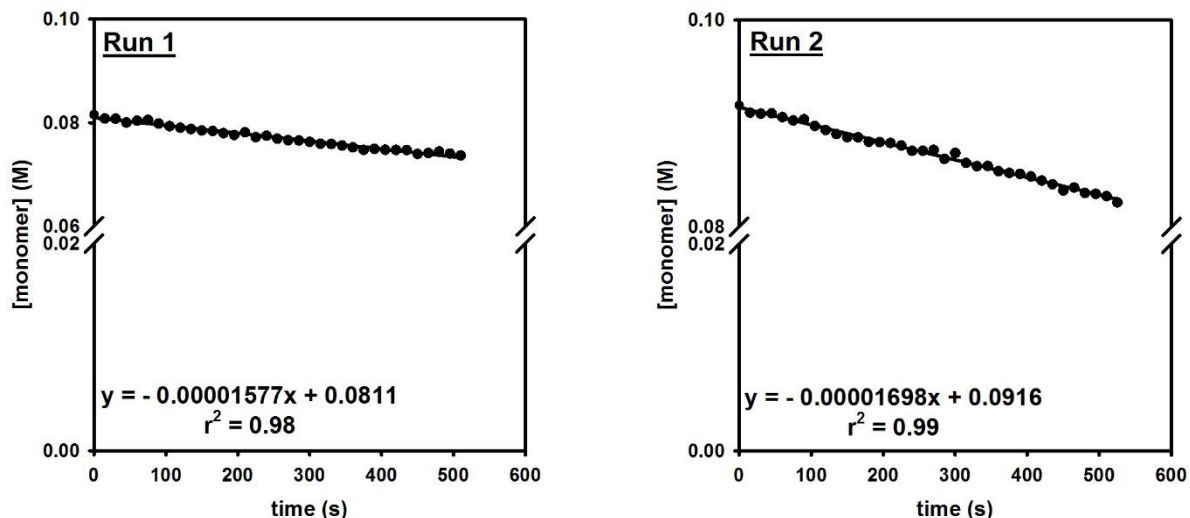


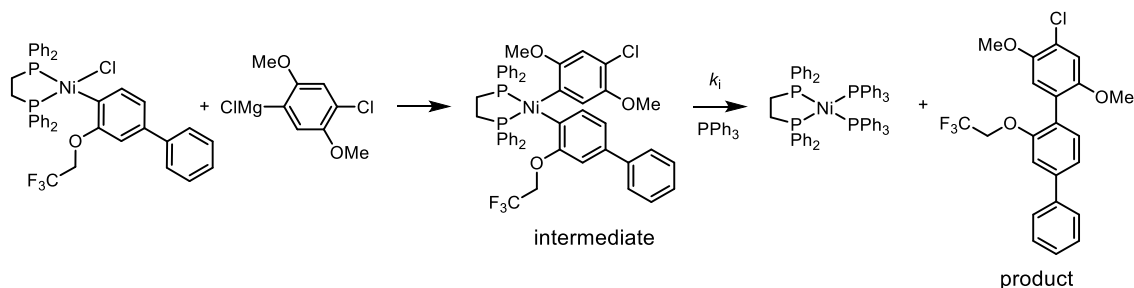
Figure S1.19. Plot of [monomer] versus time for the polymerization catalyzed by **2f**. (temp = 0 °C, [2f] = 0.0015M, [monomer] = 0.08M (Run 1), 0.09M (Run 2)). *Due to low solubility of precatalyst **2f**, a more dilute catalyst solution (3.0 mL, 0.005M, 0.015 equiv) was used.

Table S1.7. Table of data for the plot in **Figure S1.19**. The initiation rate constant k_i was not calculated because equation 1 fails when $k_{obs} > k_p$.

Run	Initial rate ($10^{-6} \times \text{M s}^{-1}$)	k_{obs} ($10^{-3} \times \text{s}^{-1}$)	Time at 10% conversion (s)	Calculated k_i ($10^{-3} \times \text{s}^{-1}$)
1	15.77	10.5	570	n/a
2	16.98	11.3	465	n/a
average	16.4 ± 0.9	10.9 ± 0.6		n/a

Representative Procedure for Performing ^{19}F NMR Spectroscopy Studies

In a glovebox under an N_2 atmosphere a stock solution of precatalyst **2e** (19.8 mg, 0.0265 mmol) and PPh_3 (15.1 mg, 0.0557 mmol) was prepared in THF (1 mL). To this stock solution, α,α,α -trifluoromethyltoluene (26 μL , 1.0M in THF) was added as an internal standard. A J. Young NMR tube was charged with this solution (0.8 mL), sealed with a septum, and cooled to 0 $^\circ\text{C}$ in the spectrometer for approx. 45 min. A solution of (4-chloro-2,5-dimethoxyphenyl)magnesium chloride (0.2 mL, 0.2M in THF, 2.0 equiv) was added, and the tube was inverted once to mix. The final solution contained 0.02 mmol precatalyst, 0.04 mmol PPh_3 , 0.02 mmol α,α,α -trifluoromethyltoluene, and 0.04 mmol (4-chloro-2,5-dimethoxyphenyl)magnesium chloride. All ^{19}F NMR spectra were acquired with acquisition time = 1.5 s, relaxation time = 3 s, scan size = 4.



Scheme S1.1. Initiation of precatalyst **2e**

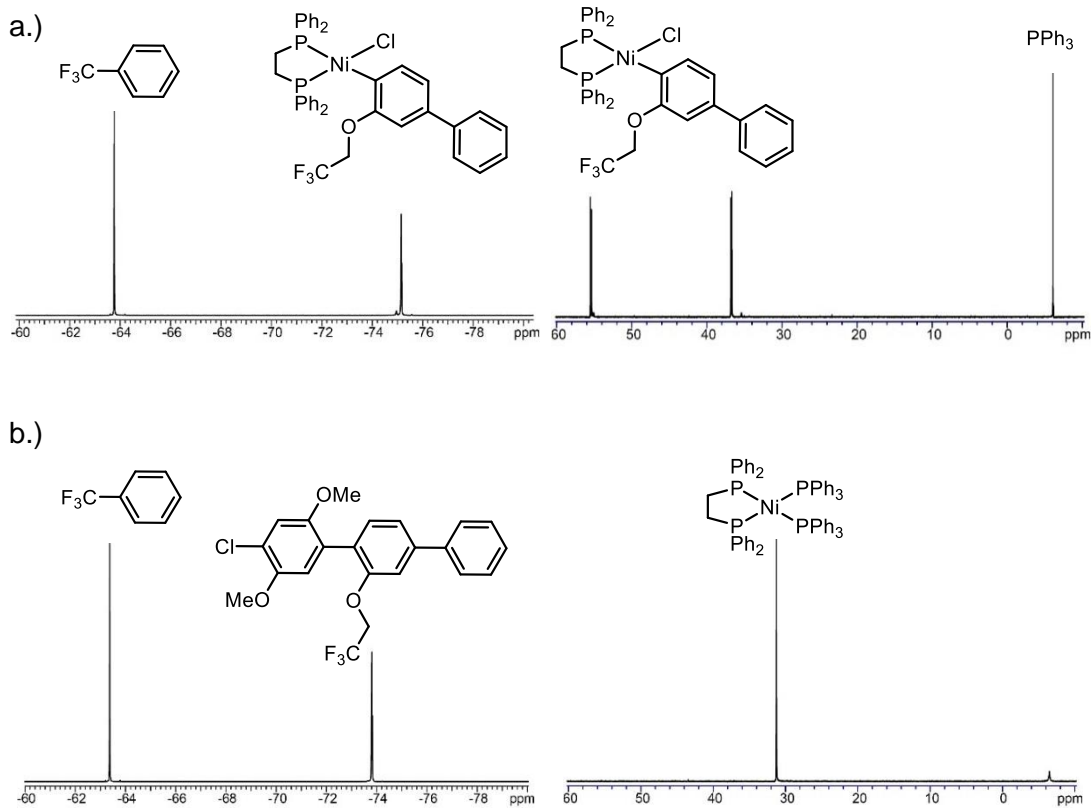
^{19}F NMR spectra **^{31}P NMR spectra**

Figure S1.20. (a) ^{19}F and ^{31}P NMR spectra at the beginning and (b) end of the reaction in **Scheme S1.1**.

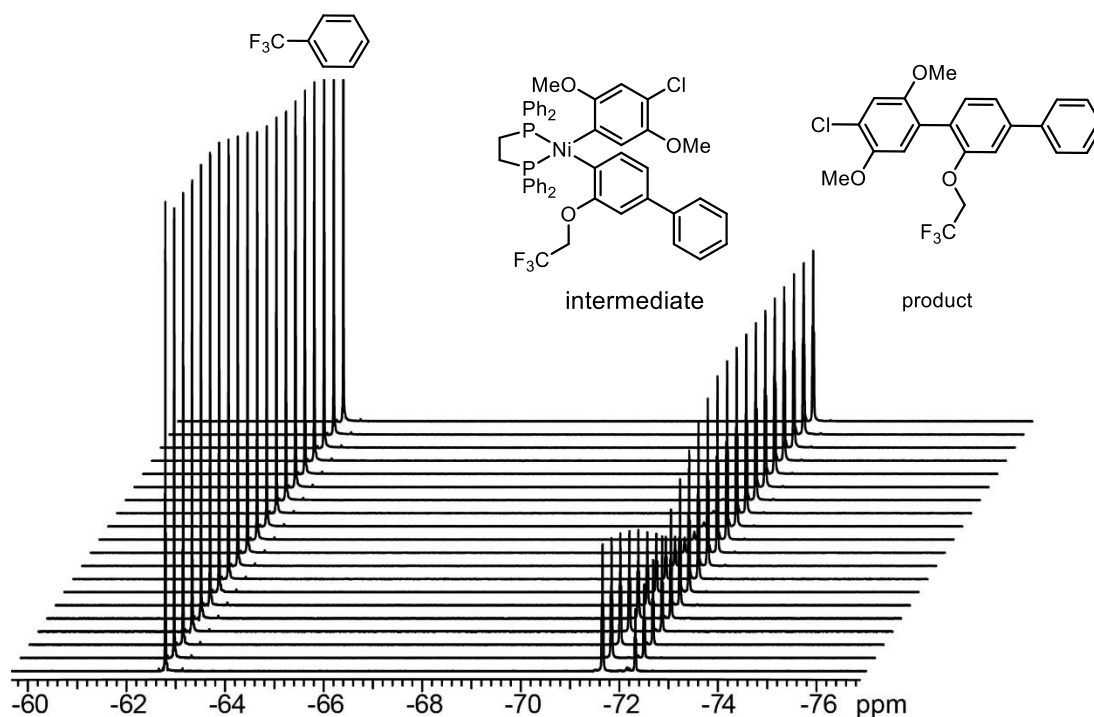


Figure S1.21. Representative ^{19}F NMR spectral array for precatalyst **2e**. Concentrations were calculated relative to an internal standard, α,α,α -trifluoromethyltoluene.

Procedure for Calculating Concentrations from Integrals

The internal standard concentration was used to calculate the ratio of integration:concentration, which was then used to calculate concentrations of the intermediate and product peaks from the integrals.

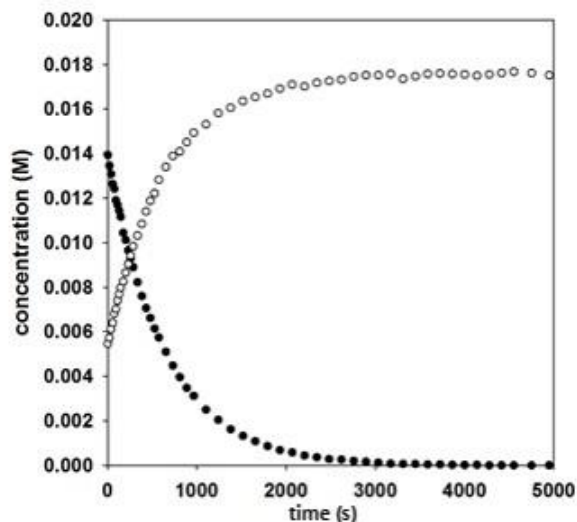


Figure S1.22. Plot of concentration of intermediate (●) and product (○) versus time for the data in **Figure S1.21**.

Procedure for Calculating Rate Constants in Igor Pro

Initiation rate constants were calculated using Igor Pro v.6.22A, following the procedure in “Fitting to Differential equations in Igor Pro” provided by the Collum group⁴ and using Collum Kinetic 5000 as the master procedure file. The data was fit to the following equations:

$$\frac{d[\textit{intermediate}]}{dt} = -k_i \times [\textit{intermediate}] \quad (2)$$

$$\frac{d[\textit{product}]}{dt} = k_i \times [\textit{intermediate}] \quad (3)$$

Table S1.8. Initiation rate constants for **2e**

Run	k_i ($10^{-3} \times \text{s}^{-1}$)
1	1.310
2	1.307
average	1.309 ± 0.002

VII. Polymerization

Representative Procedure for M_n and \bar{D} versus Conversion Studies Utilizing *in situ* React IR Spectroscopy:

The IR probe was inserted through an O-ring-sealed 14/20 ground-glass adapter (custom-made) into an oven-dried 50 mL 2-neck flask equipped with a stir bar. The other neck was fitted with a three-way flow-control adapter with a septum for injections/aliquot sampling and an N₂ line. The oven-dried flask was cooled under vacuum, then filled with N₂. The flask was re-evacuated and filled for two additional cycles. The flask was charged with THF (6.7 mL) and cooled to 0 °C for 15 min. After recording a background spectrum, monomer **1** (2.3 mL, 0.44 M in THF, 1.0 equiv) was added by syringe and equilibrated at 0 °C for at least 5 min. Then the precatalyst solution (1.0 mL, 0.015 M, 0.015 equiv) was injected and spectra were recorded every 15 s. To account for mixing and temperature equilibration, spectra recorded in the first 60 s were not analyzed. Aliquots (approx. 0.5 mL) were taken via syringe and immediately quenched with aq. HCl (approx. 1 mL, 12 M). The resulting solution was then extracted with CH₂Cl₂ (2 x 1.5 mL) (with mild heating if polymer had precipitated), dried over MgSO₄, filtered, and then concentrated. At approximately 80% conversion, the polymerization was poured into aq. HCl (20 mL, 12 M), extracted with CH₂Cl₂ (3 x 25 mL), washed with H₂O (1 x 25 mL), brine (1 x 25 mL), dried over MgSO₄, filtered, and concentrated. The samples (both aliquots and the final reaction mixture) were each dissolved in THF (with heating), and passed through a 0.2 μm poly(tetrafluoroethylene) filter for analysis by gel permeation chromatography (GPC). The monomer conversion versus time data was calculated from the IR spectra using a calibration curve.

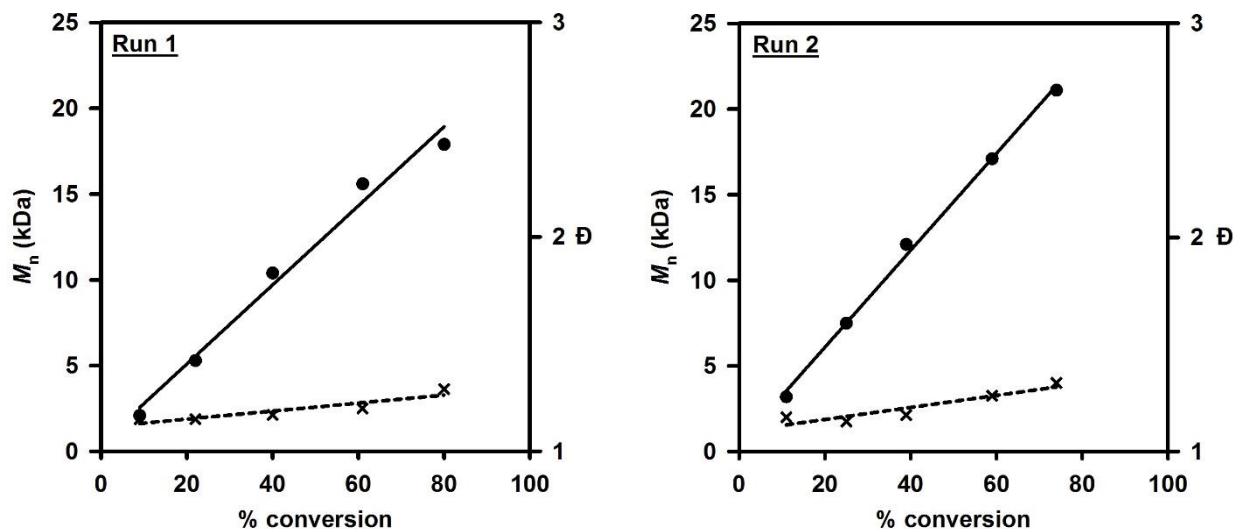


Figure S1.23. Plot of M_n (●) and \bar{D} (x) versus conversion for **2b** (temp = 0 °C, [2b] = 0.0015M, [monomer] = 0.11M (Run 1), 0.11M (Run 2)).

Table S1.9. Data for the plot in **Figure S1.23**, Run 1.

% Conversion	M_n (kDa)	\bar{D}
9	2.1	1.15
22	5.3	1.15
40	10.4	1.17
61	15.6	1.20
80	17.9	1.29

Table S1.10. Data for the plot in **Figure S1.23**, Run 2.

% Conversion	M_n (kDa)	\bar{D}
11	3.2	1.16
25	7.5	1.14
39	12.1	1.17
59	17.1	1.26
74	21.1	1.32

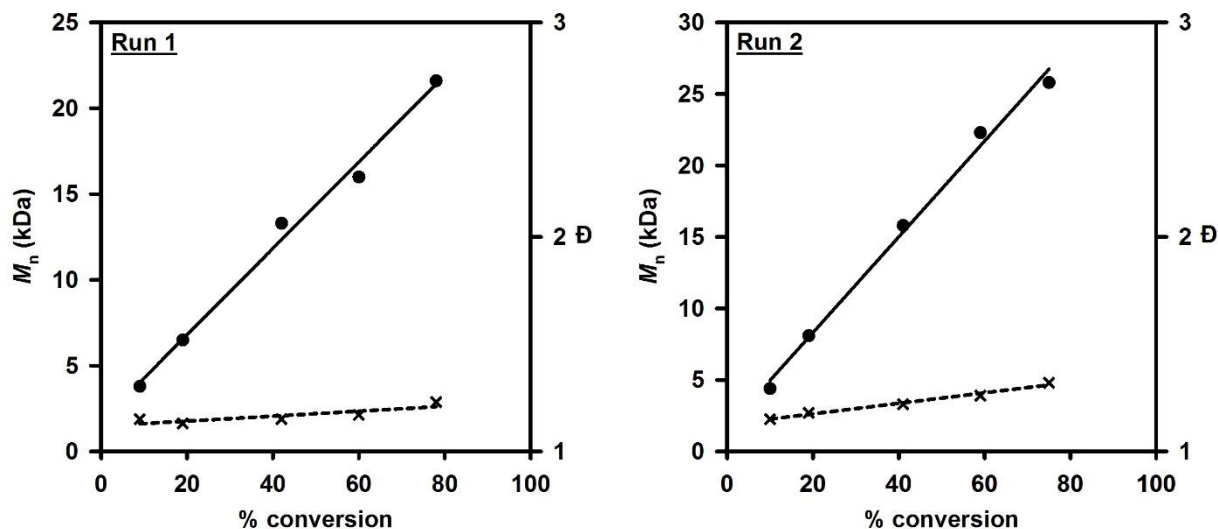


Figure S1.24. Plot of M_n (●) and \bar{D} (x) versus conversion for **2c** (temp = 0 °C, $[2c] = 0.0015M$, $[\text{monomer}] = 0.10M$ (Run 1), $0.10M$ (Run 2)).

Table S1.11. Data for the plot in **Figure S1.24**, Run 1.

% Conversion	M_n (kDa)	\bar{D}
9	3.8	1.15
19	6.5	1.13
42	13.3	1.15
60	16.0	1.17
78	21.6	1.23

Table S12. Data for the plot in **Figure S24**, Run 2.

% Conversion	M_n (kDa)	\bar{D}
10	4.4	1.15
19	8.1	1.18
41	15.8	1.22
59	22.3	1.26
75	25.8	1.32

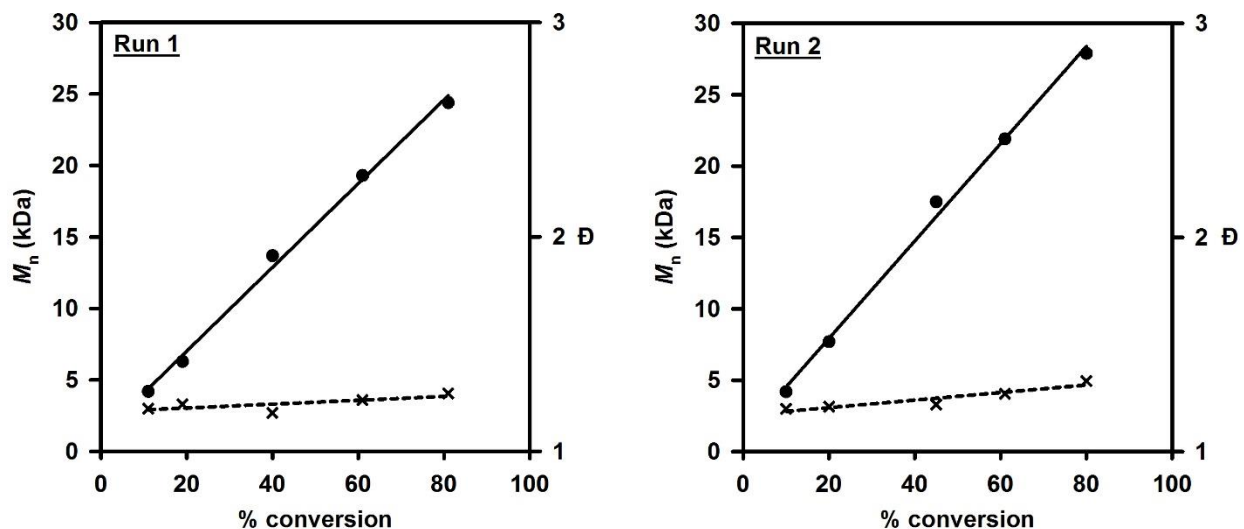


Figure S1.25. Plot of M_n (●) and \bar{D} (x) versus conversion for **2d** (temp = 0 °C, [2d] = 0.0015M, [monomer] = 0.10M (Run 1), 0.11M (Run 2)). *Due to low solubility of precatalyst **2d**, a dilute precatalyst solution (2.0 mL, 0.0075M, 0.015 equiv) was used.

Table S1.13. Data for the plot in **Figure S1.25**, Run 1.

% Conversion	M_n (kDa)	\bar{D}
11	4.2	1.20
19	6.3	1.22
40	13.7	1.18
61	19.3	1.24
81	24.4	1.27

Table S1.14. Data for the plot in **Figure S1.25**, Run 2.

% Conversion	M_n (kDa)	\bar{D}
10	4.2	1.20
20	7.7	1.21
45	17.5	1.22
61	21.9	1.27
80	27.9	1.33

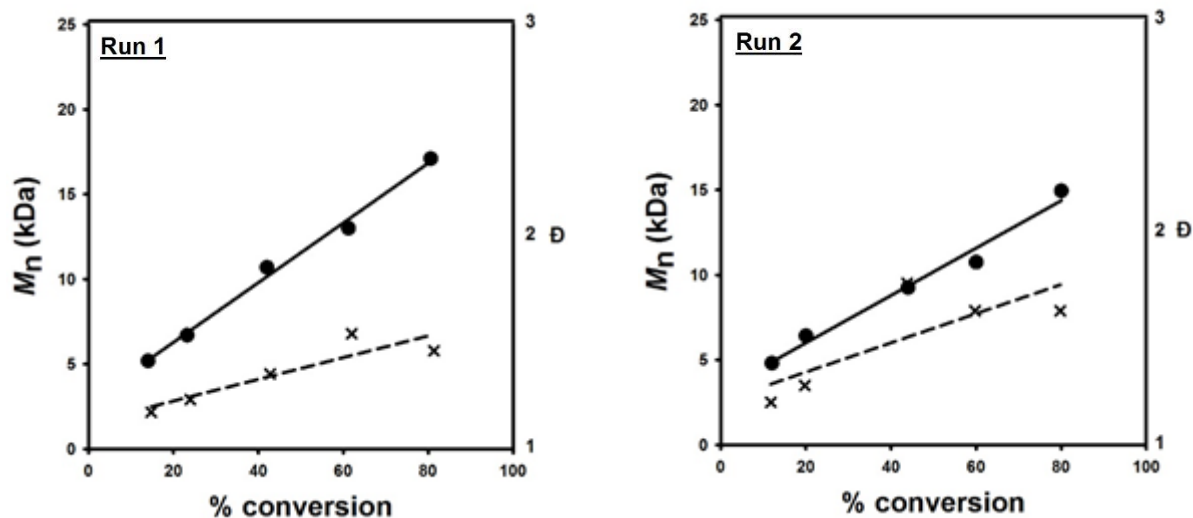


Figure S1.26. Plot of M_n (●) and \bar{D} (x) versus conversion for **2e** (temp = 0 °C, $[2e] = 0.0015M$, $[monomer] = 0.10M$ (Run 1), $0.11M$ (Run 2)).

Table S1.15. Data for the plot in **Figure S1.26**, Run 1.

% Conversion	M_n (kDa)	\bar{D}
14	5.2	1.16
23	6.7	1.22
42	10.7	1.34
61	13.0	1.53
81	17.1	1.45

Table S1.16. Data for the plot in **Figure S1.26**, Run 2.

% Conversion	M_n (kDa)	\bar{D}
12	4.8	1.19
20	6.4	1.27
44	9.3	1.55
60	10.8	1.75
80	15.0	1.62

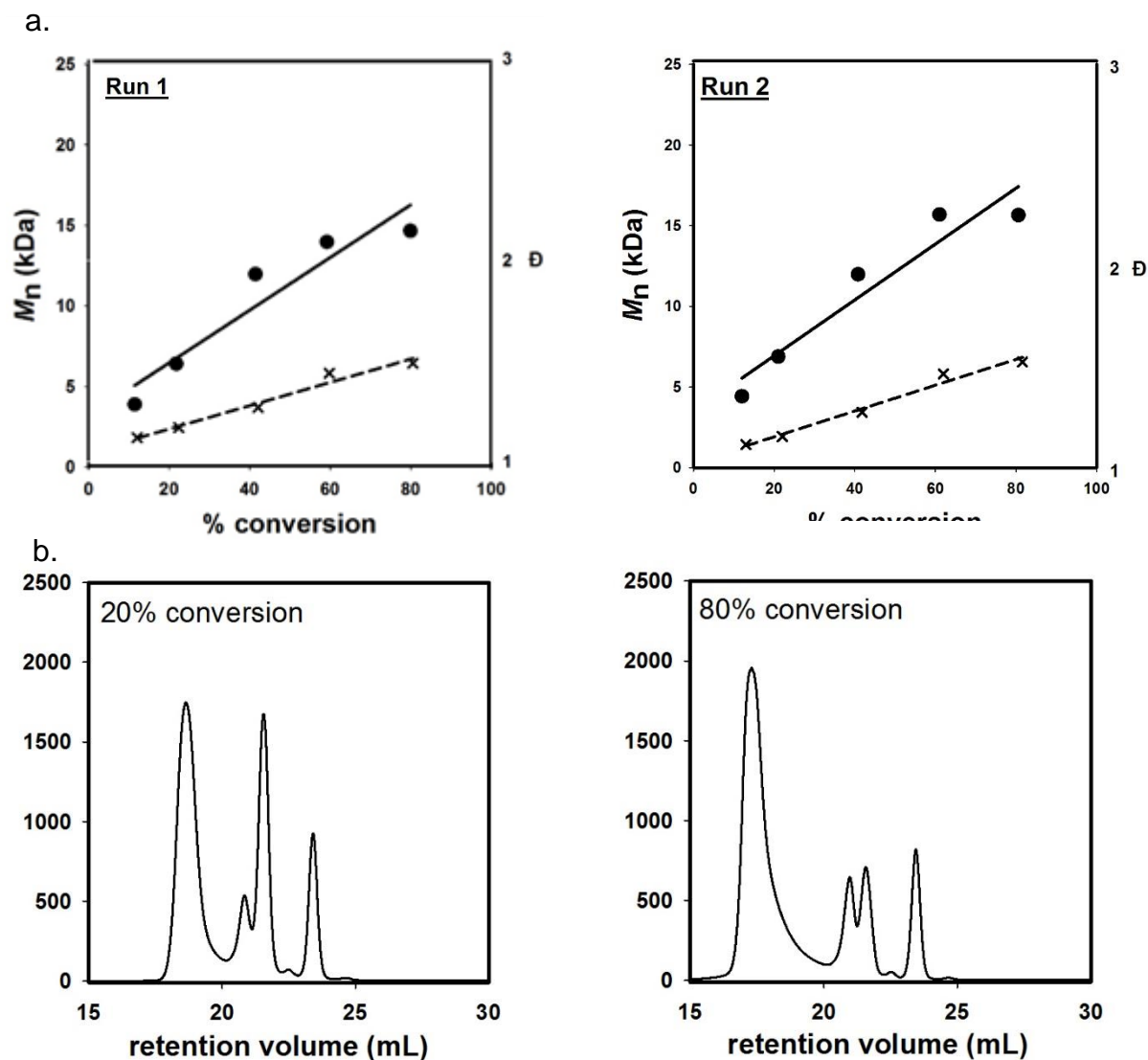


Figure S1.27. a.) Plot of M_n (●) and \bar{D} (x) versus conversion for **2f** (temp = 0 °C, [**2f**] = 0.0015M, [monomer] = 0.082M (Run 1), 0.90M (Run 2)). *Due to low solubility of precatalyst **2f**, a dilute catalyst solution (3.0 mL, 0.005M, 0.015 equiv) was used. b.) GPC curves of aliquots removed at 20 and 80% monomer conversion during Run 1.

Table S1.17. Data for the plot in **Figure S1.27a**, Run 1.

% Conversion	M_n (kDa)	\bar{D}
11	3.9	1.12
22	6.4	1.17
41	12.0	1.27
59	14.0	1.44
80	14.7	1.49

Table S1.18. Data for the plot in **Figure S1.27b**, Run 2.

% Conversion	M_n (kDa)	\bar{D}
12	4.4	1.13
21	6.9	1.17
41	12.0	1.29
61	15.7	1.48
81	15.6	1.54

VIII. MALDI-TOF-MS Analysis

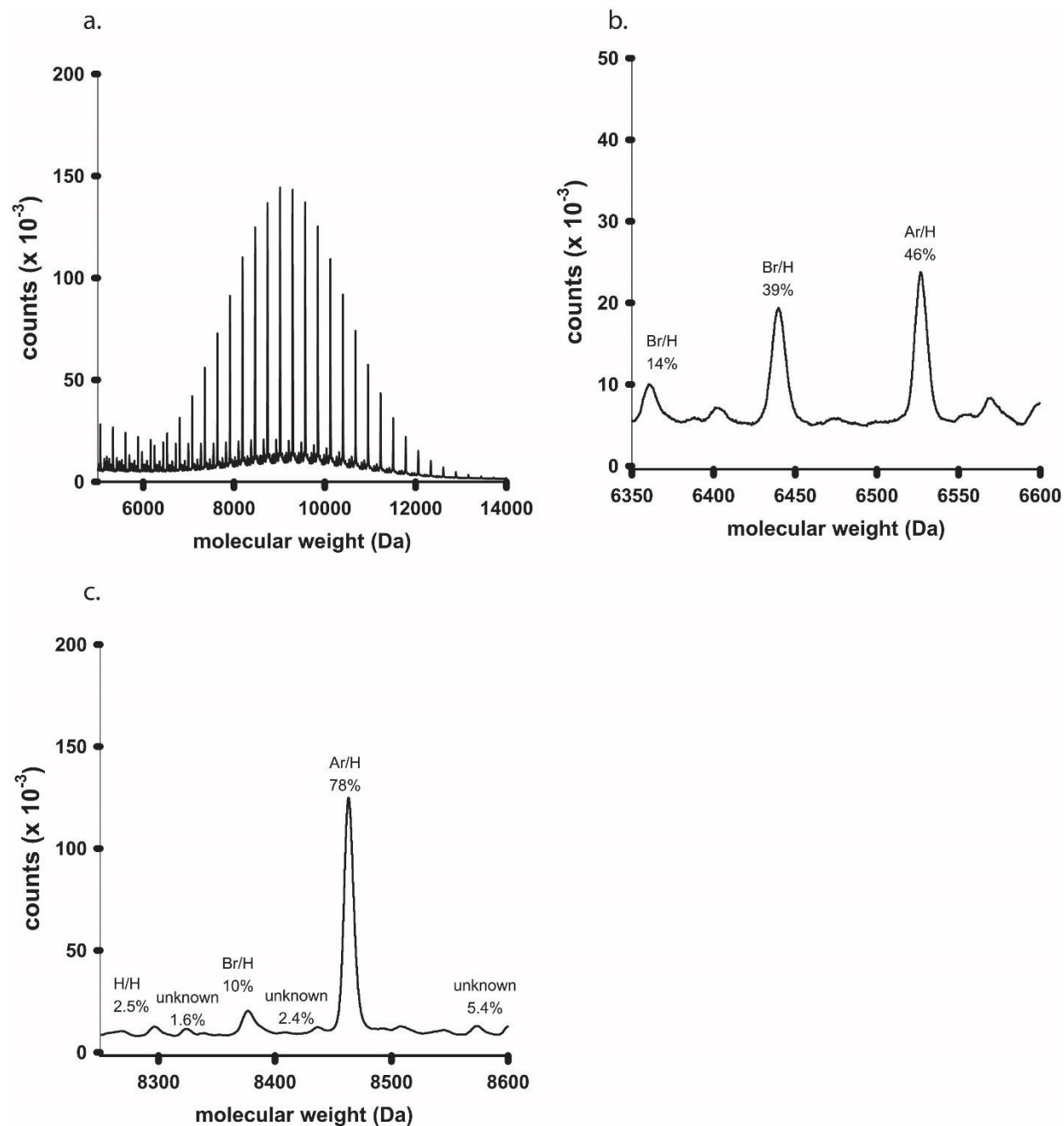


Figure S1.28. a. Full MALDI-TOF MS spectrum of polyphenylene initiated with precatalyst **2b**, b., MALDI-TOF MS spectrum at 23 repeat units, and c., MALDI-TOF MS spectrum at 30 repeat units. The polymer sample analyzed was from an aliquot was taken at 20% conversion for the polymer described in **Figure S1.23**. Lower molecular weight polymers had a higher percentage of Br/H terminated polymers.

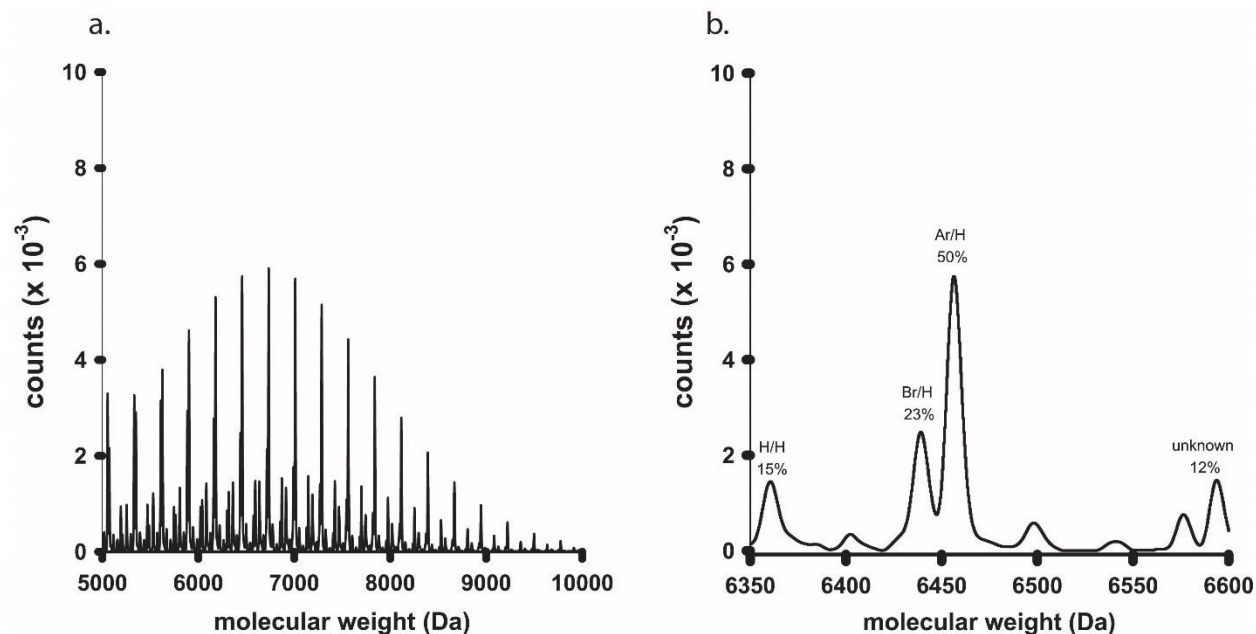


Figure S1.29. a. Full MALDI-TOF MS spectrum of polyphenylene initiated with precatalyst **2c**, and b., MALDI-TOF MS spectrum at 23 repeat units. The polymer sample analyzed was from an aliquot was taken at 20% conversion for the polymer described in **Figure S1.24**.

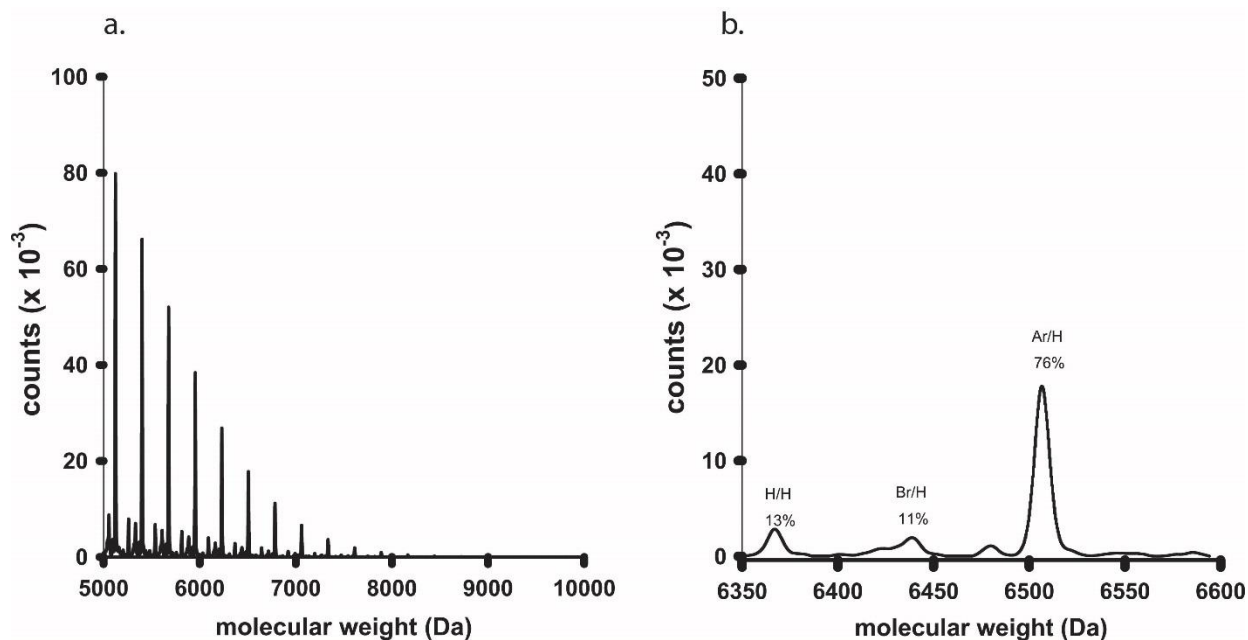
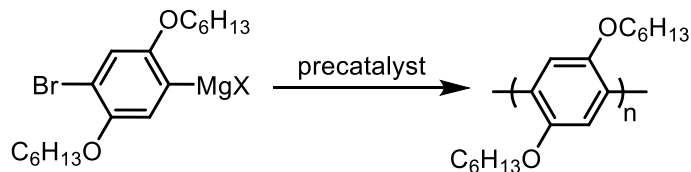


Figure S1.30. a. Full MALDI-TOF MS spectrum of polyphenylene initiated with precatalyst **2d**, and b., MALDI-TOF MS spectrum at 23 repeat units. The polymer sample analyzed was from an aliquot was taken at 20% conversion for the polymer described in **Figure S1.25**.

Representative Procedure for Preparation of Polymers to Compare End-group Fidelity with Three dppe-Based Precatalysts:



In a glovebox, a precatalyst stock solution was made by combining **2f** (11.2 mg, 0.0165 mmol) with THF (3.3 mL) in a 4 mL vial. (Note: For Ni(dppe)Cl₂, a pre-initiation protocol was followed wherein monomer **1** (0.23 mL, 5 equiv) was added to the precatalyst and stirred until homogeneous). The precatalyst solution (3.0 mL, 0.015 mmol, 1 equiv) and THF (3.8 mL) were combined in a 50 mL Schlenk tube, sealed with a Teflon stopper, and then removed from the glovebox and put under N₂ pressure. The solution was cooled to 0 °C for 20 min. Then monomer solution (3.2 mL, 1.0 mmol, 66 equiv) was added. After 30 min, an aliquot was removed by syringe, then quenched with aq. HCl (approx. 1.0 mL, 12 M), extracted with CH₂Cl₂ (2 x 1 mL), dried over MgSO₄, filtered, concentrated, and then analyzed by MALDI-TOF MS analysis (SI). After 4 h, the polymerization was poured in aq. HCl (20 mL, 12 M), extracted with CH₂Cl₂ (3 x 25 mL), washed with water (1 x 25 mL), brine (1 x 25 mL), dried over MgSO₄, filtered, and concentrated. Both the aliquot and the bulk polymerization were analyzed by GPC.

Precatalyst	<i>M_n</i> (kDa)	Đ
2f	16.1	1.45
Ni(dppe)(tol)Br	18.4	1.54
Ni(dppe)Cl ₂	23.0	1.41

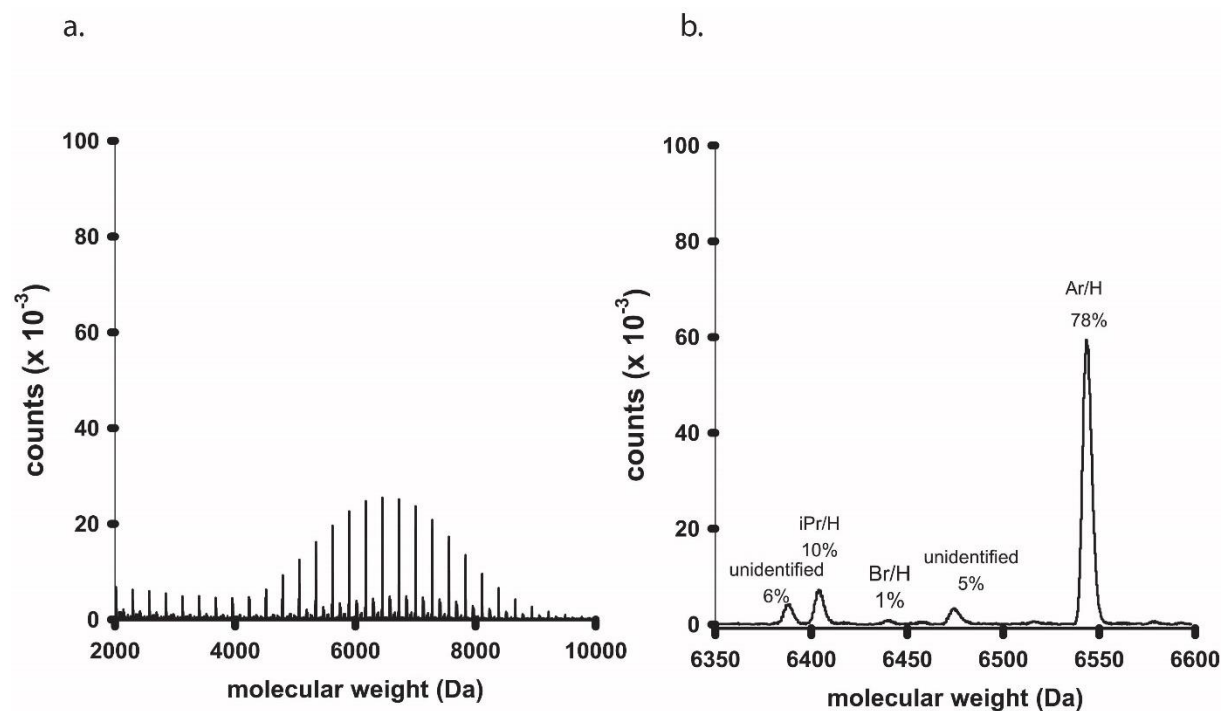


Figure S1.31. a. Full MALDI-TOF MS spectrum of polyphenylene initiated with precatalyst **2f**, and b., MALDI-TOF MS spectrum at 23 repeat units.

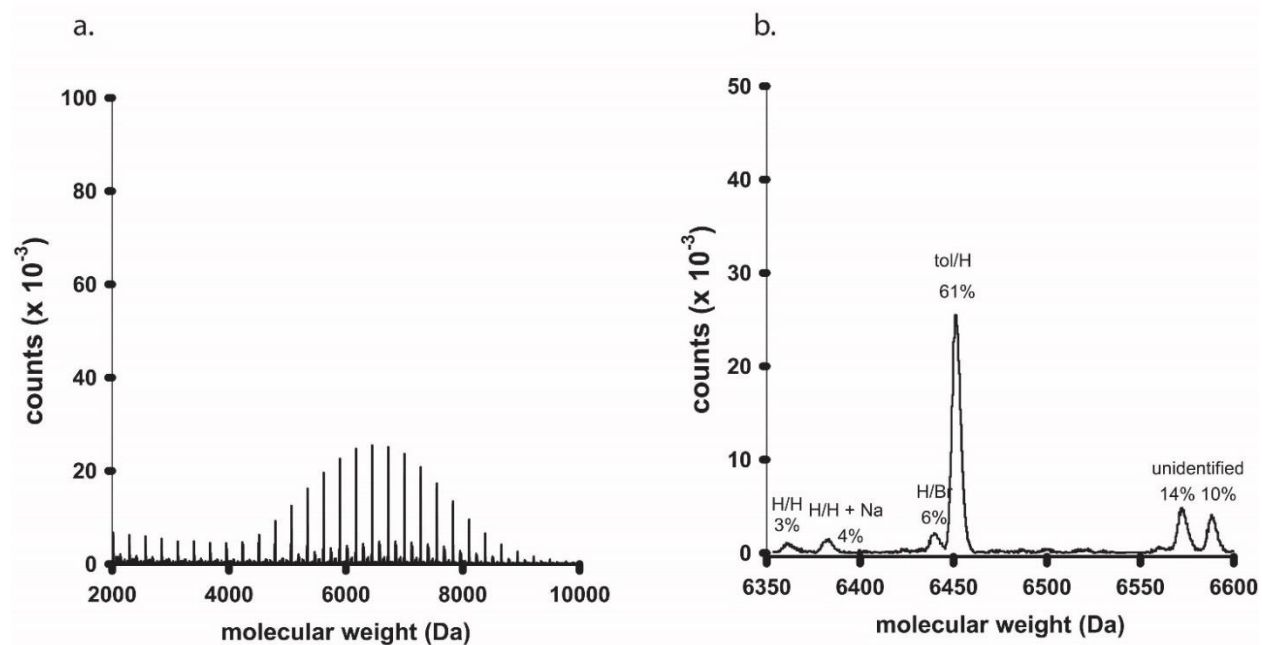


Figure S1.32. a. Full MALDI-TOF MS spectrum of polyphenylene initiated with Ni(dppe)tolBr, and b., MALDI-TOF MS spectrum at 23 repeat units.

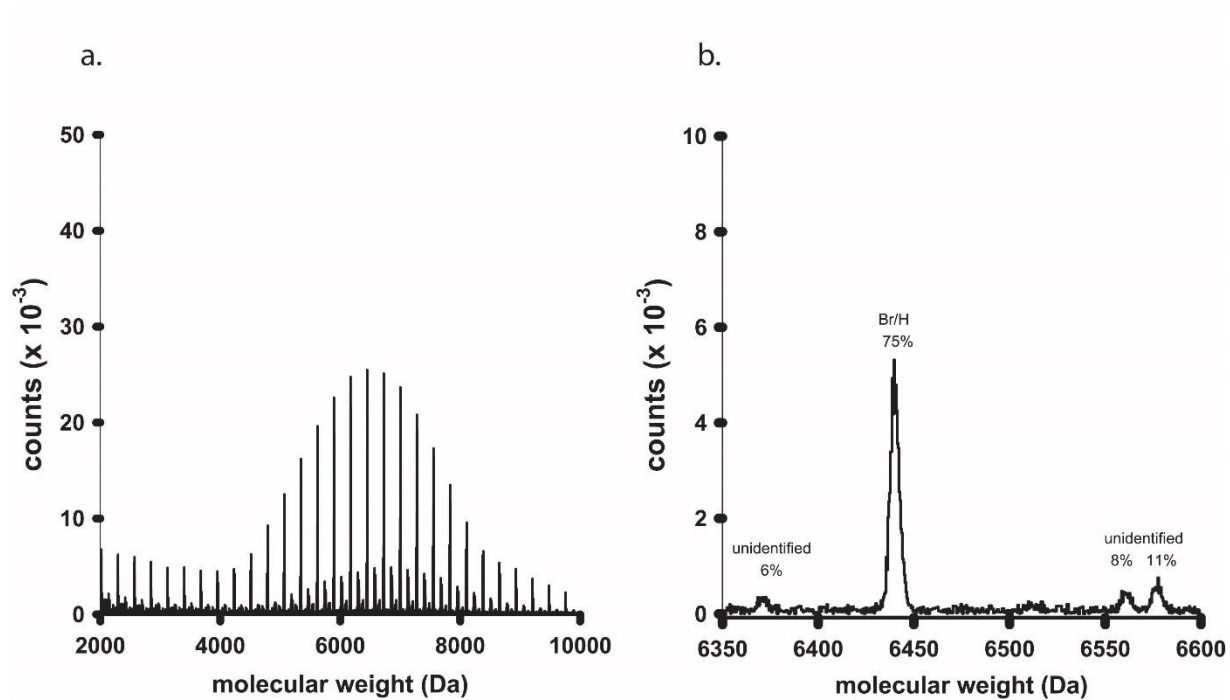


Figure S1.33. a. Full MALDI-TOF MS spectrum of polyphenylene initiated with Ni(dppe)Cl₂, and b., MALDI-TOF MS spectrum at 23 repeat units.

X. Computational Data

Computations were performed with the BP86 DFT functional⁵ paired with the 6-311+G(d) basis set⁶ was used for all non-metal atoms and the SDB-cc-pVTZ basis set with the small core, fully relativistic effective core potential⁷ was used for Ni. All computations were performed using Gaussian09.

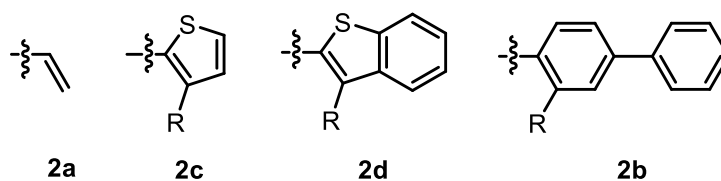
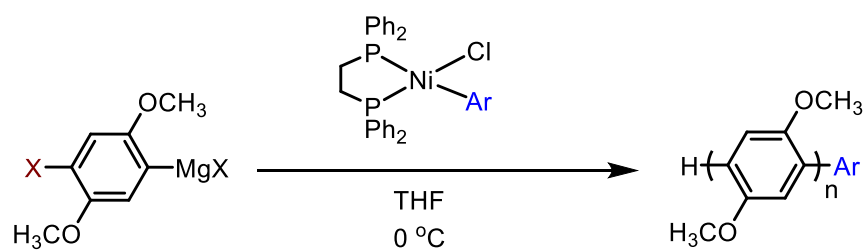


Table S1.19. Absolute electronic energies (E) and free energies (G), in hartrees, for reactants and transition states (TS), along with the corresponding change in NPA charges for select species (Δq).

A _r	X	R	E(Reactant)	G(Reactant)	E(TS)	G(TS)	Δq
1	B _r	--	- 4971.90540 4	- 4971.38789 8	- 4971.89431 1	- 4971.37756 7	--
2	B _r	CH ₃	- 5485.72532 8	- 5485.16936 1	-5485.70677	- 5485.15114 5	--
3	B _r	CH ₃	- 5639.40893 1	- 5638.81039 5	- 5639.38939 8	- 5638.79143 1	--
4	B _r	CH ₃	- 5396.01706 1	- 5395.35623 6	-5395.99755	- 5395.33812 9	0.24 4
5	B _r	OCH ₃	- 5471.25594 3	- 5470.59185 8	- 5471.23810 4	- 5470.57520 8	0.24 7
5	B _r	OCH ₂ CH ₃	- 5510.57899 5	- 5509.88910 1	- 5510.56134 4	- 5509.87206 4	0.24 9
5	B _r	OCH ₂ CF ₃	- 5808.41091 5	- -5807.74857	- 5808.39191 1	- 5807.72867 1	0.25 9
1	Cl	CH ₃	- 2857.76516 3	- 2857.24519 1	- 2857.75425 7	- 2857.23428 1	--
2	Cl	CH ₃	- 3371.58451 3	- -3371.02894	- 3371.56753 6	- 3371.01124 8	--
3	Cl	CH ₃	- 3525.26891 3	- -3524.66836	- 3525.24928 8	- 3524.64757 2	--
4	Cl	CH ₃	- 3281.87684 7	- 3281.21468 2	- 3281.85638 1	- 3281.19354 2	--

References

- (1) Collins, E.A.; Garcia-Losada, P.; Hamdouchi, C.; Hipskind, P.A.; Lu, J.; T. Takakuwa, T. Imidazopyridazine compounds WO/2006/107784 A1.
- (2) Lee, S. R.; Bloom, J. W. G.; Wheeler, S. E.; McNeil, A.J. Accelerating Ni(II) Precatalyst Initiation Using Reactive Ligands and its Impact on Chain-Growth Polymerizations *Dalton Trans.* **2013**, *42*, 4218–4222.
- (3) Love, B.E.; Jones, E.G. The Use of Salicylaldehyde Phenylhydrazone as an Indicator for the Titration of Organometallic Reagents *J. Org. Chem.* **1990**, *45*, 1924–1930.
- (4) http://collum.chem.cornell.edu/documents/Fitting_to_Differential_Equ_IgorPro.pdf
Accessed December 2016
- (5) (a) Becke, A.D. Density-Functional Exchange-Energy Approximation with Correct Asymptotic Behavior *Phys. Rev. A* **1988**, *38*, 3098–3100. (b) Perdew, J.P. Density-Functional Approximation for the Correlation Energy of the Inhomogeneous Electron Gas *Phys. Rev. B* **1986**, *33*, 8822–8824.
- (6) (a) Raghavachari, K.; Binkley, J.S.; Seeger, R.; Pople, J.A. Self-Consistent Molecular Orbital Methods. XX. A Basis Set for Correlated Wave Functions *J. Chem. Phys.* **1980**, *72*, 650–654. (b) McLean, A.D.; Chandler, G.S. Contracted Gaussian Basis Sets for Molecular Calculations. I. Second Row Atoms, Z=11–18 *J. Chem. Phys.* **1980**, *72*, 5639–5648. (c) Clark, T.; Chandrasekhar, J.; Spitznagel, G.W.; Schleyer, P.v.R. Efficient Diffuse Function-Augmented Basis Sets for Anion Calculations. III. The 3-21+G Basis Set for First-Row Elements, Li–F *J. Comp. Chem.* **1983**, *4*, 294–301.
- (7) (a) Dolg, M.; Wedig, U.; Stoll, H.; Preuss, H.; Energy-Adjusted ab initio Pseudopotentials for the First Row Transition Elements *J. Chem. Phys.* **1987**, *86*, 866–872. (b) Martin, J.M.L.; Sundermann, A. Correlation Consistent Valence Basis Sets for Use with the Stuttgart–Dresden–Bonn Relativistic Effective Core Potentials: The atoms Ga–Kr and In–Xe *J. Chem. Phys.* **2001**, *114*, 3408–3420.

Appendix 2

Supporting Information for Chapter 3:

Limitations of Using Small Molecules to Identify Catalyst-Transfer Polymerization Reactions

I. Materials

Flash chromatography was performed on SiliCycle silica gel (40-63 μm) and thin layer chromatography was performed on Merck TLC plates pre-coated with silica gel 60 F254. 4-*t*-Butylphenylmagnesium bromide (**S6**) (0.5 M in THF), Pd-PEPPSI-IPr, and Buchwald precatalysts were purchased from Aldrich. All other reagent grade materials and solvents were purchased from Aldrich, Acros, EMD, Strem, or Fisher and used without further purification unless otherwise noted. THF was dried and deoxygenated using an Innovative Technology (IT) solvent purification system composed of activated alumina, copper catalyst, and molecular sieves. THF was dried and deoxygenated using an MBraun solvent purification system composed of activated alumina, copper catalyst, and molecular sieves. All glassware was oven-dried at 120 °C for at least 1 h before use. Compounds **S2**¹, **S3**², **1**², **S1**³, **6**³, **S7**⁴, **S8**⁴, **S9**⁴, and **S10**⁵ were prepared according to modified literature procedures.

II. General Experimental

NMR Spectroscopy. ¹H, ¹³C NMR, and ³¹P spectra for all compounds were acquired at rt in CDCl₃, CD₂Cl₂, or C₆D₆ on a Varian VNMRs 500 operating at 500, 126, and 202 MHz or a Varian VNMRs 700 operating at 700 and 176 MHz. For ¹H, ¹³C NMR, and ³¹P spectra in deuterated solvents, the chemical shift data are reported in units of δ (ppm) relative to tetramethylsilane (TMS) and referenced with residual solvent. Multiplicities are reported as follows: singlet (s), doublet (d), triplet (t), quartet (q), and multiplet (m). * indicates residual H₂O

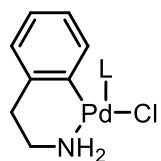
Gel-Permeation Chromatography: Polymer molecular weights were determined by comparison with polystyrene standards (Varian, EasiCal PS-2 MW 580-377,400) on a Waters 1515 HPLC instrument equipped with column guard and three Phenogel columns (4.6 x 30 cm, 10^2 Å, 10^3 Å, 10^4 Å) in sequence and analyzed with Waters 2487 dual absorbance detector (254 nm), or on a Malvern Viscotek GPCMax VE2001 equipped with two Viscotek LT-5000L 8 mm (ID) x 300 mm (L) columns and analyzed with Viscotek TDA 305 (with R.I., UV-PDA Detector Model 2600 (190-500 nm), RALS/LALS, and viscometer). Samples were dissolved in THF (with mild heating) and passed through a 0.2 µm PTFE filter prior to analysis.

Titrations of the Grignard Reagents: In the glovebox, an accurately weighed sample of salicylaldehyde phenylhydrazone (typically between 290-310 mg) was added to a 5 mL volumetric flask and dissolved with THF. Next, 0.50 mL of this solution was transferred to a 4 mL vial and stirred at rt while ArMgBr was added dropwise using a 500 µL syringe. The initial solution was yellow and turns bright orange at the end-point.⁶

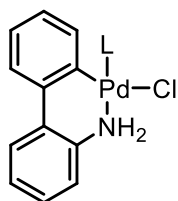
Gas Chromatography: Gas chromatography was carried out using a Shimadzu GC 2010 containing a Shimadzu SHR5 (crossbound 5% diphenyl – 95% dimethyl polysiloxane; 15 m, 0.25 mm ID, 0.25 µm df) column.

III. Structure Chart

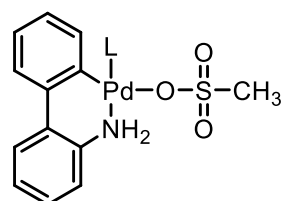
Generation 1-3 precatalysts



Gen 1

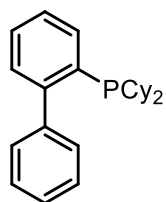


Gen 2

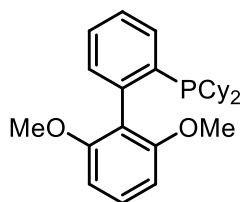


Gen 3

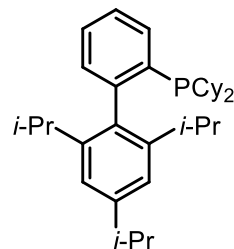
Buchwald phosphine ligands



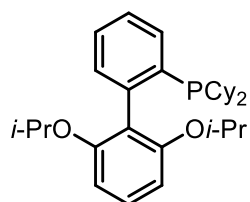
CyJohnPhos



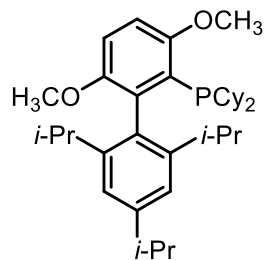
SPhos



XPhos

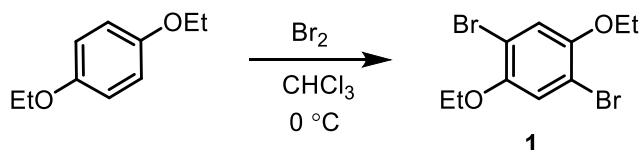


RuPhos

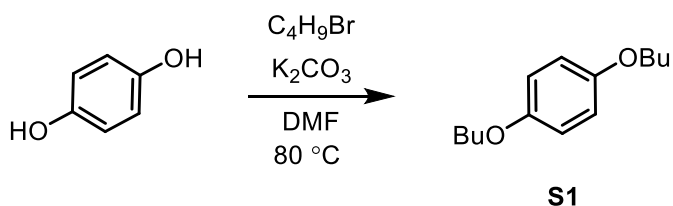


BrettPhos

IV. Synthetic Procedures

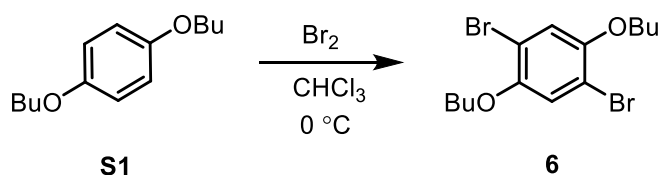


1.² A 500 mL round-bottom flask was equipped with a stir bar. Sequentially, 1,4-diethoxybenzene (13.0 g, 78.2 mmol, 1.0 equiv), and CHCl_3 (90 mL) were added to the flask. The reaction flask was cooled to $0\text{ }^\circ\text{C}$ in an ice/water bath and fitted with an addition funnel. Bromine (10.0 mL, 195 mmol, 2.5 equiv) was added dropwise under N_2 and the pressure was vented through a solution of aq satd Na_2SO_3 and NaHCO_3 (50:50). After 3 h, the reaction was quenched with an aq satd solution of Na_2SO_3 (100 mL) and stirred vigorously until colorless. The aqueous mixture was extracted with DCM (3 x 100 mL). The organic layers were combined and washed with water (2 x 200 mL) and brine (1 x 200 mL), dried over MgSO_4 , filtered, and concentrated in vacuo. The residue was recrystallized from DCM/methanol to produce 21.3 g of **1** as a white solid (84% yield). HRMS (EI): Calculated for $\text{C}_{10}\text{H}_{12}\text{O}_2\text{Br}_2$, 321.9204 [M+]; found, 321.9197.

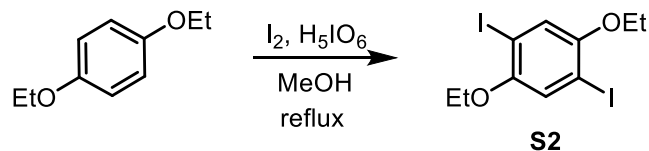


S1.³ A 500 mL round-bottom flask was equipped with a stir bar. Sequentially, hydroquinone (20.0 g, 0.182 mol, 1.0 equiv), anhydrous DMF (120 mL), and 1-bromobutane (49.0 mL, 0.454 mol, 2.5 equiv) were added to the flask. The flask was put under N_2 and stirred vigorously while heated to $80\text{ }^\circ\text{C}$. Once at $80\text{ }^\circ\text{C}$, K_2CO_3 (62.2 g, 0.454 mmol, 2.5 equiv) was slowly added over 10 min and subsequently put under N_2 again for 5 d. After cooling to rt, the reaction mixture was poured into water (400 mL). The

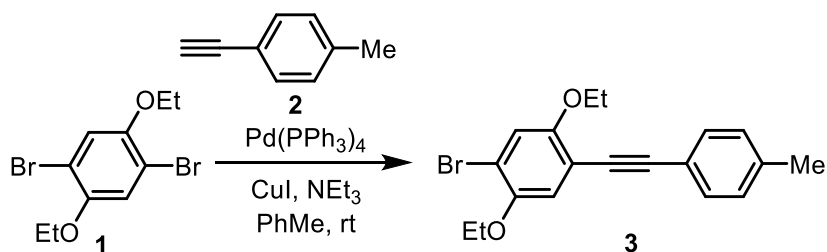
reaction mixture was extracted with hexanes (3 x 200 mL). The organic layers were combined and washed with water (2 x 200 mL) and brine (1 x 200 mL), dried over MgSO₄, filtered, and concentrated in vacuo. The resulting oil was passed through silica gel with 100% DCM as the eluent. Recrystallization from hot methanol produced 34.7 g of **S1** as a white crystalline solid (86% yield). HRMS (EI): Calculated for C₁₄H₂₂O₂, 222.1620 [M⁺]; found, 222.1626.



6.³ A 500 mL round-bottom flask was equipped with a stir bar. Sequentially, **S1** (17.3 g, 77.7 mmol, 1.0 equiv), and CHCl₃ (90 mL) were added to the flask. The reaction flask was cooled to 0 °C in an ice/water bath and fitted with an addition funnel. Bromine (10.0 mL, 194 mmol, 2.5 equiv) was added dropwise under N₂ and the pressure was vented through a solution of aq satd Na₂SO₃ and NaHCO₃ (50:50). After 3 h, the reaction was quenched with an aq satd solution of Na₂SO₃ (100 mL) and stirred vigorously until colorless. The aqueous mixture was extracted with DCM (3 x 100 mL). The organic layers were combined and washed with water (2 x 200 mL) and brine (1 x 200 mL), dried over MgSO₄, filtered, and concentrated in vacuo. The residue was recrystallized from DCM/methanol to produce 23.3 g of **6** as a white solid (79% yield). HRMS (EI): Calculated for C₁₄H₂₀Br₂O₂, 377.9830 [M⁺]; found, 377.9824.

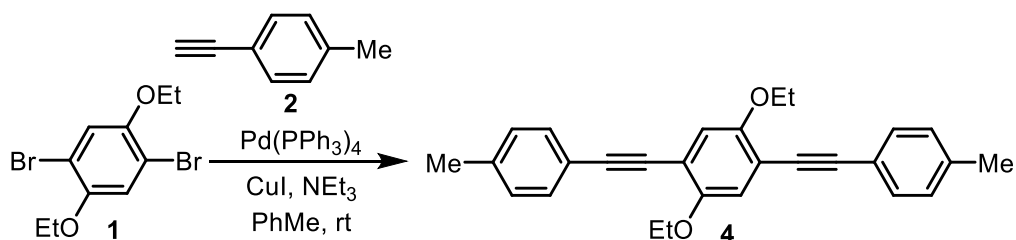


S2.¹ A 100 mL round-bottom flask was equipped with a stir bar. Sequentially, 1,4-diethoxybenzene (5.00 g, 30.1 mmol, 1.0 equiv), and MeOH (50 mL) were added to the flask. Iodine (7.64 g, 30.1 mmol, 1.0 equiv) and periodic acid (6.86 g, 30.1 mol, 1.0 equiv) were added with stirring. This was then heated to reflux and put under N₂ atmosphere. After 4 h, the reaction was quenched with an aq satd solution of Na₂SO₃ (50 mL) and stirred vigorously until colorless. The aqueous mixture was extracted with DCM (3 x 50 mL). The organic layers were combined and washed with water (2 x 50 mL) and brine (1 x 50 mL), dried over MgSO₄, filtered, and concentrated in vacuo. The residue was recrystallized from DCM/methanol to produce 7.29 g of **S2** as a white solid (58% yield). HRMS (EI): Calculated for C₁₀H₁₂O₂I₂, 417.8927 [M⁺]; found, 417.8927.

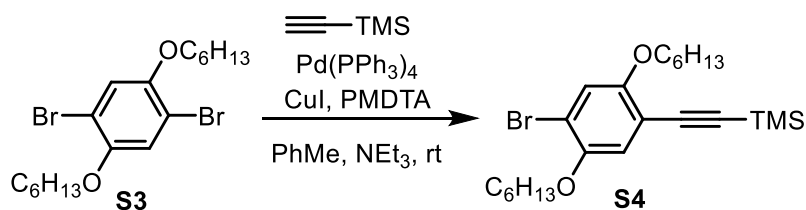


3. A 200 mL Schlenk flask was equipped with a stir bar, the chamber was evacuated for 5 min, and then charged with N₂. Sequentially, **1** (2.00 g, 6.17 mmol, 1.0 equiv), Pd(PPh₃)₄ (360 mg, 0.312 mmol, 5 mol %), CuI (120 mg, 0.620 mmol, 10 mol %) were all added and placed under vac for 20 min. The flask was then placed under N₂ atmosphere. Next, PhMe (60 mL) was added with stirring. Once dissolved, NEt₃ (30 mL, 33% by volume), and **2**

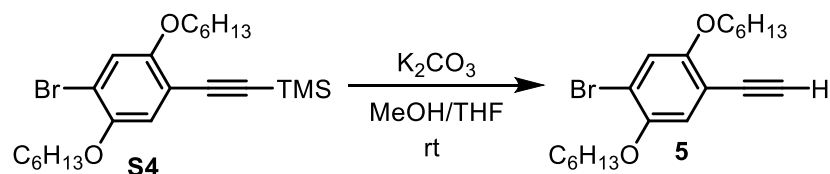
(0.78 mL, 6.2 mmol, 1.0 equiv) were added. The reaction was left for 14 h at rt. This reaction was quenched with aq satd NH₄Cl (50 mL) and extracted with DCM (3 x 50 mL), the organic layers were combined and washed with brine (50 mL), dried over MgSO₄, filtered, and concentrated in vacuo. The resulting oil was passed through silica gel with DCM/hexanes (20:80) as the eluent to produce 1.22 g of **3** as an off-white solid (55% yield). HRMS (ESI⁺): Calculated for C₁₉H₁₉BrO₂, 359.0641 [M+H]⁺; found, 359.0641.



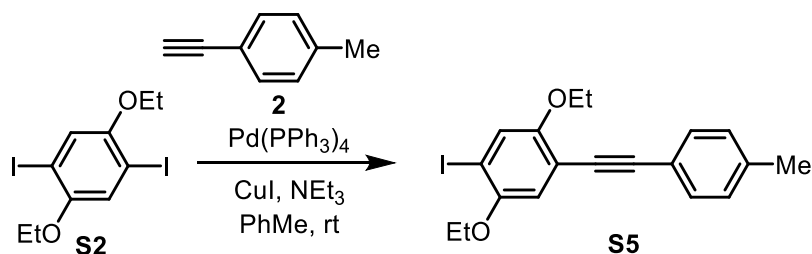
4. A 200 mL Schlenk flask was equipped with a stir bar, the chamber was evacuated for 5 min, and then and charged with N₂. Sequentially, **1** (2.00 g, 6.17 mmol, 1.0 equiv), Pd(PPh₃)₄ (360 mg, 0.312 mmol, 5 mol %), CuI (120 mg, 0.620 mmol, 10 mol %) were all added and placed under vac for 20 min. The flask was then placed under N₂ atmosphere. Next, PhMe (60 mL) was added with stirring. Once dissolved, NEt₃ (30 mL, 33% by volume), and **2** (1.95 mL, 15.4 mmol, 2.5 equiv) were added. The reaction was left for 14 h at rt. This reaction was quenched with aq satd NH₄Cl (50 mL) and extracted with DCM (3 x 50 mL), the organic layers were combined and washed with brine (50 mL), dried over MgSO₄, filtered, and concentrated in vacuo. The resulting oil was passed through silica gel with DCM/hexanes (20:80) as the eluent to produce 1.98 g of **4** as an off-white solid (81% yield). HRMS (ESI⁺): Calculated for C₂₈H₂₆O₂, 395.2006 [M+H]⁺; found, 395.2010.



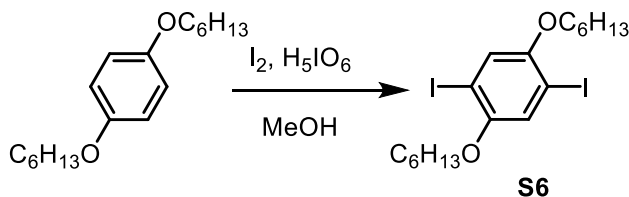
S4. In the glovebox, a 20 mL vial was equipped with a stir bar. Then, **S3** (500 mg, 1.15 mmol, 1.5 equiv), trimethylsilylacetylene (0.11 mL, 0.76 mmol, 1.0 equiv), Pd(PPh₃)₄ (44 mg, 0.038 mmol, 5 mol %), CuI (14 mg, 0.076 mmol, 10 mol %), PMDTA (16 μL, 0.076 mmol, 10 mol %), PhMe (10 mL), and NEt₃ (5 mL) were all added. The reaction was left to stir overnight at rt. The solution was quenched with aq satd NH₄Cl (10 mL). The solution was extracted with DCM (3 x 25 mL). The organic layers were combined and washed with water (2 x 25 mL) and brine (1 x 25 mL), dried over MgSO₄, filtered, and concentrated in vacuo. The product was purified by column chromatography (20% DCM/80% hexanes) to produce 252 mg of **S4** (73% yield). HRMS (ESI⁺): Calculated for C₂₃H₃₇BrO₂Si, 453.1819 [M+H]⁺; found, 453.1821.



5. A 250 mL round bottom flask was equipped with a stir bar and charged with **S4** (2.00 g, 4.41 mmol, 1.0 equiv), K₂CO₃ (10 g, excess), THF (50 mL), and MeOH (50 mL). The reaction was stirred for 2 h at rt. The reaction was filtered and washed with THF (25 mL), the filtrate was then concentrated in vacuo. This oil was purified by column chromatography (20% DCM/80% hexanes) to produce 1.56 g of **5** (93% yield). HRMS (ESI⁺): Calculated for C₂₀H₂₉BrO₂, 381.1424 [M+H]⁺; found, 381.1423.

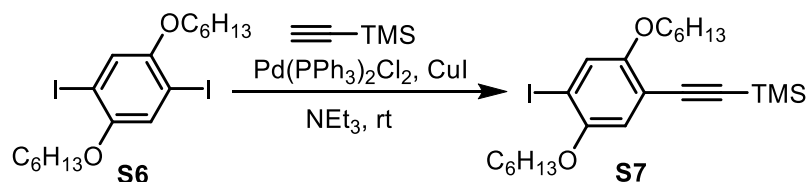


S5. A 200 mL Schlenk flask was equipped with a stir bar, the chamber was evacuated for 5 min, and then charged with N₂. Sequentially, **S2** (2.00 g, 4.78 mmol, 1.0 equiv), Pd(PPh₃)₄ (276 mg, 0.239 mmol, 5 mol %), CuI (91.1 mg, 0.478 mmol, 10 mol %) were all added and placed under vac for 20 min. The flask was then placed under N₂ atmosphere. Next, PhMe (60 mL) was added with stirring. Once dissolved, NEt₃ (30 mL, 33% by volume), and tolyl-acetylene (0.61 mL, 4.8 mmol, 1.0 equiv) were added. The reaction was left for 14 h at rt. This reaction was quenched with aq satd NH₄Cl (50 mL) and extracted with DCM (3 x 50 mL), the organic layers were combined and washed with brine (50 mL), dried over MgSO₄, filtered, and concentrated in vacuo. The resulting oil was passed through silica gel with DCM/hexanes (20:80) as the eluent to produce 932 mg of **S5** as an off-white solid (48% yield). HRMS (ESI⁺): Calculated for C₁₉H₁₉I₂O₂, 407.0502 [M+H]⁺; found, 407.0512.

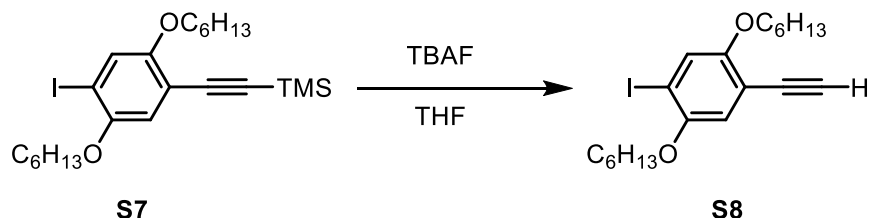


S6.¹ A 25 mL round-bottom flask was equipped with a stir bar and reflux condenser. Sequentially, 1,4-dihexyloxybenzene (1.12 g, 4.01 mmol, 1.0 equiv), and MeOH (7 mL) were added to the flask. Iodine (1.07 g, 4.01 mmol, 1.0 equiv) and periodic acid (0.914 g, 4.01 mol, 1.0 equiv) were added with stirring. The reaction mixture was then heated to reflux and placed under N₂ atmosphere. After 6 h, the reaction was quenched with an aq satd solution of Na₂SO₃ (30 mL) and stirred vigorously until colorless. The aqueous mixture was extracted with DCM (3 x 25 mL). The organic layers were combined and

washed with water (1 x 25 mL) and brine (1 x 25 mL), dried over MgSO₄, filtered, and concentrated in vacuo. The residue was recrystallized from DCM/methanol to produce 1.41 g of **S2** as a white solid (66% yield). HRMS (EI): Calculated for C₁₈H₂₈O₂, 530.0179 [M⁺]; found, 530.0192.

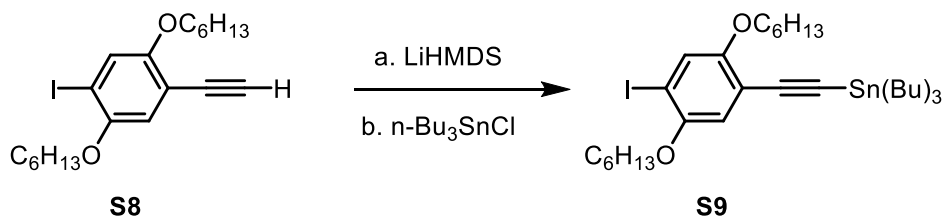


S7. In the glovebox, a 20 mL vial was equipped with a stir bar. Then, **S6** (532 mg, 1.00 mmol, 1.5 equiv), trimethylsilylacetylene (0.10 mL, 0.70 mmol, 0.7 equiv), Pd(PPh₃)₂Cl₂ (35 mg, 0.05 mmol, 5 mol%), CuI (1.9 mg, 0.01 mmol, 1 mol %), and NEt₃ (11.5 mL) were all added. The reaction was stirred for 6 h at rt. The solution was quenched with aq satd NH₄Cl (30 mL), then extracted with hexanes (3 x 25 mL). The organic layers were combined and washed with water (1 x 25 mL) and brine (1 x 25 mL), dried over MgSO₄, filtered, and concentrated in vacuo. The product was purified by column chromatography with PhMe/hexanes(20:80) as the eluent to produce 187.6 mg of **S7** (53% yield) as a yellow oil. HRMS (EI): Calculated for C₂₃H₃₇IO₂Si, 500.1608 [M⁺]; found, 500.1607

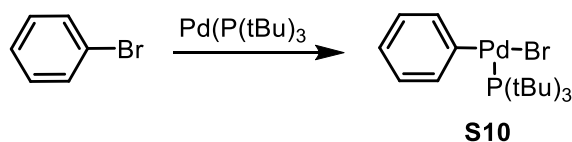


S8. In a 25 mL round-bottom flask, **S7** (319.0 mg, 0.64 mmol, 1 equiv) was dissolved in THF (8 mL), then tetrabutyl ammonium fluoride (1 M in THF, 0.96 mL, 1.5 equiv) was added and the solution was stirred 10 min at rt. DI water (10 mL) was added and the aqueous solution was extracted with diethyl ether (3 x 20 mL). The organic layers were combined and washed with water (1 x 20 mL) and brine (1 x 20 mL), dried over MgSO₄, filtered, and concentrated in vacuo. The product was purified by column chromatography

with DCM/hexanes (10:90) as the eluent to produce 220.10 mg of **S8** (81% yield) as a yellow solid. HRMS (EI+): Calculated for C₂₀H₂₉IO₂, 428.1212 [M+]; found, 428.1199.



S8. In a 50 mL Schlenk flask, **S8** (190.1 mg, 0.44 mmol, 1 equiv) was dissolved in anhydrous THF (8 mL), and cooled to -78 °C. Then, LiHMDS (0.75 M in THF, 0.77 mL, 1.3 equiv) was added dropwise, and the solution was stirred at -78 °C for 1 h. Tri-*n*-butyltin chloride (0.16 mL, 0.58 mmol, 1.3 equiv) was added, then the dry ice bath was removed and the solution was stirred for 90 min. The reaction was quenched with sat. aqueous NH₄Cl (5 mL), then extracted with diethyl ether (2 x 15 mL). The organic layers were combined and washed with water (1 x 15 mL) and brine (1 x 15 mL), dried over MgSO₄, filtered, and concentrated in vacuo. The product was dried under vacuum overnight, giving 303.2 mg of a yellow oil (95%), and used without further purification. HRMS (EI): Calculated for C₃₂H₅₅IO₂Sn, 661.1564 [M-Bu]⁺; found, 661.1567



S10. In a glovebox, a 20 mL vial was charged with bis(tri-*t*-butylphosphine)palladium (153.3 mg, 0.300 mmol, 1 equiv) and bromobenzene (1.5 mL, 14.1 mmol, 47 equiv). The reaction mixture was stirred at 70 °C for 2.5 h, then poured into cold pentane, causing immediate precipitation of a yellow solid. The product was isolated by vacuum filtration, then washed with pentane (5 x 3 mL), giving 41.3 mg of a yellow solid (29%).

V. NMR Spectra

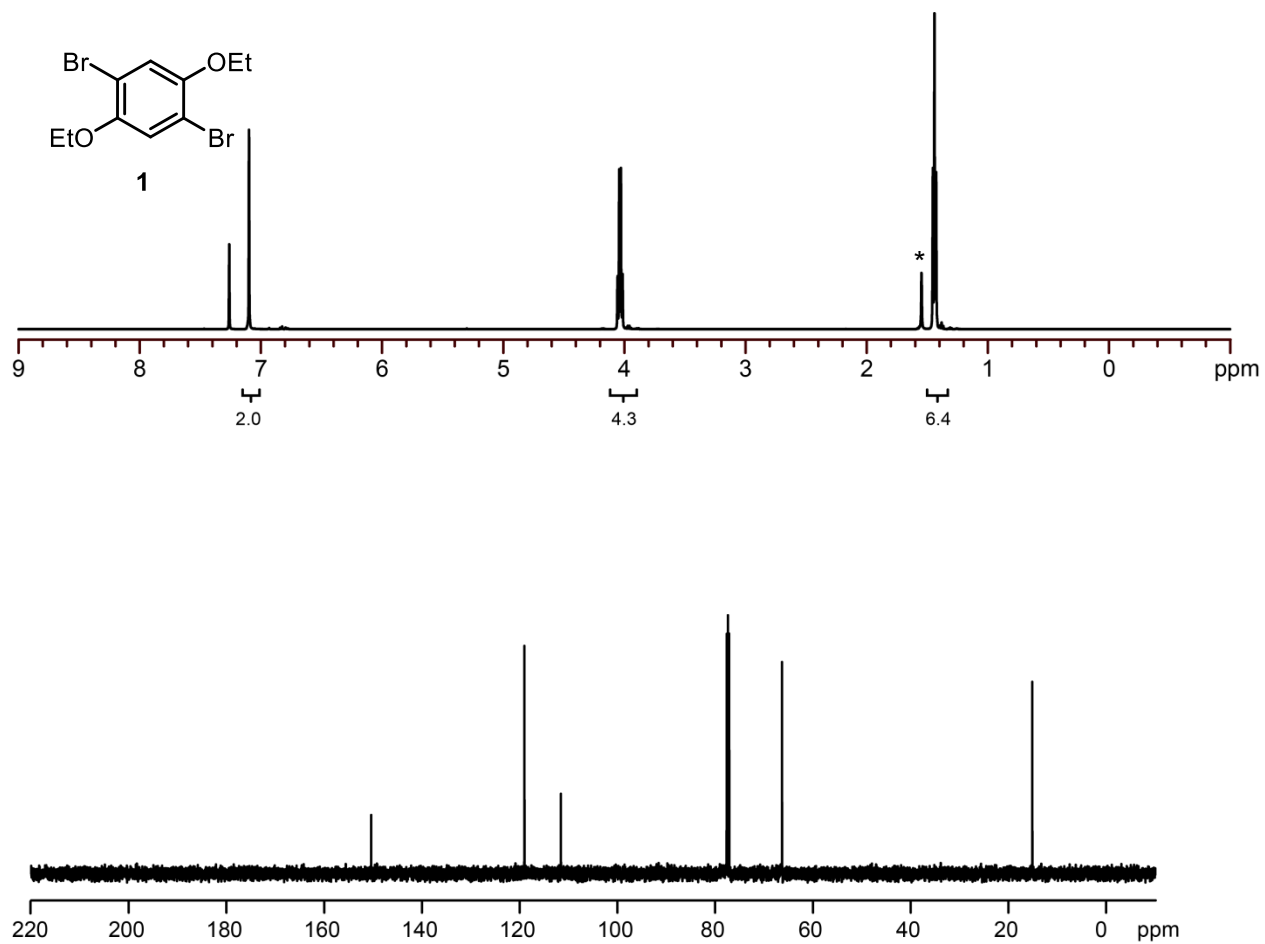


Figure S2.1. ¹H and ¹³C NMR spectra for 1. ¹H NMR (500 MHz, CDCl₃) δ 7.10 (s, 2H), 4.04 (q, *J* = 7.1 Hz, 4H), 1.47 (t, *J* = 7.1 Hz, 6H). * indicates residual H₂O. ¹³C NMR (126 MHz, CDCl₃) δ 150.00, 118.65, 111.85, 65.94, 14.73.

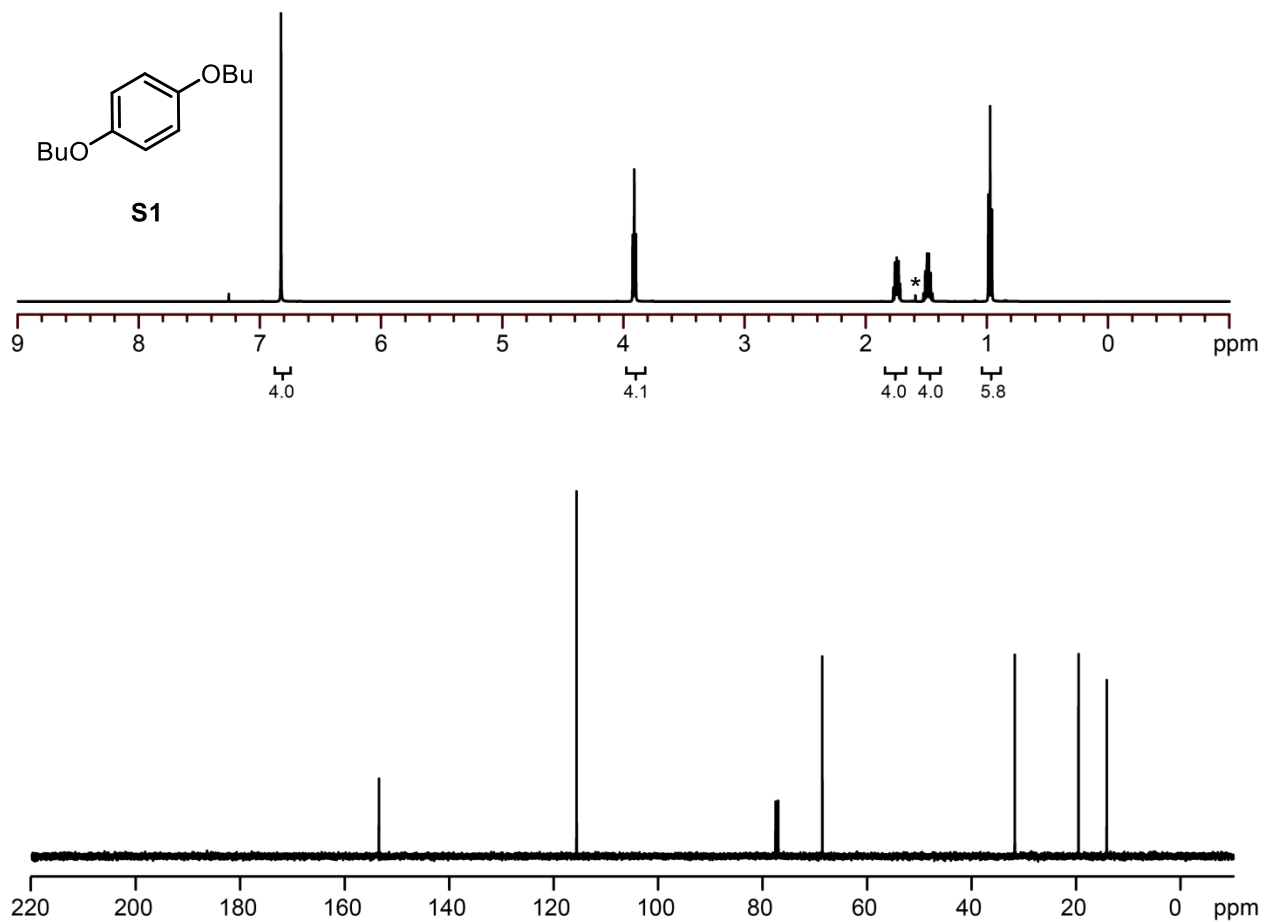


Figure S2.2. ^1H and ^{13}C NMR spectra for **S1**. ^1H NMR (500 MHz, CDCl_3) δ 6.83 (s, 4H), 3.92 (t, $J = 7.0$ Hz, 4H), 1.80–1.73 (m, 4H), 1.55–1.46 (m, 4H), 0.98 (t, $J = 7.3$ Hz, 6H). * indicates residual H_2O . ^{13}C NMR (126 MHz, CDCl_3) δ 153.19, 115.36, 68.30, 31.45, 19.24, 13.84.

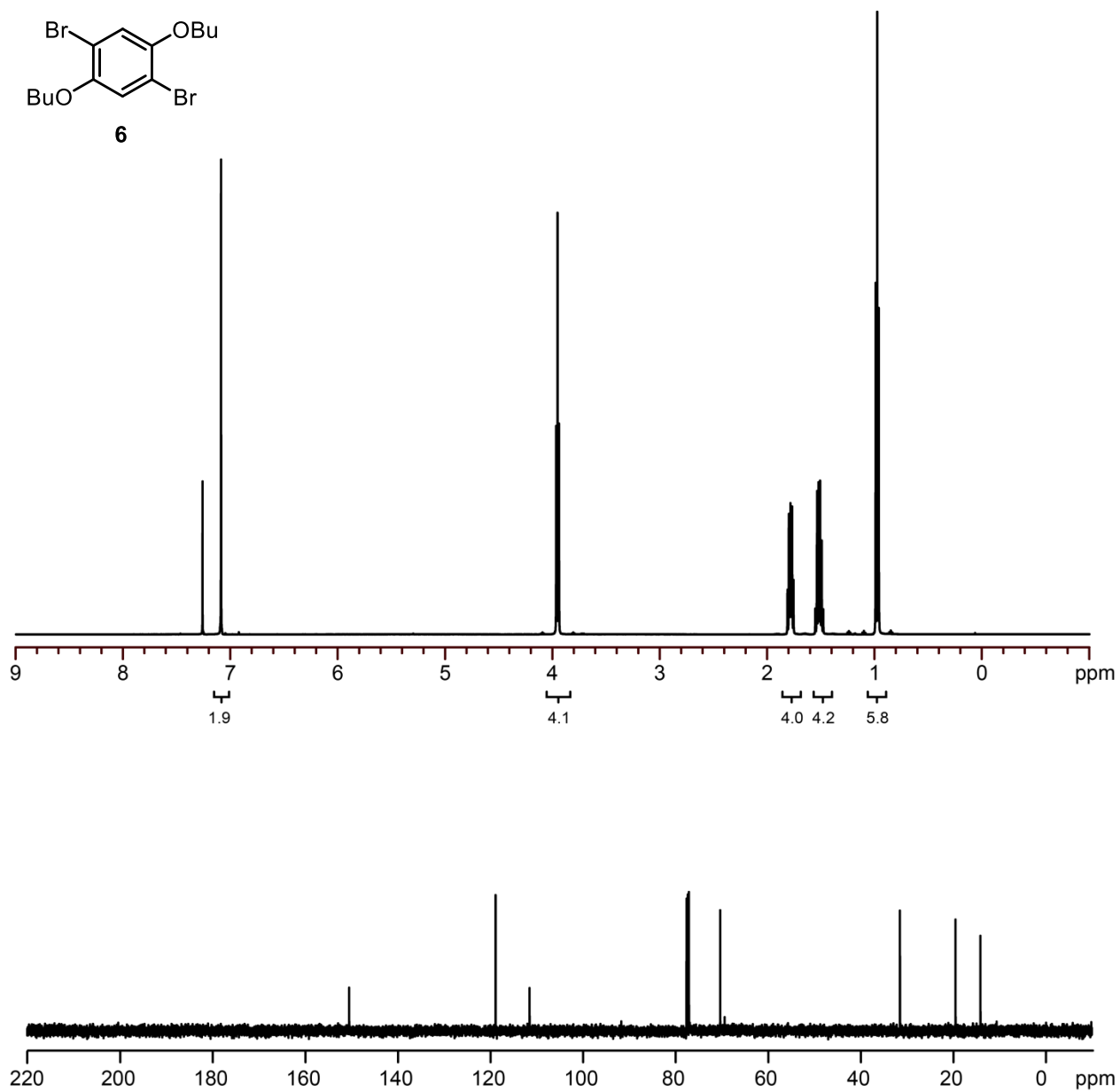


Figure S2.3. ^1H and ^{13}C NMR spectra for **6**. ^1H NMR (500 MHz, CDCl_3) δ 7.09 (s, 2H), 3.96 (t, $J = 6.7$ Hz, 4H), 1.84–1.77 (m, 4H), 1.58–1.49 (m, 4H), 0.98 (t, $J = 7.2$ Hz, 6H). ^{13}C NMR (126 MHz, CDCl_3) δ 150.08, 118.46, 111.13, 69.99, 31.19, 19.19, 13.81.

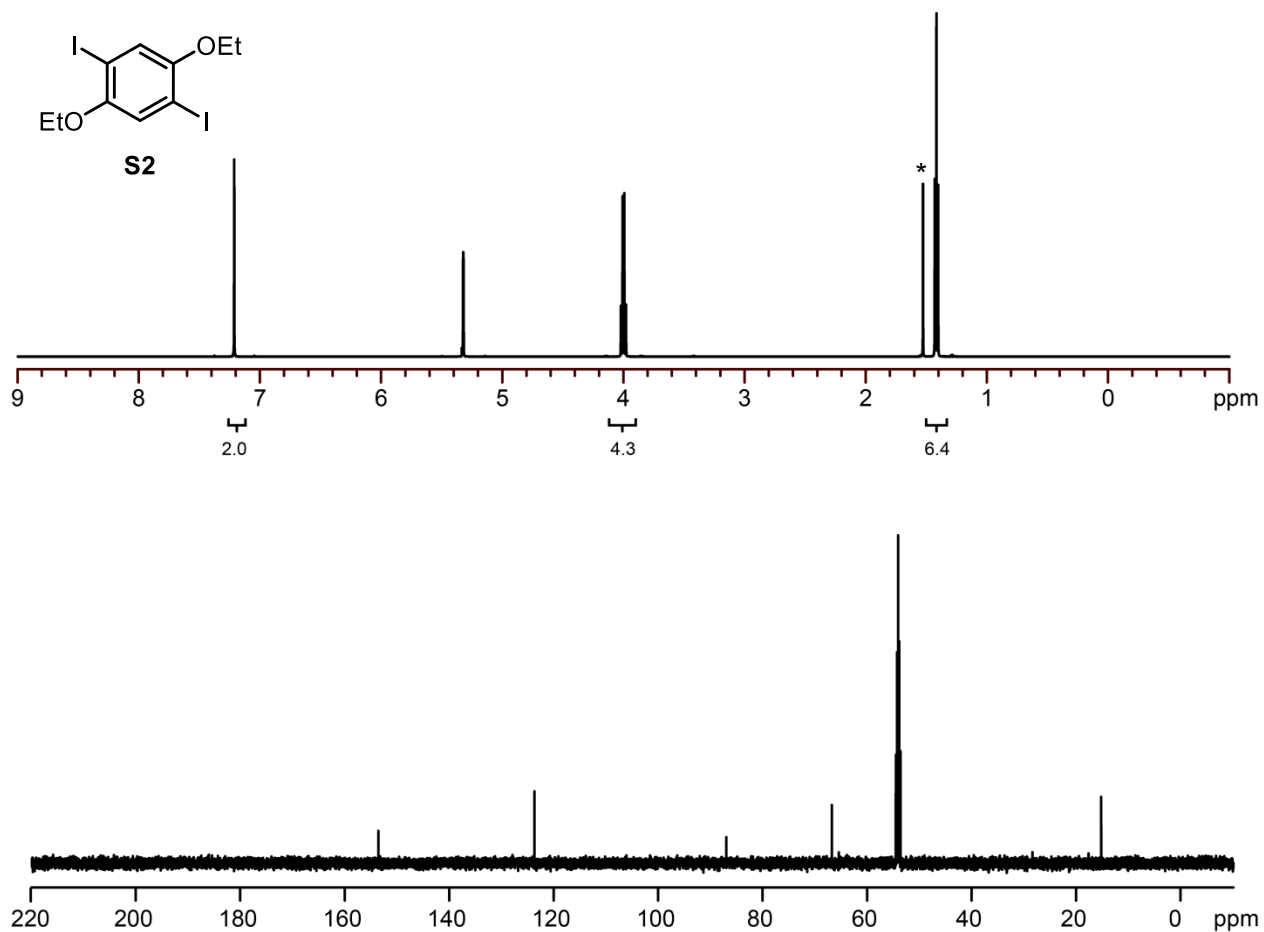
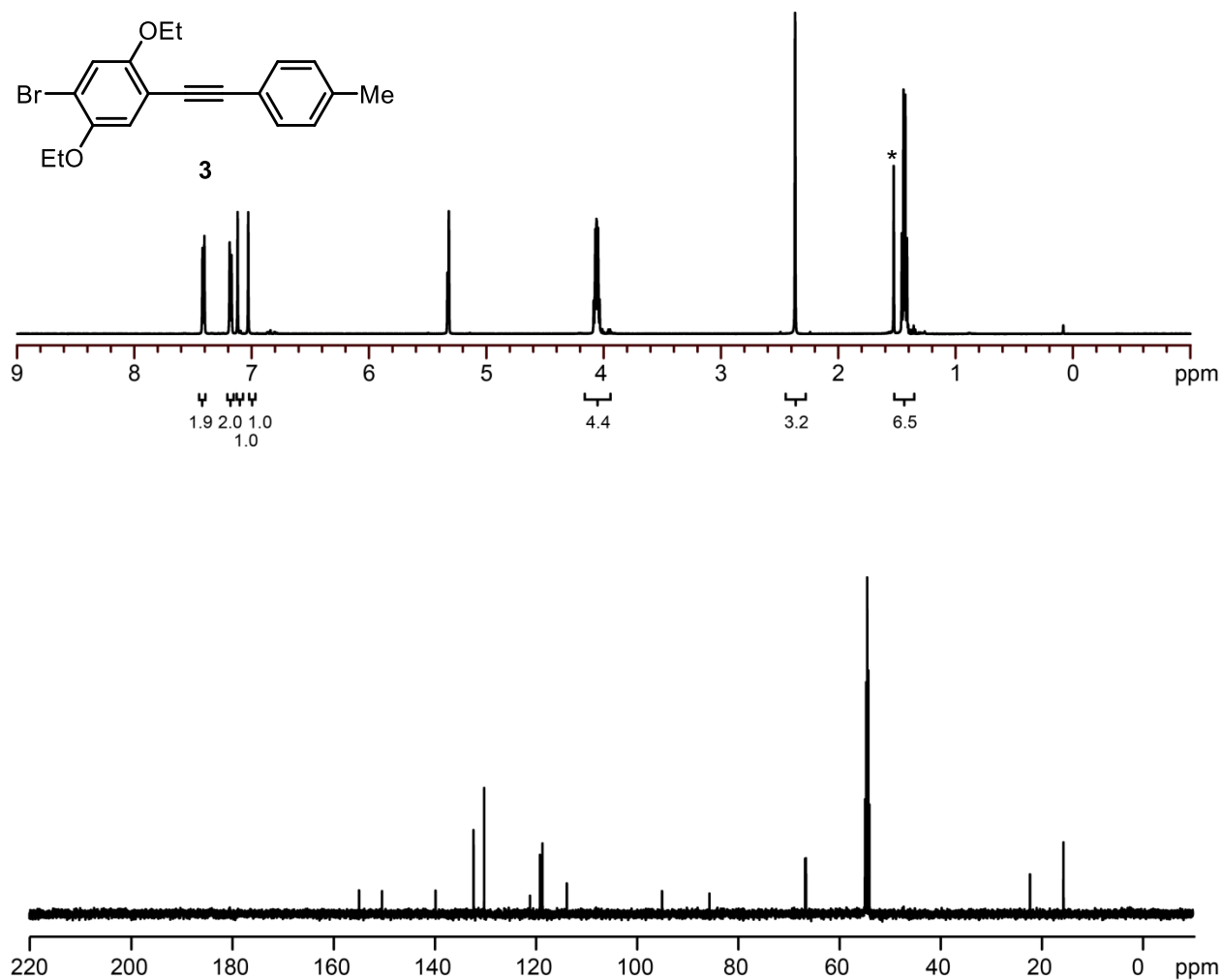


Figure S2.4. ^1H and ^{13}C NMR spectra for **S2**. ^1H NMR (500 MHz, CD_2Cl_2) δ 7.21 (s, 2H), 4.01 (q, $J = 7.0$ Hz, 4H), 1.42 (t, $J = 7.0$ Hz, 6H), * indicates residual H_2O . ^{13}C NMR (126 MHz, CD_2Cl_2) δ 153.66, 123.80, 87.09, 66.92, 15.40.



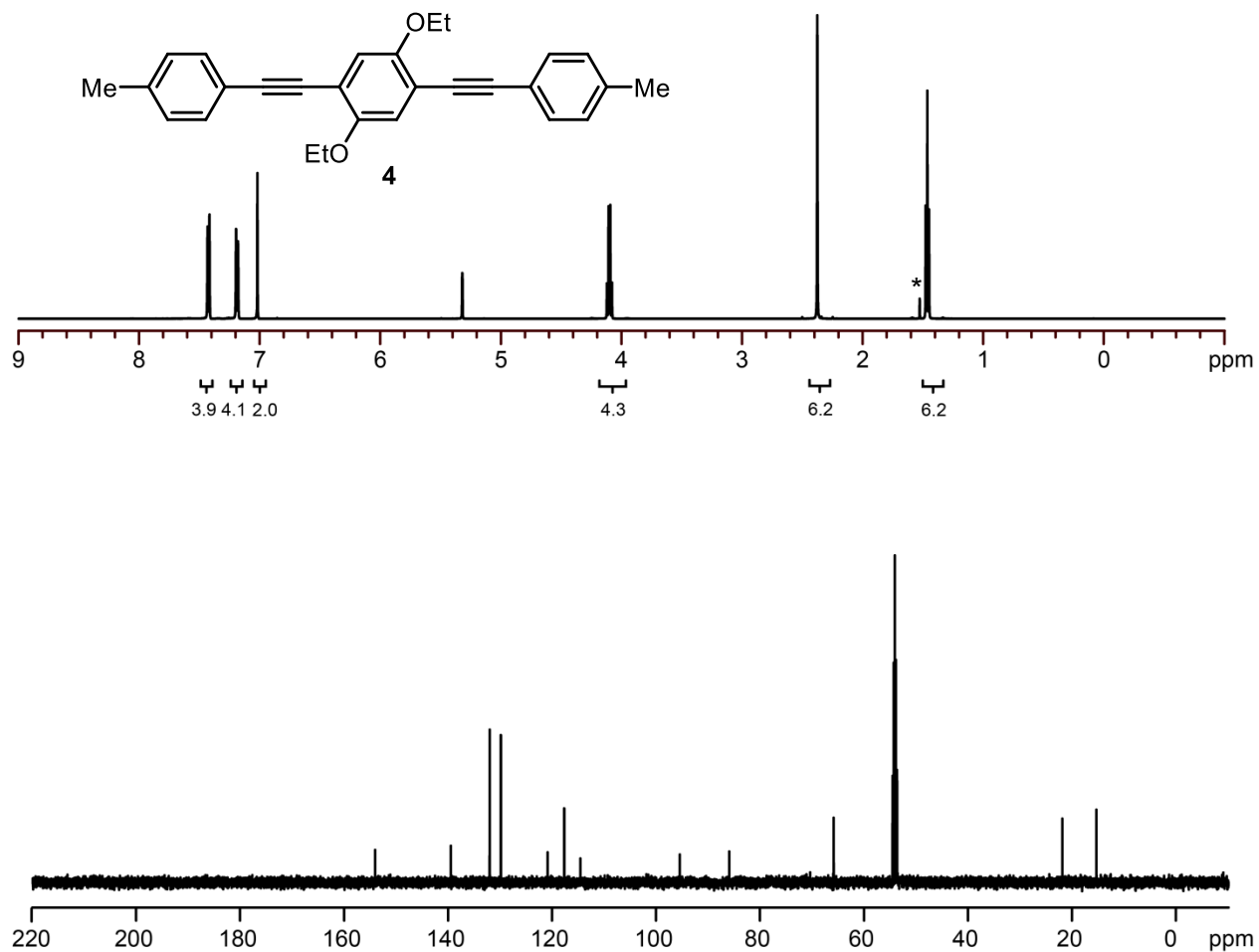


Figure S2.6. ^1H and ^{13}C NMR spectra for **4**. ^1H NMR (500 MHz, CD_2Cl_2) δ 7.42 (d, J = 8.4 Hz, 4H), 7.19 (d, J = 7.9 Hz, 4H), 7.02 (s, 2H), 4.12–4.08 (m, 4H), 2.38 (s, 6H), 1.46 (t, J = 7.0 Hz, 6H). * indicates residual H_2O . ^{13}C NMR (126 MHz, CD_2Cl_2) δ 153.35, 138.79, 131.33, 129.18, 120.18, 116.99, 113.88, 94.79, 85.27, 65.19, 21.23, 14.69.

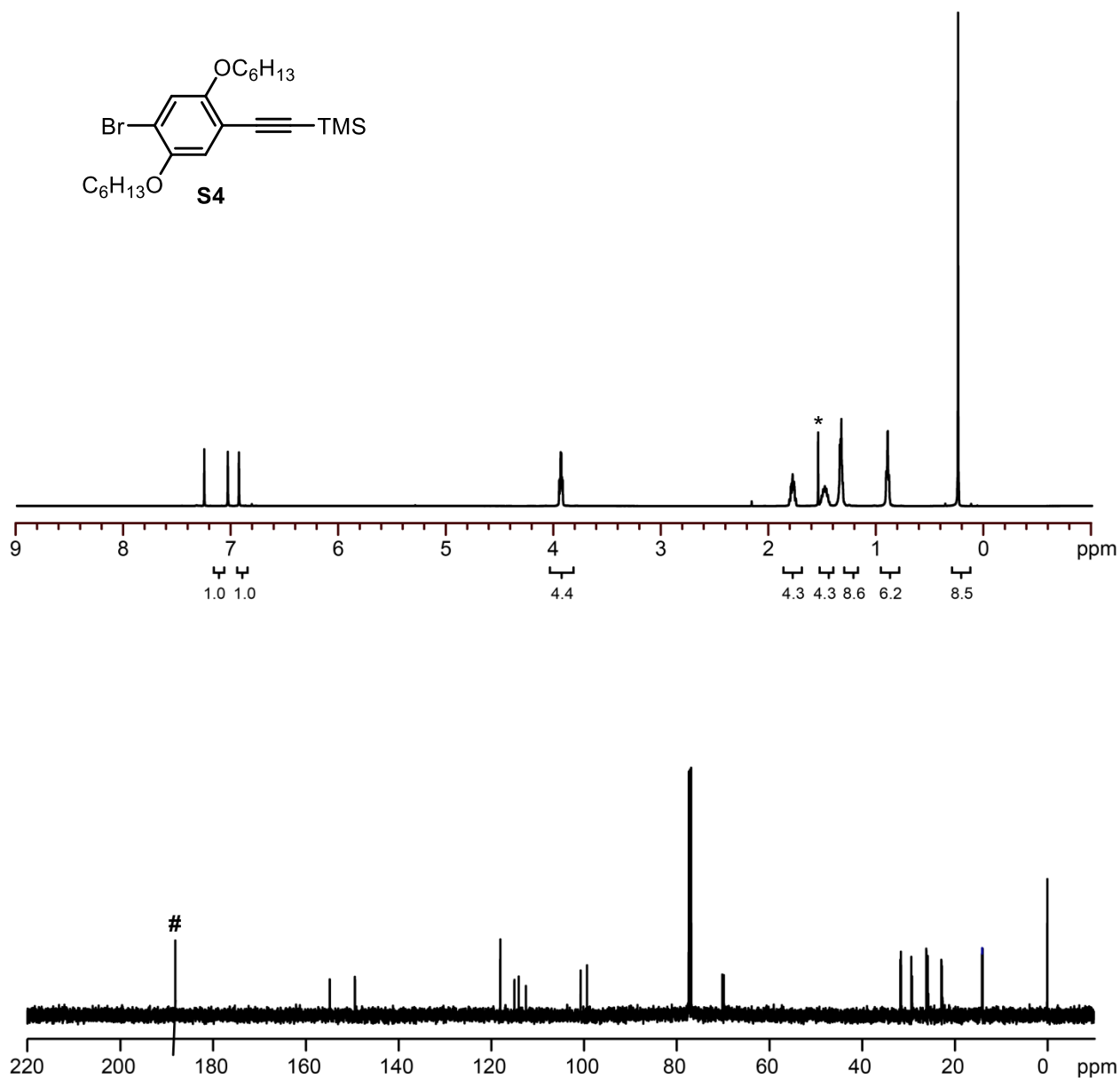


Figure S2.7. ^1H and ^{13}C NMR spectra for **S4**. ^1H NMR (500 MHz, CDCl_3) δ 7.04 (s, 1H), 6.94 (s, 1H), 3.97-3.91 (m, 4H), 1.83-1.75 (m, 4H), 1.54-1.43 (m, 4H), 1.39-1.30 (m, 8H), 0.95-0.87 (m, 6H), 0.26 (s, 9H). * indicates residual H_2O . ^{13}C NMR (126 MHz, CDCl_3) δ 154.71, 149.29, 117.93, 114.89, 113.56, 112.40, 100.61, 99.22, 70.08, 69.72, 31.60, 31.58, 29.25, 29.24, 25.67, 25.65, 22.58, 22.57, 14.05, 14.02, -0.06. # indicates NMR instrument artifact

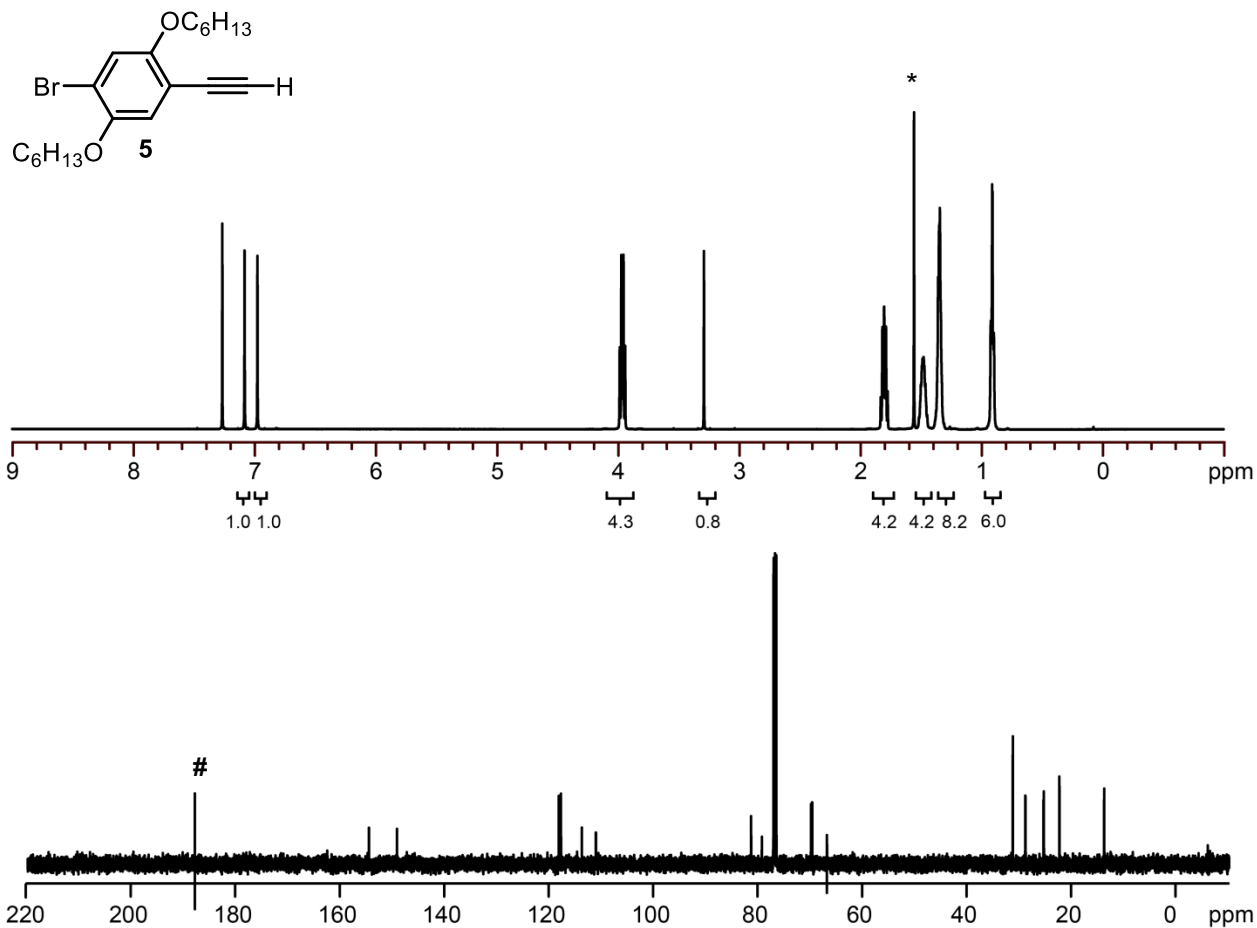


Figure S2.8. ^1H and ^{13}C NMR spectra for **5**. ^1H NMR (500 MHz, CDCl_3) δ 7.08 (s, 1H), 6.97 (s, 1H), 3.99–3.93 (m, 4H), 3.29 (s, 1H), 1.84–1.76 (m, 4H), 1.52–1.43 (m, 4H), 1.39–1.31 (m, 8H), 0.94–0.88 (m, 6H). * indicates residual H_2O . ^{13}C NMR (126 MHz, CD_2Cl_2) δ 154.72, 149.34, 118.38, 117.96, 113.96, 111.28, 81.58, 79.52, 70.13, 69.89, 31.50, 29.94, 29.11, 29.05, 25.63, 25.55, 22.57, 22.57, 14.02, 14.00. # indicates NMR instrument artifact

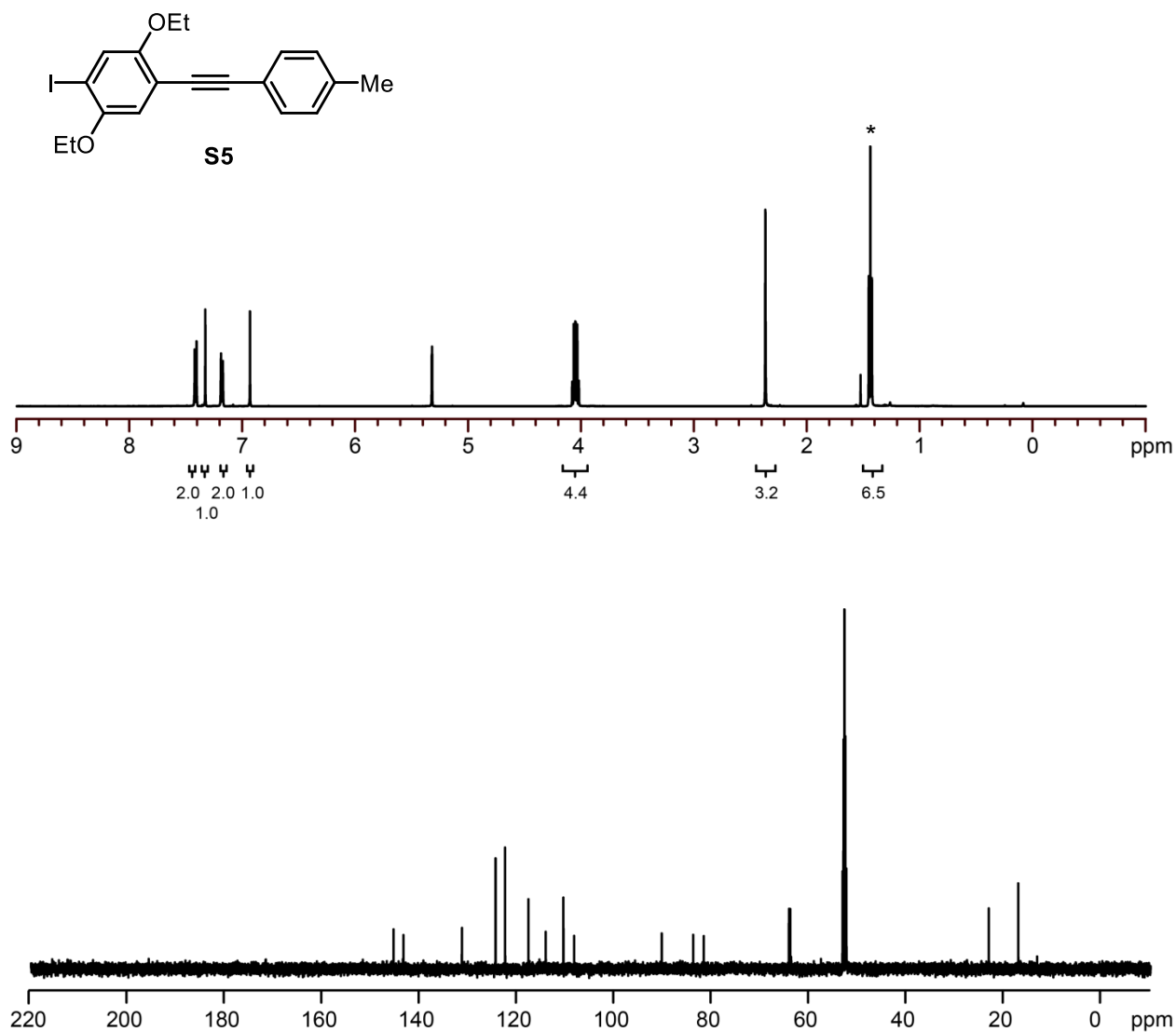


Figure S2.9. ^1H and ^{13}C NMR spectra for **S5**. ^1H NMR (500 MHz, CD_2Cl_2) δ 7.41 (d, J = 7.9 Hz, 2H), 7.33 (s, 1H), 7.18 (d, J = 7.9 Hz, 2H), 6.93 (s, 1H), 4.08–4.01 (m, 4H), 2.37 (s, 3H), 1.44 (t, J = 7.0 Hz, 6H). * indicates residual H_2O . ^{13}C NMR (126 MHz, CD_2Cl_2) δ 154.87, 152.64, 139.62, 132.09, 129.97, 124.76, 120.90, 116.95, 114.56, 95.00, 87.99, 85.62, 66.10, 66.32, 22.03, 15.45.

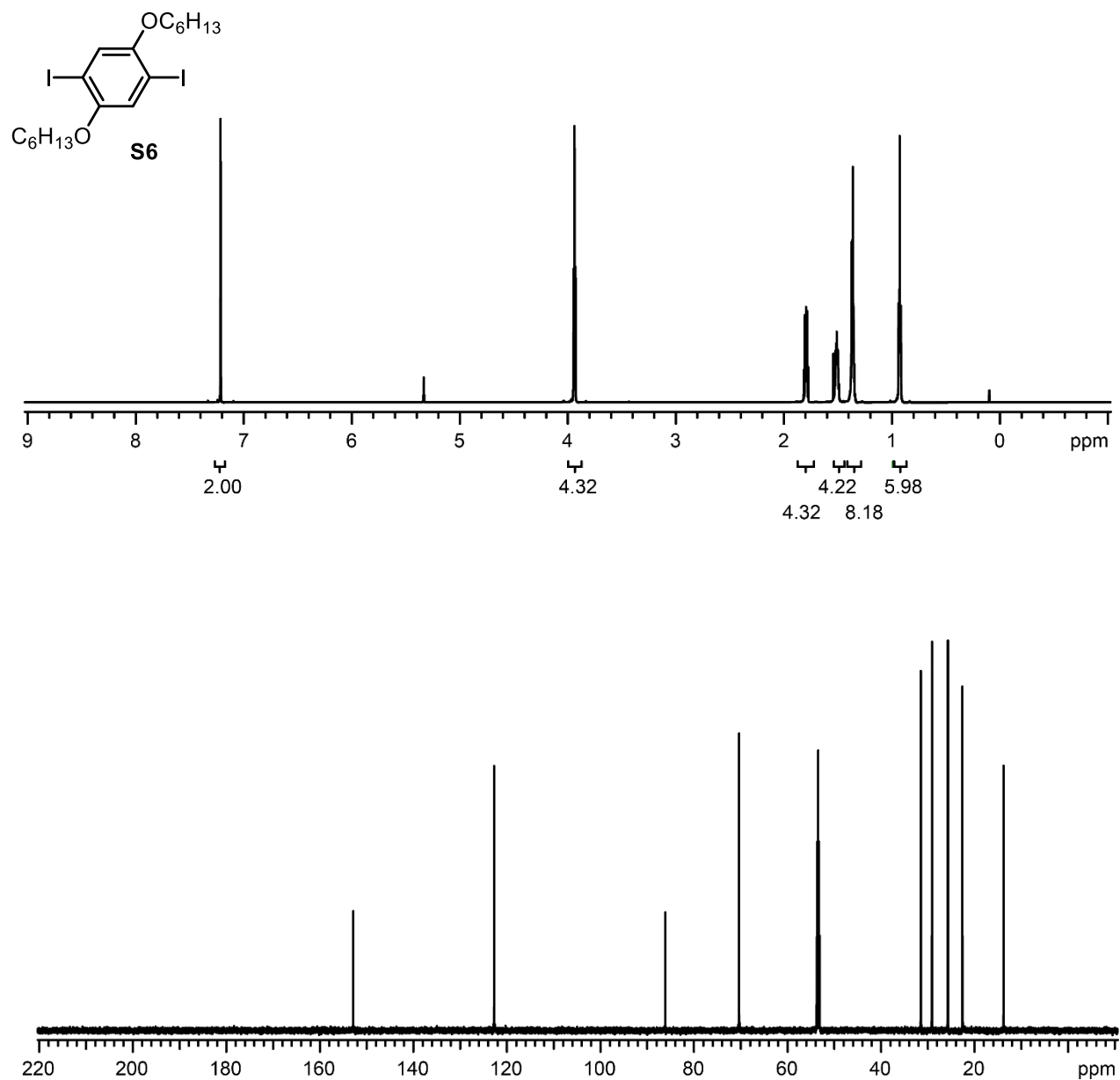


Figure S2.10. ^1H and ^{13}C NMR spectra for **S6**. ^1H NMR (700 MHz, CD_2Cl_2) δ 7.21 (s, 2H), 3.94 (t, $J = 6.3$, 4H), 1.81–1.77 (m, 4H), 1.53–1.49 (m, 4H), 1.39–1.34 (m, 8H), 0.94–0.91 (m, 6H). ^{13}C NMR (126 MHz, CD_2Cl_2) δ 152.84, 122.72, 86.10, 70.35, 31.45, 29.09, 25.67, 22.57, 13.79.

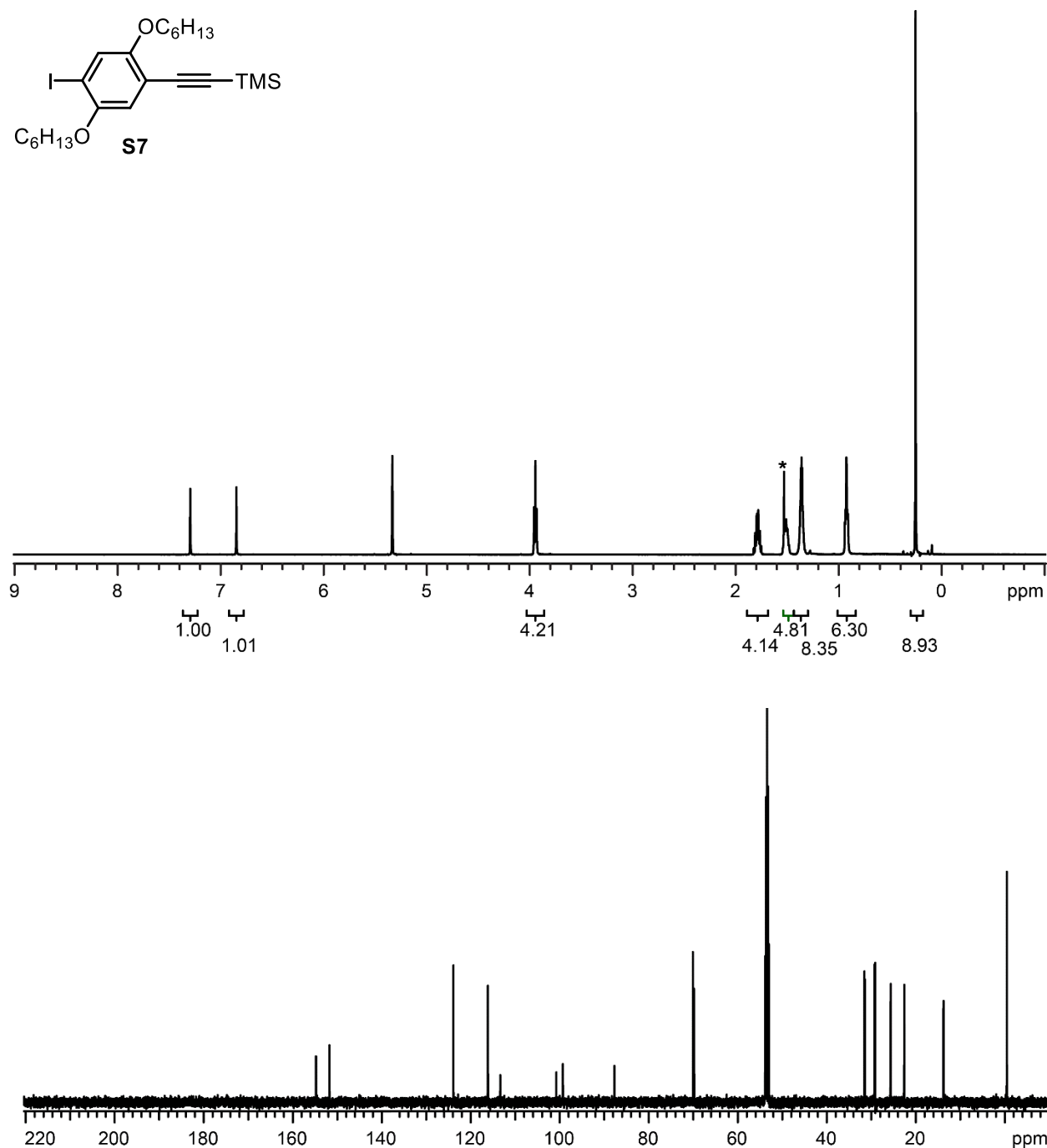
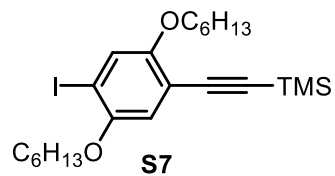


Figure S2.11. ^1H and ^{13}C NMR spectra for **S7**. ^1H NMR (500 MHz, CD_2Cl_2) δ 7.27 (s, 1H), 6.82 (s, 1H), 3.92 (t, $J = 5.8$ Hz, 4H), 1.80–1.73 (m, 4H), 1.51–1.47 (m, 4H), 1.35–1.32 (m, 8H), 0.92–0.89 (m, 6H), 0.24 (s, 9H). ^{13}C NMR (126 MHz, CD_2Cl_2) δ 1549.76, 151.72, 123.88, 116.14, 113.34, 100.76, 99.27, 87.68, 70.08, 69.80, 31.54, 31.45, 29.24, 29.10, 25.68, 25.61, 22.60, 22.57, 13.79, 13.76, 0.47.

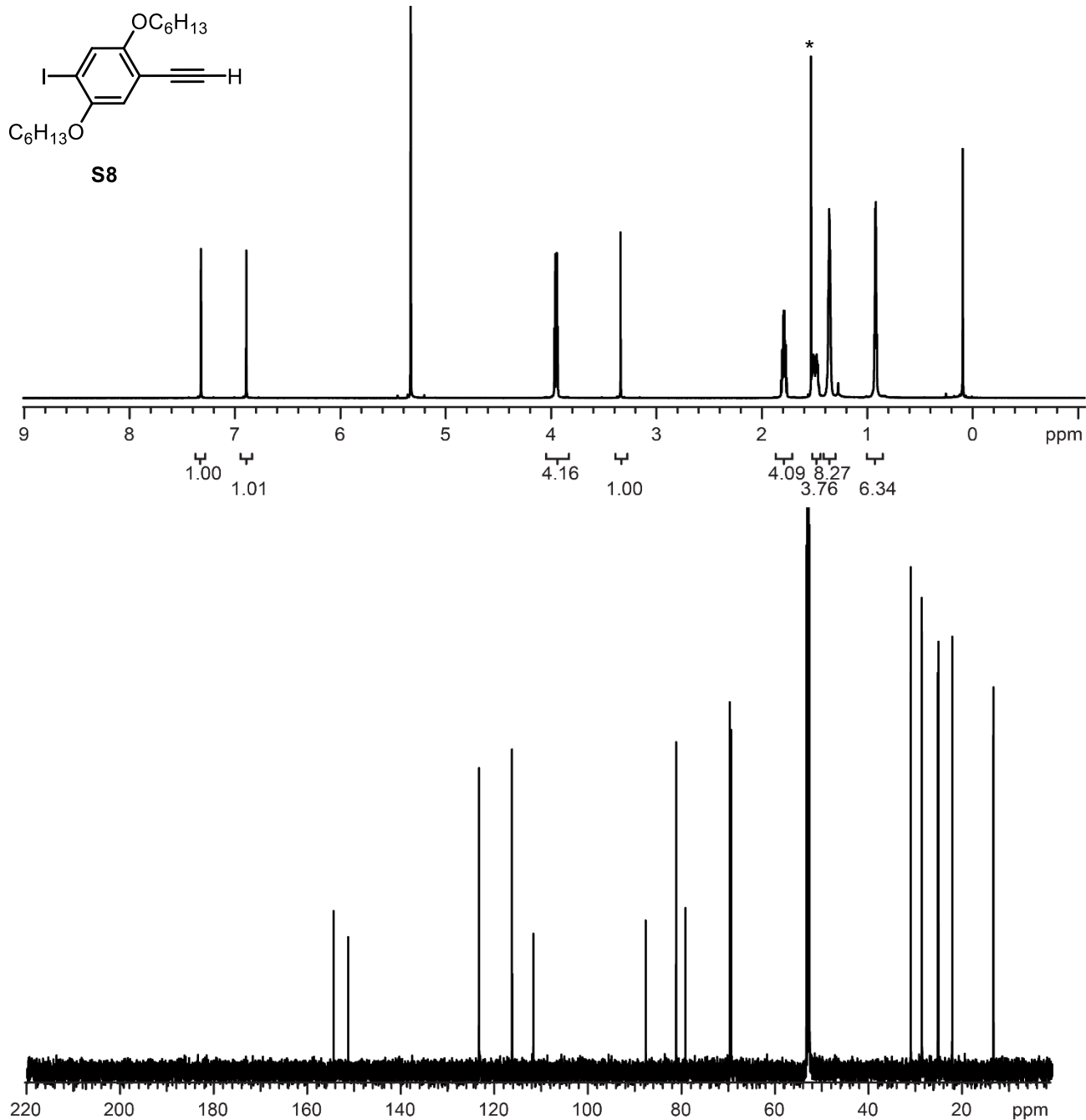
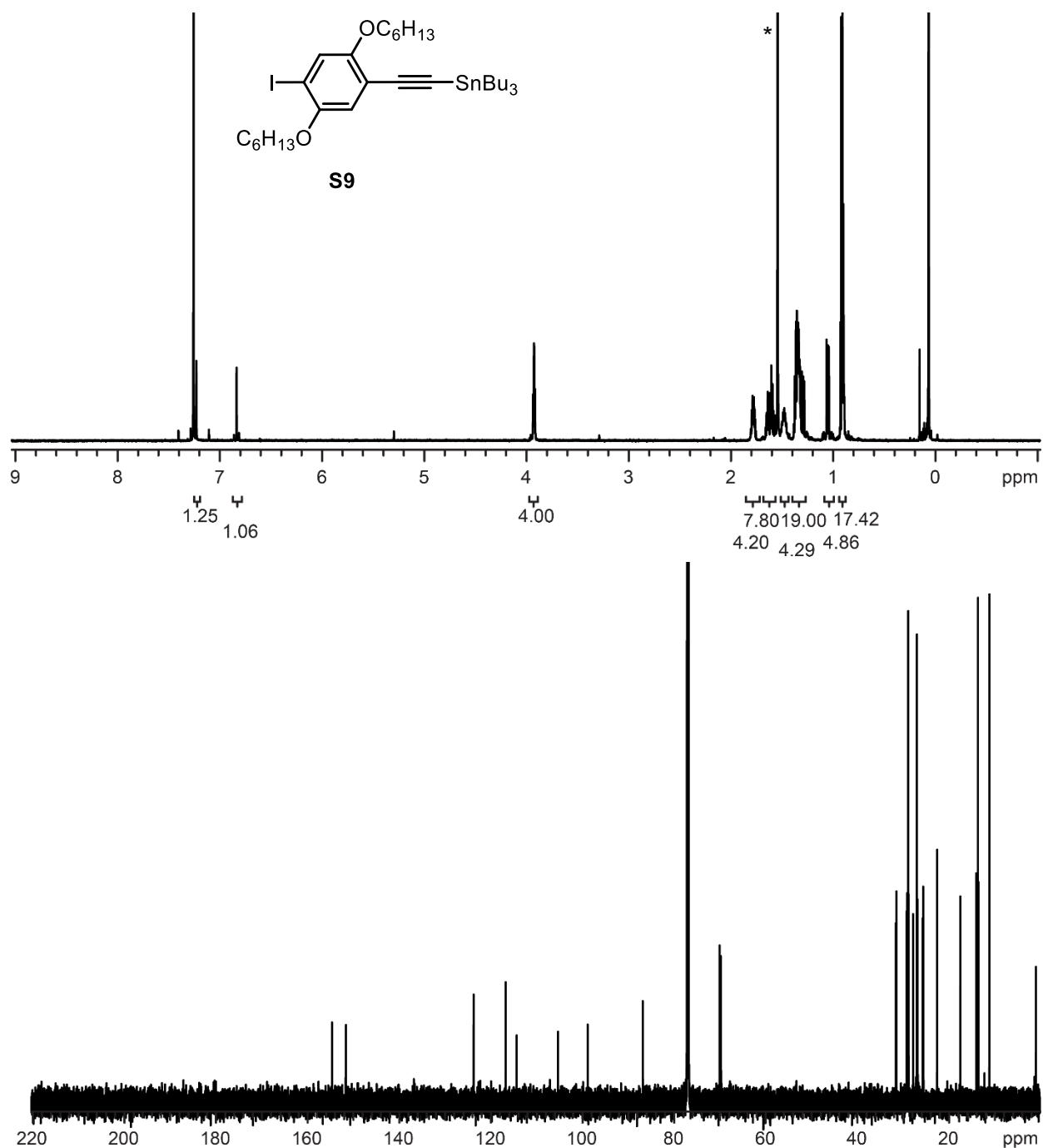


Figure S2.12. ^1H and ^{13}C NMR spectra for **S8**. ^1H NMR (700 MHz, CD_2Cl_2) δ 7.32 (s, 1H), 6.89 (s, 1H), 3.97–3.94 (m, 4H), 3.34 (s, 1H), 1.81–1.76 (m, 4H), 1.53–1.47 (m, 4H), 1.37–1.34 (m, 8H), 0.93–0.91 (m, 6H). ^{13}C NMR (176 MHz, CD_2Cl_2) δ 154.82, 151.72, 123.73, 116.67, 112.12, 88.10, 81.59, 79.59, 70.12, 69.83, 31.47, 31.45, 29.09, 29.07, 25.68, 25.51, 22.57, 22.55, 13.77, 13.75.



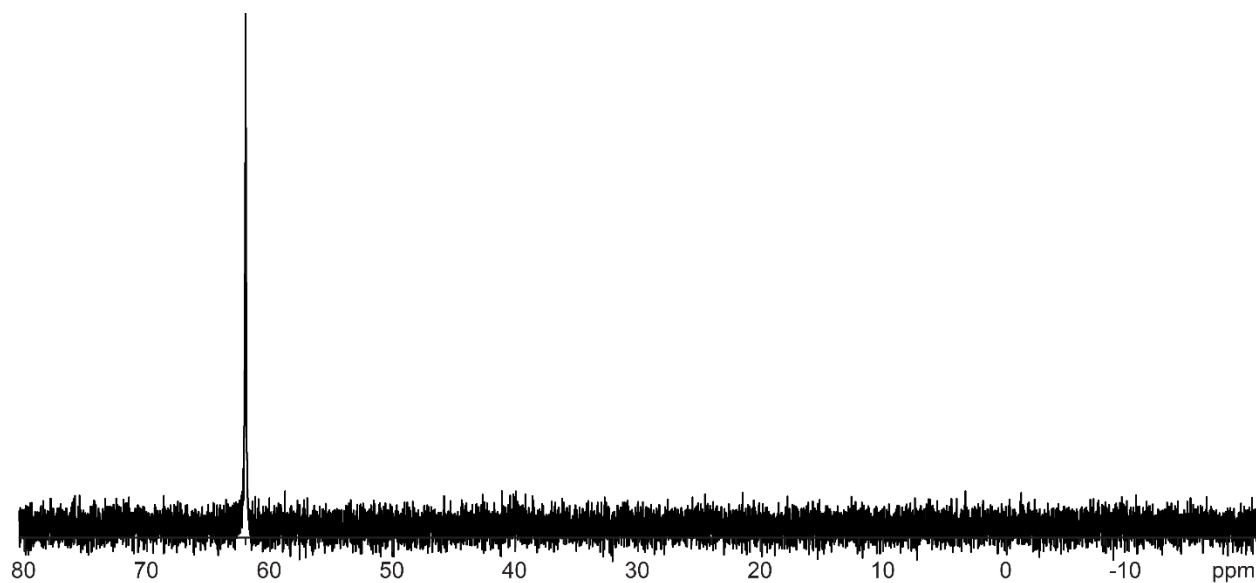
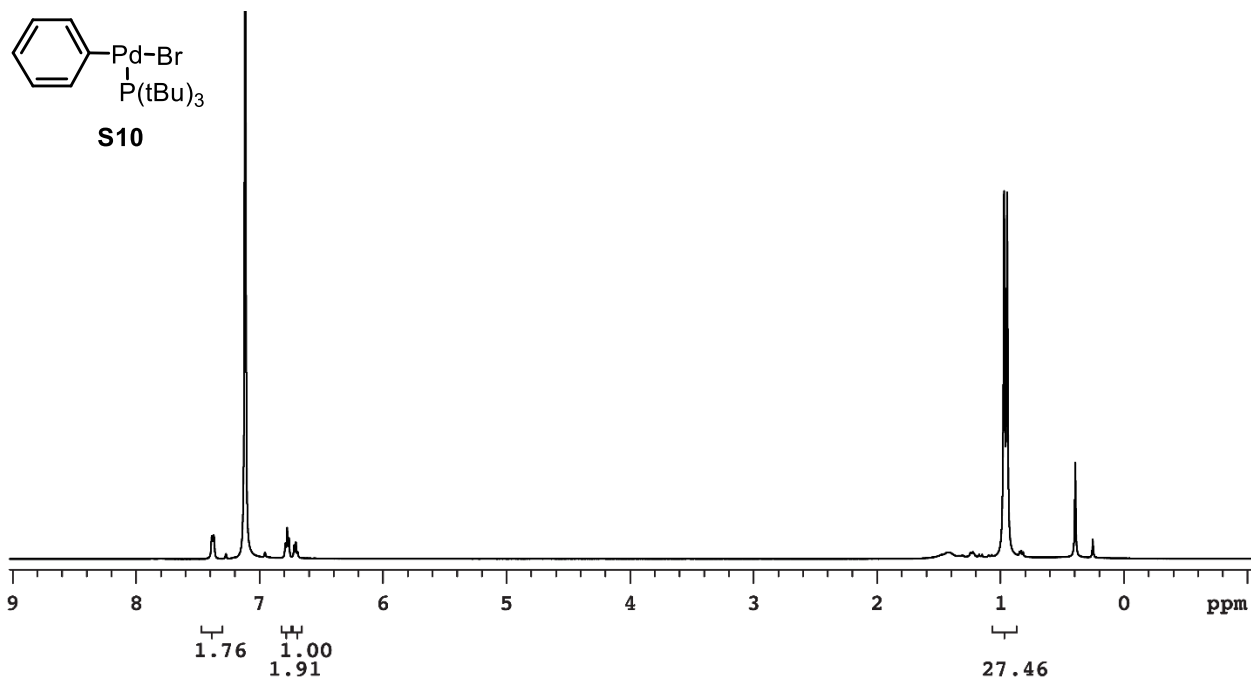
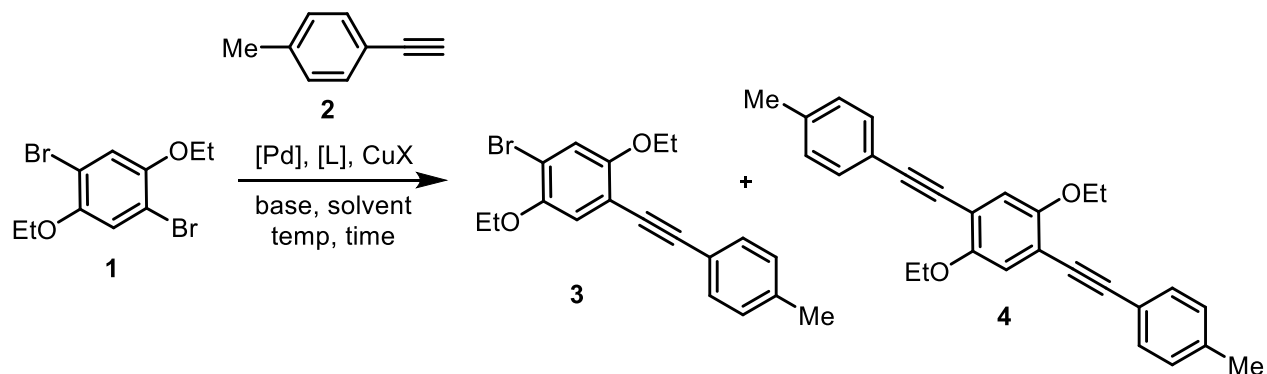
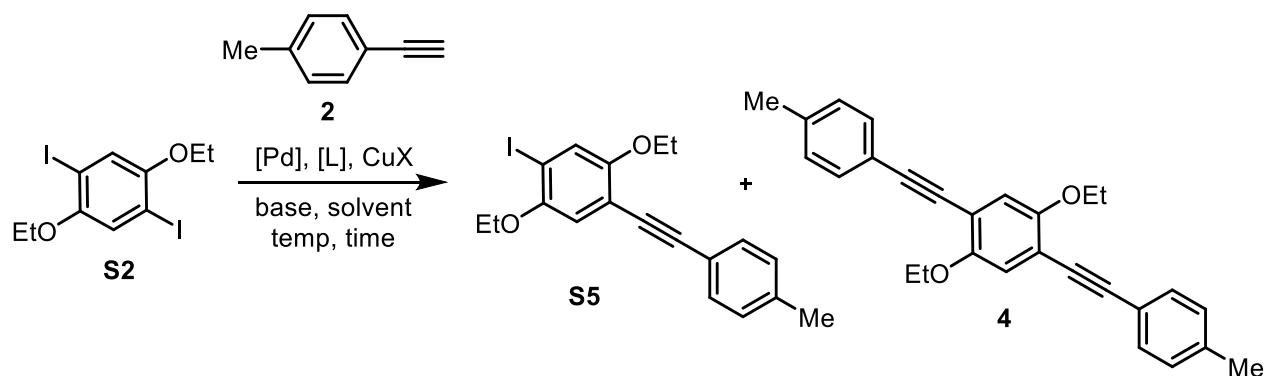


Figure S2.14. ^1H and ^{31}P NMR spectra for **S10**. ^1H NMR (500 MHz, C_6D_6) δ 7.42 (d, $J = 6.5$ Hz, 2H), 6.82 (t, $J = 7.5$ Hz, 2H), 6.75 (t, $J = 7.0$ Hz, 1H), 1.00 (d, $J_{P-H} = 12.5$, 27 H). ^{31}P NMR (202 MHz, C_6C_6) δ 61.98.

VI. Small Molecule Screens

The small molecule screens outlined in this section reflect a small percentage of the total number performed. We initially began screening small molecules utilizing 1,4-diiodo-2,5-diethoxybenzene (**S2**), however we observed aryl iodide decomposition in solution over time. We switched to 1,4-dibromo-2,5-diethoxybenzene (**1**) and observed higher selectivity for the di-functional product (**4**). All small molecule screens listed are using **S2** unless noted. The amount of 1,1'-(1,2-ethynediyl)bis(4-methylbenzene) formed was less than 3% unless stated otherwise.



Representative Procedure for Small Molecule Screens:

Prior to starting each batch of reactions, separate stock solutions in PhMe were made for C₁₉H₄₀ internal standard (0.050 M), **1** (0.20 M), CuI/PMDTA (0.050 M). Similarly, a stock solution of the phosphine ligand (0.020 M) was also prepared when needed.

In the glovebox, a 4 mL vial was equipped with a stir bar. Pd catalyst (0.0025 mmol, 1.0 equiv) was then carefully measured out in the vial, and the mass was recorded. Sequentially phosphine ligand* (0.25 mL of 0.02 M stock solution, 2.0 equiv), CuI/PMDTA (0.25 mL of 0.050 M stock solution, 5.0 equiv), **1** (1.0 mL of 0.20 M stock solution, 80 equiv), C₁₉H₄₀ internal standard (0.25 mL of 0.050 M stock solution, 5.0 equiv), and 0.25 mL PhMe were added with stirring to reach a total volume of 2.0 mL PhMe. Next, NEt₃ (1 mL, 33% by volume) and **2** (13 μ L, 0.10 mmol, 40 equiv) were added to the vial. The cap was secured tightly and the reaction was stirred for 2 days at rt. The vial was removed from the glovebox and the reaction was quenched with HCl (12.1 M, 3 mL) and subsequently diluted with water (8 mL). The reaction mixture was then extracted with DCM (3 x 3 mL), and the combined organic layers were dried over MgSO₄, filtered through a 0.2 μ m PTFE filter, and subjected to GC analysis.

Table S2.1. Data for reactions with 0-2 equiv of SPhos.
Conditions: Solvent = PhMe/NEt₃ (67/33 vol. ratio, 3 mL total vol.), temperature = rt, Pd = Gen 2 SPhos (1 equiv) + n SPhos, CuI/PMDTA = 5 equiv (1:1 ratio).

SPhos (equiv)	% Conv. 2	μ mol S5	μ mol 4	S5/4 ratio
0	100	13.6	56.4	20/80
1	63	12.0	8.2	60/40
2	52	8.5	2.0	81/19

Table S2.2. Data for reactions with variable Pd precatalysts.

Conditions: Solvent = PhMe/NEt₃ (67/33 vol. ratio, 3 mL total vol.), temperature = rt, Pd = **precatalyst** (1 equiv), CuI/PMDTA = 5 equiv (1:1 ratio).

Catalyst	% Conv. 2	μmol S5	μmol 4	S5/4 ratio
Gen 1 SPhos	80	19.0	39.0	33/67
Gen 2 SPhos	100	11.9	76.1	14/84
Gen 3 SPhos	100	13.9	68.7	17/83
Gen 1 XPhos	100	25.0	38.4	39/61
Gen 2 XPhos	100	26.1	40.1	39/61
Gen 3 XPhos	100	34.6	68.8	33/67
Gen 1 BrettPhos	100	38.8	19.3	67/33
Gen 2 BrettPhos	100	40.1	25.6	61/39
Gen 2 RuPhos	100	18.9	33.1	36/64

Table S2.3. Data for reactions with variable Pd catalysts.

Conditions: Solvent = PhMe/NEt₃ (67/33 vol. ratio, 3 mL total vol.), temperature = rt, Pd = **precatalyst** (1 equiv) or **PdL₂** (1 equiv), CuI/PMDTA = 5 equiv (1:1 ratio).

ArX ₂	Catalyst	% Conv. 2	μmol 3 or S5	μmol 4	3/4 or S5/4 ratio
S2	Gen 1 SPhos	80	16.3	28.1	37/63
S2	Gen 2 SPhos	100	11.8	37.9	24/76
S2	Gen 1 XPhos	100	25.5	45.1	36/64
S2	Gen 2 XPhos	100	21.5	45.5	32/68
S2	Pd(PhCN)Cl ₂ + XPhos	70	26.0	36.3	36/64
S2	Pd(OAc) ₂ + XPhos	100*	17.1	19.4	47/53
1	Pd(OAc) ₂ + CyJohnPhos	100 [^]	64.8	25.2	72/28

*This reaction produced 12% yield of 1,1'-(1,2-ethynediyl)bis(4-methylbenzene) as a side-product. [^]These conditions resulted in 51% isolated yield of **3** when scaled to a 1 g of **1**.

Table S2.4. Data for reactions with 5-20 equiv PMDTA.

Conditions: Solvent = PhMe/NEt₃ (67/33 vol. ratio, 3 mL total vol.), temperature = rt, Pd = Gen 2 SPhos (1 equiv), CuI/PMDTA (1:n ratio) = 5 equiv.

PMDTA (equiv)	% Conv. 2	μmol S5	μmol 4	S5/4 ratio
5	100	9.0	25.3	26/74
10	100	9.1	20.6	31/69
15	93	8.8	25.1	31/69
20	94	9.1	19.4	32/68

Table S2.5. Data for reactions with 1-20 equiv CuI/PMDTA (1:1 ratio).

Conditions: Solvent = PhMe/NEt₃ (67/33 vol. ratio, 3 mL total vol.), temperature = rt, Pd = Gen 2 SPhos (1 equiv), CuI/PMDTA = n equiv (1:1 ratio).

CuI + PMDTA (equiv)	% Conv. 2	μmol S5	μmol 4	S5/4 ratio
1	95	16.6	60.6	22/78
5	100	14.0	44.3	24/76
10	100	13.3	34.3	28/72
20	100	13.3	30.3	31/69

Table S2.6. Data for reactions with 0.2-5 equiv of Gen 2 SPhos

Conditions: Solvent = PhMe/NEt₃ (67/33 vol. ratio, 3 mL total vol.), temperature = rt, Pd = Gen 2 SPhos (n equiv), CuI/PMDTA = 5 equiv (1:1 ratio).

Gen 2 SPhos (equiv)	% Conv. 2	μmol S5	μmol 4	S5/4 ratio
0.2	100	21.3	61.1	26/74
1	100	13.6	56.3	20/80
5	100	7.4	18.3	29/71

Table S2.7. Data for reactions with various bases.

Conditions: Solvent = PhMe/**base** (67/33 vol. ratio, 3 mL total vol.), temperature = rt, Pd = Gen 2 SPhos (1 equiv), Cu/PMDTA = 5 equiv (1:1 ratio).

Base	pKa	% Conv. 2	μmol S5	μmol 4	S5/4 ratio
HNPh ₂	1	42	2.8	0.0	100/0
NBn ₃	4	71	5.4	0.1	97/3
NEt ₃	9	100	11.8	37.9	24/76
NHiPr ₂	11	100	11.1	27.5	29/71
DBU	14	100	25.8	11.8	69/31
KOtBu	18	83*	6.1	1.1	85/15

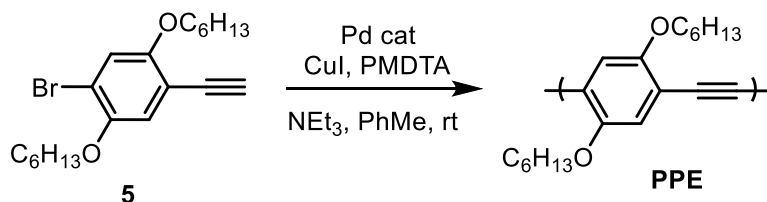
*This reaction produced 17% yield of 1,1'-(1,2-ethynediyl)bis(4-methylbenzene) as a side-product.

Table S2.8. Data for reactions with 15-100% NEt₃ volume ratio.

Conditions: Solvent = PhMe/NEt₃ (**n** vol. ratio, 3 mL total vol.), temperature = rt, Pd = Gen 2 SPhos (1 equiv), Cu/PMDTA = 5 equiv (1:1 ratio).

ArX ₂	NEt ₃ (% vol)	% Conv. 2	μmol 3 or S5	μmol 4	3/4 or S5/4 ratio
S2	15	12	18.1	8.3	69/31
S2	25	46	24.7	30.1	45/55
S2	33	69	22.1	40.6	35/65
S2	50	94	16.0	58.8	21/79
S2	75	100	11.0	63.4	15/85
S2	100 (neat)	100	6.5	76.0	8/92
1	100 (neat)	100	1.2	55.5	4/96
1	100 (neat)	100	1.0	56.0	2/98

VII. Polymerization Results



Representative Procedure for PPE Polymerizations:

Prior to starting each batch of reactions, separate stock solutions in PhMe were made for **5** (0.050 M) with added internal standard ($\text{C}_{22}\text{H}_{46}$, ~3 mg), and CuI/PMDTA (0.050 M).

In the glovebox, a 4 mL vial was equipped with a stir bar. Gen 2 SPhos (1.3 μmol , 0.94 mg, 1.0 equiv) was then carefully measured out in the vial, and the mass was recorded. Sequentially, CuI/PMDTA (0.13 mL of 0.050 M stock solution, 5.0 equiv), and 0.11 mL PhMe were added with stirring to reach a total volume of 0.24 mL PhMe. Next, NEt_3 (1 mL, 33% by volume) and **5** (1.76 mL of 0.050 M stock solution, 67 equiv) were added to the vial. The cap was secured tightly and the reaction was stirred for 2 days at rt. The vial was removed from the glovebox, quenched with HCl (12.1 M, 1 mL), and subsequently diluted with water (4 mL). The reaction was then extracted with DCM (3 x 3 mL). The combined organic layers were dried over MgSO_4 . Conversion was determined relative to the initial concentration, using the internal standard as a reference via GC. To measure molecular weight and molecular weight distribution, the organic phase was concentrated in vacuo, redissolved in THF (~1.5 mL) with mild heating and passed through a 0.2 μm PTFE filter for GPC analysis.

Table S2.9. Data for polymerization screens with NEt₃ (variable volume)

Conditions: Solvent = PhMe/NEt₃ (n vol. ratio, 3 mL total vol.), temperature = rt, Pd = Gen 2 SPhos (1 equiv), CuI/PMDTA = 5 equiv (1:1 ratio).

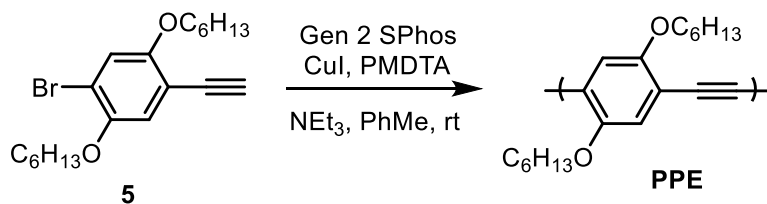
NEt ₃ (% vol)	% Conv. 5	M _n (predicted)	M _n (measured)	Đ
33	100	20.2	7.2	1.57
50	100	20.2	7.8	1.61

Table S2.10. Data for reactions with variable Pd precatalysts.

Conditions: Solvent = PhMe/NEt₃ (50/50 vol. ratio, 3 mL total vol.), temperature = rt, Pd = **precatalyst** (1 equiv), CuI/PMDTA = 5 equiv (1:1 ratio).

Catalyst	% Conv. 5	M _n (predicted)	M _n (measured)	Đ
Gen 1 SPhos	100	15.1	4.6	4.29
Gen 2 SPhos	100	24.8	10.1	4.76
Gen 3 SPhos	100	23.3	10.3	6.08
Gen 1 XPhos	100	22.0	8.2	1.99
Gen 2 XPhos	100	23.6	12.5	2.79
Gen 3 XPhos	100	25.4	11.9	3.00

VIII. M_n and \bar{D} versus Conversion



Representative Procedure for M_n and \bar{D} versus Conversion Studies utilizing GC analysis:

Prior to starting each batch of reactions, separate stock solutions in PhMe were made for **5** (0.50 M) with added internal standard (C₂₂H₄₆, ~3 mg), and CuI/PMDTA (0.050 M).

In the glovebox, a 20 mL vial was equipped with a stir bar. Gen 2 SPhos (0.013 mmol, 9.1 mg, 1.0 equiv) was then carefully measured out in the vial, and the mass was recorded. Sequentially, CuI/PMDTA (1.26 mL of 0.050 M stock solution, 5.0 equiv), and 4.54 mL PhMe were added with stirring to reach a total volume of 5.80 mL PhMe. Next, NEt₃ (2.5 mL, 25% by volume) and **5** (1.70 mL of a 0.50 M stock solution, 67 equiv) were added to the vial. The cap was secured tightly and the reaction was stirred for 30 h at rt. Samples (~0.5 mL) were taken periodically and removed from the glovebox, quenched with HCl (12.1 M, 1 mL), and subsequently diluted with water (4 mL). The sample was then extracted with DCM (3 x 3 mL). The combined organic layers were dried over MgSO₄. Conversion was determined relative to the initial concentration, using the internal standard as a reference via GC. To measure molecular weight and molecular weight distribution, the organic phase was concentrated in vacuo, redissolved in THF (~1.5 mL) with mild heating and passed through a 0.2 μm PTFE filter for GPC analysis.

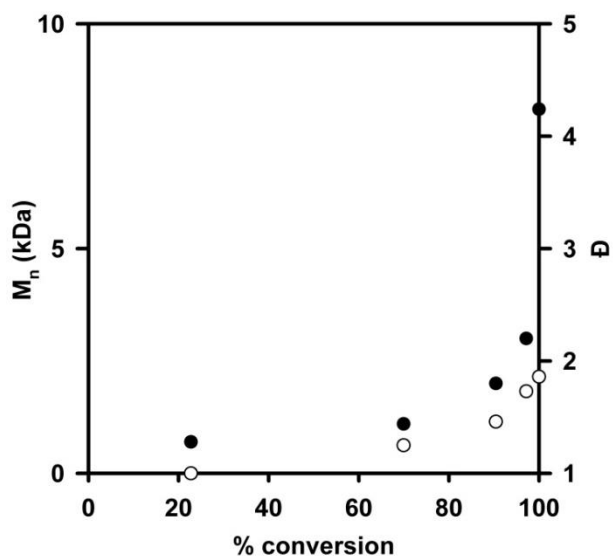


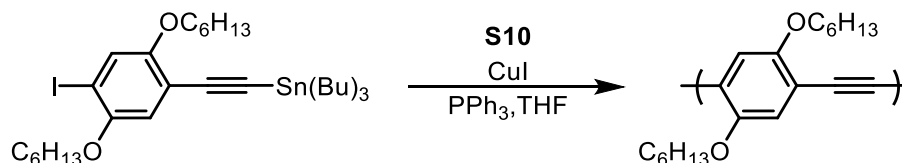
Figure S2.15. Plot of M_n (•) and \bar{D} (◦) versus conversion utilizing the most favorable small molecule conditions.

Table S2.11. Data for the plot in **Figure S2.15**.

Time (min)	% Conv. 5	M_n	\bar{D}
50	23	0.7	1.00
125	70	1.1	1.25
190	90	2.0	1.46
240	97	3.0	1.73
1770	100	8.1	1.86

Procedures for M_n and \mathcal{D} versus Time Studies utilizing **S9** Monomer:

Method A:



In the glovebox, a 20 mL vial was equipped with a stir bar and charged with CuI (1.9 mg, 0.01 mmol, 0.1 equiv) and triphenylphosphine (2.6 mg, 0.1 mmol, 0.1 equiv), then **S9** (4 mL of a 0.025 M stock solution in THF, 0.10 mmol, 1 equiv) and **S10** (0.2 mL of a 0.01 M solution in THF, 0.02 equiv) were added. The reaction was stirred for 12 h at rt. Samples (~0.5 mL) were taken periodically and removed from the glovebox, quenched with DI water/MeOH (1:4, 1 mL), and subsequently extracted with DCM (2 x 3 mL). The combined organic layers were dried over MgSO₄. To measure molecular weight and molecular weight distribution, the organic phase was concentrated in vacuo, redissolved in THF (~1.5 mL) with mild heating and passed through a 0.2 μm PTFE filter for GPC analysis.

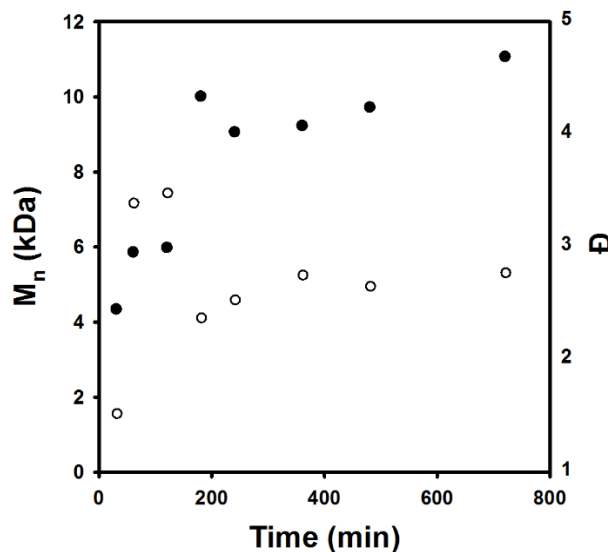
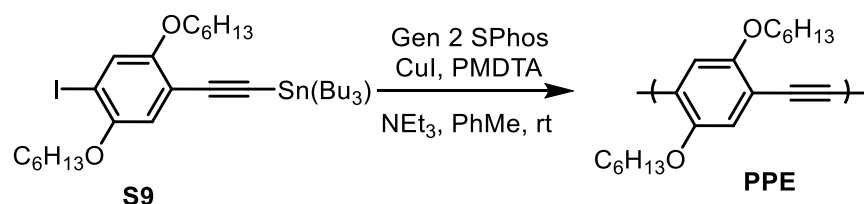


Figure S2.16. Plot of M_n (•) and \mathcal{D} (°) versus time utilizing **S9** monomer and previously reported chain-growth conditions.⁴

Table S2.12. Data for the plot in **Figure S2.16.**

Time (min)	M _n	Đ
30	4.4	1.49
60	5.9	3.36
120	6.0	3.45
180	10.0	2.34
240	9.1	2.50
360	9.2	2.72
480	9.7	2.62
720	11.1	2.74

Method B:



In the glovebox, a 20 mL vial was equipped with a stir bar. Gen 2 SPhos (0.0026 mmol, 1.9 mg, 1.0 equiv) was then carefully measured out in the vial. Sequentially, an aliquot of a stock solution (0.19 mL) containing CuI (0.050 M) and PMDTA (0.050 M) and PhMe (1.6 mL) were added with stirring to reach a total volume of 1.79 mL PhMe. Next, NEt₃ (1.47 mL, 25% by volume) and **S9** (2.6 mL of a 0.050 M stock solution, 50 equiv) were added to the vial. The cap was secured tightly and the reaction was stirred for 12 h at rt. Samples (~0.5 mL) were taken periodically and removed from the glovebox, quenched with HCl (12.1 M, 1 mL), and subsequently diluted with water (4 mL). The sample was then extracted with DCM (3 x 3 mL). The combined organic layers were dried over MgSO₄. To measure molecular weight and molecular weight distribution, the organic phase was concentrated in vacuo, redissolved in THF (~1.5 mL) with mild heating and passed through a 0.2 μm PTFE filter for GPC analysis.

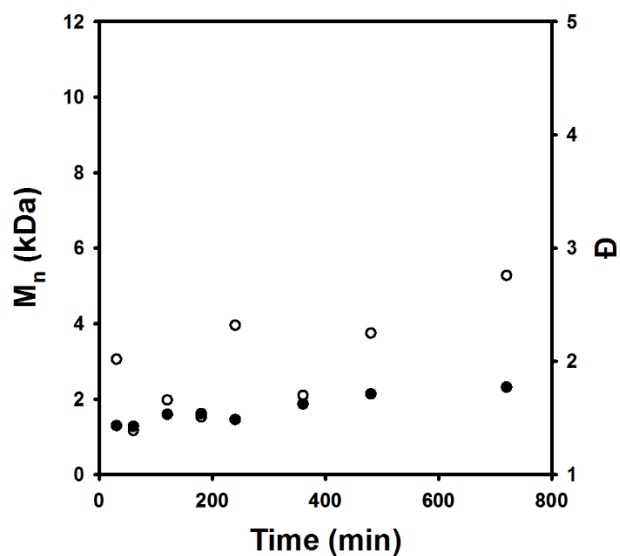
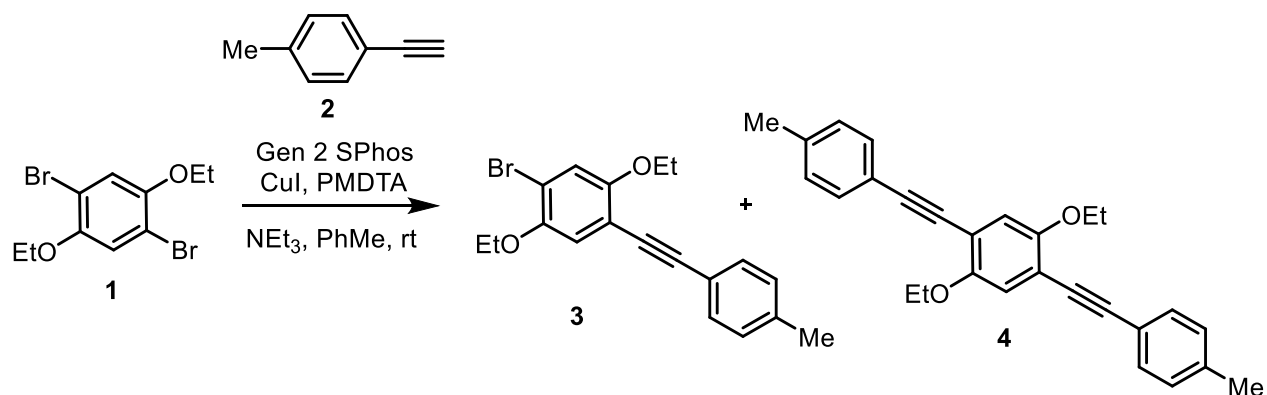


Figure S2.17. Plot of M_n (•) and \bar{D} (◦) versus time utilizing **S9** monomer and the most favorable small molecule conditions.

Table S2.13. Data for the plot in **Figure S2.17**

Time (min)	M_n	\bar{D}
30	1.3	2.02
60	1.3	1.39
120	1.6	1.66
180	1.6	1.51
240	1.5	2.32
360	1.9	1.7
480	2.1	2.25
720	2.3	2.76

IX. Small Molecule Reaction Profiles



Representative Procedure for Sonogashira Small Molecule Reaction Profile utilizing GC analysis:

Prior to starting each batch of reactions, separate stock solutions in PhMe were made for **1** (0.50 M), **2** (0.50 M) with added internal standard (C₂₂H₄₆, ~3 mg), and CuI/PMDTA (0.050 M).

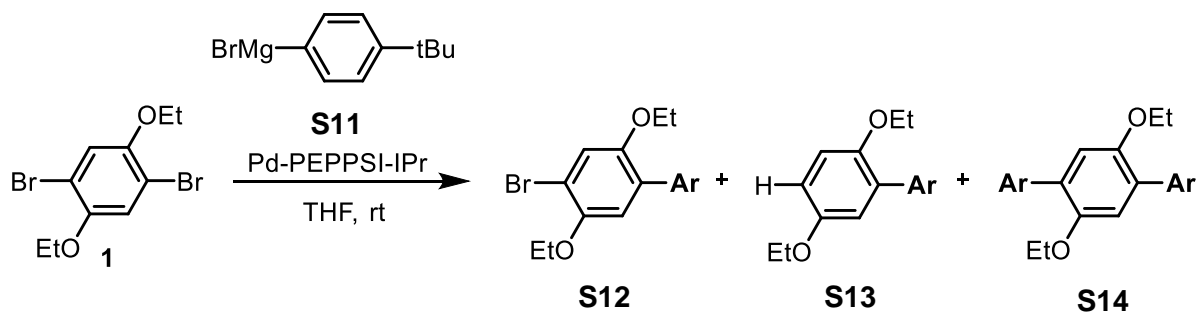
In the glovebox, a 20 mL vial was equipped with a stir bar. Gen 2 SPhos (5.8 mg, 0.0075 mmol, 1.0 equiv) was then carefully measured out in the vial, and the mass was recorded. Sequentially CuI/PMDTA (0.76 mL of 0.050 M stock solution, 5.0 equiv), **1** (1.2 mL of 0.50 M stock solution, 80 equiv), and 3.84 mL PhMe were added with stirring to reach a total volume of 5.80 mL PhMe. Next, NEt₃ (6 mL, 50% by volume) and **2** (0.2 mL of 0.50 M stock solution, 40 equiv) were added to the vial. The cap was secured tightly and the reaction was stirred for 24 h at rt. Samples (~0.5 mL) were taken periodically and removed from the glovebox, quenched with HCl (12.1 M, 1 mL), and subsequently diluted with water (4 mL). The sample was then extracted with DCM (2 x 3 mL). The combined organic layers were dried over MgSO₄. Conversion was determined relative to the initial concentration, using the internal standard as a reference via GC.

Table S2.14. Data for Sonogashira small molecule reaction profile, trial 1.

Time (h)	% Conv. 2	% 3	% 4
1	6	100	0
2	19	92	8
3	27	77	23
5	46	37	63
22	100	9	91

Table S2.15. Data for Sonogashira small molecule reaction profile, trial 2.

Time (h)	% Conv. 2	% 3	% 4
2	18	100	0
3	28	95	5
4	52	50	50
5	57	36	64
22	100	9	91



Representative Procedure for Sonogashira Small Molecule Reaction Profile utilizing GC analysis:¹

Prior to starting each batch of reactions, separate stock solutions in THF were made for **1** (0.50 M), Pd-PEPPSI-IPr (0.050 M), and **S11** (0.25 M) with added internal standard (C₂₂H₄₆, ~3 mg).

In the glovebox, a 20 mL vial was equipped with a stir bar. Pd-PEPPSI-IPr (0.15 mL of 0.050 M stock solution, 1.0 equiv) was then added to the vial with stirring. Sequentially **1** (1.2 mL of 0.50 M stock solution, 80 equiv), and 9.45 mL THF were added with stirring to reach a total volume of 10.80 mL THF. Next, **S11** (1.2 mL of 0.25 M stock solution, 40 equiv) were added to the vial. The cap was secured tightly and the reaction was stirred for 60 min at rt. Samples (~0.5 mL) were taken periodically and removed from the glovebox, quenched with HCl (12.1 M, 1 mL), and subsequently diluted with water (4 mL). The sample was then extracted with DCM (2 x 3 mL). The combined organic layers were dried over MgSO₄. Conversion was determined relative to the initial concentration, using the internal standard as a reference via GC.

¹ Structures **S11–S14** were labeled as **S6–S9** in the original publication, but have been changed here as **S6–S9** are different synthetic intermediates.

Table S2.16. Data for Kumada small molecule reaction profile, trial 1

Time (min)	% Conv. S11	% S12	% S13 + S14
0.5	25	0	100
1.5	32	1	99
2.5	39	0	100
3.5	45	5	95
5	49	6	94
7	53	7	93
60	100	8	92

Table S2.17. Data for Kumada small molecule reaction profile, trial 2.

Time (min)	% Conv. S11	% S12	% S13 + S14
0.5	30	0	100
2	44	0	100
2.5	50	3	97
3	55	4	96
3.5	60	7	93
4.5	64	8	92
5	77	8	92
60	100	9	91

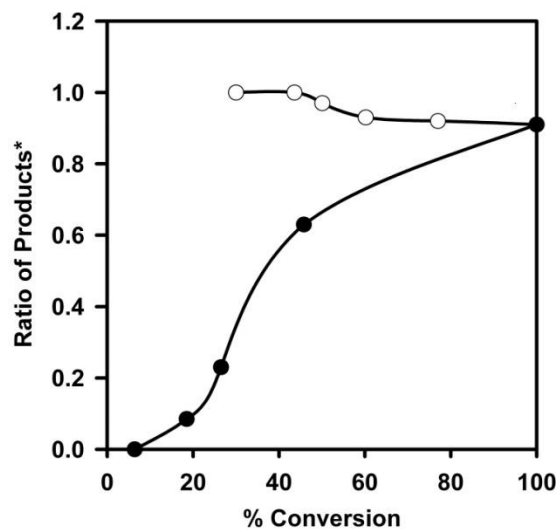


Figure S2.18. Plot of product ratios versus conversion from **Table S2.14** and **Table S2.17**. For Sonogashira (•) small molecule reactions, the product ratio is of compounds **4:3**. For Kumada (°) small molecule reactions, the product ratio is of compounds (**S13 + S14**):**S12** as both **S13** and **S14** stem from intramolecular pathways.

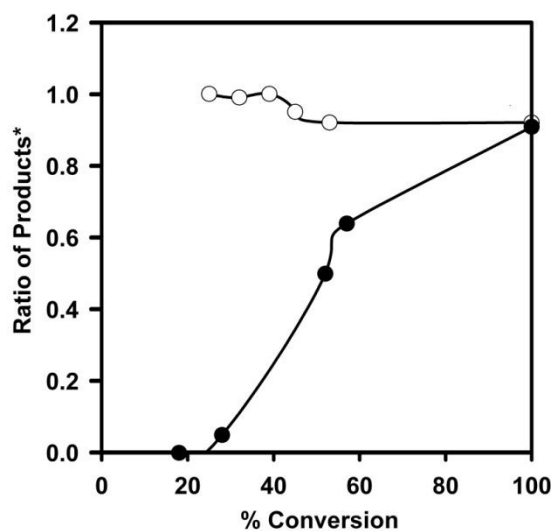
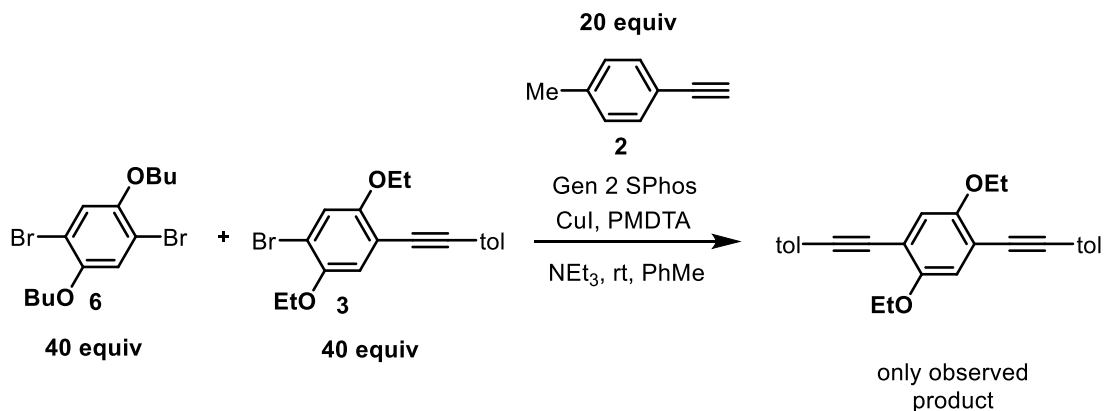


Figure S2.19. Plot of product ratios versus conversion from **Table S2.15** and **Table S2.16**. For Sonogashira (•) small molecule reactions, the product ratio is of compounds **4:3**. For Kumada (°) small molecule reactions, the product ratio is of compounds (**S13 + S14**):**S12** as both **S13** and **S14** stem from intramolecular pathways.

X. Competition Experiments



Representative Procedure for Sonogashira Reactivity Competition Experiments:

Prior to starting each batch of reactions, separate stock solutions in PhMe were made for C₁₉H₄₀ internal standard (0.050 M), **6** (0.20 M), **3** (0.20 M), and CuI/PMDTA (0.050 M).

In the glovebox, a 4 mL vial was equipped with a stir bar. Pd catalyst (1.9 mg, 0.0025 mmol, 1.0 equiv) was then carefully measured out in the vial, and the mass was recorded. Sequentially, CuI/PMDTA (0.25 mL of 0.050 M stock solution, 5.0 equiv), **6** (0.50 mL of 0.20 M stock solution, 40 equiv), **3** (0.50 mL of 0.20 M stock solution, 40 equiv), C₁₉H₄₀ internal standard (0.25 mL of 0.050 M stock solution, 5.0 equiv), and 0.50 mL PhMe were added with stirring to reach a total volume of 2.0 mL PhMe. Next, NEt₃ (1 mL, 33% by volume) and **2** (13 μ L, 0.10 mmol, 40 equiv) were added to the vial. The cap was secured tightly and the reaction was stirred for 2 days at rt. The vial was removed from the glovebox and the reaction was quenched with HCl (12.1 M, 3 mL) and subsequently diluted with water (8 mL). The reaction mixture was then extracted with DCM (2 x 3 mL), and the combined organic layers were dried over MgSO₄, filtered through a 0.2 μ m PTFE filter, and subjected to GC analysis.

GC analysis showed exclusively conversion of the mono-functionalized starting material (**3**), and also showed only formation of the di-functionalized product (**4**) labeled with

ethoxy side-chains, indicating that it originated from **3**. This experiment was performed twice with the same results.

XI. Calibration Curves

Representative Procedure for Preparing Calibration Curves:

A stock solution was made by weighing ~75 mg of each compound into a 25 mL volumetric flask which was then filled with DCM. A separate stock solution of internal standard ($C_{19}H_{40}$) was also made by placing ~75 mg into a 25 mL volumetric flask and then diluting with DCM. These stock solutions were used to make 5 samples with known concentrations within the expected range of concentrations of the experiment (0.05 mmol – 0.0005 mmol for compounds **4**, 0.1 mmol – 0.01 mmol for compound **3**). Each of these samples was analyzed by GC and the areas plotted against the known concentrations to produce a calibration curve. The process was performed twice per compound and the ratios were averaged.

These calibration curves were used to convert the GC product area ratio of **3:4** into mol product ratios of **3:4**. These calibration curves were also used to determine the conversion of **2**, the μmol of **S5**, the μmol of **3**, and μmol of **4** found in **VI** (small molecule screens).

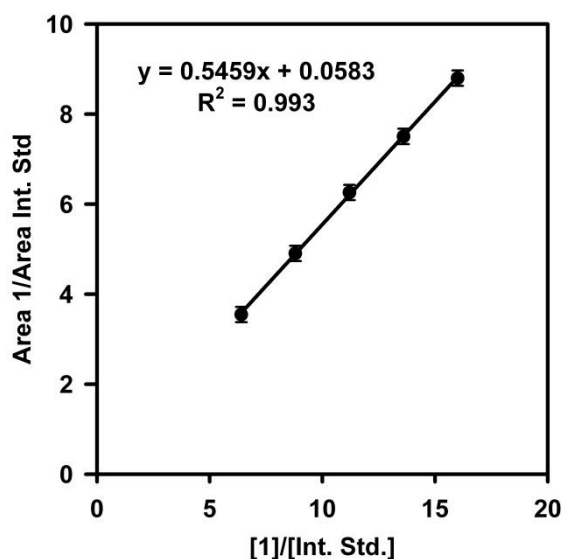


Figure S2.20. Calibration curve for **1**, points include error bars.

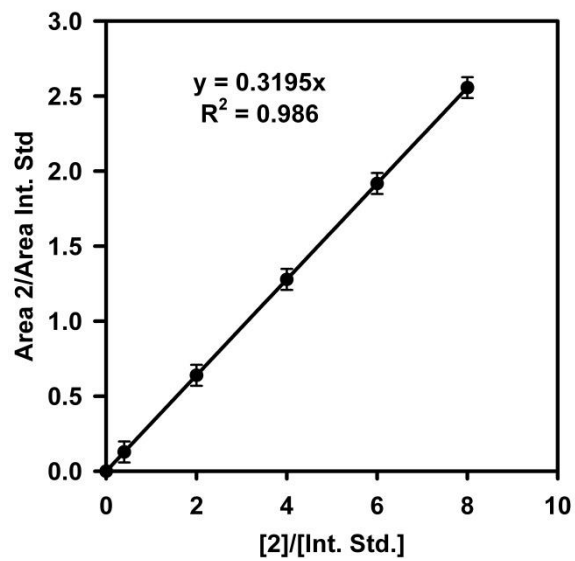


Figure S2.21. Calibration curve for 2, points include error bars.

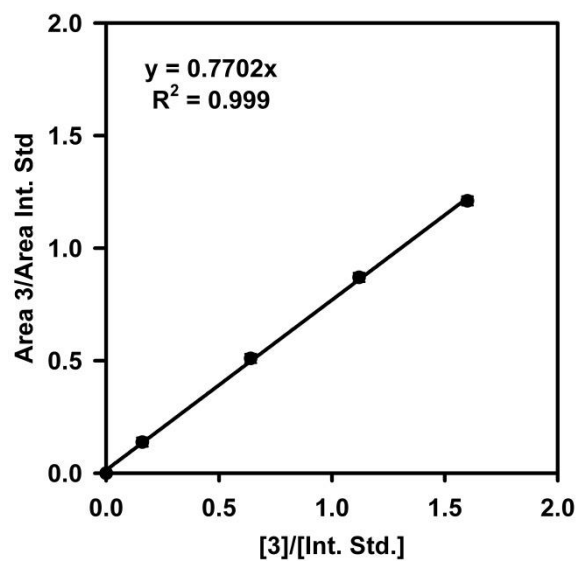


Figure S2.22. Calibration curve for 3, points include error bars.

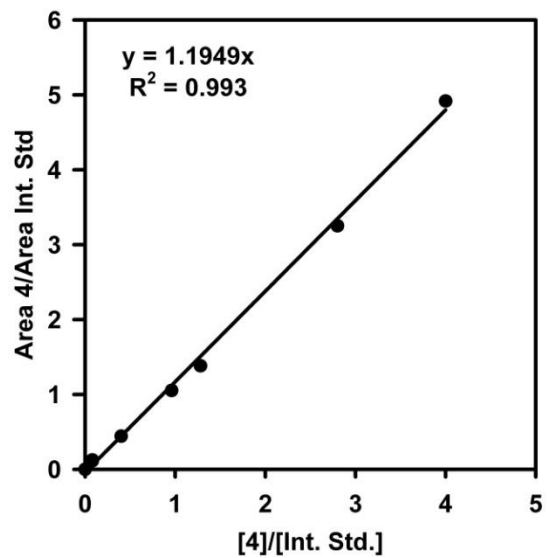


Figure S2.23. Calibration curve for 4.

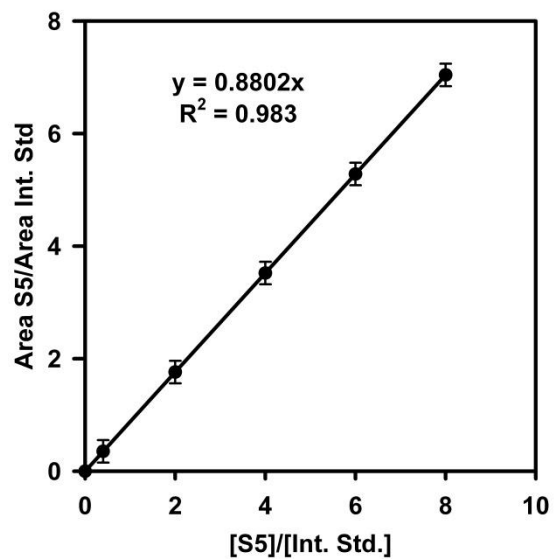


Figure S2.24. Calibration curve for S5, points include error bars.

XII. References

- (1) Wild, A.; Winter, A.; Hager, M. D.; Schubert, U. S. Fluorometric, Water-based Sensors for the Detection of Nerve Gas G Mimics DMMP, DCP and DCNP *Chem. Commun.* **2012**, *48*, 964–966.
- (2) Lanni, E. L.; McNeil, A. J. Mechanistic Studies on Ni(dppe)Cl₂-catalyzed Polymerizations: Evidence for Rate-Determining Reductive Elimination. *J. Am. Chem. Soc.* **2009**, *131*, 16573–16579.
- (3) Bryan, Z. J.; McNeil, A. J. Evidence for a Preferential Intramolecular Oxidative Addition in Ni-catalyzed Cross-coupling Reactions and their Impact on Chain-growth Polymerizations *Chem. Sci.* **2013**, *4*, 1620–1624.
- (4) Kang, S.; Ono, R.J.; Bielawski, C.W. Controlled Catalyst Transfer Polycondensation and Surface-Initiated Polymerization of a p-Phenyleneethynylene-Based Monomer *J. Am. Chem. Soc.* **2013**, *135*, 4984–4987.
- (5) Stambuli, J. P.; Incarvito, C. D.; Bühl, M.; Hartwig, J. F. Synthesis, Structure, Theoretical Studies, and Ligand Exchange Reactions of Monomeric, T-Shaped Arylpalladium(II) Halide Complexes with an Additional, Weak Agostic Interaction *J. Am. Chem. Soc.* **2004**, *126*, 1184–1194.
- (6) Love, B. E.; Jones, E. G. The Use of Salicylaldehyde Phenylhydrazone as an Indicator for the Titration of Organometallic Reagents *J. Org. Chem.* **1999**, *64*, 3755–3756.

Appendix 3

Supporting Information for Chapter 4

Single-Electron Methods for Conjugated Polymer Synthesis

I. Materials

iPrMgCl (in THF) was purchased in 100 mL quantities from Aldrich and titrated with phenylhydrazone salicylaldehyde¹ before each use. Compounds **1**, **2**, and **3** were purchased from Solarmer, Inc. The ionic liquid 1-ethyl-3-methylimidazolium bis(trifluoromethanesulfonyl)imide ([EMIM]NTf₂) was purchased from TCI America. All other reagent grade materials and solvents were purchased from Aldrich or Fisher and used without further purification unless otherwise noted. THF was dried and deoxygenated using an Innovative Technology (IT) solvent purification system composed of activated alumina, copper catalyst, and molecular sieves. Flash chromatography was performed on SiliCycle silica gel (40–63 μm) and thin layer chromatography was performed on Merck TLC plates pre-coated with silica gel 60 F254. Preparative size-exclusion chromatography was performed with BioRad S-X1 bio-beads (200–400 mesh). Compounds **S1**,² **4**,³ **PDI**,⁴ and **LiTDBB**⁵ prepared from modified literature procedures. The procedures for attempted S_{RN}1⁶ and electrochemical polymerization were also adapted from the literature.⁷

II. General Experimental

NMR spectroscopy. Unless otherwise noted, ¹H and ¹³C spectra for all compounds were acquired at rt in CD₂Cl₂ or CDCl₃ on a Varian vnmrs 700 operating at 700 and 176 MHz and Varian vnmrs 500 operating at 500 and 126 MHz, respectively. For ¹H and ¹³C spectra in deuterated solvents, the chemical shift data are reported in units of δ (ppm) relative to tetramethylsilane (TMS) and referenced with residual solvent. Multiplicities are reported

as follows: singlet (s), doublet (d), doublet of doublets (dd), triplet (t), multiplet (m), broad resonance (br), and apparent triplet (at).

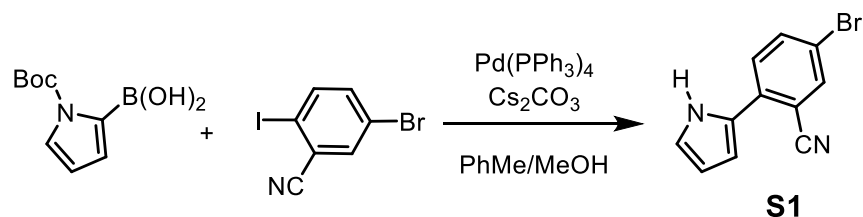
Mass spectrometry: HRMS data were obtained on a Micromass AutoSpec Ultima Magnetic Sector mass spectrometer.

Gel-permeation chromatography: Polymer molecular weights were determined by comparison with polystyrene standards (Varian, EasiCal PS-2 MW 580-377,400) on a Malvern Viscotek GPCMax VE2001 equipped with two Viscotek LT-5000L 8 mm (ID) × 300 mm (L) columns and analyzed with Viscotek TDA 305 (with RI, UV-PDA Detector Model 2600 (190–500 nm), RALS/LALS, and viscometer). Samples were dissolved in THF (with mild heating) and passed through a 0.2 μm PTFE filter prior to analysis. PhMe was used as an internal reference to standardize retention volume.

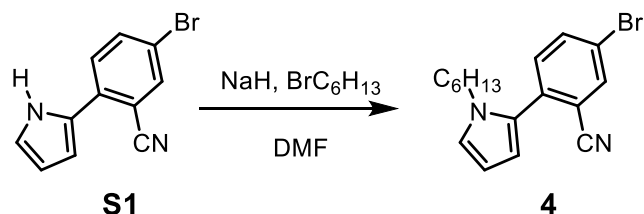
Electropolymerization: Constant current and constant potential electrolysis was performed using a CHI 760C potentiostat with a glassy carbon working electrode ($d = 3.0$ mm), a sacrificial zinc electrode (99.999% pure zinc foil, 150 x 75 mm), and a reference electrode containing Ag/AgNO₃ (0.10 M in MeCN). The zinc foil was degreased by sequential sonication in hexanes, acetone, methanol, and DI H₂O.

Cyclic voltammetry: Cyclic voltammograms were obtained using a CHI 760C potentiostat with a glassy carbon working electrode ($d = 3.0$ mm), a platinum wire counter electrode, and a reference electrode containing Ag/AgNO₃ (0.10 M in MeCN) at a scan rate of 0.10 V/s.

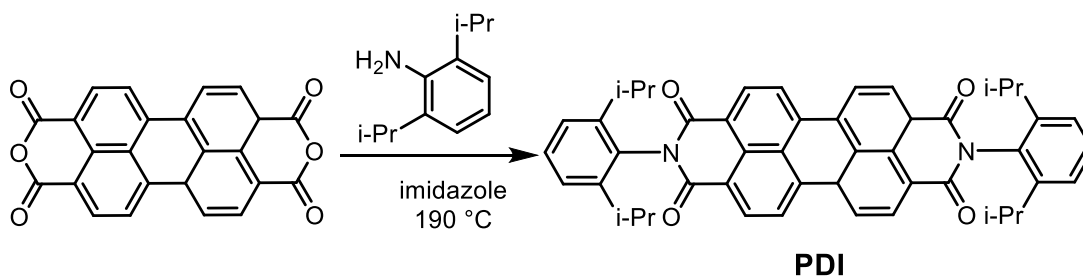
III. Synthetic Procedures



5-bromo-2-(1H-pyrrol-2-yl)benzonitrile (S1). In a glovebox, a 250 mL 2-neck round-bottom flask equipped with a stir bar was charged with palladium tetrakis(triphenylphosphine) (174 mg, 0.150 mmol, 0.050 equiv). The flask was removed from the glovebox and equipped with a reflux condenser, and put under nitrogen. Then, 5-bromo-2-iodobenzonitrile (3.00 mmol, 923 mg, 1.00 equiv) and cesium carbonate (6.00 mmol, 1.96 g, 2.00 equiv) were added to the 2-neck flask, followed by toluene (60 mL). In a separate vial, (1-tert-butoxycarbonylpyrrol-2-yl)boronic acid (3.60 mmol, 760 mg, 1.20 equiv) was dissolved in a 10:3 mixture of toluene:MeOH (39 mL; MeOH was sparged with nitrogen for 20 min). The reaction mixture was heated to 100 °C, and the boronic acid solution was added dropwise via syringe drive addition over 5.5 h. The reaction mixture was then stirred 11 h at 100 °C. The reaction was cooled to rt, then DI H₂O (30 mL) was added, and the product was extracted with DCM (3 x 25 mL), washed with DI H₂O (30 mL), and brine (30 mL), then dried over MgSO₄, filtered, and concentrated, giving a brown solid. The product was purified by column chromatography in toluene, giving 481 mg of **S1** as a yellow solid (65% yield). HRMS (ESI⁺): [M+H] Calcd for C₁₁H₈BrN₂, 246.9865; found, 246.9860.



5-bromo-2-(1-hexylpyrrol-2-yl)benzonitrile (M4). A 25 mL Schlenk flask equipped with a stir bar was evacuated and refilled with nitrogen 3x, then charged with 5-bromo-2-(1H-pyrrol-2-yl)benzonitrile (494 mg, 2.00 mmol, 1.00 equiv) and anhydrous DMF (10 mL). Then, NaH (60% in mineral oil, 240 mg, 6.00 mmol, 3.00 equiv) was added, and the mixture was cooled for 10 min with an ice-water bath. Then, 1-bromohexane (0.56 mL, 4.0 mmol, 2.0 equiv) was added via syringe, and the ice-water bath was removed. The mixture was stirred at rt for 18 h. The reaction mixture was cooled with an ice-water bath, then DI H₂O (20 mL) was slowly added. The solution was extracted with EtOAc (3 x 25 mL), washed with DI H₂O (25 mL), and brine (25 mL), then dried over MgSO₄, filtered, and concentrated. The product was purified by column chromatography (9:1 hexanes:diethyl ether), giving 527 mg of a viscous yellow oil, 80% yield. HRMS (ESI⁺): [M+H]⁺ Calcd for C₁₇H₂₀BrN₂, 331.0804; found, 331.0801.



2,9-bis(2,6-diisopropylphenyl)-3a,12b-dihydroanthra[2,1,9-def:6,5,10-d'e'f']diisoquinoline-1,3,8,10(2H,9H)-tetraone (PDI). An oven-dried 25 mL Schlenk flask was cooled under nitrogen, then 3,4,9,10-perylenetetracarboxylic dianhydride (0.25 mmol, 98 mg, 1.0 equiv), 2,6-diisopropylaniline (0.19 mL, 1.0 mmol, 4.0 equiv) and imidazole (750 mg, 11.0 mmol, 44.0 equiv) were added. The reaction mixture was heated

to 190 °C. After 24 h, the reaction mixture was cooled to rt, then EtOH (5 mL) and aq. HCl (2M, 6 mL) was added and the reaction mixture was stirred an additional 3 h. The crude product was collected by vacuum filtration, and purified by column chromatography in 100% DCM, giving a dark red powder (94.7 mg, 53%). HRMS (ESI+): [M+Na] Calcd for C₄₈H₂₂N₂O₄Na, 733.3037; found 733.3030

IV. NMR Spectra

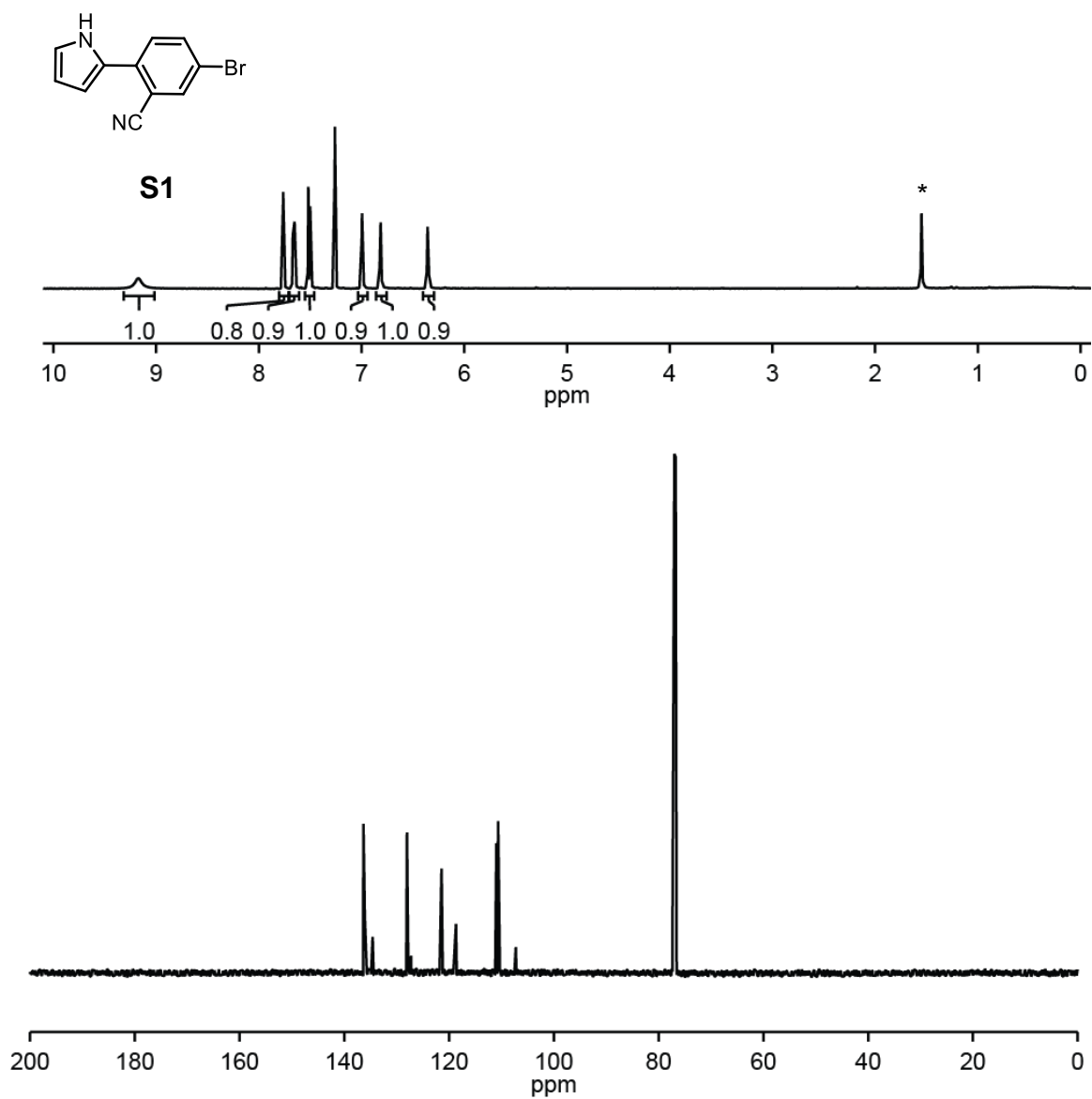


Figure S3.1. ¹H and ¹³C NMR spectra of **S1** ¹H NMR (500 MHz, CDCl₃) 9.17 (br s, 1H), 7.76 (d, *J* = 2.0 Hz, 1H), 7.66 (dd, *J* = 8.7, 2.0 Hz, 1H), 7.51 (d, *J* = 8.6, 1H), 6.99–6.98 (m, 1H), 6.82–6.80 (m, 1H), 6.36–6.34 (m, 1H). *denotes residual H₂O
¹³C NMR (126 MHz, CDCl₃) 136.36, 136.12, 134.61, 128.06, 127.28, 121.46, 118.83, 118.69, 110.98, 110.65, 107.27.

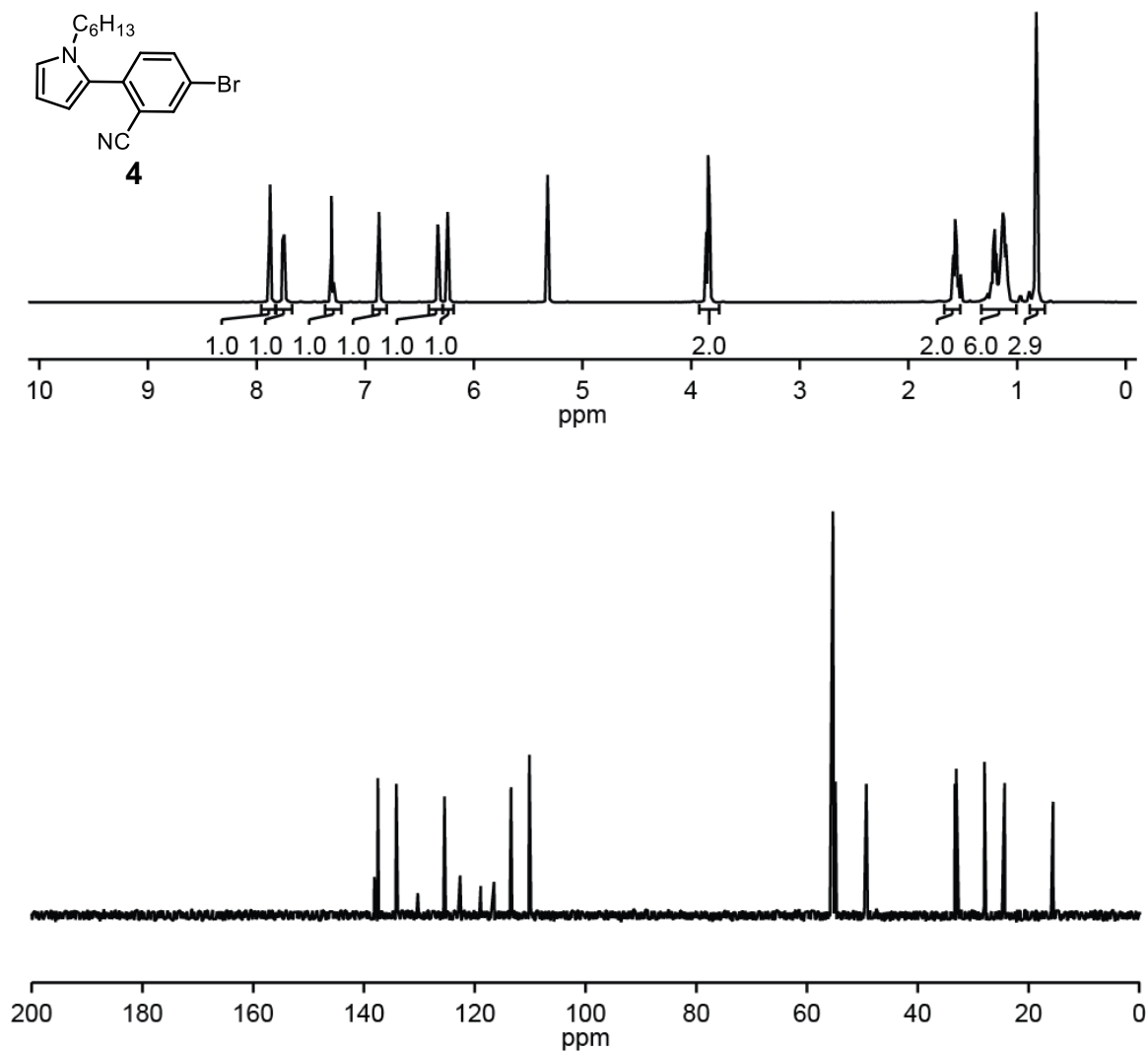


Figure S3.2. ^1H and ^{13}C NMR spectra of **4**.

^1H NMR (500 MHz, CD_2Cl_2) 7.89 (d, $J = 2.0$ Hz, 1H), 7.76 (dd, $J = 8.3, 2.0$ Hz, 1H), 7.31 (d, $J = 8.5$ Hz, 1H), 6.89 (t, $J = 2.0$ Hz, 1H), 6.35–6.34 (m, 1H), 6.25 (t, $J = 3.5$ Hz, 1H), 3.86 (t, $J = 7.0$ Hz, 1H), 1.57–1.60 (m, 2 H), 1.11–1.22 (m, 6 H), 0.84 (t, $J = 7.1$ Hz, 3H).

^{13}C NMR (126 MHz, CDCl_3) 138.15, 137.68, 137.50, 134.17, 130.30, 125.46, 122.65, 118.92, 116.53, 113.45, 110.15, 49.30, 33.29, 33.08, 27.96, 24.33, 15.58.

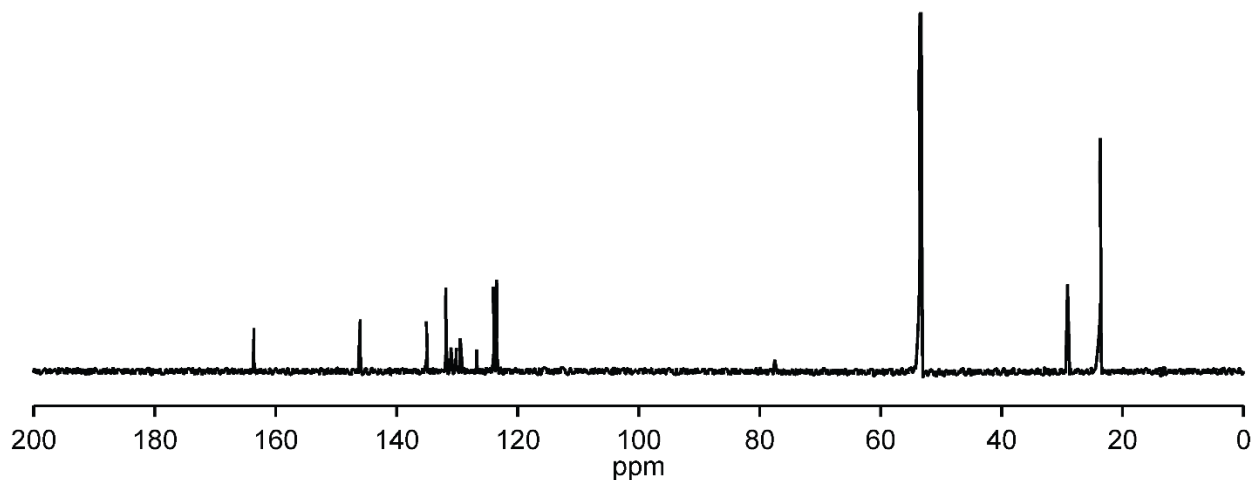
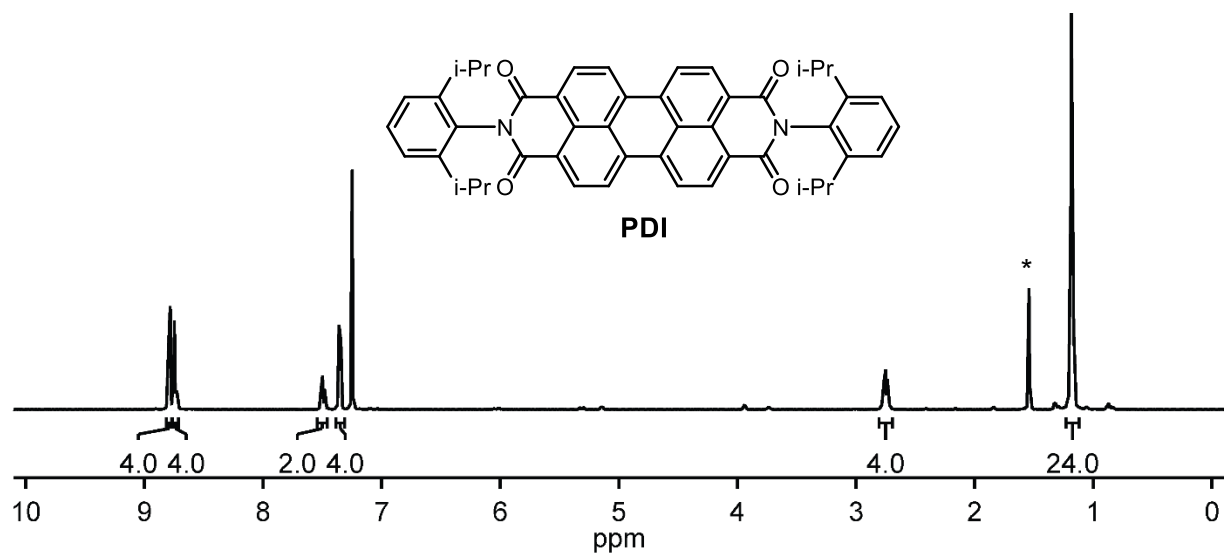


Figure S3.3. ^1H and ^{13}C NMR spectra of **PDI**.

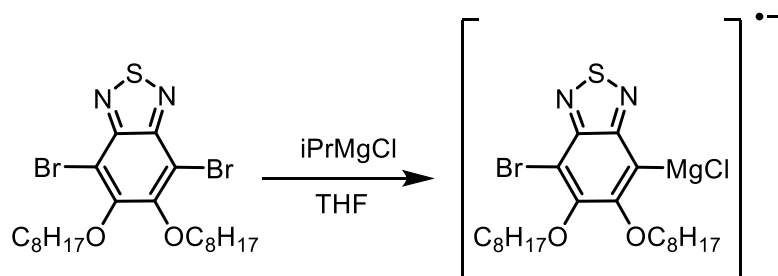
^1H NMR (500 MHz, CDCl_3) 8.81 (d, $J = 7.8$ Hz, 4H), 8.76 (d, $J = 8.0$ Hz, 4H), 7.52 (t, $J = 7.8$ Hz, 2H), 7.37 (d, $J = 7.8$ Hz, 4H), 2.80–2.75 (m, 4H), 1.21 (d, $J = 6.8$ Hz, 24H).

*denotes residual H_2O .

^{13}C NMR (176 MHz, CDCl_3) 163.61, 146.04, 135.13, 131.87, 131.05, 130.16, 129.50, 126.82, 124.08, 123.52, 123.33, 29.11, 23.69.

V. Attempted spontaneous radical polymerization

General activation procedure:



In a glovebox, 4,7-dibromo-5,6-bis(octyloxy)benzo[c][1,2,5]thiadiazole (**2**) (99 mg, 0.18 mmol, 1.0 equiv) was dissolved in THF (0.60 mL) in a 4 mL vial, and a portion of the solution (0.1 mL) was transferred to an EPR tube. A solution of iPrMgCl (1.70 M, 0.095 mL, 0.90 equiv) was added to the remaining **2** solution, causing a color change from colorless to dark red. The reaction was stirred for 10 min at rt in the glovebox, then a portion (0.10 mL) was transferred to a separate EPR tube. The iPrMgCl solution (0.10 mL) was added to a third EPR tube, and the three tubes were sealed with Teflon stoppers, removed from the glovebox and immediately frozen in liquid nitrogen. The three samples were analyzed by EPR spectroscopy. The remaining reaction was left stirring in the glovebox for 24 h, then removed, poured into DI H₂O (2 mL), extracted with CHCl₃ (3 x 2 mL), dried over MgSO₄, filtered, concentrated, and analyzed by GPC.

The activation procedure was repeated using the same scale and reaction time with 4,9-dibromo-2,7-bis(2-decyltetradecyl)benzo(lmn)[3,8]phenanthroline-1,3,6,8(2H,7H)-tetraone (**3**) and 3,6-bis(5-bromothiophen-2-yl)-2,5-bis(2-octyldecyl)pyrrolo[3,4-c]pyrrole-1,4-(2H,5H)-dione (**1**).

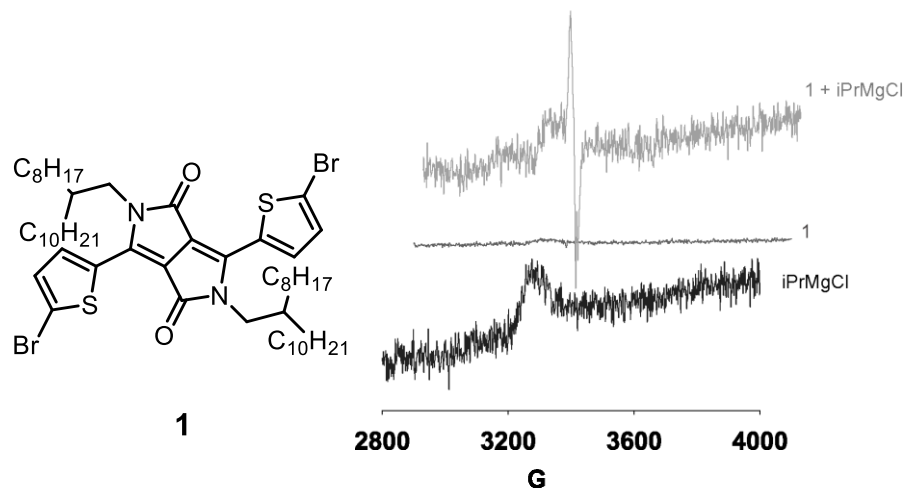


Figure S3.4. EPR spectra of **1**, *iPrMgCl*, and the reaction of **1** + *iPrMgCl*

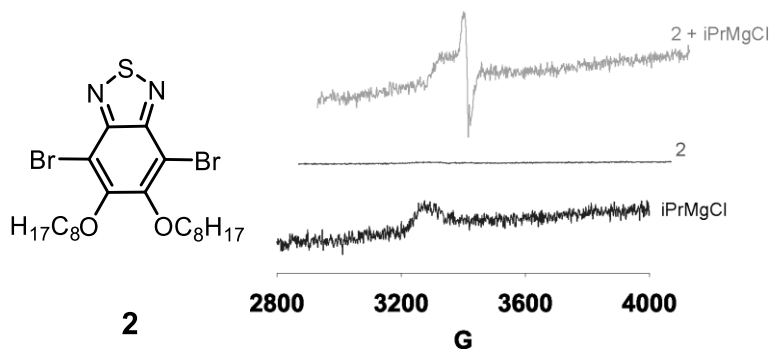


Figure S3.5 EPR spectra of **2**, *iPrMgCl*, and the reaction of **2** + *iPrMgCl*

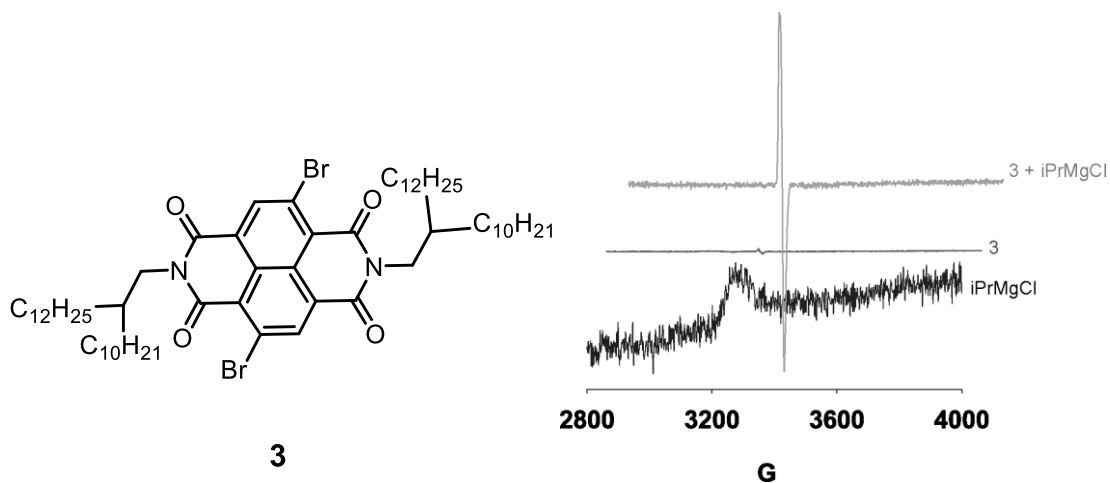
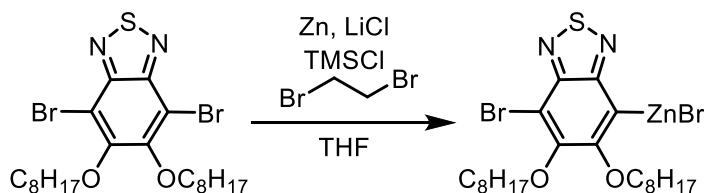


Figure S3.6 EPR spectra of **3**, *iPrMgCl*, and the reaction of **3** + *iPrMgCl*

VI. Zinc activation and attempted polymerization of 4,7-dibromo-5,6-bis(octyloxy)benzo[c][1,2,5]thiadiazole

Activation procedure:



In a glovebox, zinc powder (29 mg, 0.45 mmol, 1.5 equiv) and lithium chloride (42 mg, 0.15 mmol, 1.5 equiv) were weighed into a 4 mL vial, and THF (0.40 mL) was added. A stock solution of TMSCl (4.3 μ L, 0.050 mmol) and 1,2-dibromoethane (6.4 μ L, 0.050 mmol) in THF (1.0 mL) was prepared. Then the stock solution (0.30 mL, 0.015 mmol TMSCl, 0.015 mmol 1,2-dibromoethane, 0.15 equiv of each) was transferred to the vial containing zinc, which was then stirred for 30 min at rt. Then, 4,7-dibromo-5,6-bis(octyloxy)benzo[c][1,2,5]thiadiazole (0.55 mg, 0.10 mmol, 1.0 equiv) was dissolved in THF (1.0 mL) and added to the reaction mixture, which was then stirred for 24 h at rt. The mixture turned from colorless to pink. The reaction mixture was filtered through a 0.2 μ m PTFE filter.

This procedure was repeated and the reaction was quenched with approx. 1 mL HCl, extracted with DCM (2 x 1.5 mL), washed with sat. NaHCO₃, (approx. 2 mL) and dried over MgSO₄. The product was purified by column chromatography (9:1 hexanes:EtOAc), then analyzed by NMR spectroscopy (Figure S3.4). A new singlet was observed in the aromatic region.

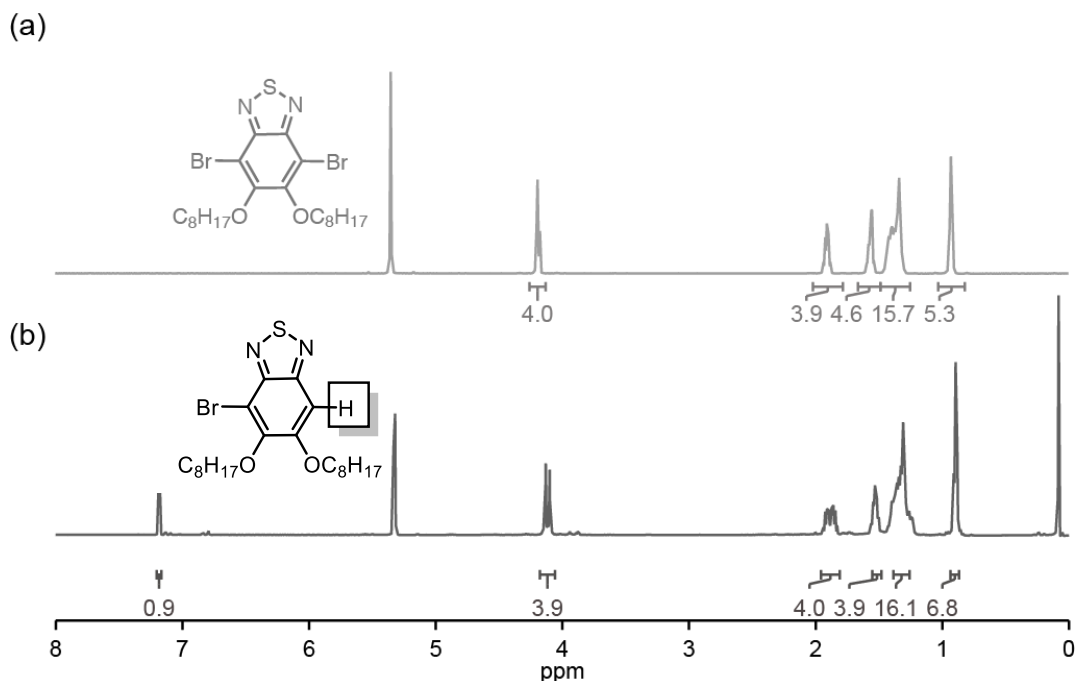
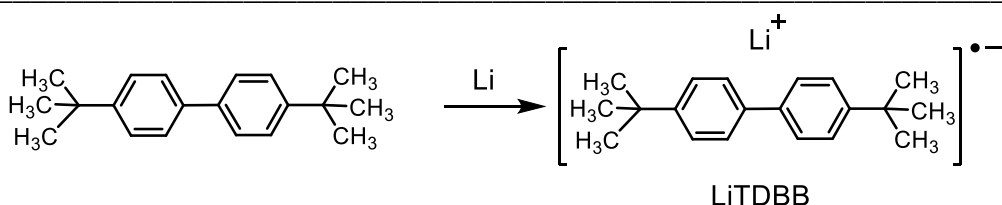


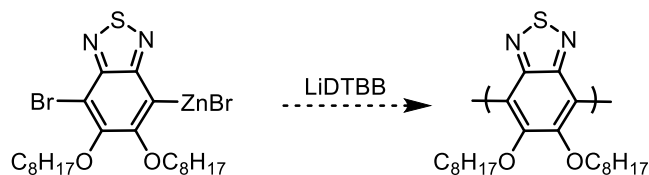
Figure S3.7. (a) ^1H NMR spectrum of unreacted **2** (b). ^1H NMR spectrum of **2** after Zn activation and quenching

Synthesis of sacrificial electron donor:



A 25 mL Schlenk flask equipped with a stir bar was evacuated and refilled with nitrogen 3x, then 1-tert-butyl-4-(4-tert-butylphenyl)benzene (107 mg, 0.400 mmol, 1.00 equiv) and THF (5 mL) were added. Lithium metal (30.0 mg, 4.30 mmol, 10.9 equiv) was washed with hexanes and added under nitrogen pressure. The reaction mixture was sonicated for five min, then stirred for 2 h, turning dark blue after 10 min. The blue solution was cannula transferred to a Schlenk tube and brought into the glovebox, where it was used immediately.

Attempted radical polymerization:



In a glovebox, a solution of **2** (0.057M in THF, 2.5 mL, 0.14 mmol) was transferred to a 20 mL vial and diluted with THF (2 mL), then LiTDBB was added (0.89 mL, 0.008M in THF, 0.05 equiv). Aliquots (approx. 0.1 mL) were removed at 0, 3, and 21, quenched with HCl (approx. 1 mL), extracted with DCM (2 x 1.5 mL), washed with sat. $NaHCO_3$, (approx. 2 mL) and dried over $MgSO_4$, then analyzed by GC and GPC. GC showed no conversion after 21 h. Additional LiDTBB (1 equiv) was added after 24 h, but no conversion was observed after an additional 10 h. GPC showed no polymer formation.

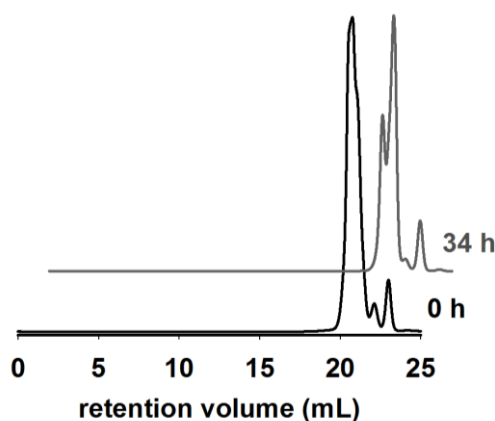


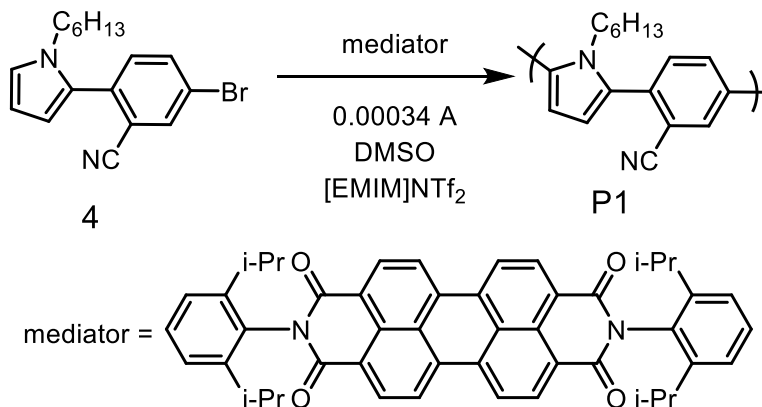
Figure S3.8. GPC traces for the attempted polymerization of **2**.

Table S3.1. GC areas for attempted polymerization of **2**.

Reaction time:	area% quenched monomer	area% unactivated monomer
0 h	91	8.8
3 h	90.5	9.5
21 h	91.2	8.8
34 h	91.3	8.7

VII. Electrochemical polymerizations

Undivided cell procedure



An undivided cell equipped with a stir bar was charged with **4** (33 mg, 0.10 mmol, 1 equiv) and **PDI** (varying equiv; see Table **S3.2**). Then, a solution of [EMIM]NTf₂ (0.15M in anhydrous DMSO) (7.5 mL) was added and the solution was sparged with argon for 10 min, then put under positive argon pressure. The cell was equipped with a glassy carbon working electrode ($d = 0.3$ mm), a sacrificial zinc counter electrode (150 x 75 mm), and a Ag/AgNO₃ reference electrode (0.10 M in MeCN). A constant current of 0.00034 A was applied for 3000 s (or 7000 s), during which time the color gradually changed from bright pink to dark purple. The potential of the solution was recorded during the reaction (Figure S3.7). The reaction was poured into DI H₂O (10 mL), extracted with hot CHCl₃ (3 x 10 mL), washed with DI H₂O (3 x 20 mL), and brine (20 mL), then dried over MgSO₄, filtered, and concentrated. The resulting pink solid was analyzed by GPC.



Figure S3.9. Undivided cell setup for polymerizing **4**

Table S3.2. Results for polymerizing **4** in an undivided cell with varying equivalents of PDI.

equiv PDI:	M_n (kDa)
0.05	11.5
0.10	6.22
0.50	no polymer
0.05 (t = 7000 s)	insoluble powder

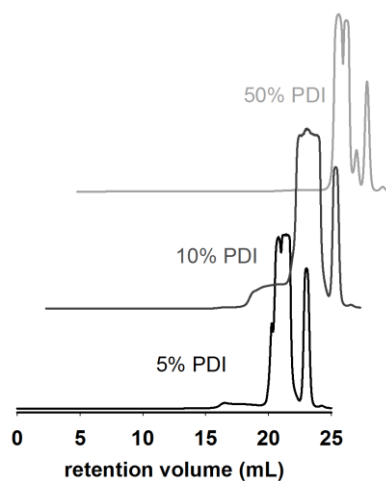


Figure S3.10. GPC traces for polymerizing **4** in an undivided cell. The peak at 20 mL is PDI.

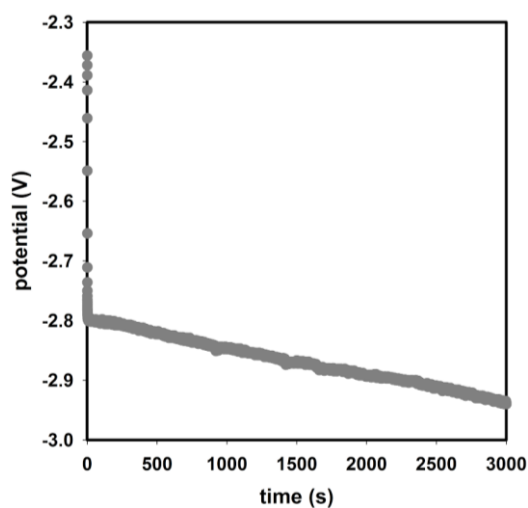


Figure S3.11. Plot of potential (V) vs time (s) for polymerizing **4** in an undivided cell at a constant current of 0.00034 A.

Polymer purification procedure:

Polymer (from reaction with 10% mediator) was isolated using size-exclusion BioBeads. The beads were swelled overnight in THF. The column was run using THF as the eluent

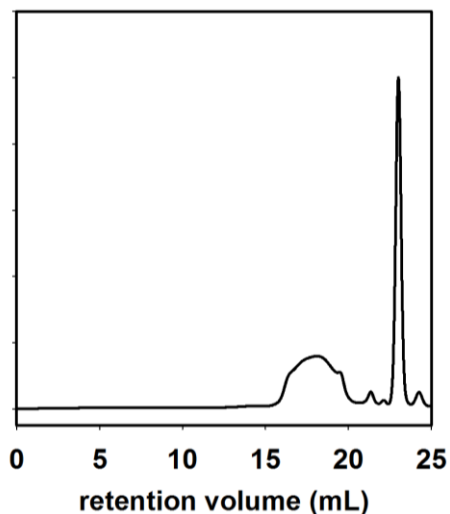


Figure S3.12. GPC trace of isolated **P1**. $M_n = 6.2$ kDa, $\mathcal{D} = 2.9$.

and fractions were collected by color. The first fraction, which was colorless, was concentrated and analyzed by GPC.

Divided cell procedure

A solution of **4** (33 mg, 0.10 mmol, 1 equiv), **PDI** (7.1 mg, 0.010 mmol, 1.0 equiv) and [EMIM]NTf₂ (0.15 M) in anhydrous DMSO (7.5 mL) was prepared and a portion (2.0 mL) was added to the cathodic chamber of a divided cell (Figure S3.9). The solvent/electrolyte solution ([EMIM]NTf₂ (0.15M in anhydrous DMSO) (7.5 mL) was added to the anodic chamber. The bright pink solution in the cathodic chamber was bubbled with argon for 10 min. The cathodic chamber was equipped with a glassy carbon working electrode and a Ag/AgNO₃ reference electrode (0.10M in MeCN), while the anodic chamber was equipped with a sacrificial zinc counter electrode (150 x 75 mm). A constant current of 0.00034 A was applied for 14 h. The reaction mixture was initially a bright pink color, and turned to dark purple during the reaction. To quench, the reaction was poured into DI H₂O (10 mL), extracted with hot CHCl₃ (3 x 10 mL), washed with DI H₂O (3 x 20 mL), and brine (20 mL), then dried over MgSO₄, filtered, and concentrated. The resulting pink solid was analyzed by GPC. No polymer was observed.



Figure S3.13. Divided cell for polymerizing **4**

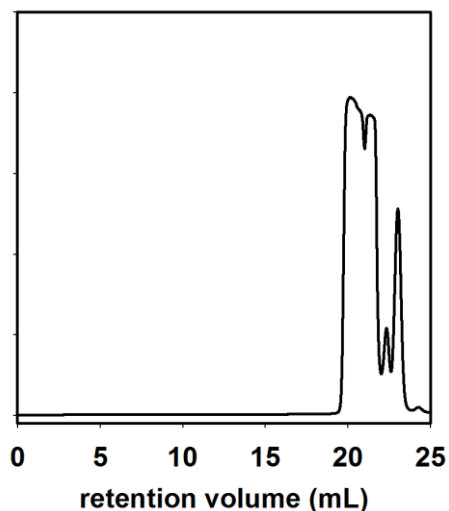


Figure S3.14. GPC trace of product isolated from polymerizing **4** in a divided cell

Control polymerizations

A. Monomer alone

An undivided cell equipped with a stir bar was charged with 5-bromo-2-(1-hexyl-1H-pyrrol-2-yl)benzotrile (33 mg, 0.10 mmol.) Then, a solution of [EMIM]NTf₂ (0.15M in anhydrous DMSO) (7.5 mL) was added. The colorless solution was sparged with argon for 10 min. The cell was equipped with a glassy carbon working electrode, a sacrificial zinc counter electrode (150 x 75 mm), and a Ag/AgNO₃ (0.10M in MeCN) reference electrode. A constant current of 0.00034 A was applied for 3000 s. After 3000 s elapsed, the solution was poured into DI H₂O (10 mL), extracted with hot CHCl₃ (3 x 10 mL), washed with DI

H₂O (3 x 20 mL), and brine (20 mL), then dried over MgSO₄, filtered, and concentrated. The resulting brown oil was analyzed by GPC. No polymer was observed.

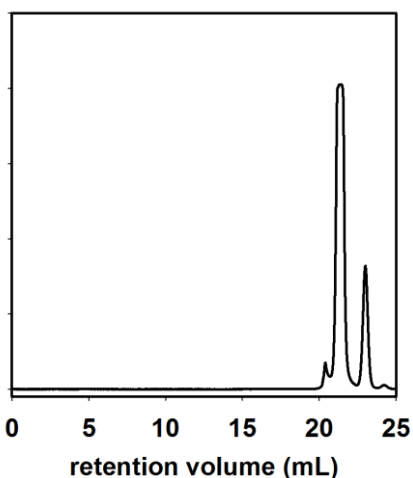


Figure S3.15. GPC trace for treating **4** with constant current in the absence of **PDI**

B. PDI alone

An undivided cell equipped with a stir bar was charged with PDI (7.1 mg, 0.01 mmol). Then, a solution of [EMIM]NTf₂ (0.15M in anhydrous DMSO) (7.5 mL) was added. The bright pink solution was sparged with argon for 10 min. The cell was equipped with a glassy carbon working electrode, a sacrificial zinc counter electrode (150 x 75 mm), and a reference electrode of Ag/AgNO₃ (0.10 M in MeCN). A constant current of 0.00034 A was applied for 3000 s. The reaction mixture was initially a bright pink color, and turned to dark purple during the reaction. After 3000 s elapsed, the solution was poured into DI H₂O (10 mL), extracted with hot CHCl₃ (3 x 10 mL), washed with DI H₂O (3 x 20 mL), and brine (20 mL), then dried over MgSO₄, filtered, and concentrated. The resulting pink solid was analyzed by GPC. No polymer was observed.

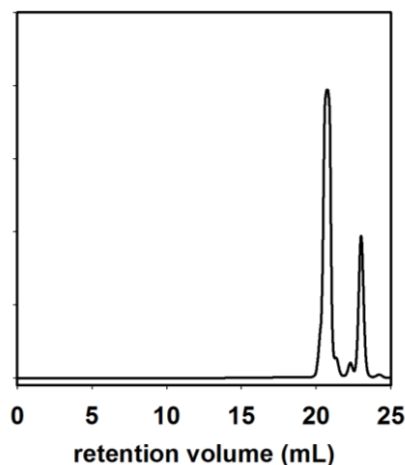


Figure S3.16. GPC trace for treating **PDI** with constant current in the absence of **4**

C. Zinc, **4** and **PDI** in the absence of current

An undivided cell equipped with a stir bar was charged with 5-bromo-2-(1-hexyl-1H-pyrrol-2-yl)benzotrile (33 mg, 0.10 mmol, 1 equiv) and **PDI** (7.1 mg, 0.010 mmol 0.10 equiv). Then, a solution of [EMIM]NTf₂ (0.15M in anhydrous DMSO) (7.5 mL) was added. The bright pink solution was sparged with nitrogen for 10 min, then a piece of zinc foil (150 x 75 mm) was added. The reaction mixture was initially a bright pink color, and turned to dark purple during the reaction. After 12 h elapsed, the solution was poured into DI H₂O (10 mL), extracted with hot CHCl₃ (3 x 10 mL), washed with DI H₂O (3 x 20 mL), and brine (20 mL), then dried over MgSO₄, filtered, and concentrated. The resulting pink solid was analyzed by GPC. No polymer was observed.

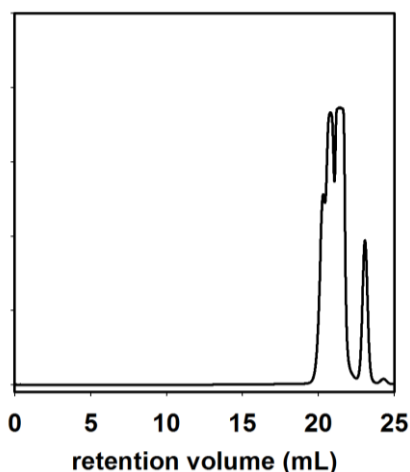


Figure S3.17. GPC trace for combining **4**, **PDI**, and zinc foil in the absence of current

Constant potential polymerization procedure:

An undivided cell equipped with a stir bar was charged with 5-bromo-2-(1-hexyl-1H-pyrrol-2-yl)benzotrile (33 mg, 0.10 mmol, 1 equiv) and PDI (0.10 equiv). Then, a solution of [EMIM]NTf₂ (0.15 M) in DMSO (7.5 mL) was added. The bright pink solution was bubbled with argon for 10 min. The cell was equipped with a glassy carbon working electrode, a sacrificial zinc counter electrode (150 x 75 mm), and a Ag/AgNO₃ (0.10M in MeCN) reference electrode. A constant potential of -2.9 V was applied for 1 h. Then, a constant potential of -1.1 V was applied for 12 h. The reaction mixture was initially a bright pink color, and turned to dark purple during the reaction. After the electrolysis finished, the reaction was poured into DI H₂O (10 mL), extracted with hot CHCl₃ (3 x 10 mL), washed with DI H₂O (3 x 20 mL), and brine (20 mL), then dried over MgSO₄, filtered, and concentrated. The resulting pink solid was analyzed by GPC. No polymer was observed.

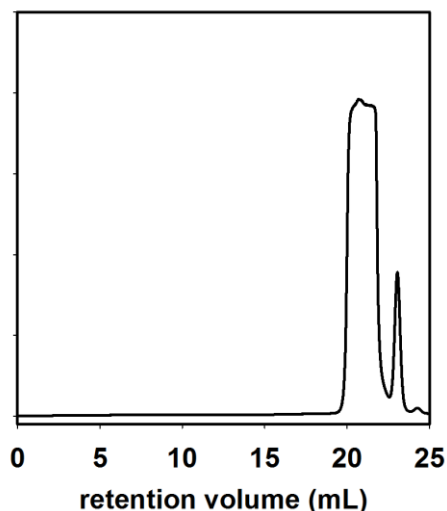


Figure S3.18. GPC trace for polymerizing **4** with constant potential

VIII. Cyclic voltammetry

Procedure:

Cyclic voltammograms were obtained using a CHI 760C potentiostat with a glassy carbon working electrode ($d = 3.0$ mm), a platinum wire counter electrode, and a reference electrode containing Ag/AgNO₃ (0.10 M in MeCN), at a scan rate of 0.10 V/s. Samples were dissolved in DMSO with [EMIM]NTf₂ (0.15 M) as the supporting electrolyte.

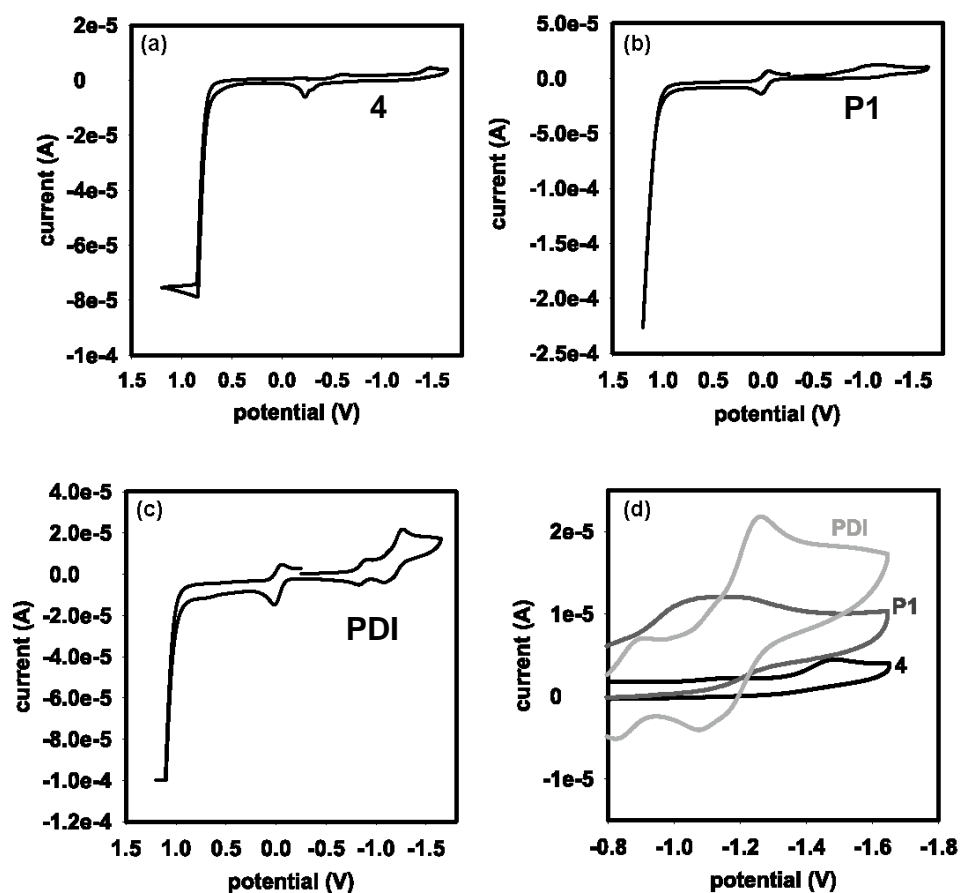


Figure S3.19. Cyclic voltammograms of (a) **4**, (b) **P1**, (c) **PDI**, and (d) **M4**, polymer, and **PDI** overlaid

Table S3.3. Cyclic voltammetry results for **4**, **P1**, and **PDI**

compound:	PDI	P1	4
E_p (V):	-0.915, -1.27	-1.16	-1.49

IX. References

- (1) Love, B.E.; Jones, E.G. The Use of Salicylaldehyde Phenylhydrazone as an Indicator for the Titration of Organometallic Reagents *J. Org. Chem.* **1990**, *45*, 1924–1930.
- (2) Alešković, M.; Basarić, N.; Mlinarić-Majerski, K. Optimization of the Suzuki coupling reaction in the synthesis of 2-[(2-substituted)phenyl]pyrrole derivatives *J. Heterocyclic Chem.* **2011**, *48*, 1329–1335.
- (3) Zhou, Y.; Liu, X-W.; Gu, Q.; You, S-H. Enantioselective Synthesis of Tetrahydroindolizines via Ruthenium–Chiral Phosphoric Acid Sequential Catalysis *Synlett* **2016**, *27*, 586–590.
- (4) Ramana, C.; Smeigh, A.L.; Anthony, J.E.; Marks, T.J.; Wasielewski, M.R. Competition between Singlet Fission and Charge Separation in Solution-Processed Blend Films of 6,13-Bis(triisopropylsilylethynyl)pentacene with Sterically-Encumbered Perylene-3,4:9,10-bis(dicarboximide)s *J. Am. Chem. Soc.* **2012**, *134*, 386–397.
- (5) Freeman, P.K.; Hutchinson, L.L. Alkylolithium Reagents From Alkyl Halides and Lithium Radical Anions *J. Org. Chem.* **1980**, *45*, 1924–1930.
- (6) Smith, M.L.; Leone, A.K.; Zimmerman, P.M.; McNeil, A.J. Impact of Preferential π -Binding in Catalyst-Transfer Polycondensation of Thiazole Derivatives *ACS Macro Lett.* **2016**, *5*, 1411–1415.
- (7) Sun, G.; Ren, S.; Zhu, X.; Huang, M.; Wan, Y. Direct Arylation of Pyrroles via Indirect Electroreductive C–H Functionalization Using Perylene Bisimide as an Electron-Transfer Mediator *Org. Lett.* **2016**, *18*, 544–547.